AD_____

Award Number: W81XWH-10-1-0971

TITLE: The Neurophysiology of Autonomic Dysfunction in SCI: Plasticity in the Input and Output Neurons

PRINCIPAL INVESTIGATOR: Keith Tansey, MD, PhD

CONTRACTING ORGANIZATION: Emory University School of Medicine
Atlanta, GA 30322-1018

REPORT DATE: April 2014

TYPE OF REPORT: Final

PREPARED FOR: U.S. Army Medical Research and Materiel Command
Fort Detrick, Maryland 21702-5012

REPORT DOCUMENTATION PAGE

Form Approved
OMB No. 0704-0188

1. REPORT DATE	2. REPORT TYPE	3. DATES COVERED
April 2014	Final	27 Sep 2010 - 26 Jan 2014

4. TITLE AND SUBTITLE
The Neurophysiology of Autonomic Dysfunction in SCI: Plasticity in the Input and Output Neurons

5a. CONTRACT NUMBER

5b. GRANT NUMBER
W81XWH-10-1-0971

5c. PROGRAM ELEMENT NUMBER

6. AUTHOR(S)
Keith Tansey, MD, PhD

E-Mail: ktansey@emory.edu

5d. PROJECT NUMBER

5e. TASK NUMBER

5f. WORK UNIT NUMBER

7. PERFORMING ORGANIZATION NAME(S) AND ADDRESS(ES)
Emory University
Atlanta, GA 30322

8. PERFORMING ORGANIZATION REPORT NUMBER

9. SPONSORING / MONITORING AGENCY NAME(S) AND ADDRESS(ES)
U.S. Army Medical Research and Materiel Command
Fort Detrick, Maryland 21702-5012

10. SPONSOR/MONITOR'S ACRONYM(S)

11. SPONSOR/MONITOR'S REPORT NUMBER(S)

12. DISTRIBUTION / AVAILABILITY STATEMENT
Approved for Public Release; Distribution Unlimited

13. SUPPLEMENTARY NOTES

14. ABSTRACT: The overall aim of this research project was to evaluate neural plasticity in the nociceptive input afferents and preganglionic sympathetic output neurons in autonomic dysfunction following spinal cord injury (SCI). Over the last three years, we have characterized the physiological changes in cardiovascular responses after ceNicalspinalcord injury and matched those with anatomical changes (sprouting) in nociceptive cutaneous afferents compared to the baseline physiology and anatomy of this system in normal animals. In regards to the preganglionic sympathetic output neurons, we have developed a monoaminergic receptor profile for these neurons and measured sensorimotor plasticity in those neurons in an *in vitro* preparation.

15. SUBJECT TERMS- Nociceptive afferents, sprouting, cardiovascular plasticity, sympathetic preganglionic neurons, HB9, autonomic dysreflexia

16. SECURITY CLASSIFICATION OF:			17. LIMITATION OF ABSTRACT	18. NUMBER OF PAGES	19a. NAME OF RESPONSIBLE PERSON
a. REPORT	b. ABSTRACT	c. THIS PAGE			USAMRMC
U	U	U	UU	113	19b. TELEPHONE NUMBER *(include area code)*

Table of Contents

Introduction

The overall aim of this research project was to evaluate neural plasticity in nociceptive afferents and preganglionic sympathetic neurons in autonomic dysfunction following spinal cord injury (SCI). Over the last three years, we have made significant progress as listed below. In the first aim regarding afferent inputs, we have characterized the physiological changes of cardiovascular responses in cervical spinal cord injury and matched those with anatomical changes of nociceptive afferents compared to the baseline physiology and anatomy in normal animals. In the second aim regarding sympathetic outputs, we have developed monoaminergic receptor profiles of preganglionic sympathetic neurons and measured sensorimotor plasticity of those neurons in an *in vitro* preparation. We also requested a 3 month no cost extension at the end of the grant's three year term to finalize data collection and complete its analysis.

Body

Scope of work

	Year 1				Year 2				Year 3				Year 4
	Q1	Q2	Q3	Q4	Q1	Q2	Q3	Q4	Q1	Q2	Q3	Q4	Q1
Specific Aim 1: We propose to study plastic mechanisms associated with high SCI-induced Autonomic Disreflexia that is circuit-based in the in vivo adult rat													
1.1 Prepare animal protocol and train postdoc and technician	Emory University												
Milestone 1: Animal Use approval postdoc trained and technician trained	Emory University												
1.2 characterize the stimulation strengths and frequencies sufficient to generate increases in blood pressure			Animals Used 40 rats										
Milestone 2:			Stimulation paradigms determined and anesthetic or decerebration determined										
1.3 Histological evaluation of spinal cord injury		40 Animals used degree of injury determined											
1.4 Compare the magnitude of plasticity in BP responses after injury				40 animals used									
1.5 Histological evaluation of dorsal cutaneous nerves by TEM			10 animals										
Milestone 3: Analysis and Publication												Emory University	

Specific aim 2: We propose to study cell based changes associated with spinal cord injury-induced autonomic disreflexia													
2.1 Prepare animal protocol and train postdoc	Emory University												
Milestone 1: Animal Use approval postdoc trained	Emory University												
2.2 Characterize dysreflexia in HB9 mice		5 recordings (8 mice) used											
Milestone 2:		dysrelexia seen in HB9 mice											
2.3 Patch clamp recordings in control mice			50 cells (57 mice) used										
Milestone 3:			baseline patch clamp recordings are completed in rostral and caudal thoracic of normal mice										
2.4 Patch clamp recordings in SCI mice				50 cells (72 mice) used									
Milestone 4: Analysis and publication											Emory University		

Specific Aim 1
Aim 1.1 Achieved

Aim 1.2

We have first characterized blood pressure (BP) and heart rate (HR) changes evoked by electrical stimulation of nociceptive cutaneous afferents at different stimulation strengths, stimulation frequencies, and spinal levels in normal animals. Dorsal cutaneous nerves (DCNs) from L1 to T6 on the left side of the animal were isolated and stimulated with bipolar electrodes one at a time under pentobarbital anesthesia. BP and HR were recorded at the right carotid artery cannulated with PE 10 tubing and connected to a pressure transducer. The DCNs were stimulated at either 0.5 or 5 mA at different frequencies (1, 2, 5 and 10 Hz) for 20 seconds each.

We have found that in normal animals the DCN stimulation generated overall BP depressor and increased HR across stimulation strengths, stimulation frequencies, and spinal levels in normal animals. However, we were able to analyze detailed parameters of the autonomic responses (e.g. magnitude, latency, and duration as well as relationship between BP and HR) and found an apparently distinct organization of those responses across stimulation strengths, stimulation frequencies, and spinal levels. Shown are normalized BP and HR changes at 0.5 mA (red) or 5 mA (green) at different stimulation frequencies (each row) and at different spinal levels (each column). This data also revealed that DCN stimulation at 0.5 mA which activates only myelinated A delta fibers preferentially generated HR increases but relatively less BP decreases. Stimulation at 5 mA which activates both myelinated A delta fibers and unmyelinated C fibers generated similar HR increases but greater BP increases. This implies a selective cardiovascular response depending on which pain afferents are stimulated: A delta for cardiac/HR and C fiber for vascular tone/BP.

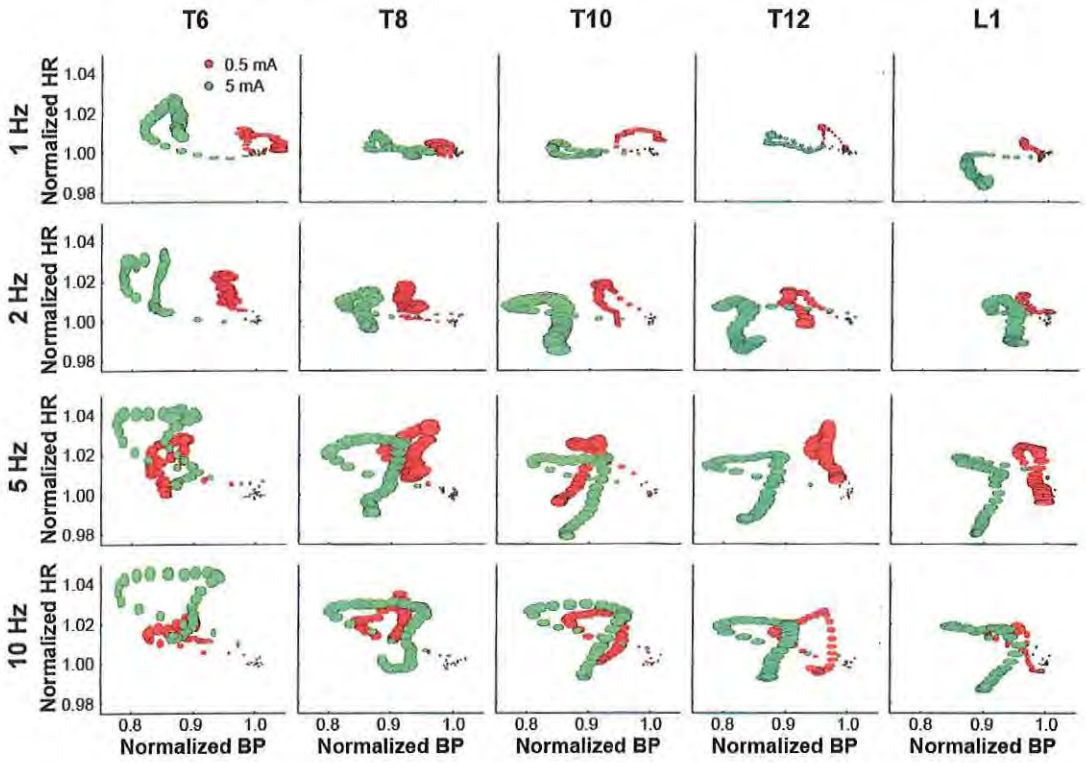

Aim 1.3

Histological evaluations of SCI were designed to address the extent of loss of supraspinal connection to spinal autonomic neural circuitry as the extent to which this occurs appears in our pilot data to influence the magnitude of the expression of dysautonomia and frank autonomic dysreflexia. Serial cross sections (20 μm thick) of injured cervical spinal cord were subjected to histological staining and injury measurement has been done using a light microscope equipped with motorized stage. Borders of injured tissue were traced along glial limitants based on cytoarchitectonics on each section stained with cressyl violoet and percent areas of spared tissue on dorsal half were measured at the injury epicenter where the most injury occurred. However, the injury measurement around the glial border seemed to overestimate spared tissue areas where actually axons remained. The spared tissue areas measured at the glial borders were much greater than the remained axon areas which can be measured with sections stained both with cressyl violet and luxol fast blue shown as a pilot data in our original proposal. We are now measuring the spared axon areas in those sections to compare the extent of injury to the extent of autonomic dysfunction seen neurophysiologically.

Aim 1.4

As the physiological parameters of cardiovascular responses evoked by DCN stimulations have been characterized in normal animals (Aim 1.2), we have performed the same experiments (except 0.5 mA stimulation) in animals with cervical SCI. After 2-4 weeks post injury, DCN stimulations generated three patterns of BP changes including depressors (normal-like), pressor (frank autonomic reflexia), and mixed responses depending on spinal levels (dysautomonia). Normalized BP (1st row) and HR (2nd row) changes across DCNs are shown below on 3D plots at 5 Hz (left three columns) and 10 Hz (right columns). Bar graphs shows delta changes at the peak of BP (3rd row) and HR (4th row) while early delta changes during the first 9 second of stimulation were shown as red boxes.

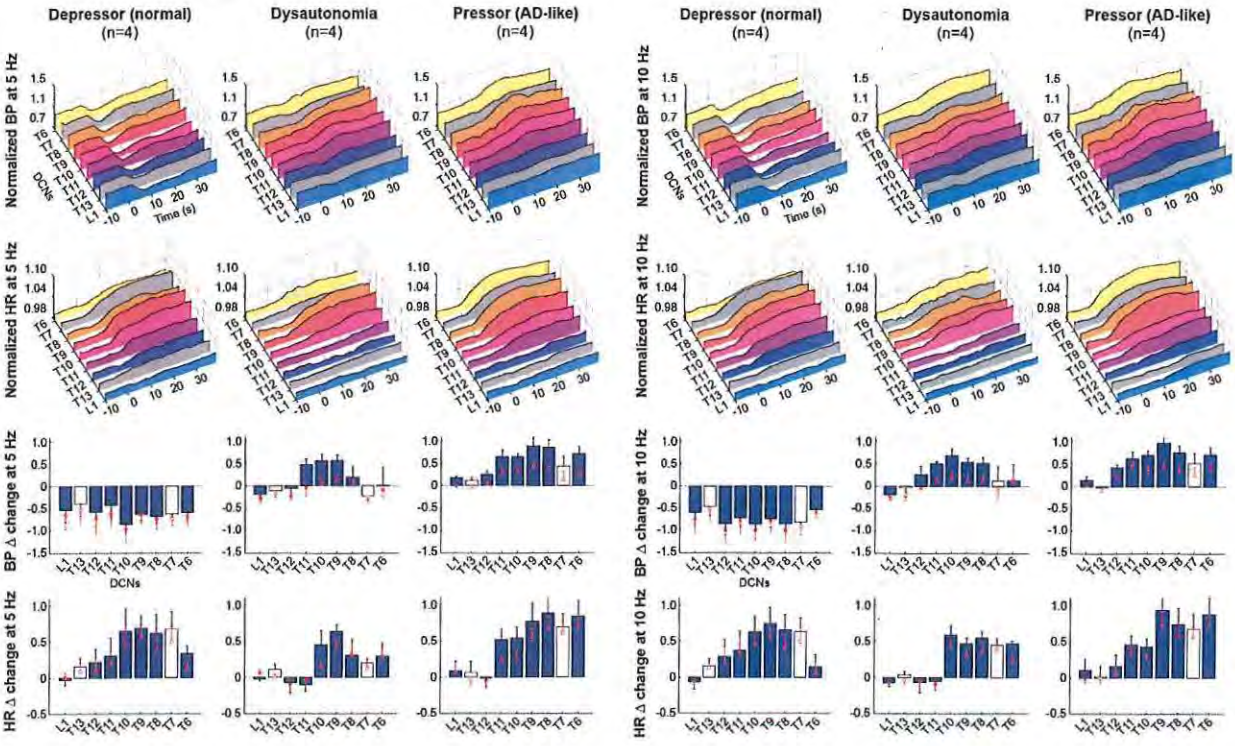

We have also analyzed BP and HR relationship patterns in animals with cervical SCI. Plotted below are normalized BP and HR at 5 mA across stimulation frequencies (each row) and spinal levels (each column) in depressor (green), dysautonomia (blue), and pressor (red) groups after SCI. The extent to which BP and HR changes i.e. spatial distribution of bubbles indicated that BP and HR responses were greater at higher frequencies (1, 2 Hz vs 5, 10 Hz) and also greater in rostral levels (L1, T12 vs T6, T8). BP responses in the depressor group in SCI were similar with those BP responses in uninjured normal animals since the subgroups were determined based on the BP responses. However, the relationship between BP and HR in depressor group appeared apparently different from normal animals (see also Aim 1.2). HR increased to a greater extent and recovered slower in injured depressor group than in normal animals. This pattern of HR change was also observed in all three injured groups. Taken all together, these findings demonstrate that stimulation of pain afferents in SCI generates cardiovascular plasticity resulting in, at least, three different patterns of autonomic dysfunction.

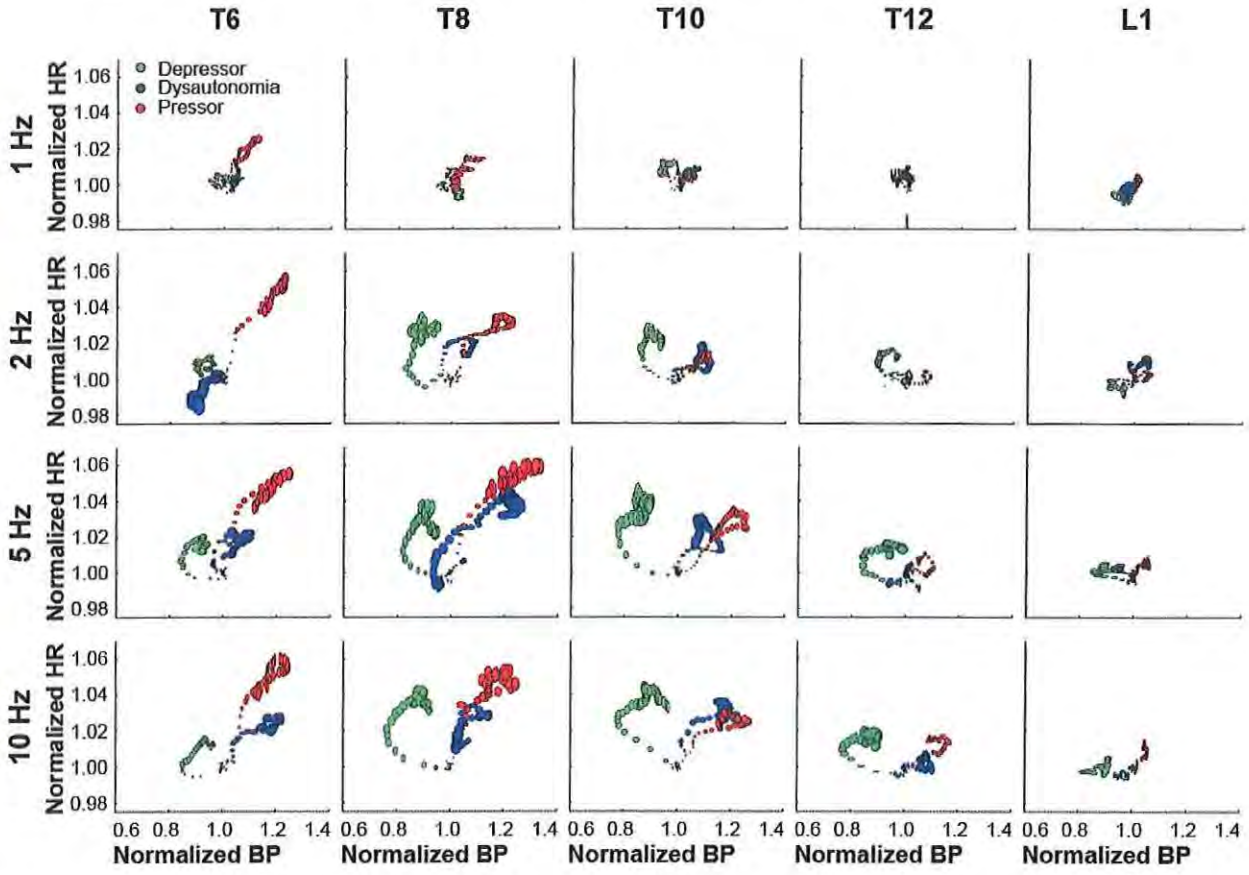

Aim 1.5

In order to examine whether the autonomic plasticity seen electrophysiologically is related to any anatomical plasticity in pain afferents, we next performed histological evaluation of the DCNs to investigate the numbers and types of pain afferents in each segmental nerves (Aim 1.5.1) and their central projection patterns into the spinal cord dorsal horn (Aim 1.5.2).

1.5.1
To examine whether pain afferents in peripheral DCNs contribute to the physiological characteristics of CTM reflex e.g. somatotopic arrangement of motor and autonomic responses,

we have analyzed numbers of axon subtypes in each DCN from T6 to L1 in normal animals. DCNs were harvested and processed for electron microscopy. Myelinated axons were identified in fascicles of each DCN (blue circles in panels A and B) on light microscopic images (10X). Axon diameters were analyzed for each myelinated axon while Aδ and Aα/β axons were distinguished based on the threshold diameter of 6 μm (left bottom panel). Unmyelinated C fibers were counted on high power cross section images (1000X) seen as blue pluses (panel C in figure). Axon numbers of all subtypes were not significantly different across spinal levels (right bottom panel) suggesting that the number of axons in peripheral DCNs does not explain the physiological somatotopic arrangement seen in evoked motor and autonomic responses.

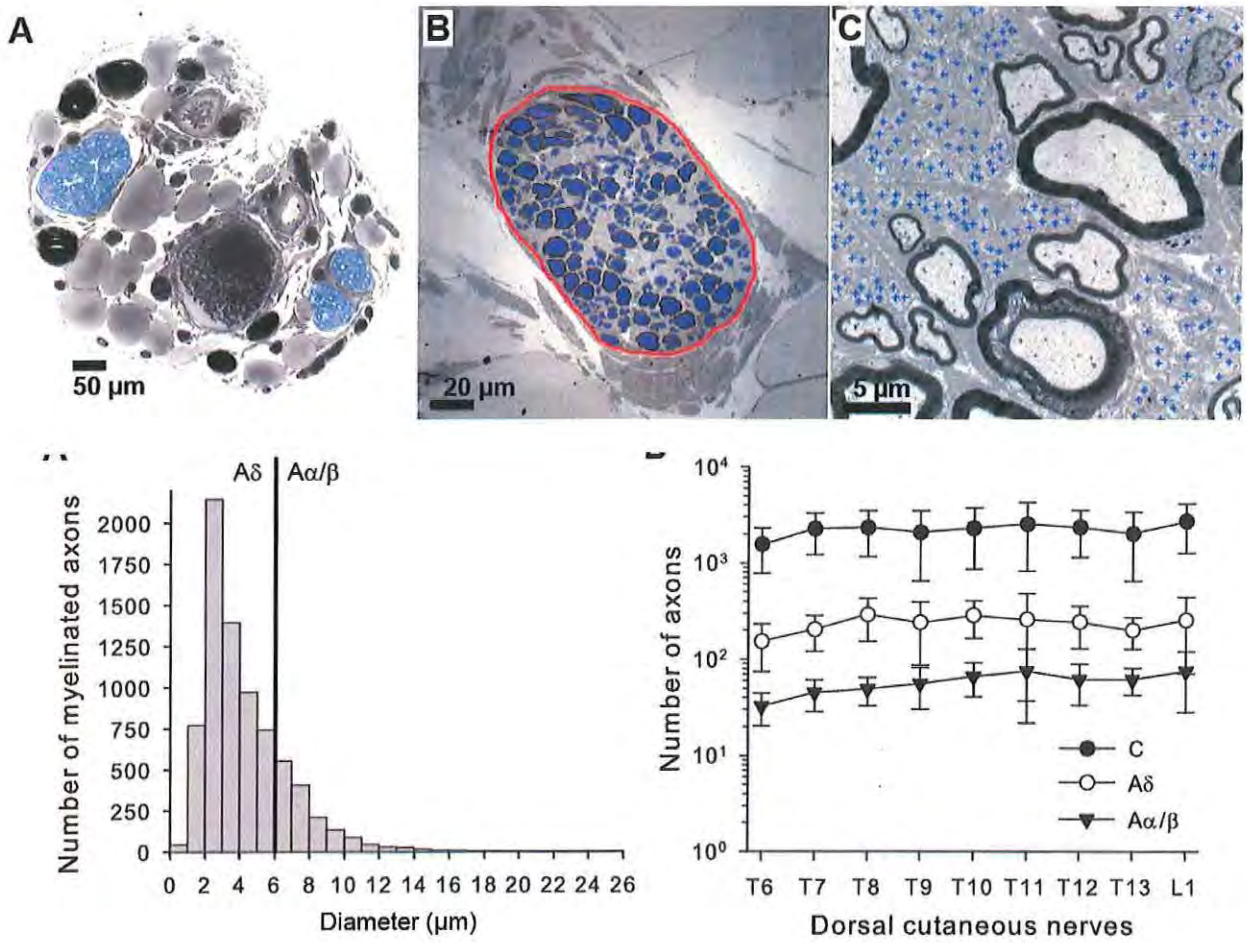

1.5.2

We have next analyzed projection patterns of DCN afferents in the dorsal horn to develop a central projection profile in normal animals. Transganglionic axon tracers, isolectin B4 (IB4) for unmyelinated C fibers and cholera toxin subunit B (CTB) for myelinated A fibers, were injected in peripheral T7 and T13 DNCs to label their afferents selectively, one tracer on one side, the other on the other side of animal. Immunohistochemistry were performed to visualize $IB4^+$ C fibers and CTB^+ A fibers on cross sections of superficial dorsal horns in T7 and T13 spinal cords (panel A in figure). To examine the spatial profile in terms of laminar, medial/lateral, dorsal/ventral, and rostral-caudal distribution, $IB4^+$ C fibers and CTB^+ A fibers were identified as immunoreactive particles on confocal images based on threshold gray values (panel B) and

overlaid on a dorsal horn diagram (panel C) according to dorsal horn borders (arrows) and laminar distributions approximated to VGLUT1 and DAPI staining profiles (panels A and C).

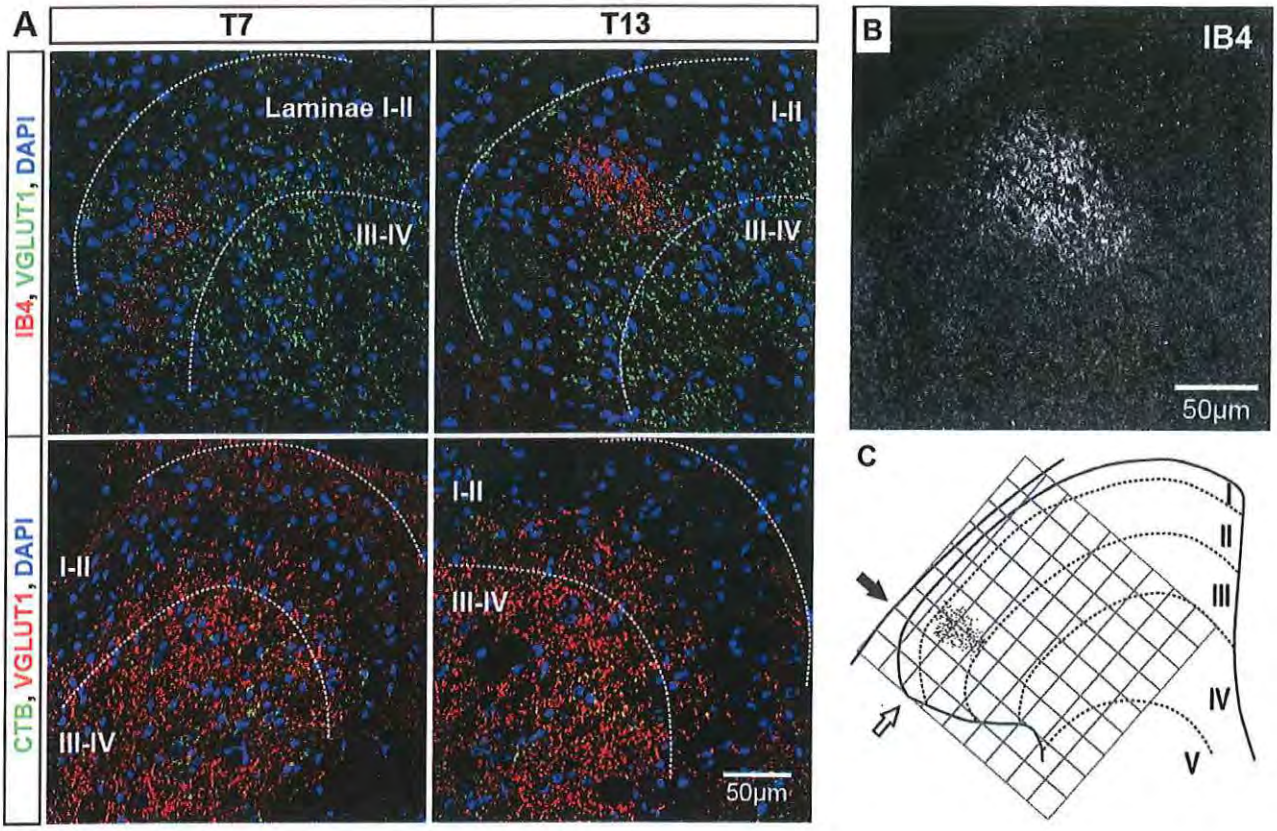

Immunoreactive areas and densities in the dorsal horn area of both $IB4^+$ C fibers and CTB^+ A fibers were measured on serial cross sections in normal animals (data shown in the previous annual report). These data suggested that distinct projection patterns of A and C fiber in T7 and T13 might be associated with the somatotopic arrangement of evoked CTM reflex responses and autonomic responses by DCN stimulations. Therefore, we have next performed the axon labeling experiments in cervical SCI to evaluate any anatomical plasticity of DCN pain afferents in association with the pathophysiological plasticity seen as cardiovascular changes.

The cervical injured animals used in BP and HR measurements were subjected to axon tracer injection in T7 and T13 DCNs three days prior to the terminal electrophysiological experiments as described above. Immunoreactive area measurements (data not shown) showed an overall increase of axon projections in both $IB4^+$ C fibers and CTB^+ A fibers across spinal levels (T7 and T13) in cervical SCI compared to normal animals although there was relatively large variability within the injured animals when all 3 pathophysiology groups were combined. Shown below are representative spatial distribution of immunoreactive axon particles overlaid on dorsal horn diagrams at given rostral/caudal locations from dorsal horn entry zone (DREZ) at each T7 and T13 levels in typical normal (left 2 columns) and injured (right 2 columns) animals of which axon areas were most close to the group mean values. The distributions of both A and C fiber projections expanded in both rostral and caudal directions after injury. When there was greater area of labeled A and C fiber neurites, they also covered a greater territory of the dorsal horn after injury.

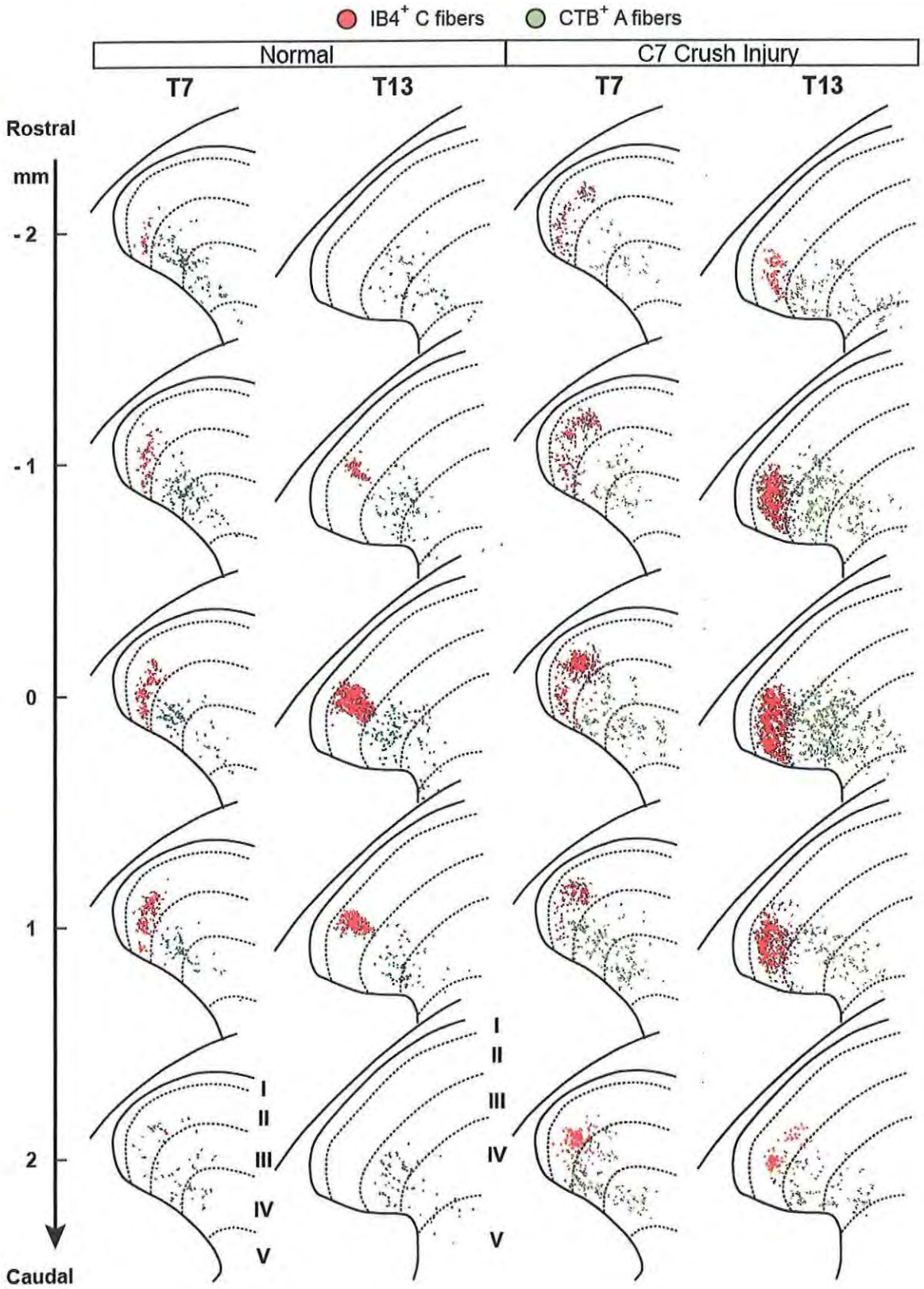
IB4+ C fibers
CTB+ A fibers
Normal
C7 Crush Injury
T7
T13
T7
T13
Rostral
mm
-2
-1
0
1
2
Caudal
I
II
III
IV
V
I
II
III
IV
V

We have also analyzed immunoreactive axon areas in three pathophysiological groups following cervical SCI. Per cent changes from uninjured normal animals are shown below for each group in both IB4$^+$ C fibers and CTB$^+$ A fibers at T7 and T13. A fiber projections increased in all injured animal groups even though the BP responses varied from the normal-like depressor to the frank pressor. As we have seen in the electrophysiological experiments, HR responses in all injured animal groups, even in the injured depressor group, showed greater increases and slower recovery in HR compared to normal uninjured animals (see Aim 1.5). These data demonstrate that the changes of A fiber projections might contribute to the altered HR but, to a lesser extent, to the BP pathology following SCI. C fibers projections, however, showed a trend of being greater over each BP category of worsening autonomic pathology. C fiber projections in the injured depressor group were slightly fewer than, or the same as, in uninjured animals in both T7 and T13 DCN levels whereas the dysautonomia and pressor response groups showed a subtle or significant sprouting depending on the spinal levels being greater in T7 than in T13. This is consistent with that the stimulation of rostral DCNs (T6 or T8) generated greater BP pressor responses than the stimulations of caudal DCNs (T12 or L1) (see Aim 1.4). Taken all together, cervical SCI generated anatomical plasticity in association with the spectrum of cardiovascular responses: A delta fiber changes preferentially affect HR responses and C fiber changes preferentially affect BP responses.

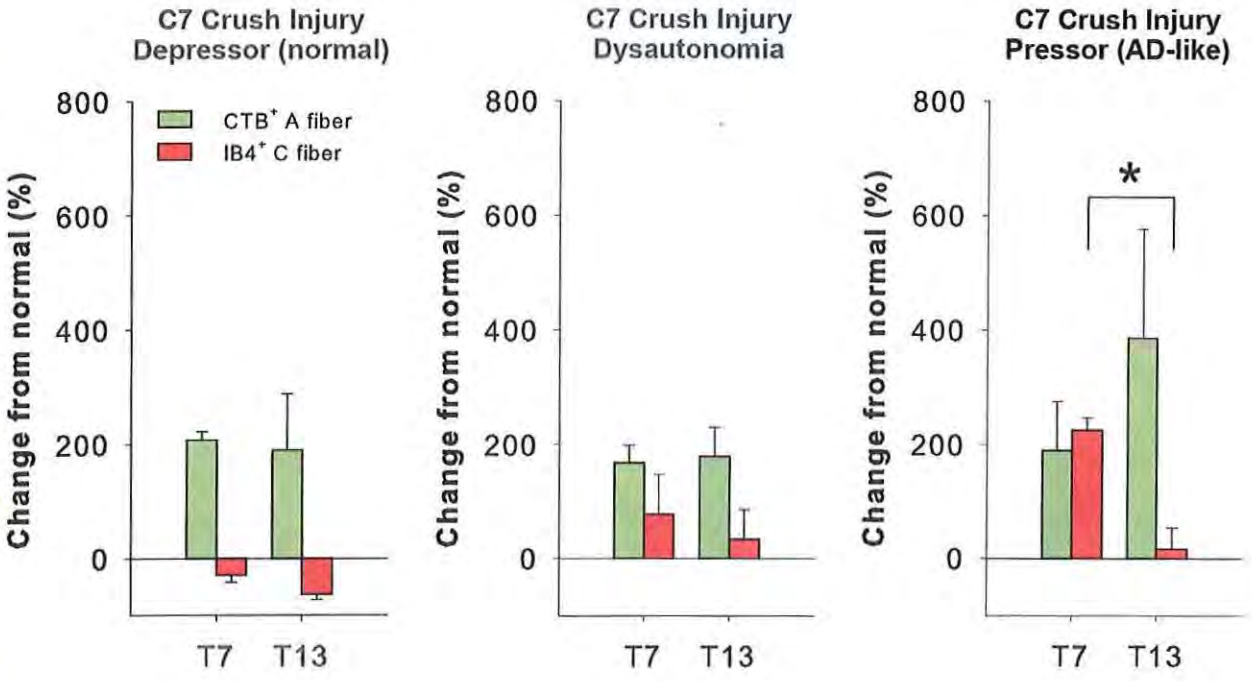

HOCHMAN co-PI progress: Specific Aim 2

Aim 2.1 achieved

Aim 2.2 Demonstrate HB9-GFP mice also express autonomic dysreflexia.

The strain of mice that HB9-GFP mice were derived is C57BL/6, and Brown and colleagues have shown that C57BL/6 mice always undergo autonomic dysreflexia (**AD**; as measured by BP responses to both caudal pinch and colon distension) after complete spinal cord transection at T2 (Jacob et al., 2003).

Mice undergoing high thoracic spinal cord injury undergo a large number of complications following surgery, making the survival rate for this procedure relatively low. However, based on studies focusing solely on care of animals undergoing high, complete spinal cord injuries (Puckett et al., 1997;Ramsey et al., 2010), we have developed a surgical protocol involving pre- and post-operative care of the animals that will significantly increase the survival rate in animals that have received a complete transection at T2-T3.

In this small aim we had originally proposed to characterize dysreflexia in the HB9 GFP mice to verify findings of T2 spinalization-induced AD in this genetic ally modified strain. However, we terminated this pursuit for two reasons. First, we found that HB9-GFP is not expressed in all sympathetic preganglionic neurons (**SPNs**) in the adult. We tested this with i.p. fluorogold injection, as this is well known to retrogradely label all SPNs (Anderson and Edwards, 1994;Cui et al., 2006). Thus, we could not reliably use the same C57BL/6 population as in the prior publication that expressed AD in 100% of the cases.

Aim 2.3 Patch recordings in control mice.

Patch clamp recordings in adult spinal cord has long been near-impossible due to the technical difficulties of keeping the tissue oxygenated throughout the dissection and preparations for recording. Moreover, SPNs in the older adults seem to be draped in perineuronal nets that are a very challenging barrier to successfully obtaining stable patch clamp recordings.

We have worked very hard on this and have run into an obstacle. SPNs in the older adults seem to be draped in perineuronal nets that are a very challenging barrier to successfully obtaining stable patch clamp recordings. Accordingly, I visited the laboratory of Ron Harris-Warrick at Cornell. His lab has been working on the same challenging barrier in another spinal neuronal population for years, and finally achieved a remarkable solution that permits stable long-duration recordings. This work was just published as "Innovative Methodology" in the Journal of Neurophysiology (Husch et al., 2011), and I wrote the invited commentary on the power of this approach (Hochman, 2011), titled: "Long-term patch recordings from adult spinal neurons herald new era of opportunity". The required approach requires the development of a series of exacting technical skills, and while we made some progress at getting there, the effort was enormous for little pay-off.

Recording from the SPNs adds the additional complication of being one of the most sensitive cell types to tissue anoxia. A postdoctoral fellow was trained to perform patch clamp recordings in spinal slice and

we were able to demonstrate that patch clamp recordings are indeed possible in SPNs of adult mice. We have found that the whole cell patch clamp technique, while possible, is not suited to long-term recordings in the adult, as the cellular properties change over time (adjacent panel A). To combat this, we began performing perforated patch clamp recordings in a subpopulation of SPNs that are genetically identified in HB9-GFP transgenic animals (adjacent panel B). The goal continued to be the original goal of this proposal, which is to examine cellular changes in neuromodulator receptor expression after spinal cord injury. Achieving this goal requires long term recordings in cells, so that we can pharmacologically dissect out changes in multiple receptors types (serotonin, dopamine and noradrenaline) in a single cell, without the experimental artifact of changing cellular properties over time. New methods were developed to achieve success as described below.

Adult mice (greater than two months of age) are immobilized with isoflurane and anesthetized with an intraperitoneal mixture of urethane (2 mg/kg), minocycline (0.08 mg/kg), and tempol (0.3 mg/kg). When withdrawal reflexes were absent, the dorsal skin was opened and the vertebral column exposed. The spinal cord was removed and sectioned using a slightly modified protocol from Husch et al, where it is described in detail (Husch et al., 2011). Briefly, a dorsal laminectomy is performed, exposing the lumbar and thoracic spinal cord. During the laminectomy, a modified ice-cold glycerol aCSF (GaCSF) is allowed to drip on the spinal cord to lower tissue temperature and decrease neuronal activity. The GaCSF contains (in mM): 222 glycerol, 3.08 KCl, 1.18 KH2PO4, 1.25 MgSO4, 2.52 CaCl2, 25 NaHCO3, and 11 D-glucose (~300 mosmol/kgH2O). The dura was then cut away from the cord,

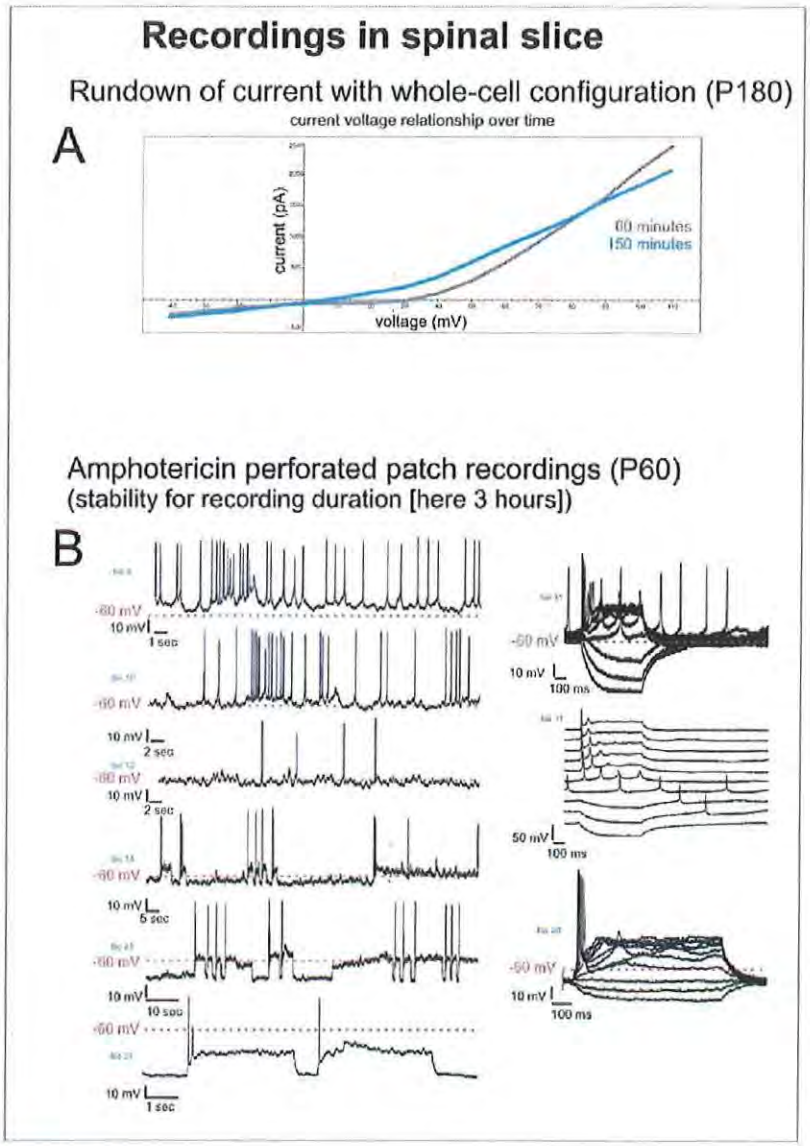

Figure 2.3.1

dorsal and ventral roots severed, and the thoracic cord removed from the vertebral column. The cord was then placed against an agar block fixed to a vibratome chuck and covered in low-melt agarose (Sigma A0701) held at ~35C. The block was then submerged in ice-cold a modified recovery aCSF (NMDG-aCSF) to allow the agarose to set. The NMDG-aCSF has been shown to aid in the recovery of adult CNS slices; it contains (in mM) 92 N-methyl-D-glucamine (NMDG), 2.5 KCl, 1.25 NaH2PO4, 30 NaHCO3, 20 HEPES, 25 glucose, 2 thiourea, 5 Na-ascorbate, 3 Na-pyruvate, 0.5 CaCl2.4H2O, and 10 MgSO4.7H2O. The pH of the solution was titrated to 7.3–7.4 with concentrated HCl (which provides Cl– counter-ions for NMDG) (Zhao et al., 2011). HEPES and thiourea plus ascorbate were included as critical components to reduce edema and oxidative damage during slicing, recovery, and extended slice incubation (Brahma et al., 2000;MacGregor et al., 2001). The thoracic cord was then sliced on Leica VT100S vibratome into 200 µm thick sections. Sections were incubated for 45 minutes in NMDG-aCSF at 35C then transferred to room temperature NMDG-aCSF.

After one hour at room temperature, slices were transferred to a recording chamber with a HEPES-buffered aCSF containing (in mM): (in mM) 92 NaCl, 2.5 KCl, 1.2 NaH2PO4, 30 NaHCO3, 20 HEPES, 25 glucose, 2 thiourea, 5 Na-ascorbate, 3 Na-pyruvate, 2 CaCl2.4H2O, and 1 MgSO4.7H2O. The pH of the solution was titrated to 7.3–7.4 with concentrated NaOH. The aCSF wass continuously oxygenated and perfused at ~2 ml/min.
Perforated patch recordings were made with thick-walled, unfilamented borosilicate glass (1.5-mm outer diameter, 1.0-mm inner diameter; PG52151-4; WPI) on a vertical puller (PC-10; Narishige) with resistances of 4–8 Mfg. The tip of the pipette was first filled with intracellular solution containing, in mM: 135 K-gluconate, 10 KCl, 10 HEPES, 0.1 EGTA, and 2 MgCl2 (adjusted to pH 7.2 with KOH, ~270 mosmol/kgH2O) by placing the pipette tip into an 1.5-ml Eppendorf tube filled with intracellular solution and applying 5–7 ml of negative pressure with a 10-ml syringe for 1 s. The pipette was then backfilled with a combination of intracellular solution, amphotericin B (A4888; Sigma) and Pluronic F-127 (P-2443; Sigma) (Herrington, Solaro et al. 1995; Lovell and McCobb 2001). To prepare the solution, 1.2 mg amphotericin B was dissolved in 20 µl DMSO (D8418; Sigma) and added to 1 mg Pluronic F-127 dissolved in 40 µl DMSO. The 60 µl amphotericin B-Pluronic F-127-DMSO mix was added and vortexed in 1 ml intracellular solution.

Current and voltage clamp recordings were undertaken at room temperature using the Multiclamp 700A amplifier (Molecular Devices, Sunnyvale, CA). Sympathetic preganglionic neurons were identified intermediolateral column using epifluorescent illumination with cell location further verified with differential-interference contrast optics (DIC), when using transgenic mice expressing HB9-eGFP (JAX laboratories), which express the green florescent protein in motor neurons, SPNs and a population of ventral horn interneurons (Zimmerman and Hochman, 2010)). SPNs were also identified in wild type mice by location and cell morphology, as the SPNs are situated in clusters in the intermediate lateral

column and just dorsal to the central canal. Voltage- and current-clamp data were acquired on a personal computer using pClamp 10 acquisition software (Molecular Devices).

New Aim 2.4 Plasticity in monoamine receptors that would facilitate expression of AD.

Figure 2.4.1. Comparison of Flouorogold anti-cy3 to HB9-GFP anti-GFP labeling in SPNs. Note top right neuron in merge is not GFP+.

Due to the very slow advances made in the aforementioned specific aim, we undertook In a parallel related but not explicitly proposed direction, we have used DoD money to try and tackle the problem by a complementary technique. As the overarching hypothesis is that monoamine receptors become constitutively active in SPNs after SCI, we explored the expression of monoamine receptor subtypes associated with SPNs. Using the proposed mouse model of AD, we compared the distribution of serotonergic 5HT2A receptors and dopaminergic D2 and D3 receptors in control cords, and following chronic injury at high thoracic levels (T1 or T2). We focused our analysis on the intermediolateral nucleus (**IML**), the location of the SPNs that will be the target of whole-cell patch clamp recordings above. Immunochemistry showed labeling of processes adjacent to the IML for 5HT2A receptors and somatic/perisomatic labeling of SPNs for D2 and D3 receptors in control tissue. Post-SCI, all receptors showed decreased expression close to the injury site (thoracic levels T2-T7). D2 and D3 receptor expression decreases extended further from the injury site (thoracic level T9-T12). In contrast, serotonergic receptor 5HT2A showed progressively increased expression in spinalized tissue in a rostrocaudal gradient moving away from the injury site, with greatest expression in lowest thoracic levels. The loss of inhibitory influences via D2 and D3 receptors and concomitant increase in excitatory influence of 5HT2A receptors is consistent with changes that would increase autonomic activity, as observed in AD. Moreover, as it is the 5-HT2 receptors that are known to increase in their constitutive activity in

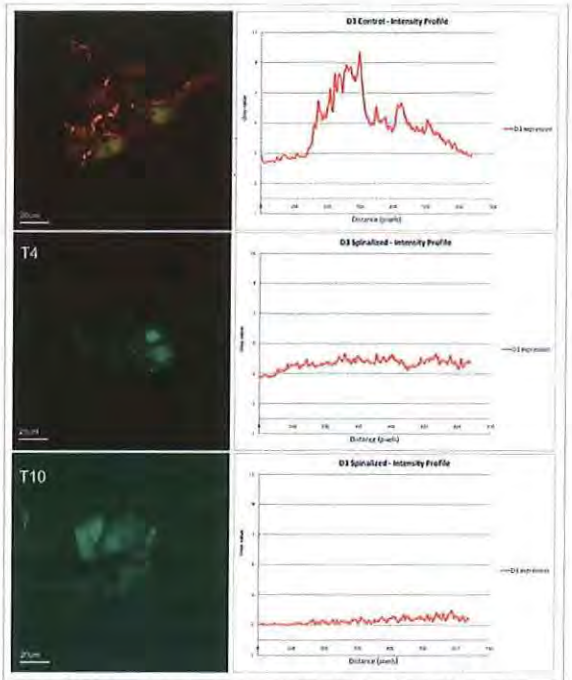

Intensity profiles for control and spinalized tissue stained for dopaminergic D3 receptor. Top panels show control tissue, middle panels show spinalized tissue at thoracic level T4, bottom panels show spinalized tissue at thoracic level T10. All images at 60x magnification.

Figure 2.4.2

motoneurons after SCI, their retained expression suggests this substrate is available to induce AD in SPNs from lower thoracic levels 3 week post-transection (Fouad et al., 2010).
In this series of experiments, control and SCI tissue sections were co□processed to facilitate reliable comparisons of immunolabeling differences. At three weeks post spinal cord lesion, adult mouse spinal cords showed a drastic decrease in expression of dopaminergic D2 and D3 receptors (Figures 2 & 3 and Tables 1 and 2, respectively; n=4). Control spinal cords showed strong coincident labeling of dopamine receptors with cells of the IML somatically and perisomatically. In contrast, spinalized tissue showed virtually no expression of dopamine receptors at either high or low thoracic levels. Table 1 compares relative receptor expression between control and SCI cord by using a thresholding technique for pixel intensity. In both upper and lower thoracic cord there is clearly a profound significant reduction in D2 immunolabeling. The table also clearly shows a lack of rostro□caudal differences in expression after injury with sites close to (upper thoracic) and further from (lower thoracic) the lesion being equally altered.

Figure 2.4.3

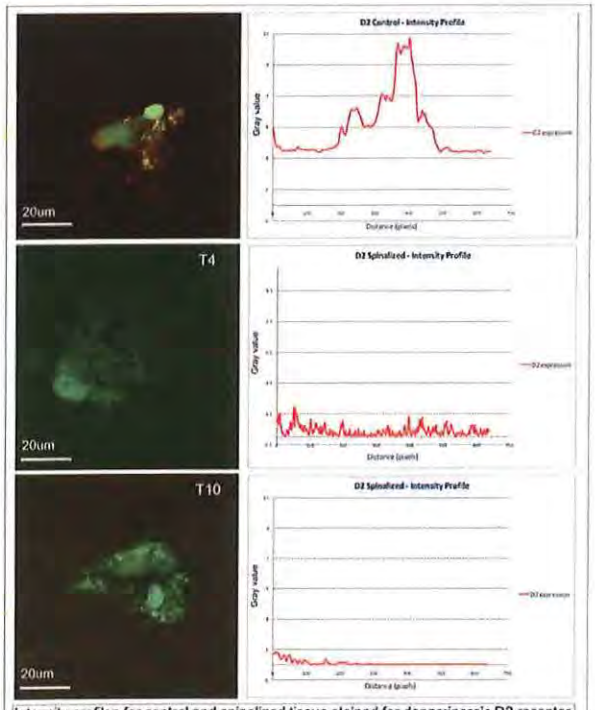

Intensity profiles for control and spinalized tissue stained for dopaminergic D2 receptor. Top panels show control tissue, middle panels show spinalized tissue at thoracic level T4, bottom panels show spinalized tissue at thoracic level T10. All images at 60x magnification.

Figure 2.4.4

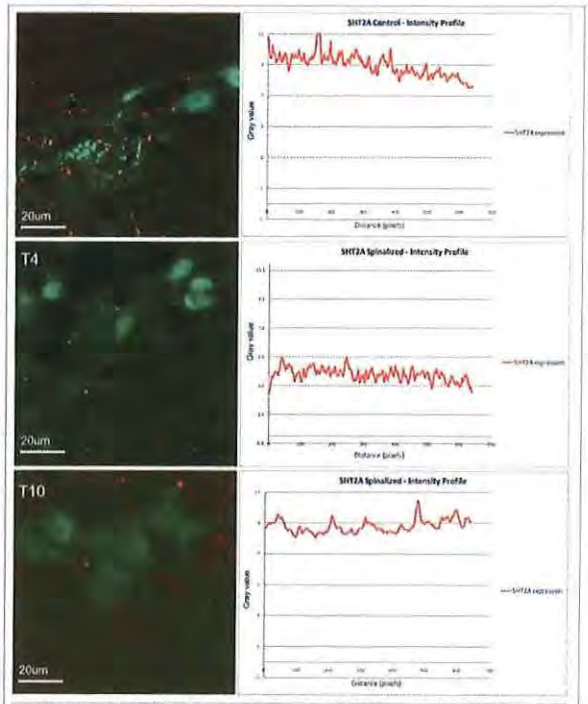

Intensity profiles for control and spinalized tissue stained for serotonergic 5HT2A receptor. Top panels show control tissue, middle panels show spinalized tissue at thoracic level T4, bottom panels show spinalized tissue at thoracic level T10. All images at 60x magnification.

Table 1

D_2: Pixels above threshold	Area 1	Area 2	Area 3	Area 4	Number of pixels fluorescing above threshold for four identical areas of IML in control cord, spinalized upper thoracic cord, and spinalized lower thoracic cord. Threshold defined using omission controls in which no primary antibodies were used. * denotes statistically significant (<.05) using Student's T-Test
Control	355	369	336	296	
Spinalized: Upper Thoracic	*32	*65	*30	*56	
Spinalized: Lower Thoracic	*56	*19	*28	*37	

Table 2

D_3: Pixels above threshold	Area 1	Area 2	Area 3	Area 4	Number of pixels fluorescing above threshold for four identical areas of IML in control cord, spinalized upper thoracic cord, and spinalized lower thoracic cord. Threshold defined using omission controls in which no primary antibodies were used. * denotes statistically significant (<.05) from control using Student's T-Test; no significant difference in upper thoracic and lower thoracic
Control	299	427	572	439	
Spinalized: Upper Thoracic	*29	*46	*24	*10	
Spinalized: Lower Thoracic	*31	*34	*14	*64	

Table 3

$5HT_{2A}$: Pixels above threshold	Area 1	Area 2	Area 3	Area 4	Number of pixels fluorescing above threshold for four identical areas of IML in control cord, spinalized upper thoracic cord, and spinalized lower thoracic cord. Threshold defined using omission controls in which no primary antibodies were used. * denotes statistically significant (<.05) using Student's T-Test
Control	451	783	824	301	
Spinalized: Upper Thoracic	*43	*30	*47	*63	
Spinalized: Lower Thoracic	208	237	279	290	

New Aim 2.5: Recording AD-related sensorimotor plasticity in an adult in vitro thoracic hemisect preparation.

In parallel with patch recordings in spinal slice, we initiated development of an adult isolated thoracic hemicord preparation. The idea was to circumvent the technical issues associated with patch recordings in spinal slice and look instead at dorsal root stimulation-evoked motor output as a proxy of population activity in SPNs. A limitation is that, while the thoracic ventral roots contain predominantly SPN axons, there is a sizeable minority of somatic motoneurons as well (Coggeshall et al., 1977). Yet even with mixed sympathetic and somatic motor output recorded in the ventral roots, an observation of afferent-evoked lasting motor responses observed only at pain afferent electrical stimulation intensities that is blocked with riluzole would support the hypothesis. The panels in the figure below show preliminary data on recording of activity in animals ranging from 2 to 6 months old. Note that these are evocable dorsal and ventral root reflexes.

The hemisected spinal cord model system to study dysautonomia

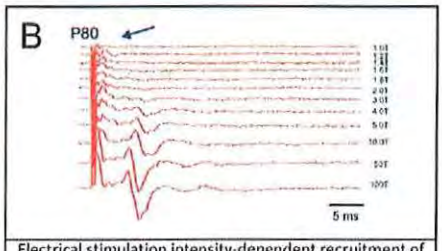

Electrical stimulation intensity-dependent recruitment of afferent fiber populations - Aβ, Aδ, and C.

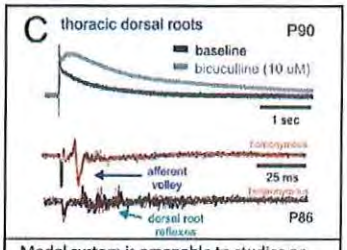

Model system is amenable to studies on presynaptic inhibition

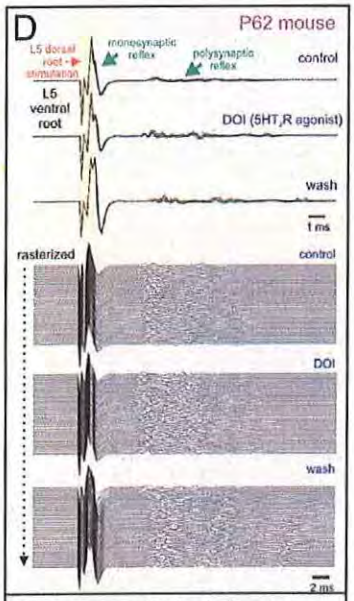

5HT$_2$ receptor activation-induced amplification of spinal reflexes in the adult spinal cord maintained in vitro

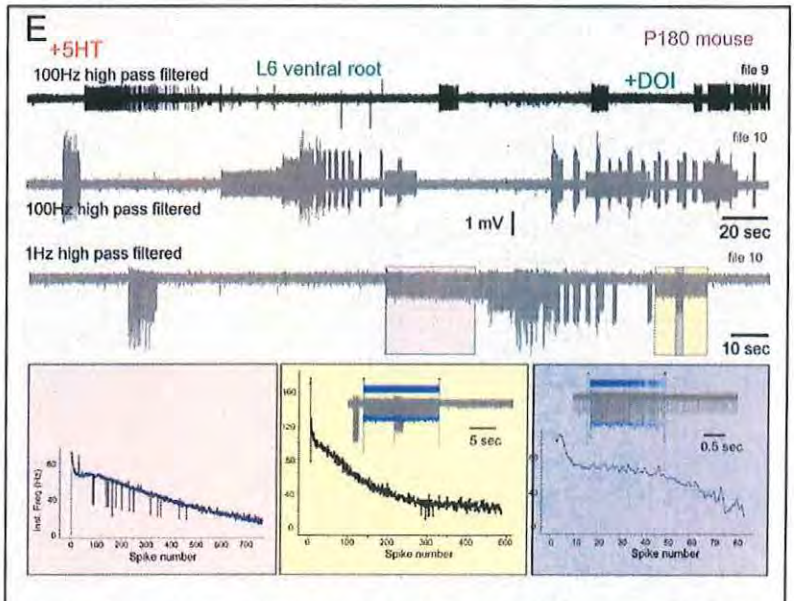

5HT receptor activation-induced recruitment of motoneurons whose individual unit activity is separable to study relative size dependent recruitment properties and firing properties

New Aim 2.6 Understanding neuromodulatory control monoamine receptor activation and autonomic function in the neonate

See attached paper in press to PLoS ONE (Zimmerman et al 2012)

New Aim 2.7 The distribution of monoamine receptors in the neonate

Serotonin receptors

As both $5HT_7$ and $5HT_2$ receptors are known to have excitatory actions on motoneurons (Holohean et al., 1990;Schmidt and Jordan, 2000;Noga et al., 2009) and implicated in 5HT actions on SPNs (Ma and Dun, 1986;Lewis et al., 1993;Madden and Morrison, 2008) we undertook immunolabeling studies to determine substrates of direct actions. Dual immunolabeling for both anti-GFP and various serotonergic receptors was assessed in the IML and intercalated nucleus (ICN). Immunohistochemistry revealed the presence of $_{5HT2A}$ and $5HT_7$ receptors on HB9+ neurons in these regions. Figure 2.7.1 displays a comparison with HB9-GFP labeling with $5HT_{2A}$ receptor labeling, showing co-labeling both perisomatically and on processes. Staining in horizontal slices revealed HB9+ processes in the dorsal-ventral direction at the level of the IML, consistent with the projections of SPN axons. Figure 2.7.2 displays a comparison between HB9-GFP labeling and $5H_7$ receptor labeling, and shows both perisomatic and process labeling in the IML. $5HT_{2c, 1d, 1f, and 5}$ receptors were also assessed, but the antibodies tested did not positively label any SPNs and are not shown.

Adrenergic receptors

Using immunohistochemistry on adult slices, both α_1 and α_2 receptors were found to label SPNs in the IML and ICN, both perisomatically and on processes. This can be seen in figure 2.7.3. and 2.7.4.

Dopaminergic receptors

Using immunohistochemistry, D_1, D_2, D_3, D_4, and D_5 receptors were tested. Of those tested, only D_2, D_3, and D_5 receptors co-labeled $HB9^+$ neurons in the IML and ICN (Figures 2.7.5-2.7.7). While D_5 receptors were found on many non-GFP+ neurons, D_2 and D_3 receptors were more localized to SPNs and motoneurons in the ventral horn.

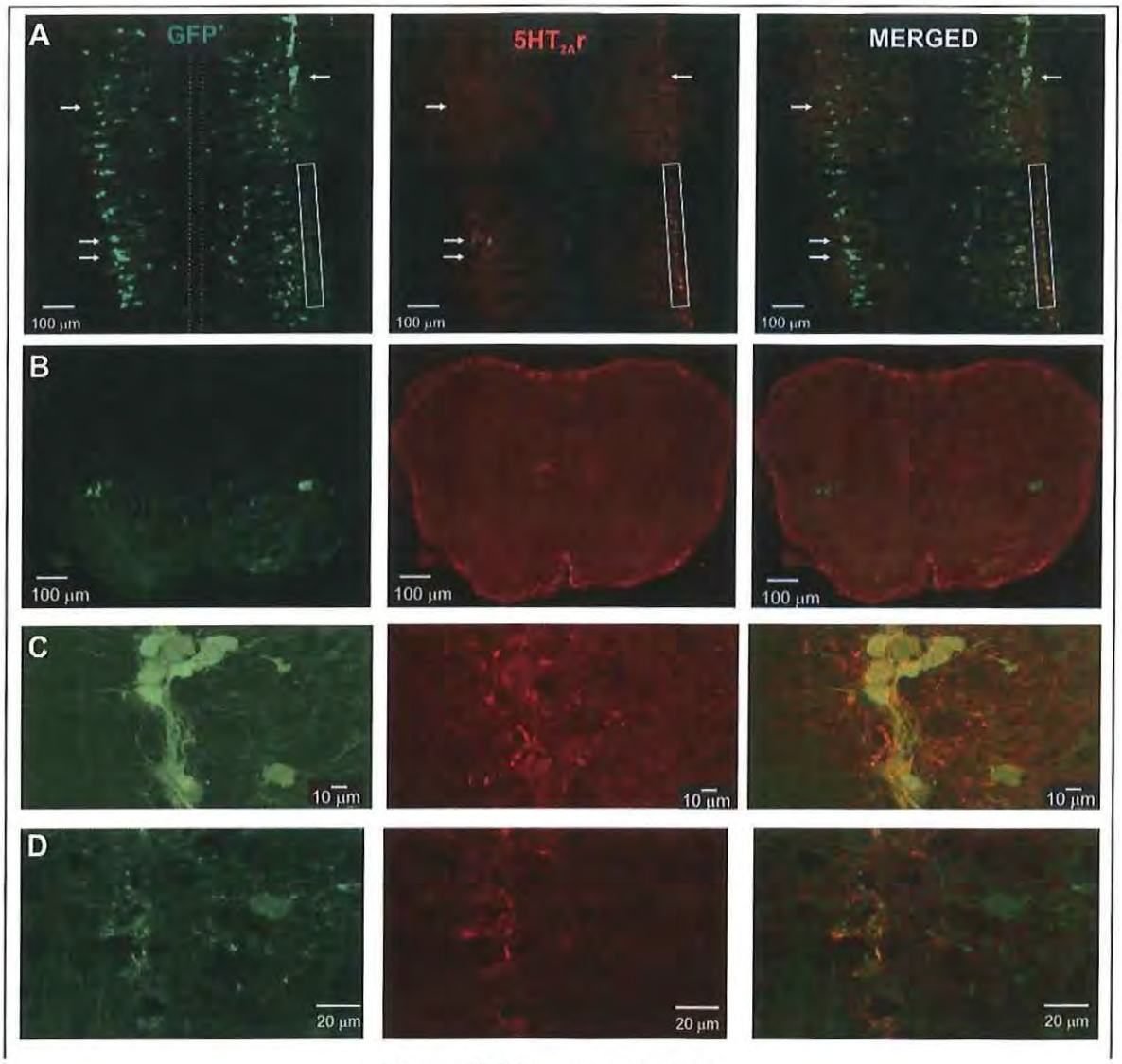

Figure 2.7.1 $_{5HT2A}$ receptors.

A. Horizontal spinal cord slice 10 mm thick, just dorsal to the central canal (at level for IMLvisualization); imaged with Nikon E800 Microscope and rendered in Neurolucida Virtual Scan software for composite shown. Dotted lines denote approximate location of central canal. Left column, GFP labeling; middle, 5HT2A receptors; right, merged image. Note some co-labelled somas (arrows) and processes, including those in the dorsal-ventral plane (boxed region). B. Low magnification confocal image of a transverse spinal cord slice, 10 mm thick. Note widespread labeling, particularly in the ventral horn and some in the IML. C. Higher magnification confocal image of IML from a horizontal slice. Image represents composite of 10 consecutive images taken at 0.3 mm optical section thickness (3 mm total thickness). Note some punctate labeling on and nearby SPN somas, as well as GFP+ process co-labeling. D. Higher magnification of boxed region in A. Confocal image of horizontal slice, single image of 0.3 mm thickness. Note co-labeling of processes going into the page, in the dorsal-ventral plane.

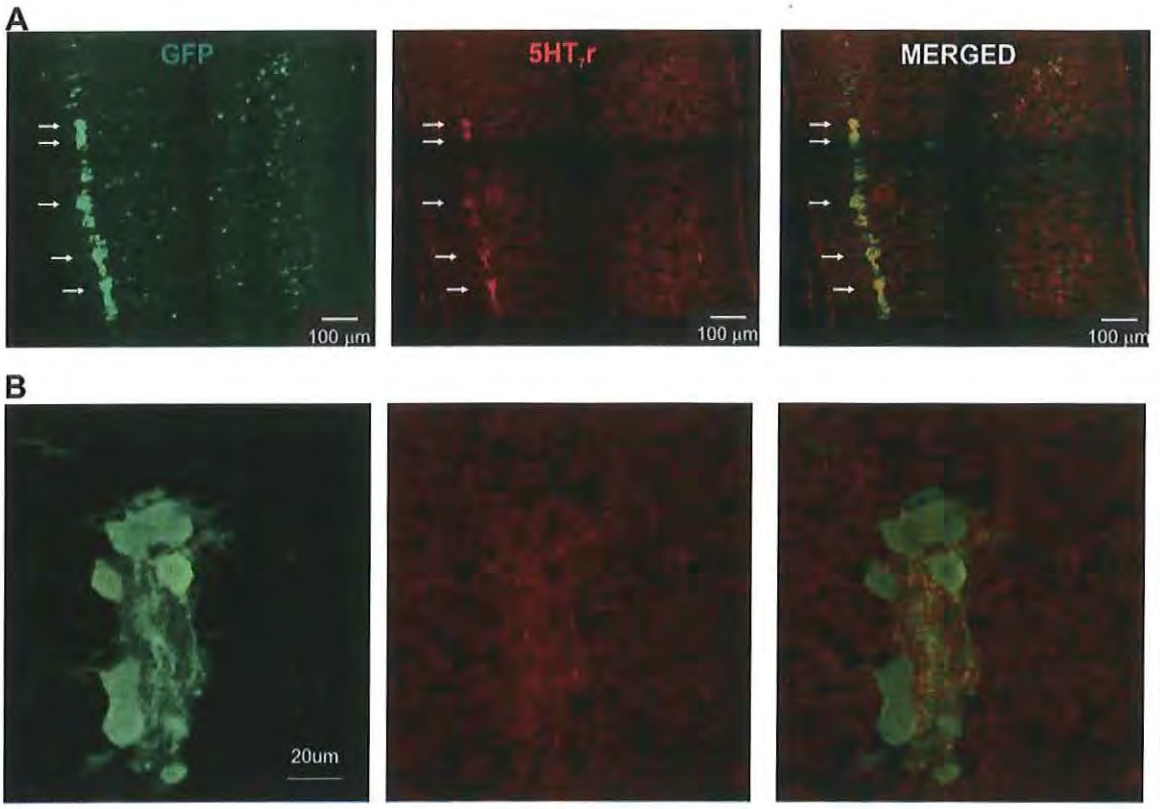

Figure 2.7.2 5HT7 receptors.

A. Horizontal spinal cord slice 10 mm thick, just dorsal to the central canal (at level for IMLvisualization); imaged with Nikon E800 Microscope and rendered in Neurolucida Virtual Scan software for composite shown. Dotted lines denote approximate location of central canal. Left column, GFP labeling; middle, 5HT7 receptors; right, merged image. Note some co-labelled somas (arrows). B. Higher magnification confocal image of IML from a horizontal slice. Image represents single optical slice of 0.3 mm thickness. Note some punctate labeling perisomatically around SPNs as well as GFP+ processes between them.

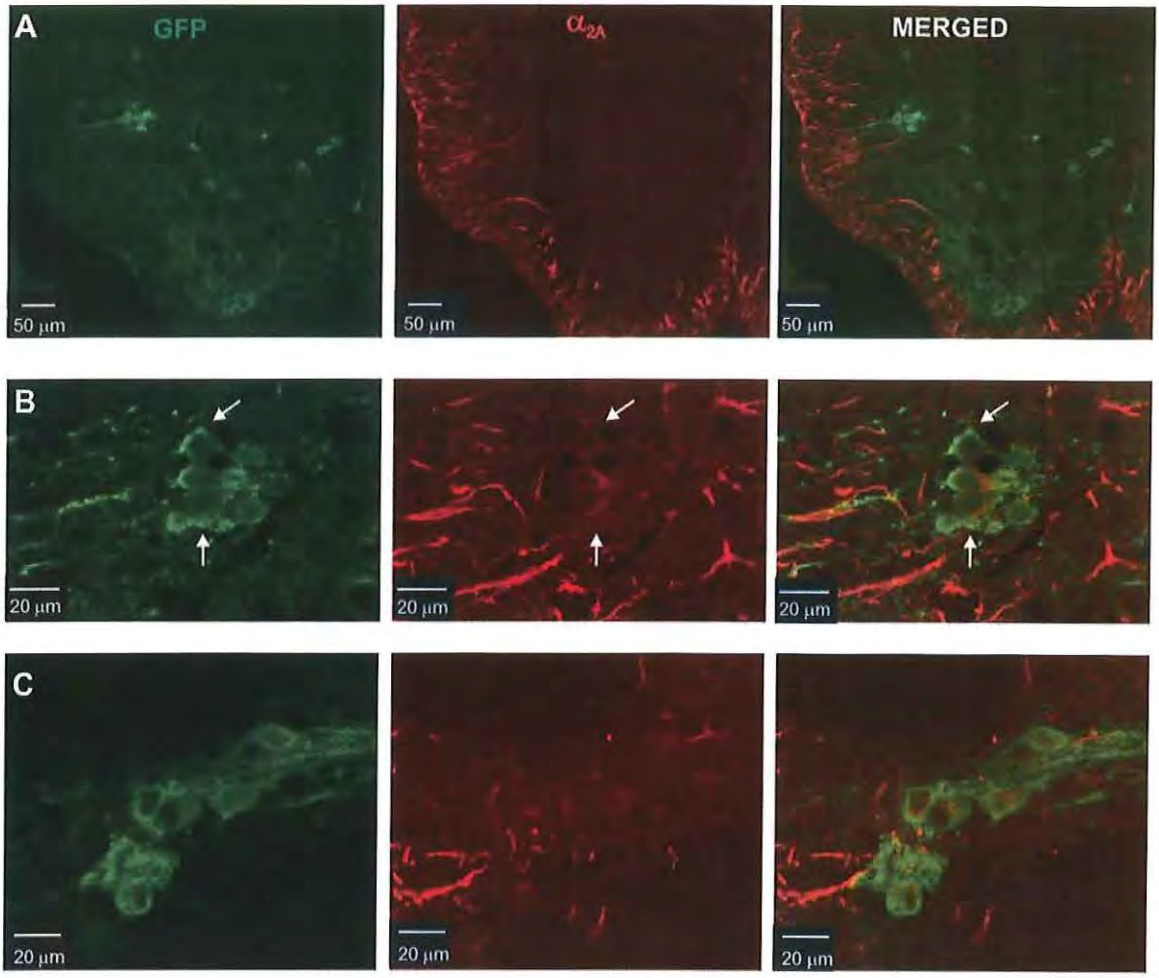

Figure 2.7.3 Adrenergic receptor α_{2A}.

A. Low power confocal image of lower thoracic spinal cord transverse slice, showing both Hb9 -GFP+ neurons and a2A adrenergic receptor labeling. Notice relatively weak labeling of spinal grey matter, compared to strong white matter labeling. B. Higher magnification of IML in same slice. Image represents single optical slice of 0.3 mm thick. Note perisomatic labeling of SPNs (arrows) C. Composite of 7 consecutive confocal images from an adjacent slice, taken at 0.3 mm optical section thickness (2.1 mm total thickness). Again, note perisomatic labeling of SPNs.

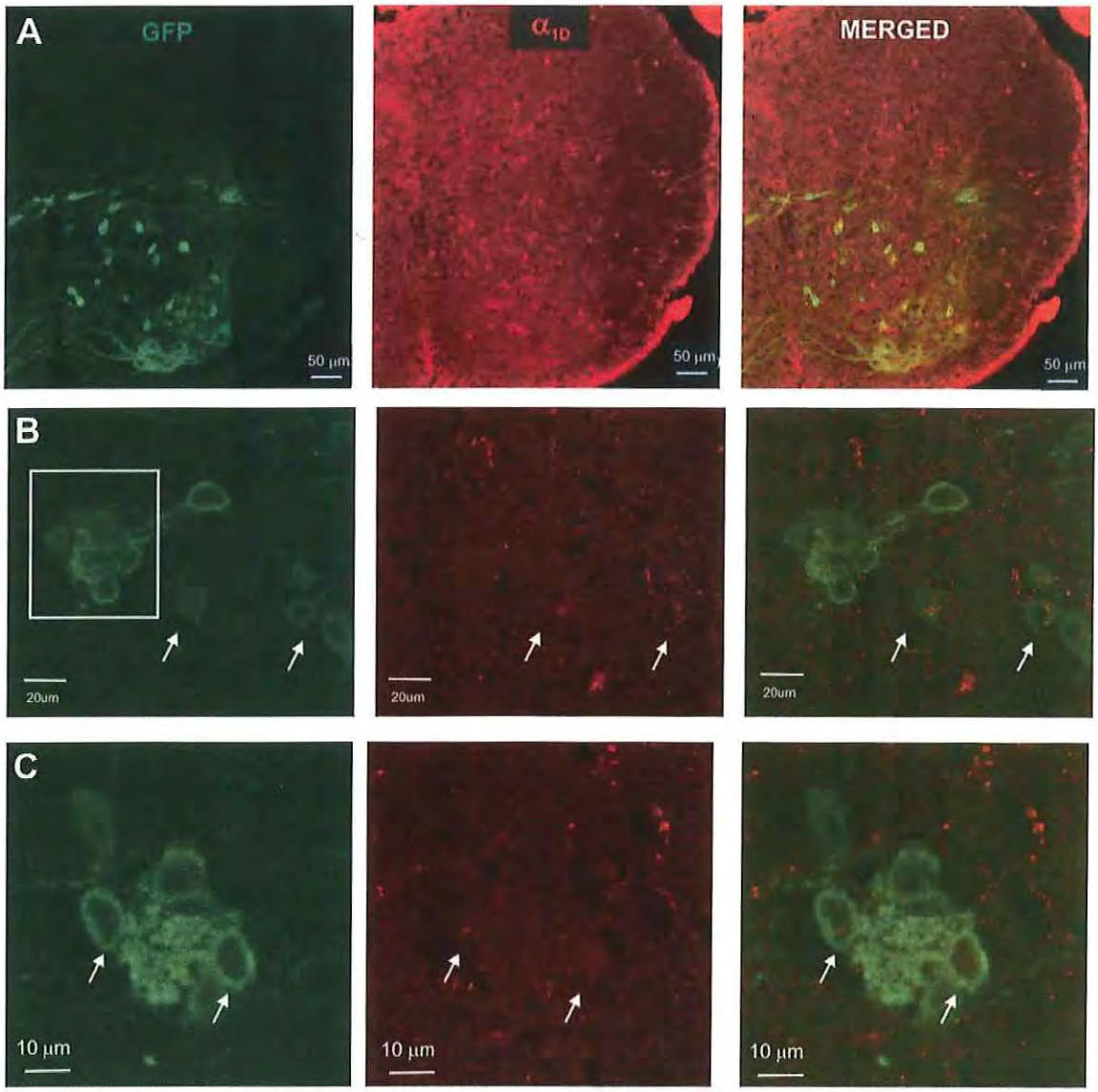

Figure 2.7.4 Adrenergic receptor α_{1D}.

A. Low power confocal image of lower thoracic spinal cord transverse slice, showing both Hb9 -GFP+ neurons and α_{1D} adrenergic receptor labeling. Notice sporatic labeling throughout the spinal cord, particularly in ventral horn. B. Higher magnification of IML in an adjacent slice. Image represents composite of 6 consecutive confocal images taken at 0.3 mm optical section thickness (1.8 mm total thickness). Note weak labeling of SPNs in the IML (boxed), but much stronger labelling of GFP+ neurons in other autonomic regions. C. Single section (0.3 mm optical thickness) deeper into the slice, showing week

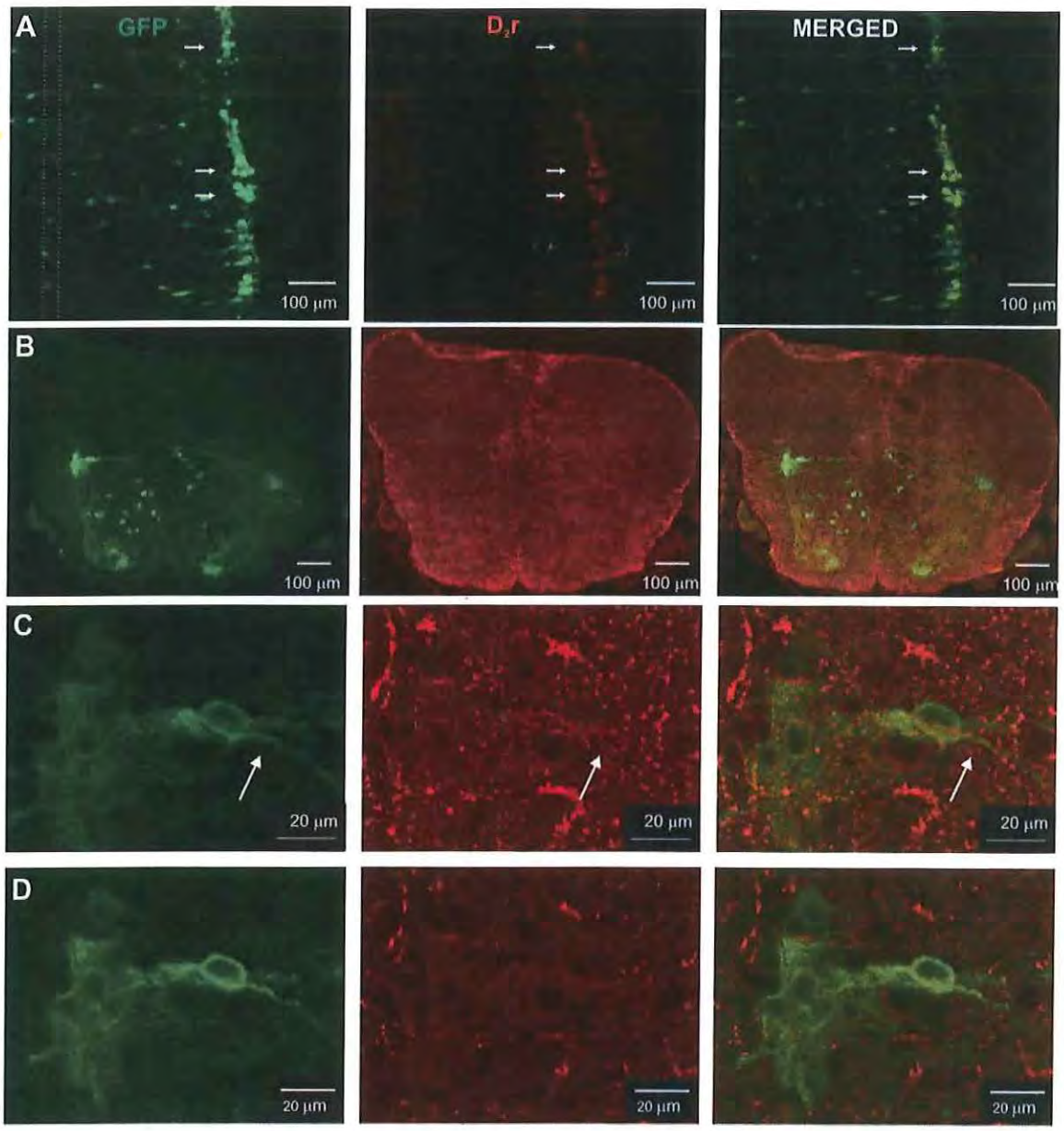

Figure 2.7.5 D_2 dopaminergic receptors.

A. Horizontal spinal cord slice 10 mm thick, just dorsal to the central canal; imaged with Nikon E800 Microscope and rendered in Neurolucida Virtual Scan software. Dotted lines denote approximate location of central canal. Left column, GFP labeling; middle, D2 receptors; right, merged image. Note some co-labelled somas (arrows) B. Low magnification confocal image of a transverse spinal cord slice in a different animal, 10 mm thick. Note widespread labeling, particularly in the ventral horn and in the IML. C. Higher magnification confocal image of IML from a transverse slice. Image represents composite of 19 consecutive images taken at 0.3 mm optical section thickness (5.7 mm total thickness). Note punctate labeling throughout the IML and surrounding region,

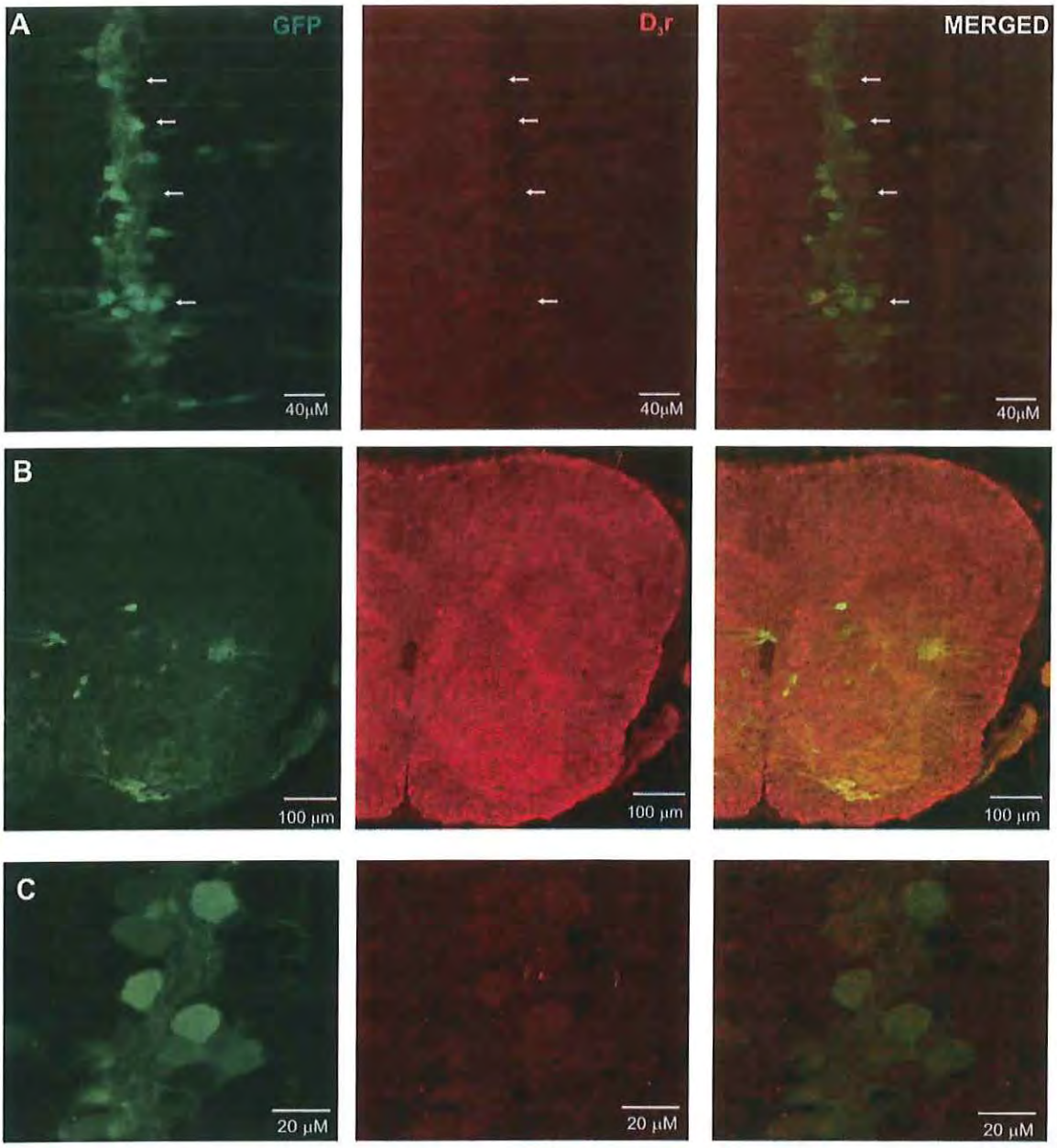

Figure 2.7.6 D_3 dopaminergic receptors.

A. Horizontal spinal cord slice 10 mm thick, just dorsal to the central canal; confocal image at low magnification. Left column, GFP labeling; middle, D3 receptors; right, merged image. Note some co-labelled somas (arrows) B. Low magnification confocal image of a transverse spinal cord slice in a different animal, 10 mm thick. C. Higher magnification confocal image of IML from a transverse slice. Single image, 0.3 mm

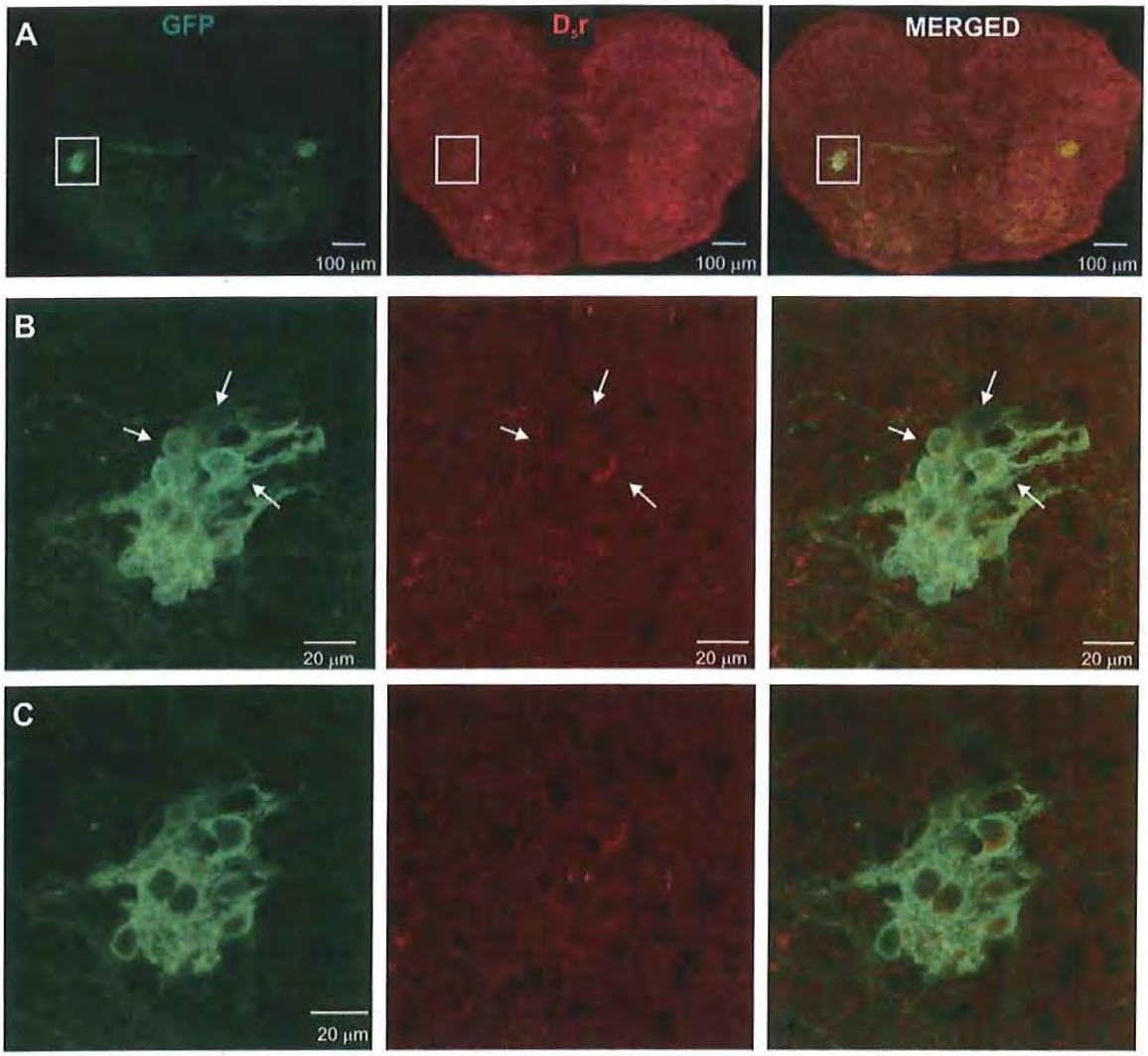

Figure 2.7.7 D3 dopaminergic receptors.

A. Transverse spinal cord slice 10 mm thick, confocal image at low magnification. Left column, GFP labeling; middle, D5 receptors; right, merged image. Note co-labeling in IML (boxed) B. Higher magnification confocal image of boxed region. Image represents composite of 20 consecutive images taken at 0.3 mm optical section thickness (6 mm total thickness). C. Single image of same region, 0.3 mm optical section thickness Note

2.8 NEW DIRECTION: Plasticity in sympathetic postganglionics comprising the thoracic sympathetic chain.

As stated in the original grant application, spinal cord injury (**SCI**) leads to devastating alterations in autonomic function (Rabchevsky and Kitzman, 2011;West et al., 2013). While the sympathetic paravertebral postganglionics (**PPNs**) located in sympathetic ganglia represent the final common sympathetic motor output, the physiological role of middle and lower thoracic ganglia in autonomic dysfunction after SCI remains unstudied. This is presumably due to their inaccessibility. Nevertheless, PPN function could be dramatically altered. Thus, an understanding of PPN function after SCI may provide novel mechanistic insights of clinical relevance. Given this, we have developed a new experimental approach that affords easy PPN experimental access and will also allow for optogenetic approaches for selective activation of neuronal subpopulations for more precise assessments of function and dysfunction.

Autonomic dysfunction after SCI may occur not within the spinal cord SPNs but rather in paravertebral sympathetic chain postganglionic neurons (PPNs). PPNs receive their input via preganglionics originating in spinal cord and represent the final common path for sympathetic output. The paravertebral ganglia control sympathetic activity to most body regions, so insight on changes in PPN function after spinal cord injury should further understanding on the etiology of autonomic dysfunction. As most paravertebral thoracic ganglia are nearly impossible to access for in vivo studies most have NEVER BEEN STUDIED DIRECTLY yet they represent the predominant sympathetic control of vascular function in upper and middle extremities as well as bronchi, lungs, heart, and esophagus. We achieved a strategic methodological advance by developing an in vitro adult mouse preparation for physiological study of intact adult mouse thoracic sympathetic chain ganglia with maintained connections to dorsal root ganglia, dorsal roots and ventral roots.

We assert that a major site of autonomic dysfunction after SCI occurs within paravertebral sympathetic postganglionic neurons (**PPNs**). We hypothesize that spinal cord injury-induced alterations in sympathetic function include aberrant integrative actions within PPNs located in the thoracic paravertebral sympathetic chain. We have begun to undertake the first physiological studies on mid- and lower-thoracic chain ganglia after SCI. Specifically, we have begun testing for (i) changes in cholinergic preganglionic synaptic transmission onto PPNs, (ii) alterations in PPN firing properties, (iii) aberrant sprouting between PPNs and visceral afferents, and (iv) aberrant sprouting between afferents and sympathetic preganglionic axons. In order to secure specific activation of axon fiber subpopulations within mixed nerves, we have begun to create transgenic mice to all for selective channelrhodopsin expression in adrenergic PPNs. Selective optogenetic recruitment of segmental preganglionics will be achieved using ChAT::CHR2 mice. While we do not as yet have CGRP-Cre mice, electrical stimulation of segmental dorsal roots can test for aberrant sensory-to-preganglionic synaptic coupling in ventral roots using advillin:CHR2 mouse.

Synapses in sympathetic ganglia are the last site for integration of CNS commands to the cardiovascular system. While synaptic transmission is presumably normally robust and stable, if ganglionic synapses malfunction due to injury or disease process, the link between the CNS and the vasculature becomes compromised and dysautonomias emerge. We are positioned to

undertake the first direct studies on mechanisms leading to dysautonomia at this vital site in thoracic ganglia after SCI.

We forward a discovery-based mouse model of SCI. We assert that a major site of autonomic dysfunction after SCI occurs within paravertebral PPNs. PPNs receive their input via preganglionics and represent the final common path for sympathetic output. The T1–L2 paravertebral sympathetic ganglia control all body regions, so studies on PPN function at and below the SCI lesion should further understanding on the etiology of sympathetic dysfunction. As these ganglia are difficult to access, studies on sympathetic chain function are shockingly scarce (Bratton et al., 2010;Undem and Potenzieri, 2012). To our knowledge there are no studies on changes in sympathetic chain function after SCI. To solve the accessibility problem and determine the extent to which paravertebral PPNs are a nodal site for vasomotor dysfunction after SCI, we achieved a strategic methodological advance by developing an *in vitro* preparation for physiological study of the intact sympathetic chain of adult mouse maintained *in situ* (Fig 2.8.1A&B). A ventral vertebrectomy is used to expose the entire spinal cord, which is carefully removed so that ventral (anterior) and dorsal (posterior) roots remain for stimulation and recording within the canal along the thoracolumbar axis, while the preganglionic connections to the sympathetic chain are intact to assess actions within associated paravertebral sympathetic chain ganglia (Fig 2.8.1A). This allows incorporation of high throughput electrophysiological, pharmacological, and transgenic approaches for studies on PPN function. As continuity with sensory afferents projecting through to the dorsal root ganglia (**DRG**) is also retained (Fig 2.8.1A), we can even test for aberrant coupling between PPNs and visceral afferents. Accordingly, stimulation of segmental preganglionics (or direct optogenetic recruitment of PPNs [see below]) can test for aberrant ***PPN-to-afferent*** synaptic coupling while stimulation of segmental dorsal roots while recording from PPNs can test for aberrant ***sensory-to-PPN*** synaptic coupling.

Approach

The proposed study will involve three mouse populations. In year one, we will only undertake experimentation in uninjured animals, as it will be necessary to more completely characterize this baseline in terms of its fundamental properties from scratch. The second year will involve comparison of changes in complete T2-T3 spinal transection and sham lesion littermate controls (identical surgery minus cord transection). Mice will be transected at six weeks of age and experiments will be undertaken 4 to 6 weeks later.

Primary afferents are not thought to synapse directly on sympathetic preganglionic neurons (**PPNs**) (Laskey and Polosa, 1988). If true and this remains so after SCI, nociceptor-driven hyperactivity could be due to afferent, interneuronal, and/or efferent changes in the spinal circuitry or changes in sympathetic postganglionic neurons located in the paravertebral sympathetic chain. A few labs have investigated the SCI-induced changes in synaptic input to PPNs (Ida J. Llewellyn-Smith, 2001;Schramm and Lynne, 2006) or afferent sprouting

(Rabchevsky and Lynne, 2006;Weaver et al., 2006). However, no one has investigated whether there is sprouting visceral afferents directly onto postganglionic neurons or whether postganglionic neurons themselves undergo dramatic changes in signaling properties.

Previous reports have shown that in mice transected at T2, a dysautonomia consistent with autonomic dysreflexia was present in 100% of animals after 2 weeks (Jacob et al., 2001;Jacob et al., 2003). We hypothesize that PPN *intrinsic excitability is increased after SCI* and will assess this by comparing the evoked responses elicited following stimulation of dorsal and ventral roots. We will characterize changes along the entire thoracic chain axis to determine whether there are changes in afferent and efferents convergence and divergence along the sympathetic chain as well as preferential changes in plasticity in regions closer to the spinal cord transection level.

Description of the surgical dissection

Adult mice are anesthetized with isofluorane and i.p. injected with ketamine-xylazine solution. The vertebral column from upper thorax to high lumbar was removed and pinned dorsal up in a recording chamber so that all tissue was submerged in an oxygenated artificial CSF at room temperature. The spinal cord was exposed by dorsal laminectomy followed by a ventral vertebrectomy. Dorsal and ventral roots were cut away as close to the cord as possible then the cord was discarded. The sympathetic chain was gently and meticulously separated from fat using forceps and a glass probe.

Following surgical isolation and dissection, components of the paravertebral sympathetic chain can be easily identified as shown in Figure 2.8.1B. Tight fitting suction electrodes are used for stimulating as well as recording evoked responses on various dorsal roots, ventral roots and sympathetic chain ganglia. The experimental configuration is shown in Figure 2.8.1C. The same electrode can be used for both stimulation or recording via a switching. Evoked responses associated with paravertebral ganglia in particular require small tight fitting suction electrodes along the sympathetic chain following section of an interganglia nerve root.

Preliminary experiments (see Figs 2.8.1-6).

(1) We stimulated the sympathetic preganglionic neuron axons in the ventral roots along the entire rostrocaudal thoracic chain axis to assess axonal convergence patterns onto thoracic sympathetic chain ganglia (Figure 2.8.3A). We also stimulated individual ventral root roots containing preganglionic neurons and study their divergence onto the thoracic chain ganglia (Figure 2.8.3B). We also undertook the same stimulation protocols above except for stimulation of dorsal roots to assess their convergence and divergence patterns (Figure 2.8.3C) and examined whether they evoke synaptic actions in chain ganglia. To generally assess whether chemical synaptic transmission is present, we blocked synaptic transmission by application of a high Mg2+ / low Ca2+-containing artificial cerebrospinal fluid (aCSF) (Shreckengost et al., 2010). Use of this solution completely blocked synaptic transmission in the recordings shown in Figure 2.8.4A and B. We then tested for evidence of glutamatergic and cholinergic transmission from both dorsal and ventral roots. We are currently in possession of all three transgenic lines and have already successfully crossed ChAT-Cre and TH-Cre mice with a TD tomato Cre-dependent reporter line (e.g. Figure 2.8.7). Thus we are in a position to undertake selective optogenetic

recruitment of cholinergic or adrenergic actions to assess their plasticity independent of contamination from co-recruitment of other axons. We have also constructed a TTL triggerable blue LED fiber-optic light for activation of roots. Using a thy-CHR2 mouse, we observed spiking activity after shining the light on ventral roots in the dorsal root potential and shining the light on (Figure 2.8.7B).

Neuroanatomical plasticity after SCI (see Figure 2.8.8). Following experimentation, tissue was immersion fixed. Subsequent fluorescent labeling of preganglionics, PPNs and afferents was combined with high resolution confocal visualization to correlate physiology with anatomy and assess characteristic expression patterns within identified thoracic ganglia and correlate anatomy to observed physiology in the same mice.

Physiological experiments after SCI. We are now testing for possible sites of plasticity after SCI as depicted in Figure 2.8.2B. As shown in the figure there at least 7 possible sites. Site ❸ will not be tested. ❶Increased cholinergic transmission from pre- to post-ganglionics. ❷Preganglionic cholinergic sprouting onto primary afferents. ❸Increased postganglionic actions on vasculature and other effector organs. ❹Sympathetic postganglionic sprouting on dorsal root ganglion neurons. ❺Primary afferent sprouting onto postganglionic neurons. ❻Primary afferent sprouting onto preganglionics. ❼Primary afferent sprouting onto autonomic reflex pathways in spinal cord.

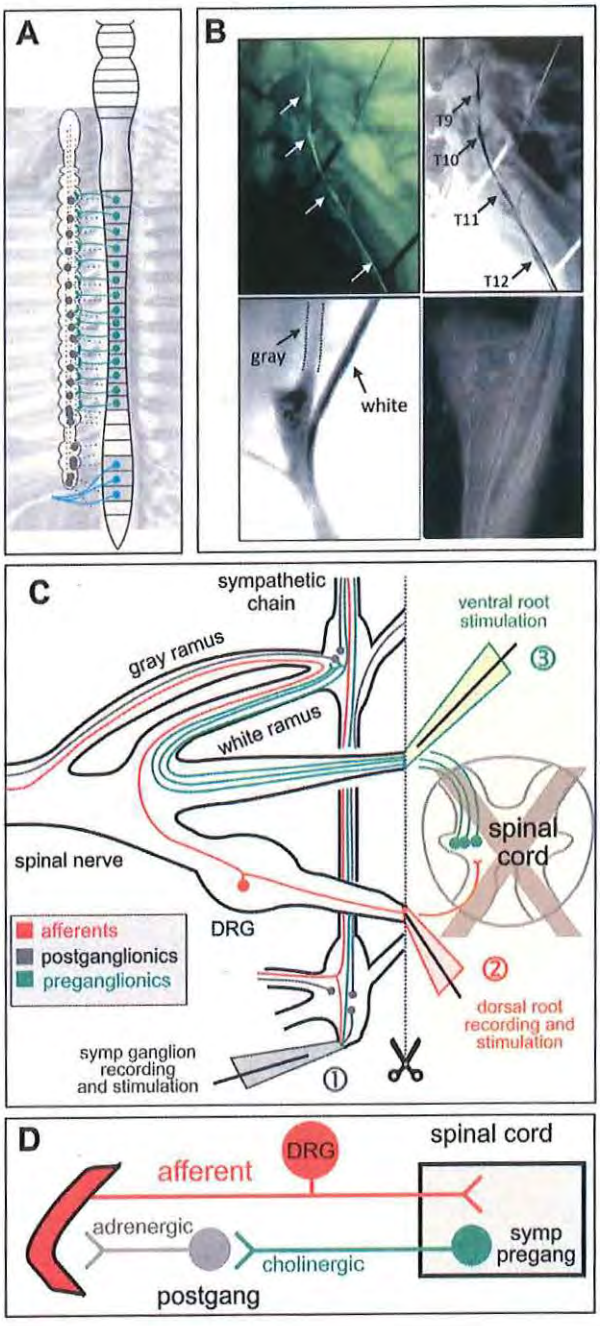

Figure 2.8.1. Sympathetic chain anatomy and recording configuration. **A.** *Organization of the autonomic nervous system.* The entire sympathetic neural output from the CNS originates in spinal thoracic and upper lumbar cord (green). In comparison, the sacral parasympathetic system controlling bowel, bladder and sexual function is found in sacral spinal segments (blue). **B.** *Example dissection of sympathetic ganglia for experimentation.* Top. Dissected live caudal thoracic paravertebral sympathetic chain from adult ChAT-GFP transgenic mouse viewed with a stereo dissecting fluorescent microscope. Sympathetic chain ganglia are numbered in grayscale copy of image at right. Bottom left. Higher magnification grayscale image of the T12 sympathetic chain with arrows pointing to gray (unmyelinated) and white (myelinated) commissure. Bottom right. Grayscale image of a more rostral ganglion showing a subpopulation of cholinergic postganglionic neurons. **C.** *Anatomical arrangement for experimentation.* Shown are two segmental paravertebral ganglia and their relation to afferent input (red) and sympathetic preganglionic efferent output (green) from the spinal cord. Electrodes are placed on dorsal and ventral roots as well as along the sympathetic chain for stimulation and/or recording. Evoked responses associated with paravertebral ganglia can be recorded with tight fitting suction electrodes along the sympathetic chain following section of an interganglia nerve root. **D.** *Schematic simplifying the anatomical connectivity shown in C.*

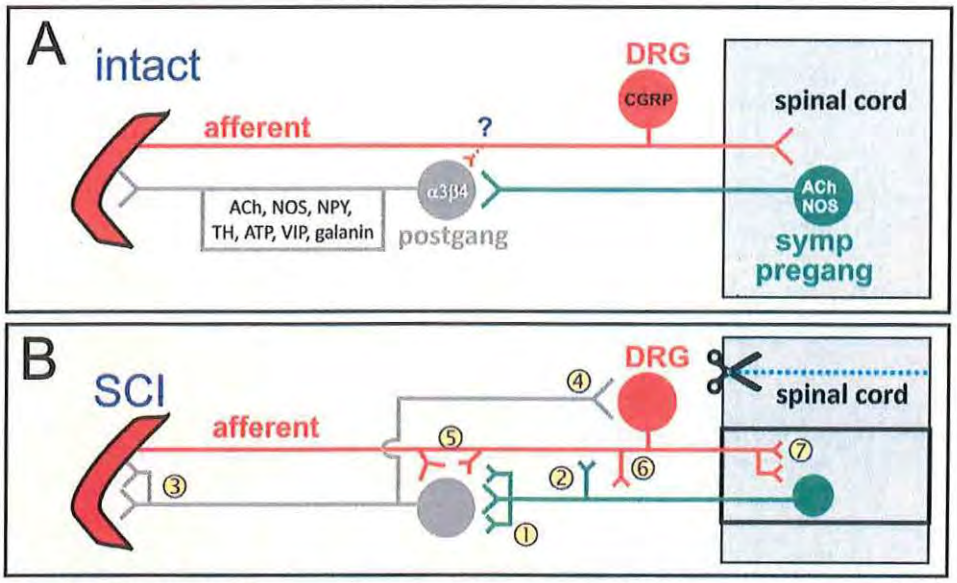

Figure 2.8.2. Possible sites of plasticity associated with neuron populations having axons within the sympathetic chain after SCI. A. *Simplification of conventional reports of organization of sympathetic pre- and postganglionic as well as afferent projections in relation to paravertebral symapthetic chain.* Adrenergic postganglionic neurons express α3β4 nicotinic cholinergic receptors. There is some anatomical evidence that CGRP+ afferents synapse onto postganglionic neurons (dotted line ?). Most sympathetic preganglionic neurons are both cholinergic and nitrergic. Postganglionic neurons have heterogeneous phenotypes including presence of neuropeptides as co-transmitters as well as the presence of purinergic cholinergic and nitrergic neurons. These are indicated within the box attached to the postganglionic peripheral projections. **B.** *Possible sites of plasticity after SCI.* ① Increased cholinergic transmission from pre- to post-ganglionics. ② Preganglionic cholinergic sprouting onto primary afferents. ③ Increased postganglionic actions on vasculature and other effector organs. ④Sympathetic postganglionic sprouting on dorsal root ganglion neurons. ⑤ Primary afferent sprouting onto postganglionic neurons. ⑥ Primary afferent sprouting onto preganglionics. ⑦ Primary afferent sprouting onto autonomic reflex pathways in spinal cord.

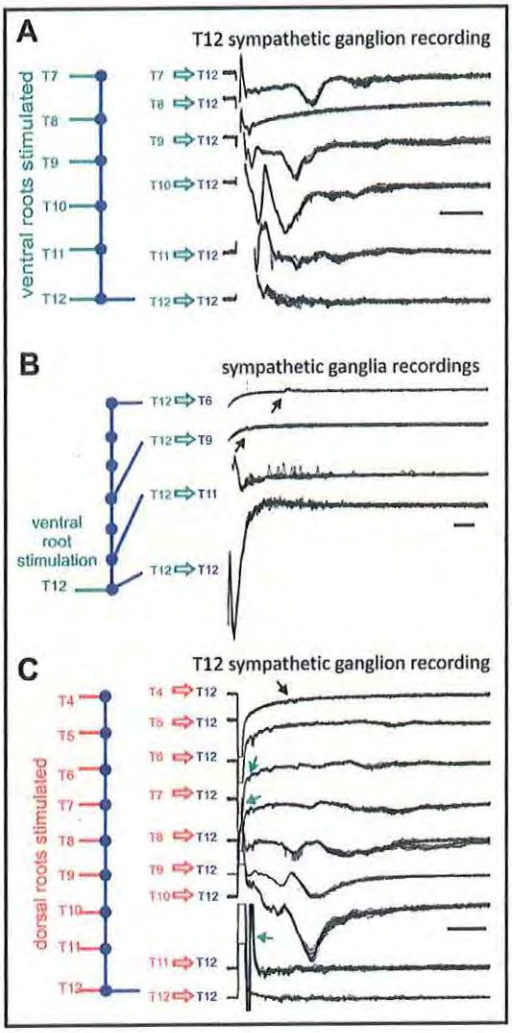

Figure 2.8.3. Multisegmental axonal composition in individual sympathetic chain ganglia. A. *Evidence that chain ganglia contain projections from many ventral roots.* Ventral roots T7-12 were sequentially stimulated while evoked population responses were recorded with a suction electrode on the T12 sympathetic chain. Primary observations are: (i) T12 sympathetic chain receive preganglionic axons from all stimulated roots, and (ii) variable longer-latency volleys are also observed following stimulation of many ventral roots. These responses may be synaptically- mediated and/or due to recruitment of unmyelinated axons. **B.** *Evidence that axons from a single ventral root evokes actions in many sympathetic chain ganglia.* Note that evoked responses in more distant ganglia were also observed (arrows) but were comparatively small. **C.** *Evidence that chain ganglia contain axons projecting to many dorsal roots.* Dorsal roots T4-12 were stimulated while evoked population responses were recorded with a suction electrode on the T12 sympathetic chain. Evoked responses were seen from all dorsal roots but very small from T4 (arrow). Broadly, thre appear to be faster conducting antidromic action potential volleys (green arrows) and slower conducting responses with greater variability suggestive of unanticipated synaptically-mediated effects. Stimuli were delivered at 1 Hz and intensities in all panels were 1 mA, 1 ms (negative polarity). Scale bar is 10 ms in all panels.

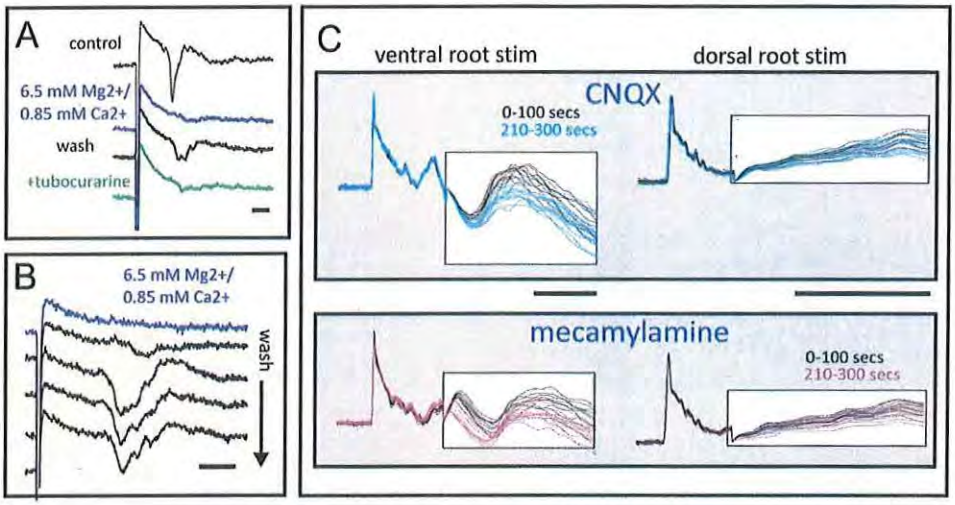

Figure 2.8.4. Synaptically mediated actions in sympathetic ganglia are sensitive to nicotinic cholinergic and non-NMDA ionotropic glutamate receptor antagonists. A. *Synaptic transmission dependent responses with cholinergic receptor sensitivity.* Evoked responses in T8 ganglion following stimulation of that T10 ventral root in a P87 male. Responses were blocked with a high Mg2+ / low Ca2+ containing saline. Following partial recovery, the evoked response was greatly attenuated with the nicotinic antagonist d-tubocurarine (20 μm). **B.** *Recovery of synaptic transmission.* Note that following return to regular saline solution the evoked volley gradually recovers with evidence of smaller spiking events superimposed. **C.** *Dorsal and ventral root-evoked responses are sensitive to glutamate and nicotinic receptor antagonists.* The T10 ventral and dorsal roots were stimulated 2 seconds apart at 0.1 Hz. Responses were recorded in the T12 ganglion. Black waveforms represent the recorded responses in the first 100 seconds following drug application. Cyan (10 μM CNQX) and purple responses (50 μM mecamylamine) represent waveforms collected at 210 to 300 seconds after drug application. Boxed region shows the integral of evoked responses to better illustrate differences. Note that longer latency responses were sensitive to glutamate and nicotinic receptor antagonists. Dorsal root evoked responses may also have sensitivity to both receptor antagonists, albeit minor. Stimulus intensities were 1 mA ,1 ms positive polarity, 500 μA 500 μs pulses polarity, and 200 μs 200 μA positive polarity in panels A, B, and C respectively. Scale bar is 10 ms in all panels.

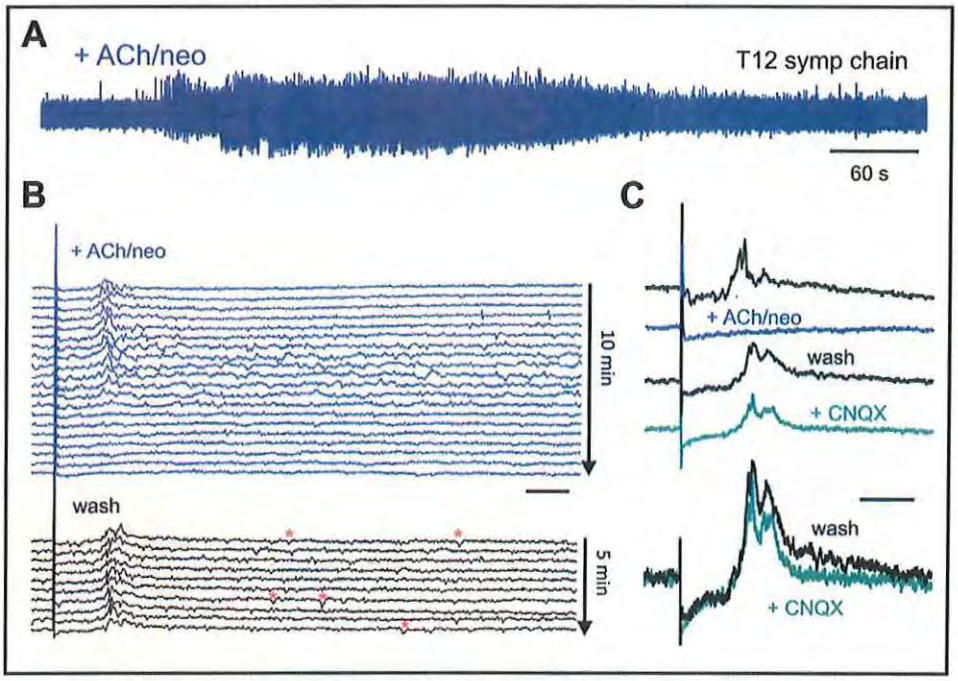

Figure 2.8.5. Activation of cholinergic receptors leads to depolarization block. Recordings are from T12 sympathetic chain following stimulation of the T10 ventral root in a 4-month old ChAT-GFP female mouse. **A.** *Acetylcholine induced increase in spontaneous postganglionic activity.* ACh (20 μM) and neostigmine (ACh/neo; 10 μM) led to a progressive increase then decrease in spontaneous activity within the sympathetic chain, supporting ACh-induced increases in neuronal excitability. **B.** *Cholinergic sensitivity of the evoked responses.* Shown is a raster display of individual evoked responses over time after application of ACh/neo. Note that depression of evoked responses coincides with loss of spontaneous activity. Following wash, evoked responses return but there is still elevated spontaneous activity (e.g. asterisks) indicative of a lasting facilitation of activity. After washout evoked responses return. **C.** *Recovered evoked responses have partial sensitivity to CNQX.* Average of evoked responses before, during ACh/neo, following washout, and following subsequent application of CNQX (10 μM). Note that later evoked responses appear to be preferentially reduced by CNQX (bottom panel with increased gain). Stimulation intensity throughout was 200 μs, 200 μA, positive polarity.

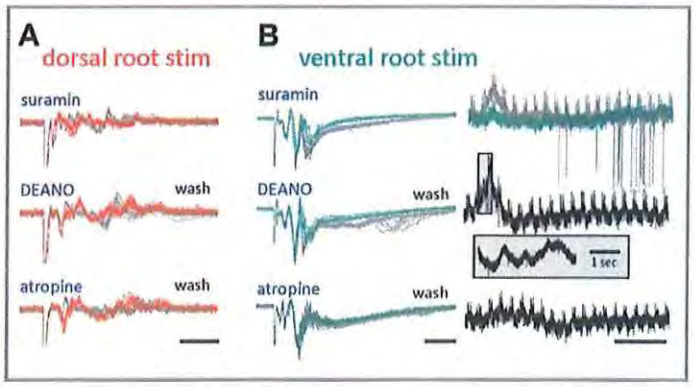

Figure 2.8.6. Evidence of purinergic nitrergic and muscarinic receptor contribution to dorsal and ventral root activity. The P2 purinoceptor antagonist suramin, the NO-donor DEANO, and the muscarinic receptor antagonist atropine were tested for modulation of evoked responses. Recordings are from T12 sympathetic chain following stimulation of the T10 dorsal and ventral roots in a 2-month old ChAT-GFP female mouse. **A.** *Suramin, DEANO and atropine broadly depress dorsal root evoked responses.* Note effects on recruited waveforms are complex. **B (left).** *Suramin, DEANO and atropine facilitated ventral root stimulation evoked responses.* **(right)** Continuous recording of T12 chain activity show that both suramin and DEANO produce hyperpolarizations (increased extracellular positivity; responses are transient due to use of 0.01 Hz high pass filter). The regular faster transients are timing of the evoked responses seen in panel A and B (right). Large spontaneous spiking events were also seen in the presence of suramin. Note that DEANO evoked hyperpolarization included th emergence of a slow superimposed membrane oscillation (enlarged box below). Atropine response involved a slower action. Suramin, DEANO and atropine were applied at 50 μM, 100 μM, 10 μM respectively. Stimulation intensity throughout was 200 μs, 200 μA, positive

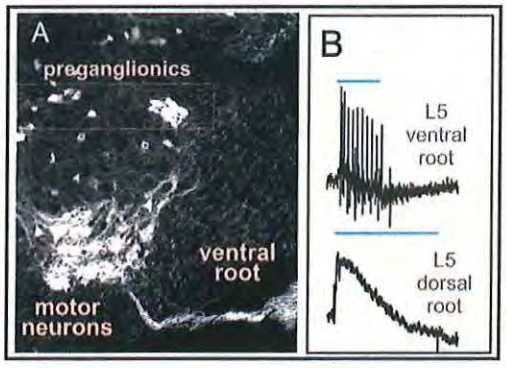

Figure 2.8.7. A. *ChAT::tdTomato in preganglionics.* **B.** *Optogenetic recruitment of root axons.* Thy1-ChR2 mouse: blue LED shone on roots for 250 ms (bar). Note evoked ventral root spiking and dorsal root potential.

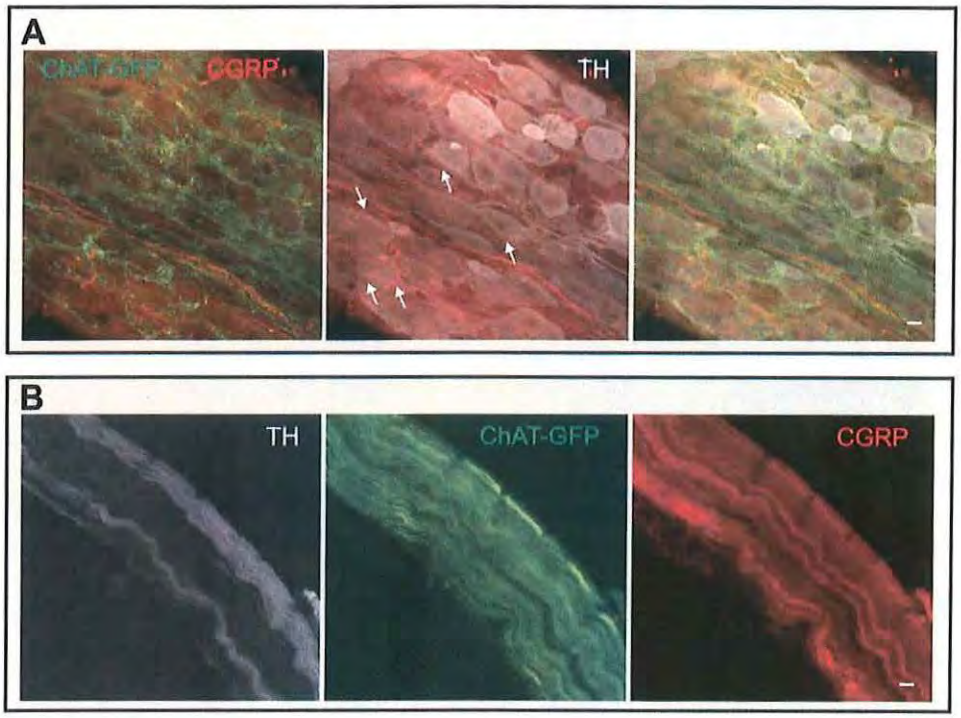

Figure 2.8.8. Confocal images from a whole-mount sympathetic chain ganglia (A) and inter-ganglia fibers (B) in a P68 female ChAT-GFP mouse after electrophysiological experimentation. Tissue was immersion fixed and processed for immunodetection of GFP+ cholinergic preganglionics, CGRP+ primary afferents and TH+ adrenergic postganglionic neurons. Tissue morphology was well preserved following 8 hours of *in vitro* experimentation. In all panels CGRP is shown as red, ChAT-GFP as green, and TH as white. **A.** *Immunolabeling within the sympathetic ganglia.* There is no overlap in immunomarkers demonstrating these populations are distinctly identifiable populations of afferents (CGRP+), preganglionics (ChAT-GFP+) and postganglionics (TH+). Note that some CGRP+ afferent axons traverse through the cell body rich region and are in a position to produce synaptic actions and injury-induced synaptic sprouting onto postganglionic neurons (arrows in middle image). Also note the extnesive putative preganglionic cholinergic synapses surrounding TH+ postganglionic somata. **B.** *Axon composition of a ganglion chain nerve bundle.* Sympathetic chain bundles contain many sensory as well as pre- and postganglionic axons. Scale bar is 10 μm in both panels.

Key research accomplishments

- Characterized the spectrum of autonomic responses (BP and HR) following cervical spinal cord injury with specific attention to cutaneous pain afferent populations, their activation frequency and their somatotopic organization.
- Characterized the anatomical changes (that is sprouting) of cutaneous pain afferent populations after cervical spinal cord injury.
- Demonstrated the relationships between afferent sprouting and autonomic responses following SCI and concluded that the A fiber sprouting seen could account for HR changes and C fiber sprouting (either a little or a lot) could account for BP changes (either dysautonomia or frank autonomic dysreflexia).
- Identified plasticity in monoamine receptors that would facilitate expression of AD. Found that monoamine receptors on preganglionic sympathetic neurons change following spinal cord injury, sometimes (serotonin) in proportion to their distance from that injury.
- Developed model system for recording AD-related sensorimotor plasticity in an adult in vitro thoracic hemisect preparation.
- Characterized neuromodulatory control monoamine receptor activation and autonomic function in the neonate
- Characterized the distribution of monoamine receptors in the neonate
- Define a completely new experimental system to be the first to study SC-induced plasticity in sympathetic postganglionics comprising the thoracic sympathetic chain.

Reportable outcomes

Papers (multiple papers are in preparation but only published papers are listed here):

1. ZIMMERMAN, A., SAWCHUK,M., & **HOCHMAN, S.** Monoaminergic modulation of spinal viscero-sympathetic function in the neonatal mouse thoracic spinal cord. PLoS One. 7(11):e47213. doi: 10.1371/journal.pone.0047213. (2012) PMID: 23144807
2. **HOCHMAN, S.,** GOZAL, E.A., HAYES, H.B., ANDERSON, J., DEWEERTH, S.D., AND CHANG, Y.-H. Enabling techniques for in vitro studies on mammalian spinal locomotor mechanisms: integrating afferent feedback and attached hindlimbs. Frontiers in Bioscience Jun 1;17:2158-80 (2012). PMID: 22652770
3. **HOCHMAN, S.** Long-term patch recordings from adult spinal neurons herald new era of opportunity. J Neurophysiol. 106: 2794–2795 (2011) PMID: 21709418

Abstracts (Hochman Lab):

1. Speigel, I.A. and Hochman, S. Selective optogenetic activation of ChAT-Cre/channelrhodopsin-expressing primary afferents. (2014) Soc. Neurosci. Abst. 40.
2. Halder, M. Sawchuk, M., and Hochman, S. Sympathetic preganglionic and afferent stimulation-evoked responses in paravertebral thoracic chain ganglia. (2014) Soc. Neurosci. Abst. 40.
3. Lam, R., Sawchuk, M., and Hochman, S. Limited incidence of tyrosine hydroxylase-expressing C-fiber low-threshold mechanoreceptors in the first two weeks of postnatal development of mouse. (2014) Soc. Neurosci. Abst. 40.
4. Watkins, K., Sawchuk, M., and Hochman, S. Light Touch: Optogenetic Activation of Tyrosine Hydroxylase-expressing C-fiber Mechanoreceptors. (2014) Soc. Neurosci. Abst. 40.
5. Losey, p. and Hochman,s. Do sympathetic preganglionic neurons modulate locomotion by intraspinal activity-dependent release of nitric oxide? (2013) Soc. Neurosci. Abst. 39.
6. Speigel, I.A., Sawchuk, M., Alvarez, F.J., Kimura, H. and Hochman, S. Visualization of putative peripheral ChAT-expressing primary afferent cell bodies and spinal projections using ChAT-cre/Gsat transgenic mice. (2013) Soc. Neurosci. Abst. 39.
7. O'Neill, E.O., Zimmerman, A., Sawchuk, M., & Hochman, S. Changes in mouse serotonin and dopamine receptor labeling in the intermediolateral nucleus after spinal cord injury. EB (2012).
8. O'Neill, B., Zimmerman, A., Sawchuk, M., Lohr, K., & Hochman, S. Monoaminergic receptors associated with autonomic and somatic motoneurons: immunocytochemical comparison and observed modulatory activities. (2010) SALK Motor Control Meeting.

Abstracts (Tansey Lab):

1. Tansey KE, Sawchuk M, Hochman S, Botterman BR. Somatotopic relationships between motor and autonomic physiology and afferent axonal anatomy in a multi-segmental spinal pain reflex. Program No. 585.9, 2010 Neuroscience Meeting Planner. San Diego, CA: Society for Neuroscience, 2010. Online.
2. White JM, Tidwell JS, Lee HJ, Deweerth SP, Tansey KE. Temporal dynamics of motor and autonomic physiology in a multi-segmental spinal cutaneous pain reflex. Program No. 804.16, 2011 Neuroscience Meeting Planner. Washington, DC: Society for Neuroscience, 2011. Online.
3. Lee HJ, Tidwell JS, White JM, Malone PS, Tansey KE. Central projection patterns of segmental cutaneous pain afferents in the rat spinal cord. Program No. 378.18, 2012 Neuroscience Meeting Planner. New Orleans, LA: Society for Neuroscience, 2012. Online.
4. Malone PS, Tidwell JS, White JM, Lee HJ, Tansey KE. Complex neural plasticity in an intersegmental cutaneous pain reflex after spinal cord injury. Program No. 378.17, 2012 Neuroscience Meeting Planner. New Orleans, LA: Society for Neuroscience, 2012. Online.

5. Malone PS, Tidwell JS, White JM, Lee HJ, Tansey KE. Complex nociceptive hypereflexia in a rat intersegmental cutaneous reflex after spinal cord injury. 4th International Congress on Neuropathic Pain, 2013, Toronto, Canada.
6. Lee HJ, Wilson NK, Chung J, Malone PS, Tidwell JS, Tansey KE. Central plasticity of segmental cutaneous nociceptive primary afferents after spinal cord hemisection injury in rats. 31st Annual Symposium of the National Neurotrauma Society, 2013, Nashville, TN. J Neurotrauma 30(15):A47-A48
7. Malone PS, Wilson NK, Chung J, Tidwell JS, White JM, Lee HJ, Tansey KE. Central plasticity of segmental cutaneous nociceptive primary afferents is associated with evoked nociceptive hypereflexia after hemisection spinal cord injury in rats. Annual meeting of the American Society of Neurorehabilitation (ASNR), 2013. San Diego, CA.
8. Lee HJ, Tidwell JS, Chung J, Wilson NK, White JM, Tansey KE. Central plasticity of segmental cutaneous nociceptive primary afferents is associated with evoked dysautonomia after cervical spinal cord injury in rats. Annual meeting of the American Society of Neurorehabilitation (ASNR), 2013. San Diego, CA.
9. Tansey KE, Malone PS, Tidwell JS, Chung J, Wilson NK, White JM, Lee HJ. Plasticity in central projections of cutaneous nociceptive afferents matches the nociceptive hypereflexia and dysautonomia seen after spinal cord injury in rats. 15th International Symposium on Neural Regeneration, 2013. Asilomar, CA.
10. Lee HJ, Chung J, Tansey KE. Cardiovascular responses to cutaneous nociceptive input after cervical spinal cord injury: role of pain afferent types and their plasticity. Society for Neuroscience, 2014.

Grants awarded (Tansey Lab):

Craig H. Neilsen Foundation Pilot Grant

Conclusion

The work done to date demonstrates strong progress on this grant. While some technical difficulties were encountered and addressed, other work, not initially proposed has been possible and has provided enlightening insights to the system under study. We feel the collective work of the PI's labs on the inputs to and outputs of the autonomic nervous system in this work make significant contributions to the field's understanding of the neurophysiology of autonomic dysfunction in spinal cord injury.

References

Anderson, C.R., and Edwards, S.L. (1994). Intraperitoneal injections of Fluorogold reliably labels all sympathetic preganglionic neurons in the rat. *Journal of Neuroscience Methods* 53, 137-141.

Brahma, B., Forman, R.E., Stewart, E.E., Nicholson, C., and Rice, M.E. (2000). Ascorbate inhibits edema in brain slices. *J Neurochem* 74, 1263-1270.

Bratton, B., Davies, P., Janig, W., and Mcallen, R. (2010). Ganglionic transmission in a vasomotor pathway studied in vivo. *J Physiol* 588, 1647-1659.

Coggeshall, R.E., Emery, D.G., Ito, H., and Maynard, C.W. (1977). Unmyelinated and small myelinated axons in rat ventral roots. *J Comp Neurol* 173, 175-184.

Cui, D., Dougherty, K.J., Machacek, D.W., Sawchuk, M., Hochman, S., and Baro, D.J. (2006). Divergence between motoneurons: gene expression profiling provides a molecular characterization of functionally discrete somatic and autonomic motoneurons. *Physiol Genomics* 24, 276-289.

Fouad, K., Rank, M.M., Vavrek, R., Murray, K.C., Sanelli, L., and Bennett, D.J. (2010). Locomotion after spinal cord injury depends on constitutive activity in serotonin receptors. *Journal of neurophysiology* 104, 2975-2984.

Hochman, S. (2011). Long-term patch recordings from adult spinal neurons herald new era of opportunity. *Journal of neurophysiology* 106, 2794-2795.

Holohean, A.M., Hackman, J.C., and Davidoff, R.A. (1990). Changes in membrane potential of frog motoneurons induced by activation of serotonin receptor subtypes. *Neuroscience* 34, 555-564.

Husch, A., Cramer, N., and Harris-Warrick, R.M. (2011). Long-duration perforated patch recordings from spinal interneurons of adult mice. *J Neurophysiol* 106, 2783-2789.

Ida J. Llewellyn-Smith, L.C.W. (2001). Changes in synaptic inputs to sympathetic preganglionic neurons after spinal cord injury. *The Journal of Comparative Neurology* 435, 226-240.

Jacob, J.E., Gris, P., Fehlings, M.G., Weaver, L.C., and Brown, A. (2003). Autonomic dysreflexia after spinal cord transection or compression in 129Sv, C57BL, and Wallerian degeneration slow mutant mice. *Experimental Neurology* 183, 136-146.

Jacob, J.E., Pniak, A., Weaver, L.C., and Brown, A. (2001). Autonomic dysreflexia in a mouse model of spinal cord injury. *Neuroscience* 108, 687-693.

Laskey, W., and Polosa, C. (1988). Characteristics of the sympathetic preganglionic neuron and its synaptic input. *Progress in Neurobiology* 31, 47-84.

Lewis, D.I., Sermasi, E., and Coote, J.H. (1993). Excitatory and indirect inhibitory actions of 5-hydroxytryptamine on sympathetic preganglionic neurones in the neonate rat spinal cord in vitro. *Brain Res* 610, 267-275.

Ma, R.C., and Dun, N.J. (1986). Excitation of lateral horn neurons of the neonatal rat spinal cord by 5-hydroxytryptamine. *Brain Res* 389, 89-98.

Macgregor, D.G., Chesler, M., and Rice, M.E. (2001). HEPES prevents edema in rat brain slices. *Neurosci Lett* 303, 141-144.

Madden, C.J., and Morrison, S.F. (2008). Brown adipose tissue sympathetic nerve activity is potentiated by activation of 5-hydroxytryptamine (5-HT)1A/5-HT7 receptors in the rat spinal cord. *Neuropharmacology* 54, 487-496.

Noga, B.R., Johnson, D.M., Riesgo, M.I., and Pinzon, A. (2009). Locomotor-activated neurons of the cat. I. Serotonergic innervation and co-localization of 5-HT7, 5-HT2A, and 5-HT1A receptors in the thoraco-lumbar spinal cord. *J Neurophysiol* 102, 1560-1576.

Puckett, W.R., Hiester, E.D., Norenberg, M.D., Marcillo, A.E., and Bunge, R.P. (1997). The astroglial response to Wallerian degeneration after spinal cord injury in humans. *Exp Neurol* 148, 424-432.

Rabchevsky, A.G., and Kitzman, P.H. (2011). Latest approaches for the treatment of spasticity and autonomic dysreflexia in chronic spinal cord injury. *Neurotherapeutics* 8, 274-282.

Rabchevsky, A.G., and Lynne, C.W.a.C.P. (2006). "Segmental organization of spinal reflexes mediating autonomic dysreflexia after spinal cord injury," in *Progress in Brain Research*. Elsevier), 265-274.

Ramsey, J.B., Ramer, L.M., Inskip, J.A., Alan, N., Ramer, M.S., and Krassioukov, A.V. (2010). Care of rats with complete high-thoracic spinal cord injury. *J Neurotrauma* 27, 1709-1722.

Schmidt, B.J., and Jordan, L.M. (2000). The role of serotonin in reflex modulation and locomotor rhythm production in the mammalian spinal cord. *Brain Res Bull* 53, 689-710.

Schramm, L.P., and Lynne, C.W.a.C.P. (2006). "Spinal sympathetic interneurons: Their identification and roles after spinal cord injury," in *Progress in Brain Research*. Elsevier), 27-37.

Shreckengost, J., Calvo, J., Quevedo, J., and Hochman, S. (2010). Bicuculline-sensitive primary afferent depolarization remains after greatly restricting synaptic transmission in the mammalian spinal cord. *J Neurosci* 30, 5283-5288.

Undem, B.J., and Potenzieri, C. (2012). Autonomic neural control of intrathoracic airways. *Compr Physiol* 2, 1241-1267.

Weaver, L.C., Marsh, D.R., Gris, D., Brown, A., Dekaban, G.A., and Lynne, C.W.a.C.P. (2006). "Autonomic dysreflexia after spinal cord injury: central mechanisms and strategies for prevention," in *Progress in Brain Research*. Elsevier), 245-263.

West, C.R., Alyahya, A., Laher, I., and Krassioukov, A. (2013). Peripheral vascular function in spinal cord injury: a systematic review. *Spinal Cord* 51, 10-19.

Zhao, S., Ting, J.T., Atallah, H.E., Qiu, L., Tan, J., Gloss, B., Augustine, G.J., Deisseroth, K., Luo, M., Graybiel, A.M., and Feng, G. (2011). Cell type–specific channelrhodopsin-2 transgenic mice for optogenetic dissection of neural circuitry function. *Nature Methods* 8, 745-752.

Zimmerman, A., and Hochman, S. (2010). Heterogeneity of membrane properties in sympathetic preganglionic neurons of neonatal mice: evidence of four subpopulations in the intermediolateral nucleus. *J Neurophysiol* 103, 490-498.

OPEN ACCESS Freely available online

PLOS ONE

Monoaminergic Modulation of Spinal Viscero-Sympathetic Function in the Neonatal Mouse Thoracic Spinal Cord

Amanda L. Zimmerman[1], Michael Sawchuk[2], Shawn Hochman[1,2]*

1 Department of Biomedical Engineering, Emory University/Georgia Institute of Technology, Atlanta, Georgia, United States of America, **2** Department of Physiology, Emory University, Atlanta, Georgia, United States of America

Abstract

Descending serotonergic, noradrenergic, and dopaminergic systems project diffusely to sensory, motor and autonomic spinal cord regions. Using neonatal mice, this study examined monoaminergic modulation of visceral sensory input and sympathetic preganglionic output. Whole-cell recordings from sympathetic preganglionic neurons (SPNs) in spinal cord slice demonstrated that serotonin, noradrenaline, and dopamine modulated SPN excitability. Serotonin depolarized all, while noradrenaline and dopamine depolarized most SPNs. Serotonin and noradrenaline also increased SPN current-evoked firing frequency, while both increases and decreases were seen with dopamine. In an *in vitro* thoracolumbar spinal cord/sympathetic chain preparation, stimulation of splanchnic nerve visceral afferents evoked reflexes and subthreshold population synaptic potentials in thoracic ventral roots that were dose-dependently depressed by the monoamines. Visceral afferent stimulation also evoked bicuculline-sensitive dorsal root potentials thought to reflect presynaptic inhibition via primary afferent depolarization. These dorsal root potentials were likewise dose-dependently depressed by the monoamines. Concomitant monoaminergic depression of population afferent synaptic transmission recorded as dorsal horn field potentials was also seen. Collectively, serotonin, norepinephrine and dopamine were shown to exert broad and comparable modulatory regulation of viscero-sympathetic function. The general facilitation of SPN efferent excitability with simultaneous depression of visceral afferent-evoked motor output suggests that descending monoaminergic systems reconfigure spinal cord autonomic function away from visceral sensory influence. Coincident monoaminergic reductions in dorsal horn responses support a multifaceted modulatory shift in the encoding of spinal visceral afferent activity. Similar monoamine-induced changes have been observed for somatic sensorimotor function, suggesting an integrative modulatory response on spinal autonomic and somatic function.

Citation: Zimmerman AL, Sawchuk M, Hochman S (2012) Monoaminergic Modulation of Spinal Viscero-Sympathetic Function in the Neonatal Mouse Thoracic Spinal Cord. PLoS ONE 7(11): e47213. doi:10.1371/journal.pone.0047213

Editor: Mark L. Baccei, University of Cincinnatti, United States of America

Received June 10, 2012; **Accepted** September 10, 2012; **Published** November 5, 2012

Funding: This work was supported by Department of Defense #10494473; National Institute of Neurological Disorders and Stroke Grant NS-65949; the Craig Neilsen Foundation #123877; and Pfizer IIR WS753331. The funders had no role in study design, data collection and analysis, decision to publish, or preparation of the manuscript.

Competing Interests: The authors have declared that no competing interests exist.

* E-mail: shawn.hochman@emory.edu

Introduction

The central nervous system receives sensory information from the visceral organs through two paths: the vagus nerve, which projects to the nucleus of the solitary tract [1] and through sympathetic and pelvic parasympathetic nerves, which pass through prevertebral and/or paravertebral ganglia to the thoracolumbar and sacral spinal cord [2,3]. It is commonly thought that nociceptive signals travel predominantly through the spinal cord path [4], and connect to somatic and sympathetic efferents through disynaptic and polysynaptic pathways [5,6]. While the role of spinally projecting visceral afferents on nociception has received considerable attention [4,7–9], little is understood on the role of visceral afferent pathways in modulating activity of primary afferents via presynaptic inhibition.

Thinly myelinated and unmyelinated visceral afferents [10,11,12] comprise a small percentage of dorsal root ganglia neurons in the thoracolumbar spinal regions [10,11,13], yet they project multi-segmentally and more diffusely than their somatic counterparts [14–16]. Visceral afferents have distinct spinal projection patterns and terminate in lamina I as well as in the deep dorsal horn (laminae IV–V), with a few collaterals reaching near lamina X [10,15,17]. The greater splanchnic nerve contains visceral afferents originating from the gut, pancreas, spleen, kidneys, testis/ovaries, and pelvic organs [8]. Stimulation of splanchnic nerve has been used to study visceral afferent inflow and has been shown to evoke both autonomic and somatic motor spinal reflexes [12,18,19,20,21].

Descending monoaminergic systems that release serotonin (5HT), noradrenaline (NA) and dopamine (DA) project densely to and have considerable modulatory actions on motor, autonomic, and sensory systems in both mammalian and non-mammalian species [22,23,24,25–29]. Studies on visceromotor and pressor responses to colorectal distension in the awake rat have indicated antinociceptive actions of NA and 5HT [9,30], and one study of spinal micturition reflexes has suggested inhibitory actions of DA [31]. The neuromodulatory role of these monoamines on intraspinal visceral afferents, interposed interneurons, and efferent

activity needs to be specifically addressed to understand their integrative actions, yet there appear to be no systematic investigations on their site of action or dose-dependent modulation.

An effective means of inhibiting primary afferent influence on central circuits is via presynaptic inhibition of their intraspinal terminals. One form of presynaptic inhibition (PSI) is ionotropic, recorded as a summed back-propagated depolarization of primary afferent terminals termed primary afferent depolarization (PAD) [32]. PAD is traditionally thought to be mediated by last order GABAergic interneurons [32,33], though ionotropic glutamate and $5HT_3$ receptors can also generate PAD [34,35]. PAD has been shown in visceral afferents in response to splanchnic nerve and sympathetic chain stimulation [36]. Though descending monoaminergic systems have been shown to play a strong role on sensory processing in spinal interneurons [37,38] and on modulating PAD in somatic afferents [39,40], their modulatory actions on visceral afferent mediated PAD have not been determined.

We developed an *in vitro* spinal cord/sympathetic chain preparation in the neonatal mouse and stimulated visceral afferents in the splanchnic nerve or sympathetic chain to record evoked PAD from thoracic dorsal roots and reflex responses from thoracic ventral roots. Since activity in thoracic ventral root recordings indicate efferent population responses of both somatic and sympathetic efferents, we sought to further clarify monoamine actions specifically on sympathetic function by recording from sympathetic preganglionic neurons (SPNs).

SPNs integrate activity from descending and sensory systems to determine the final central output of the sympathetic nervous system [41]. SPNs are located predominantly in the thoracolumbar intermediolateral column in distinct clusters that form a ladder-like distribution symmetric around the central canal [42]. Descending dopaminergic, noradrenergic, and serotonergic systems have projections corresponding to the ladder-like distribution of SPNs, suggesting a direct neuromodulatory influence [43–46]. While direct and indirect actions have been reported for NA, 5HT and DA on SPNs, conclusions as to the overall actions are often contradictory, and may partly be attributed to age and species specific differences [47–53]. Here, we used an *in vitro* slice preparation recording from fluorescently- identified SPNs in a HB9-GFP transgenic mouse line as done previously [54] to correlate the effects of the monoamines on SPN excitability with visceral afferent-evoked actions from the same mice in the intact spinal cord.

Materials and Methods

Ethical Approval

All procedures described here comply with the principles of The Care and Use of Animals outlined by the American Physiological Society and was approved by the Emory University Institutional Animal Care and Use Committee.

Splanchnic Nerve and Sympathetic Chain Immunohistochemistry

The splanchnic nerve and sympathetic chain connecting the rostral three ganglia were isolated using the dissection described below. Sympathetic chains were fixed in 4% paraformaldehyde for 1 hour, then cryoprotected in 10% sucrose plus 0.1 M PO_3 (pH 7.4) and stored at 4°C. Before staining, chains were washed overnight in 0.1M PO_3 buffered saline (PBS), then incubated with primary antibodies CGRP (goat, AbD Serotec, 1:200), TH (rabbit, Millipore, 1:1000), and anti-GFP (chicken, AbCam, 1:1000) for 48 hours at 4°C, then washed three times in PBS containing 0.3% Triton X-100 for 30 minutes each at room temperature. Primary antibodies were stained with Alexa488 anti-chicken (diluted 1:100), cy3 anti-goat (diluted 1:250), and cy5 anti-rabbit (diluted 1:100) secondary antibodies, all from Jackson Immunoresearch.

In Vitro Spinal Cord and Sympathetic Chain Preparation

In order to examine net modulatory actions on thoracic spinal efferents (whose axons predominantly originate from SPNs) and visceral afferent evoked PAD, both ventral root efferent and dorsal root afferent responses to visceral sensory stimulation were assessed with DC recordings. Electrical stimulation of the greater splanchnic nerves has often been used to study visceral afferent inflow, and this paradigm was used again here.

Dissection. All experiments were performed at postnatal day (P) 5–8 mice crossed from transgenic hemizygote HB9-eGFP females (JAX laboratories) and inbred C57/BL6 males. Mice were either HB9-eGFP$^{+/-}$ heterozygotes or wild type. Animals over age P6 were anesthetized with 10% urethane (2 mg/kg i.p.) before decapitation. All animals were decapitated and eviscerated, leaving only the vertebral column, ribcage, and surrounding tissues. The preparation was then placed in a perfusion chamber filled with low-calcium, high-magnesium artificial cerebrospinal fluid (aCSF) containing (in mM): 128 NaCl, 1.9 KCl, 1.2 KH_2PO_4, 26 $NaHCO_3$, 0.85 $CaCl_2$, 6.5 $MgSO_4$, and 10 d-glucose (pH of 7.4). A dorsal laminectomy and ventral vertebrectomy were performed to expose the dorsal and ventral sides of the spinal cord, respectively, from the upper cervical region to the mid-sacral level. Care was taken to cut medial to the aorta on the left side, to preserve the connections of the dorsal and ventral roots to the sympathetic chain. The aorta was then carefully removed, and the surrounding fascia dissected away from the left sympathetic chain. The splanchnic nerve was identified branching laterally from the sympathetic chain at T_{13} and innervating the celiac ganglia, and cut midway between the sympathetic chain and the celiac ganglia. The perfusion solution was then switched to regular aCSF (128 NaCl, 1.9 KCl, 1.2 KH_2PO_4, 26 $NaHCO_3$, 2.4 $CaCl_2$, 1.3 $MgSO_4$, and 10 D-glucose). Pancuronium bromide (25 μM) was added to limit movement of the preparation.

Recording Configuration. The recording configuration is shown in Figure 1B. Bipolar glass suction electrodes (inner diameter 60–100 μm) were used to both record slow potentials in spinal roots and stimulate the splanchnic nerve or sympathetic chain. Teflon insulated and chlorided silver ground wires were wrapped around the outside of the glass to reduce fluctuations in the DC recordings and minimize current spread to intercostal muscles. Visceral afferents were activated by stimulating the splanchnic nerve or other cut regions of the sympathetic chain at a rate of .0167 Hz (once every 60s), as responses to higher frequency stimuli were susceptible to depression [55]. Responses were recorded from the T_{11}–T_{13} dorsal and ventral roots.

Due to the mixed afferent/efferent composition, electrical stimulation of the splanchnic nerve and caudal sympathetic chain evoked short-latency orthodromically and antidromically propagating population spikes in dorsal root and ventral root recordings, respectively (Figure 1C and D). Direct electrical recruitment of axons was verified by their persistence following block of chemical synaptic transmission after exchanging the bath to a nominally Ca^{2+}-free aCSF. Orthodromic afferent volleys from splanchnic nerve were recorded in dorsal roots as far rostral as T_6, confirming direct afferent axonal projections to multiple spinal segments. Recorded DRPs from dorsal roots are produced as a result of electrotonically back-propagating depolarizing potentials (PAD) from intraspinal primary afferent terminals. PAD leads to

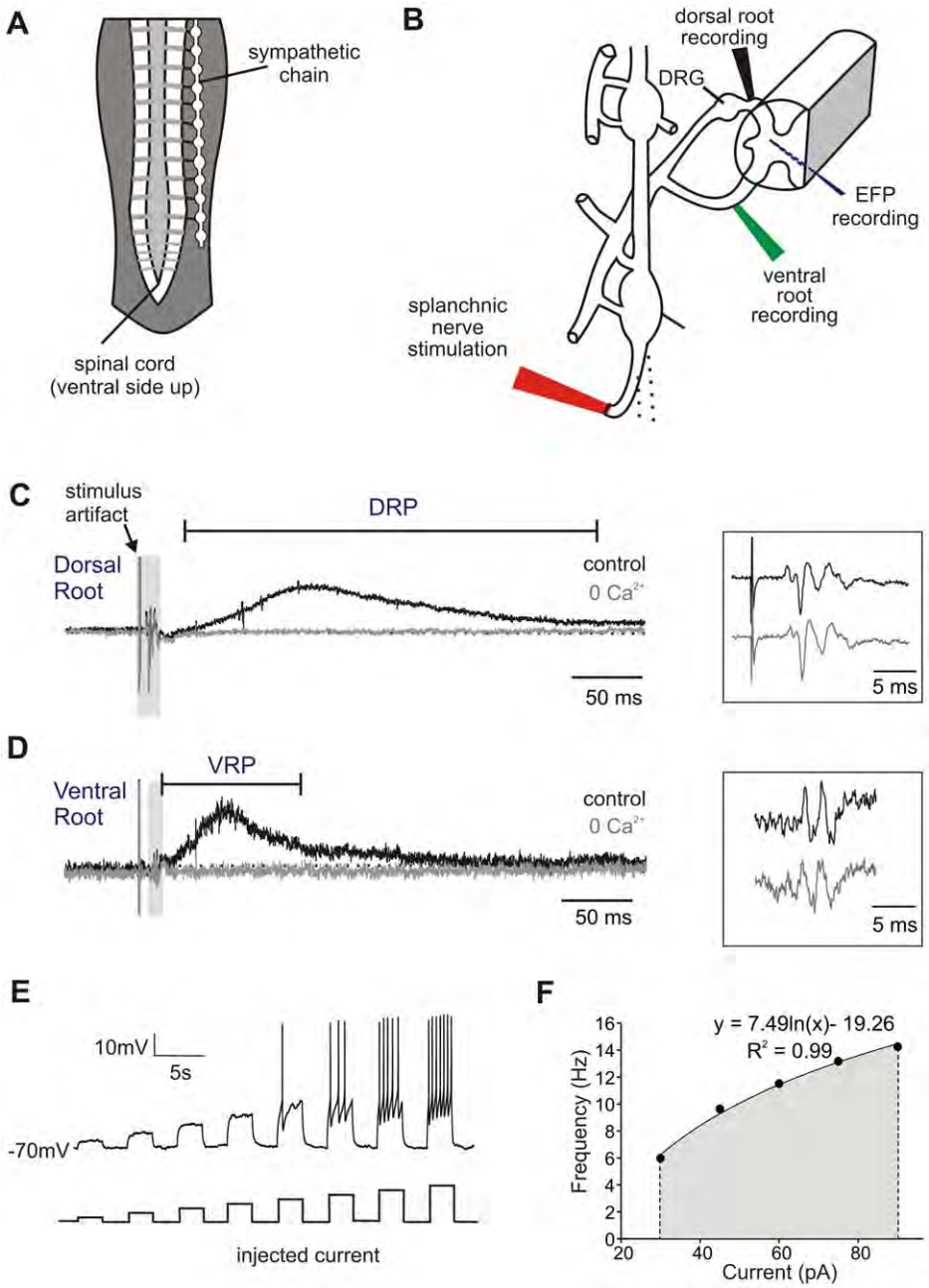

Figure 1. Sympathetic chain anatomy and example recordings. A. Schematic of the sympathetic chain and its connections to the spinal cord. B. Recording configuration, with suction stimulating electrode on greater splanchnic nerve and suction recording electrodes on dorsal and ventral roots. Field potential electrode penetrates into dorsal horn from cut surface of spinal cord. C and D. Sample recorded dorsal root potential (DRP) recorded at dorsal root entry zone (C) and ventral root potential (VRP) recorded at ventral root near exit from cord (D), both of which disappear in nominally 0 Ca^{2+} aCSF (grey traces). Higher magnification of grey highlighted orthodromic afferent (C) and antidromic efferent (D) spiking is shown in boxes at right. E. Whole-cell recorded response of a single SPN in spinal slice to increasingly depolarizing current steps (multiples of 5 pA, 1 s duration). Bottom trace shows current steps. F. Mean firing frequency for each current step plotted. Data points are best fit with a logarithmic line (equation shown). Area under this line (shaded in grey) is calculated by integrating line from first to last data point.
doi:10.1371/journal.pone.0047213.g001

presynaptic inhibition by reducing transmitter release [32], so the slow DRPs were used as a measure of the magnitude of PAD-evoked presynaptic inhibition. DRPs were recorded with a suction electrode attached *en passant* to the root as close to the entry zone as possible to minimize the distance of the recorded electrotonically decaying potential. Similarly recorded ventral root potentials (VRPs) were interpreted as compound excitatory postsynaptic potentials (EPSPs) of the combined captured axonal population of somatic and sympathetic efferents. Examples of recorded DRPs and VRPs are shown in Figure 1C and D, respectively.

Neural activity was collected on a custom built 4 channel direct current amplifiers, low pass filtered at 3 kHz, and digitized at 5 kHz (Digidata 1440) and recorded in Clampex for off-line analysis (Molecular Devices).

Extracellular Field Potentials. When extracellular field potentials (EFPs) were recorded, a 2/3 sagittal section of the

spinal cord was completed using fine insect pins. Micropipettes (tip diameter 1–2 μm, resistance 4–7 MΩ) were filled with 2 M KCl and penetrated the cut surface of the spinal cord at an approximately 35° angle until EFPs were seen in response to splanchnic nerve or caudal sympathetic chain stimulation. EFPs reflect population membrane voltage changes in the neurons around the tip of the electrode. Recording locations were approximated after the experiment using a transverse picture of the sectioned spinal cord, distance from the surface of the spinal cord marked during the experiment, and angle of micropipette penetration (see Figure 1B).

Drug Solutions and Applications. Stock solutions of drugs (10–100 mM) were made and stored at −20°C until needed. All drugs were dissolved in regular ACSF and perfused through the gravity perfusion line. For time response trials, 5–10 μM of 5-hydroxytryptamine HCl (5HT), norepinephrine bitartrate (NA), or dopamine HCL (DA) were applied for 10 minutes, then washed out with regular ACSF that continued to contain 25 μM pancuronium for at least 30 minutes. For dose-response trials, increasing dosages of 5HT, NA, or DA were applied cumulatively, with 10 minutes in between dose increments. In a few experiments, bicuculline (10–20 μM) was added to block $GABA_A$ receptor mediated transmission. All drugs were purchased from Sigma Aldrich.

Data Analysis. Changes were assessed in the evoked DRPs, VRPs, and EFPs using the following paradigm. A custom built MATLAB program was used to subtract the baseline values prior to the stimulus, low-pass filter the response at 100 Hz, find the onset of the evoked slow potential, their peak response, and their integral under the filtered response from onset to offset (defined as the time at which the slow potential decayed to 1/3 peak amplitude). This program and cutoff frequency was found to accurately capture these slow potentials. Responses were averaged for the last 5 minutes of each drug dose increment for dose response curves. For time-dependent analysis, responses were averaged over five minute intervals. In order to minimize effects of differences in suction in the dorsal and ventral root recording electrodes, and differences in EFP recordings, all evoked potentials were normalized to baseline values. Statistics were completed using a two-tailed paired t-test in Microsoft Excel. Timing of 1st afferent spikes was assessed visually in Clampfit (Molecular Devices).

Slice Electrophysiology

Dissection. All experiments were performed in transgenic mice expressing HB9-eGFP (JAX laboratories; known to label SPNs), postnatal day 3–9 as described previously [54]. Briefly, neonatal animals were decapitated, eviscerated, and the spinal cords removed, and a T_8-L_2 section isolated and sliced into thick transverse sections (400 μm). Initial removal of the spinal cord and slicing were performed in cooled, oxygenated sucrose aCSF, containing (in mM): 250 sucrose, 2.5 KCl, 2 $CaCl_2$, 1 $MgCl_2$, 25 glucose, 1.25 NaH_2PO_4, and 26 $NaHCO_3$, pH 7.4. Slices were left to recover for at least 1 hour.

The recording chamber was continuously perfused with oxygenated aCSF (composition specified above) at a rate of ~2 ml/minute. Patch clamp recordings were made from fluorescently-identified SPNs located within the intermediolateral nucleus (e.g. Fig. 2D). The intracellular recording solution was comprised of (in mM): 140 K- gluconate, 11 EGTA, 10 HEPES, 1 $CaCl_2$, and 35 KOH, pH 7.3. Cells were brought to −70 mV holding potential by injecting bias current and recorded in gap-free mode to assess effects on membrane potential. Intracellular current was injected in 1 s rectangular waveforms and incremented in magnitude in a stepwise fashion (5–30 pA increments, depending on input resistance [54]). Changes in membrane properties and excitability were quantified. Using current step sequences applied before and during drug application, mean firing frequency was calculated for each current step. Frequency – current (*f*-I) plots were then fit with a logarithmic trendline using Microsoft Excel. Matlab was then used to integrate the area under the logarithmic trendline both before and during drug application (Figure 1E, F). This integrated area was then used to quantify changes in cellular excitability, with statistical significance found using a students' paired t-test.

Application of Agonists. 5HT, NA, and DA were bath applied at 10 μM, a concentration believed to be below the concentration where nonspecific binding actions have been observed [37,56]. Each agonist was applied for 1–3 minutes, and a washout period of 10–20 minutes was allowed between drug applications. Drug order was random, and often only one or two agonists were used per cell, due to the time constraints of the recordings.

Results

$CGRP^+$ visceral afferents travel through sympathetic ganglia

While many studies have shown that visceral afferents project to dorsal root ganglia (DRG) several segments away from their spinal nerves [14–16], few have suggested they reach the appropriate DRGs by traveling within the sympathetic chain [2,57]. We therefore sought to confirm the presence of afferents in the sympathetic chain and major splanchnic nerve in the neonatal mouse model system, using immunohistochemistry on fixed tissue of dissected whole mounts of the major splanchnic nerve and sympathetic chain.

Calcitonin gene-related peptide (**CGRP**) is a peptide found in about 40–50% of DRG neurons, with a strong preference for labeling visceral afferents [58,59]. $CGRP^+$ staining was compared to tyrosine hydroxylase (**TH**), a marker for sympathetic postganglionic neurons [60], and to HB9-GFP, which labels sympathetic preganglionics [61]. Triple labeling results showed that axon bundles between ganglia contained considerable numbers of all three axon fiber types (Figure 2A–C). Within the ganglia, while many preganglionic GFP^+ axons avoided the TH^+ somas entirely, many also appeared to surround and likely synapse on them. In contrast, almost all $CGRP^+$ axons projected outside the region of TH^+ postganglionic somas, and there was no evidence of $CGRP^+$ afferents forming synapses on postganglionic cell somas (Figure 2). Additionally no overlap in labeling was seen for any of these makers, cleanly identifying these 3 axon fibers as distinct neurochemically-identifiable populations. Most importantly, our immunohistochemistry clearly demonstrates that $CGRP^+$ afferents projecting from the splanchnic nerve enter the CNS through the spinal cord via the sympathetic chain, thereby allowing for stimulation of the sympathetic chain and greater splanchnic nerve for selective stimulation of visceral afferents.

The distribution of CGRP labeling in the thoracic cord is shown in a transverse section. Note the dense labeling in the superficial dorsal horn, with additional labeling in the deep dorsal horn, and in lamina X near the central canal (Figure 2D). Note also the presence of sparse CGRP+ axons in the intermediolateral nucleus where the majority of SPNs are found. Splanchnic CGRP+ afferent labeling is not associated with superficial dorsal horn labeling [62].

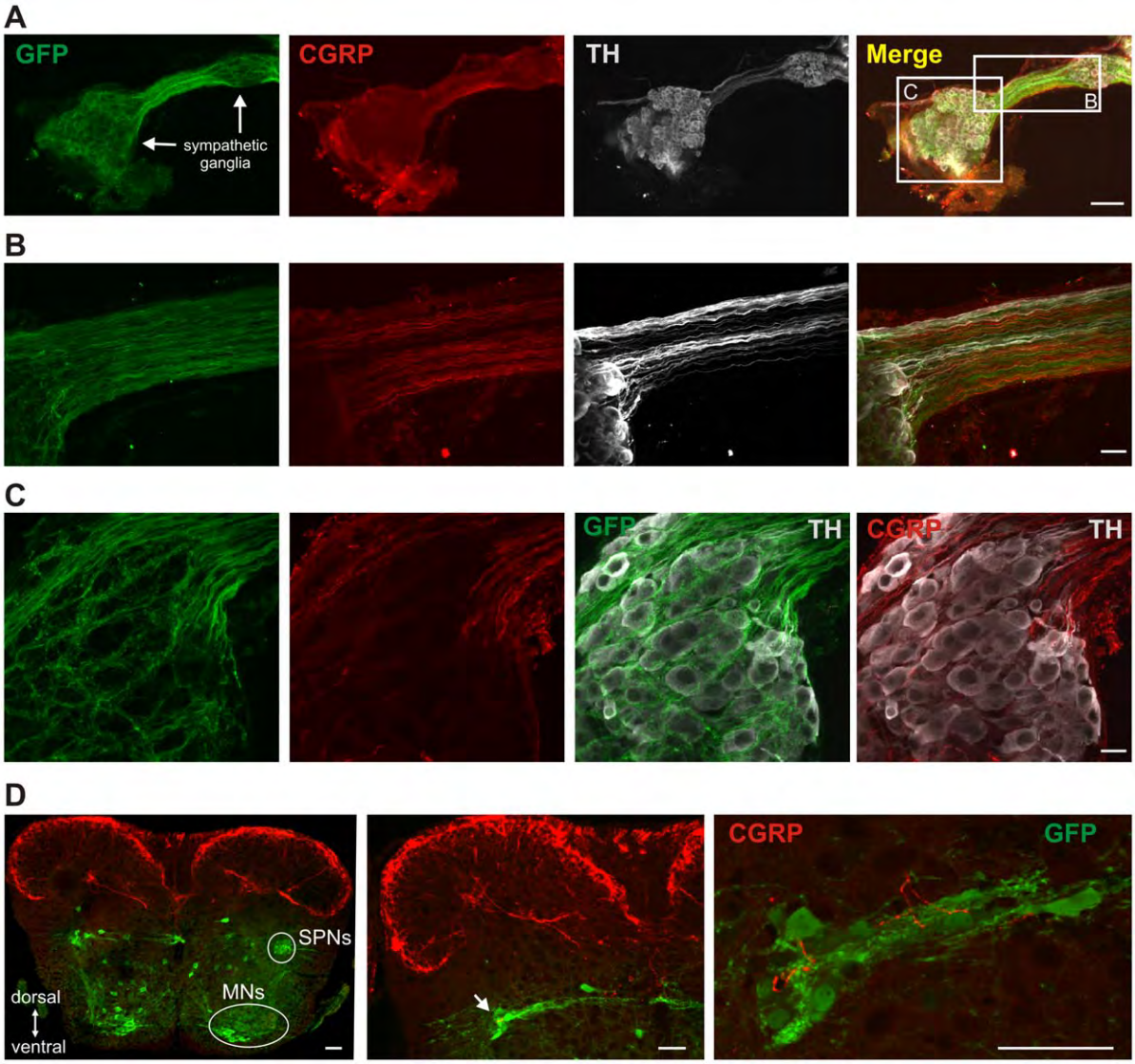

Figure 2. Axon fiber composition in paravertebral ganglia and related labeling in spinal cord. A. Lower power image of two caudal sympathetic ganglia and connecting nerve bridge showing nerve contains a mixture of at least 3 neurochemically distinct fiber populations: HB9-GFP+ sympathetic preganglionic neurons (SPNs), CGRP+ visceral afferents, and TH+ sympathetic postganglionics. Boxed regions are enlarged in B and C. B. Enlargement showing SPNs (GFP+), CGRP and TH immunolabeled axons in axon bundle between two ganglia. Image represents composite of 73 consecutive confocal images taken at 0.38 μm optical section thickness (27.74 μm total thickness). C. Enlargement of SPNs (GFP+), CGRP and TH immunolabeling in the left sympathetic ganglion. Section in central region of ganglia shows that, while SPNs appear to form basket-like synapses around postganglionics, CGRP+ afferents do not project through this region. Image is a collapsed stack of 11 consecutive confocal images (4.18 μm total). D. CGRP (red) and HB9-GFP labeling (green) in a transverse section of thoracic spinal cord. Note predominant CGRP labeling in the dorsal horn. HB9-GFP labeling of SPNs in the intermediolateral nucleus and motoneurons (MNs) in the ventral horn are identified on the right side. Middle panel shows CGRP labeling extending ventrally including into the intermediolateral nucleus (at arrow) while right panel provides a higher magnification image showing CGRP labeling intermingled with SPNs in the intermediolateral nucleus as well as along its medially oriented SPN projections. Scale bar is 100 μm in A, 20 μm in B and C, and 50 μm in D.
doi:10.1371/journal.pone.0047213.g002

Monoamines depress ventral root potentials

Application of 5–10 μM 5HT, NA, and DA significantly depressed visceral afferent- evoked VRPs recorded from T11, T12 or T13 spinal segments (Figure 3A). While the rostrocaudal extent of evoked responses was not systematically studied, evoked VRPs were seen bilaterally, and as rostral as T3 and caudal as segment S4. Combining all dose-response and time-response trials, VRP amplitude was reduced to 14.8±11.3% of control values for 5HT, 11.0±8.7% for NA, and 52.2±18% for DA. Interestingly, 5HT and NA also greatly depressed ongoing spontaneous VRPs while concomitantly increasing spontaneous spiking activity in the ventral roots (n = 4/4 and 3/3, respectively) (Figure 3C,D), overall supporting the notion that 5HT and NA have excitatory actions on efferent neurons (both somatic and autonomic), while depressing visceral afferent evoked reflexes.

Monoaminergic Actions on Spinal Sympathetic Efferents

In both the rodent and human thoracic spinal cord, the number of SPN axons in the ventral roots greatly exceeds those of somatic motoneurons [63,64]. Still, recordings from ventral roots make it

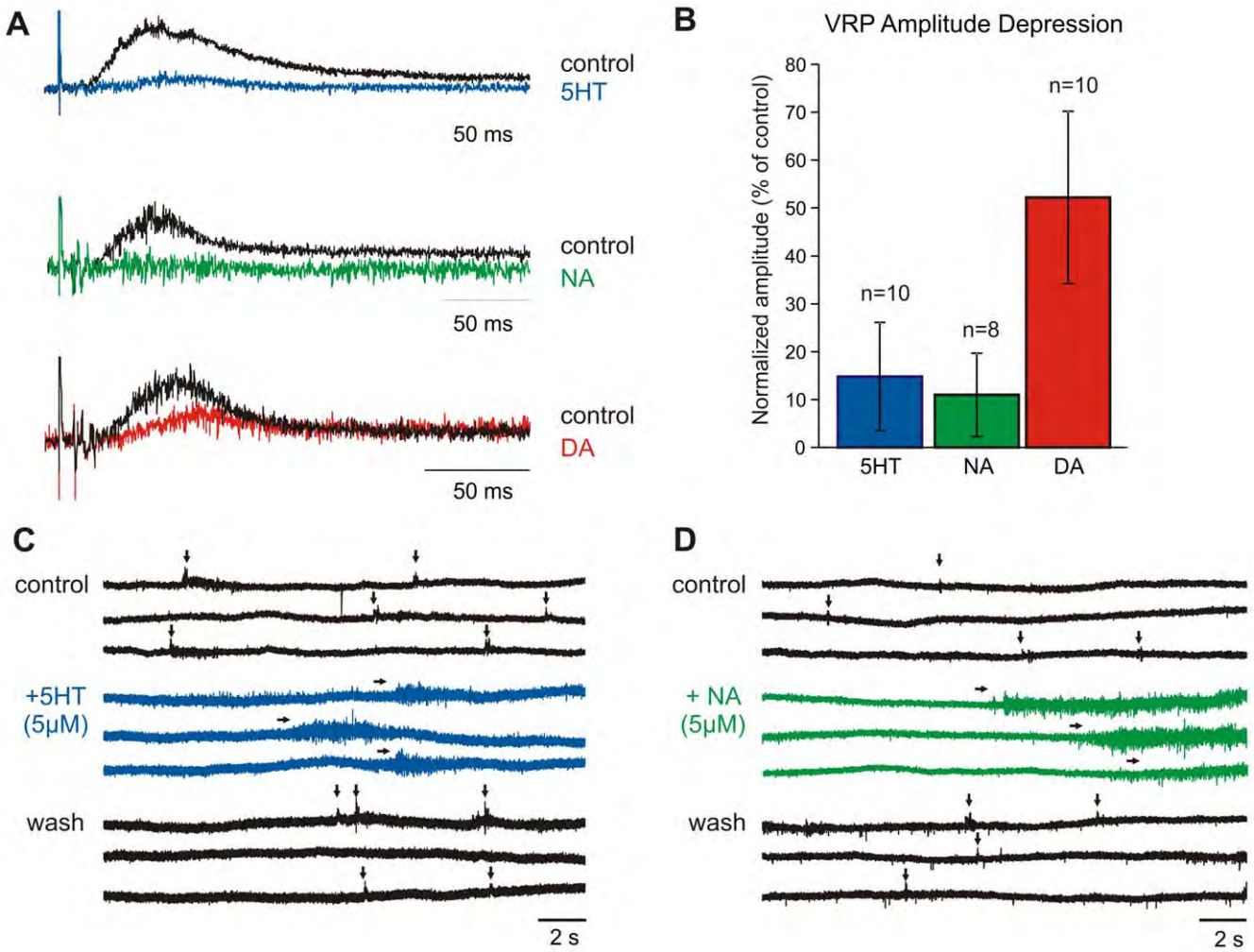

Figure 3. Monoaminergic modulation of ventral root activity. A. Example visceral afferent-evoked responses recorded from T12 ventral roots, and their modulation by 5HT, NA, and DA. Control is black, drug is in blue, green, or red, respectively. B. Combined evoked depression with 10 μM 5HT, NA, and DA across all time and dose-response trials, with standard deviation bars and number of trials displayed. C. Example change in spontaneous ventral root activity after addition of 5HT. Shown are 3 consecutive epochs during 5 minute periods for control, after 5HT (5 μM) was applied, and 15 minutes after washout. Horizontal arrows denote emergent motor bursts observed in the presence of 5HT. Vertical arrows denote spontaneous ventral root potentials, some of which reach spike threshold. D. Example change in spontaneous ventral root activity after addition of NA. Note that both 5HT and NA increased background spiking and the emergence of bursting events, while eliminating spontaneous potentials. DA had limited effects on spontaneous activity and is not displayed.
doi:10.1371/journal.pone.0047213.g003

impossible to determine whether the monoaminergic actions are on sympathetic preganglionic neurons, motor neurons, or some combination of both. Given the species-specific and seemingly contradictory actions of the monoamines previously reported on SPNs [47,48,52], we sought to characterize the effects of 5HT, NA, and DA on SPN intrinsic properties in the neonatal mouse and more clearly elucidate the effects of the monoamines on sympathetic output in the HB9-GFP mouse model. Accordingly, SPNs in the intermediolateral column were targeted for whole-cell patch clamp recordings in transverse slices of thoracic spinal cord as reported previously [54].

Serotonin. With the membrane potential held at −70 mV, bath application of 10 μM 5HT depolarized all SPNs tested (mean 4.9±2.1 mV, n = 6; Figure 4Aa). Compared to baseline values, the frequency-current (*f*-I) plots were also shifted up to the left, i.e. SPNs fired action potentials at a lower current injections and at higher rates. 5HT increased the firing response to current injection by a mean 15.9±9.2% (p = 0.04, n = 6; Figure 4B).

Noradrenaline. Bath application of NA had more diverse actions on SPN excitability. NA primarily depolarized the membrane (mean 4.7±2.2 mV, n = 4), yet hyperpolarizations (mean 3.1±0.1 mV) were also seen (n = 2) (Figure 4Ab). Regardless of the effects on the membrane, NA shifted the cell's *f*-I plot up in all neurons tested, by a mean 22±20% (p = 0.008, n = 6). This can be seen in Figure 4C.

Dopamine. DA bath application lead to both depolarizations (mean 6.0±3.5 mV, n = 7) and hyperpolarizations (mean 5.2±0.9 mV, n = 2) in SPNs (Figure 4Ac). In contrast to 5HT and NA, while DA increased the cell's firing frequency in response to current injection in the majority of neurons (mean 11.5±9.2%; p = 0.004, n = 8), decreased responses were also seen (mean −27.2±3.4%; p = 0.05, n = 3), as shown in Figure 4D. Changes in excitability were not correlated to changes in membrane potential.

Overall, 5HT, NA, and usually DA, significantly increased SPN firing in response to current injection. These upward-shifted *f*-I

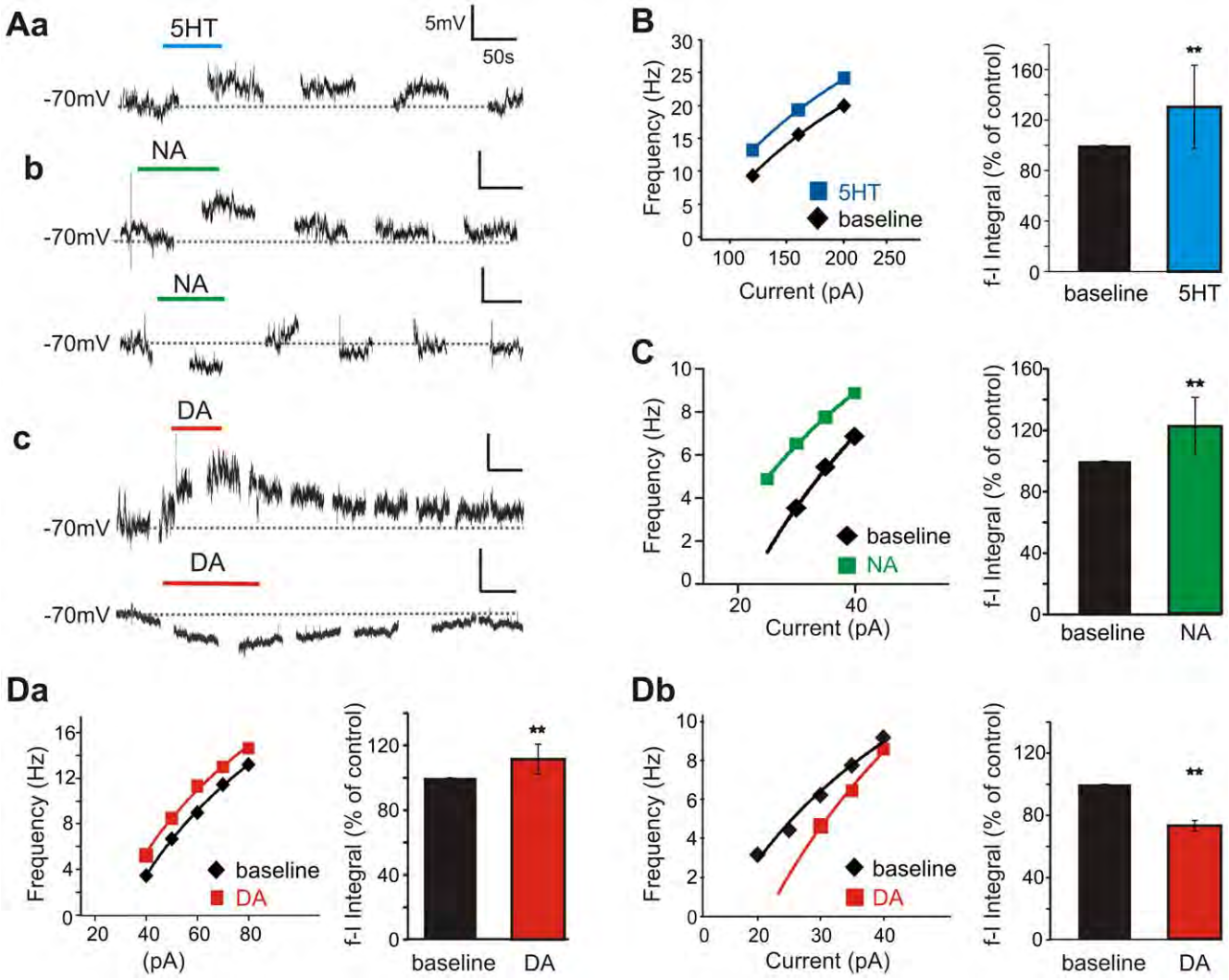

Figure 4. Monoaminergic modulation of SPNs. A. Sample of voltage traces recorded when 5HT, NA, or DA (10 μM, 60–90s) was added to the bath. Interruptions in trace represent periods where current step protocols were performed. Aa. 5HT depolarized the cell membrane in all cells tested. Ab. NA primarily depolarized the membrane, but hyperpolarizations were also seen. Ac. DA both depolarized and hyperpolarized membrane potential. B. 5HT increased cellular excitability. Shown is mean firing frequency in response to series of current steps (5–30 pA steps,1s duration) in control and during peak of 5HT application. Line demarks best fit logarithmic line, and the area under this line was calculated by integrating from first to last data point. Plot on right shows normalized integral changes with standard deviations. C. Mean firing frequency changes in the presence of NA. Regardless of action on membrane potential, NA shifted the f-I plot up and to the left. D. While DA increased cellular excitability in the majority of neurons (a), decreased excitability was also seen (b). ** denotes $p<0.05$ from a paired t-test applied to control and monoaminergic induced areas.
doi:10.1371/journal.pone.0047213.g004

plots would support a monoamine-induced increased sympathetic firing to a given excitatory drive.

Dorsal Root Potentials and Primary Afferent Depolarization

Given that the monoamines predominantly increased sympathetic efferent (SPN) excitability but decreased visceral afferent-evoked efferent synaptic responses (↓VRP), we assessed the actions of the monoamines on visceral afferent transmission and PAD-mediated presynaptic inhibition. Returning to the spinal cord and sympathetic chain preparation, we measured DRPs in the dorsal root as a measure of PAD.

Initial Characterization and Comparison to VRP. Visceral afferent stimulation-evoked DRPs were widespread throughout the thoracic spinal cord, as DRPs were recorded at the spinal levels sampled (T_9–T_{13}) with similar shape and onset. This suggests that visceral afferent stimulation-induced PAD has a broad distribution, and is consistent with the reported actions of somatosensory evoked PAD [65]. While afferent volleys could be recruited at stimulus intensities as low as 8 μA, 50 μs, greater stimulus intensities were often required to elicit a DRP (Fig. 5A). Figure 5 provides an example of the relationship between stimulus intensity and the recruitment of spike volleys, DRPs, and VRPs. Stimulus intensities above 100 μA/100 μs did not further increase DRP recruitment (Figure 5A), so this value was chosen for subsequent studies on neuromodulation. On average, the DRP onset was 31.7±6.1 ms after arrival of the first afferent volley, while the VRP onset was at 11.4±8.0 ms (n = 17). The onset of the VRP preceded the DRP therefore by 19.8±8.4 ms, suggesting that the circuitry responsible for evoking the VRP includes a distinct shorter latency pathway. DRPs lasted on average 565.6±11.8 ms, reaching their peak values

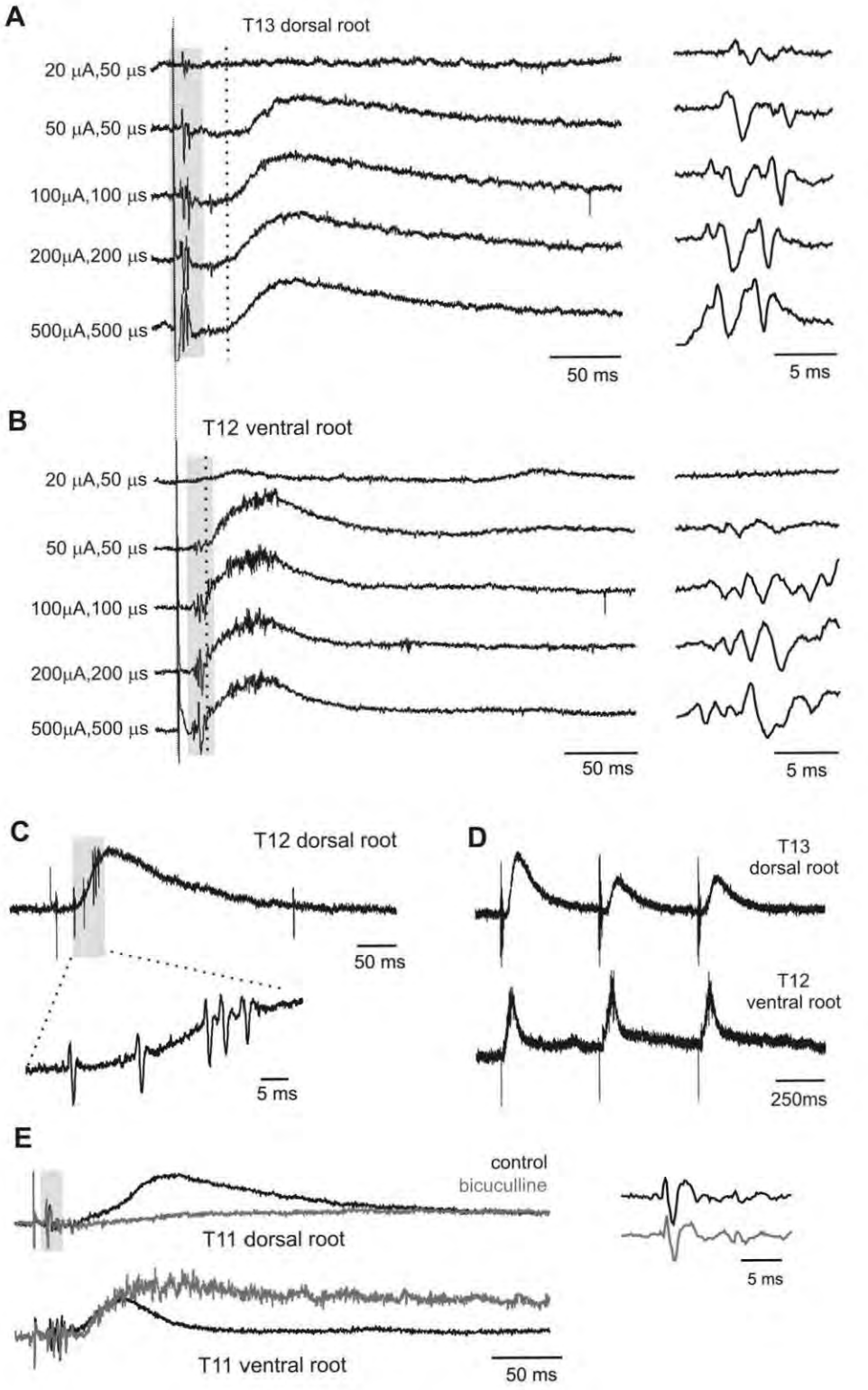

Figure 5. Differences in properties of DRPs and VRPs. A. Increasing stimulus intensities lead to increased afferent volleys and subsequent DRPs. Each trace is an average of 5 events. Note intensities greater than 100 μA, 100 μs increase afferent volley amplitudes (grey shaded region), but not the DRP. Note also that top trace has an afferent volley but no DRP. B. Increasing stimulus intensities and effects on the VRP in the same animal. Notice onset and duration difference between DRP and VRP (dotted vertical lines in A and B). Grey shading denotes orthodromic volleys, seen at higher magnification on the right. C. Single trace of an evoked dorsal root response from another experiment. Grey box and higher magnification below highlight observed dorsal root reflexes associated with the DRP. D. The DRP undergoes frequency dependent depression (here with 2 Hz stimulation). Note this is not the case for the VRP, which can follow frequencies up to 5 Hz. E. The DRP but not VRP is blocked by bicuculline. In example shown, each trace is an average of 10 sweeps, for control and 5 minutes after 20 μM bicuculline. Closeup of afferent volley at right highlights that bicuculline has no effect on the afferent recruitment.
doi:10.1371/journal.pone.0047213.g005

50.1±10.1 ms after onset. The evoked DRP was accompanied by dorsal root reflexes in 11/18 cases, (Figure 5C). Dorsal root reflexes commonly represent an intraspinal primary afferent depolarization of sufficient magnitude to be supra-threshold for antidromic action potential initiation in afferent terminals.

In addition to being quicker in onset than the DRP, the VRP had a lower threshold for recruitment in all stimulus intensity trials (n = 4/4). Also, while the visceral afferent-evoked VRP could follow stimulation up to 5 Hz without depression, the DRP was unable to follow stimulus frequencies greater than .0167 Hz (see Figure 5D). Overall, these differences in onset, frequency sensitivity and threshold for recruitment all support the notion that evoked DRPs and VRPs are mediated at least partly by distinct circuits.

$GABA_A$ Sensitivity. To test whether PAD induced by visceral afferents is $GABA_A$ receptor mediated, 10–20 μM of the competitive antagonist bicuculline was added. In all cases, bicuculline greatly depressed the DRP (mean peak depression to 20.3±3% of control values, n = 4/4). Bicuculline evoked actions were mediated by spinal circuits as there was no change in the recruitment or appearance of recorded afferent volleys. As expected, disinhibition simultaneously greatly facilitated evoked ventral root activity (Figure 5E).

Extracellular Field Potentials. Intraspinal electrodes were positioned to examine monoamine transmitter modulation of population synaptic transmission, recorded extracellularly as EFPs. Short-latency EFPs have been used to report population monosynaptic afferent transmission [66–69]. The electro-anatomic location of splanchnic visceral afferent-evoked EFPs was estimated using systematic field potential tracking; with starting locations 100–400 μm below the ventral surface of the spinal cord in dorsally-angled penetrations up to depths of 1100 μm. Sample recordings from two tracks in the same preparation can be seen in Figure 6A. Figure 6B shows approximate regions of the spinal cord where EFPs were recorded and their relative peak amplitudes in two separate preparations. EFP amplitudes were consistently estimated to be maximal in the deep dorsal horn, with evidence of an earlier arriving EFP in some tracks in the superficial dorsal horn (Figure 6C). This is consistent with known afferent termination sites of visceral afferents including CGRP+ afferents (Figure 2D) [10,15,17,62]. The earliest onset EFP in the deep dorsal horn was found to occur 4.5 ms after the first dorsal root afferent volley was seen, with a mean of 11.0±6.6 ms across trials. The largest amplitude EFPs were not necessarily the earliest in onset, with a mean onset of 12.9±5.8 ms after the first afferent spike was seen. Responses occurred on average 20.8±8.8 ms before onset of the DRP and often began before the VRP. Synaptic transmission at room temperature requires ~3 ms [70,71], so the observed central latency is sufficiently long enough to include oligosynaptic actions but may also reflect monosynaptic actions from slower conducting afferents. Regardless of whether the EFP reflects exclusively monosynaptic actions or not, their modulation would indicate actions on synaptic transmission in deep dorsal horn neurons.

Monoaminergic Depression of Evoked Responses

Overall, all visceral-afferent evoked responses were depressed by the monoamines (Figure 7). As these actions were not accompanied by a change in afferent volley amplitudes, modulatory actions were via central mechanisms. The VRP depression by all three monoamines was also accompanied by actions on the visceral afferent evoked DRP and EFP. At 5–10 μM, both 5HT and NA nearly fully blocked the DRPs (to 12.7±13.4%, n = 5, p = .04 and 5.5±2.3%, n = 4, p = 0.03, of control values, respectively). DA depressed the DRP amplitude but to a much lesser degree (to 44.1±24.9% of control; n = 7, p = .01). NA also greatly depressed the EFP (8.8±0.9% of control, p = 0.03), comparable to its depression of the DRP. In contrast, EFP depression by 5-HT was much less (48.3±3.0%; p = 0.02) than its depression of the DRP. Thus, the reduction in DRP by NA associates strongly with depressed afferent transmission in the deep dorsal horn while additional projection territories or downstream sites also contribute to 5-HT's actions.

DA had variable effects on the EFP: substantial depression in 2/5 preparations, partial depression in 2/5 preparations and facilitation in 1/5 preparations, resulting in a mean depression of 52.3±36.0% (n = 5; p = .03; Figure 7D).

Given the common presence of multiple EFPs having different latencies of onset, we questioned whether the EFP depression calculated based on changes in overall peak amplitude was representative of all evoked EFP populations. Filtered and averaged EFP traces were therefore integrated in 5 ms bins, and depression was compared across bins. No statistically significant changes were seen, indicating a uniform depression of all temporal components of the EFP (data not shown).

A time-dependent comparison was made of the relative monoamine-induced DRP and EFP depression in the same animals (Figure 8A), with data binned at 5 minute intervals. For 5HT, the peak depression of the DRP was greater and time of depression more maintained compared to the EFP (Figure 8B). In comparison, while NA depressed both the DRP and EFP to a similar extent, the DRP was depressed more rapidly, and like 5HT, the depression was maintained for a longer time than that of the EFP (Figure 8B). No statistically significant changes were seen in the time course of DA-induced depression of the DRP and EFP. Collectively, the differentiable temporal and magnitude differences in the depression of the DRP compared to the EFP for 5HT and NA support partially independent sites of actions (see Discussion).

Similar to actions reported for 5HT in lumbar spinal cord in the neonatal rat [72], both 5HT and NA depressed spontaneous DRPs in all cases where spontaneous DRPs were evident (n = 3/3 for each; not shown). Whether these DRPs were initiated by ectopic firing in primary afferents and/or exclusively via intrinsic spinal circuits was not investigated.

Dose Response Relations

To determine relative efficacies of DRP and VRP depression, cumulative dose-response curves were generated for 5HT, NA, and DA. Figure 9A shows a sample of a cumulative dose-response trial for 5HT in a single preparation. When the evoked response was normalized to the initial slow potential amplitude and compared across trials, mean IC_{50} values of 0.33 μM and 1.7 μM were calculated for 5HT on the DRP and VRP, respectively. NA had similar dose-response relations with IC_{50} values of 0.27 μM and 0.91 μM, respectively (n = 4) (Figure 9B and C). In comparison to 5HT and NA, much higher concentrations of DA were needed to suppress the evoked responses. Moreover DA had a biphasic action on the visceral afferent-evoked DRP. At low concentrations (i.e. <5 μM) DA had little effect if any, and even facilitated the DRP in the majority of trials (n = 3/5; see highlighted region in Figure 9D). On the other hand, at higher concentrations, DA dose-dependently depressed the DRP. The best-fit dose response curve calculated an IC_{50} value of 3.9 μM.

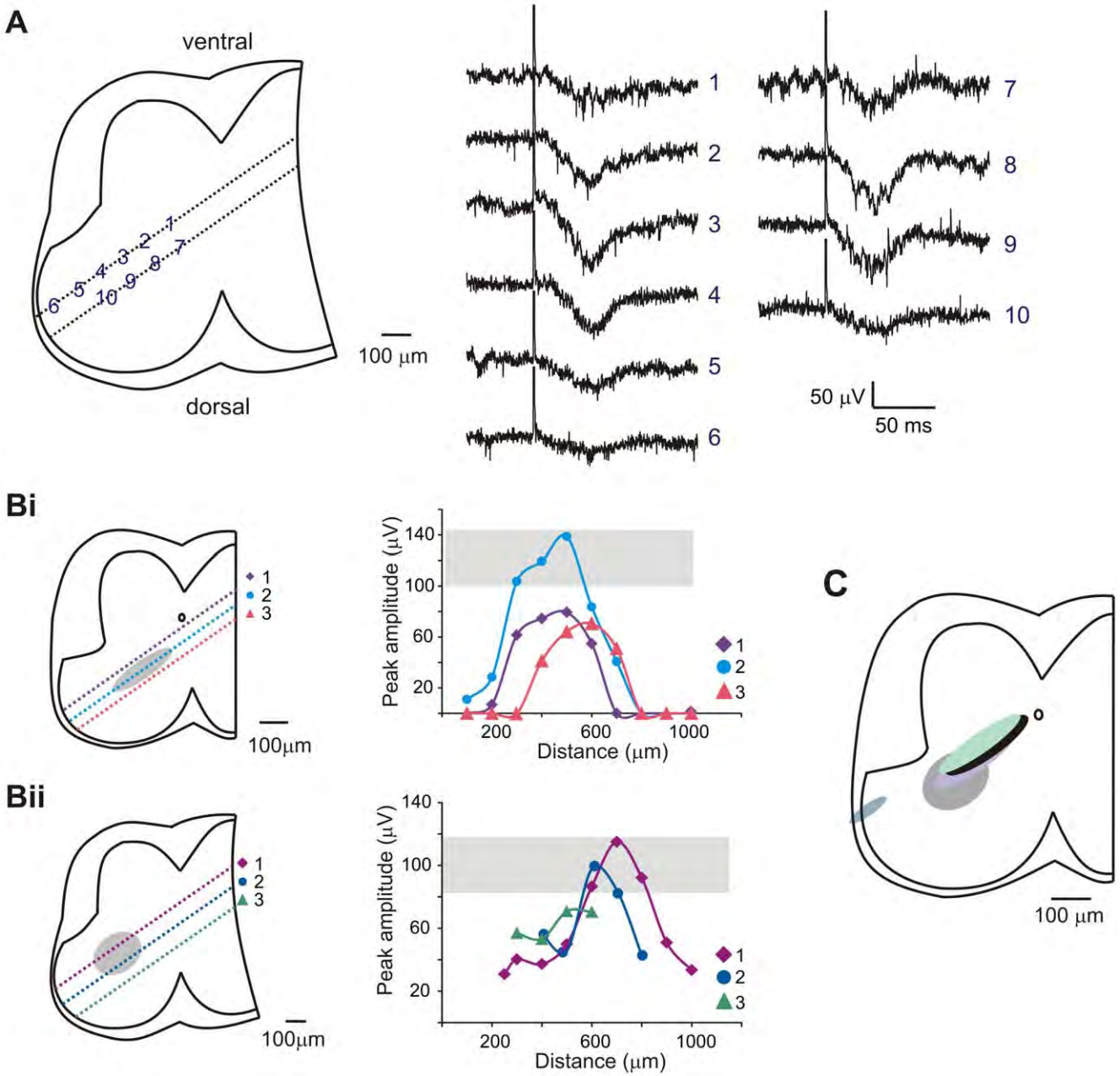

Figure 6. EFP recording locations. A. Sample traces of EFPs evoked at various recording locations marked by numbers. Each trace is an average of 5 events. B. Peak amplitude of evoked EFPs for 2 separate experimental days. Picture on left shows microelectrode paths denoted by separate numbers. Plot on right displays peak amplitude of EFP versus distance into the cord the microelectrode traveled. Grey box and oval denote largest EFP amplitudes and their locations recorded. Bii corresponds to same experiment as traces in A. C. Composite sketch estimation of where maximal EFPs were recorded, compilation of 5 experiments.
doi:10.1371/journal.pone.0047213.g006

Discussion

Spinal visceral afferents encode physiologically relevant events in the viscera and transmit this to the CNS, leading to organ regulation (including via spinal reflexes) and occasionally conscious sensation [1]. Yet, except for sacral afferents, most spinal visceral afferents are thought to lack functional specificity, responding to mechanical, chemical, and sometimes thermal stimuli (e.g. [73], see [60] for review). While some visceral afferents are active under resting conditions, many also relay visceral pain information [60,74], indicating that central mechanisms must exist to differentiate between organ regulation, non-painful sensation, and visceral pain. Indeed, organ specific presynaptic inhibition of afferents has been implicated in the control of micturition [75,76], and mutual inhibition has been demonstrated between visceral and cutaneous afferents, presumably via presynaptic mechanisms [36].

To explore the neuromodulatory control of visceral afferent encoding, this study used a novel *in vitro* spinal cord with intact sympathetic chain preparation in the neonatal mouse. An *in vitro* approach allows for greater accessibility and pharmacological control of the environment as well as the avoidance of anesthetics

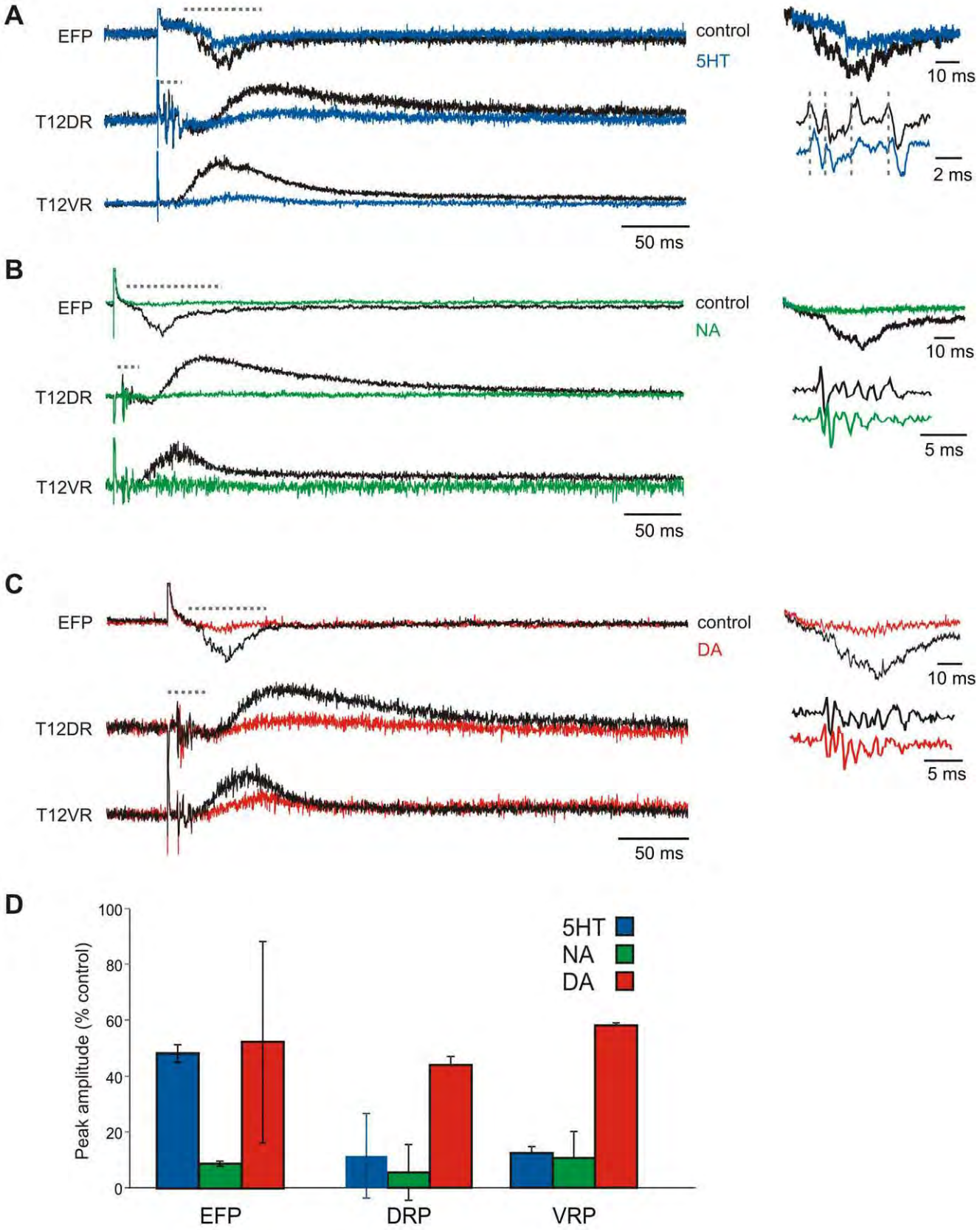

Figure 7. Monoamine effects on splanchnic evoked responses. A. Example of 5HT application on EFP, DRP, and VRP, control traces in black. Horizontal dotted lines identify magnified areas on the right for EFP (top) and DR afferent volleys (bottom). Note slight delay in afferent volley timing in the presence of 5HT. B. Example of NA application. C. Example of DA application. D. Comparison of effects of the monoamines on depression of EFP, DRP and VRP. Values are reported as mean with standard deviation bars.
doi:10.1371/journal.pone.0047213.g007

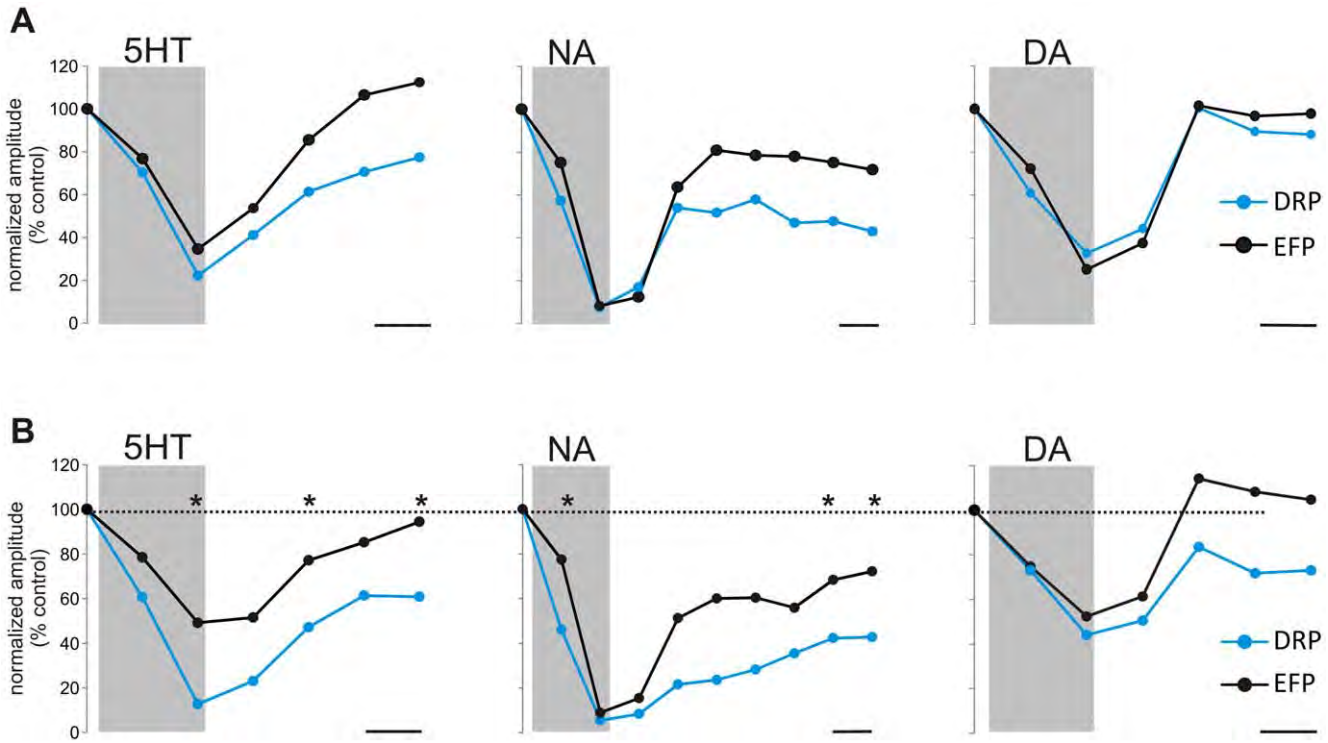

Figure 8. Comparing time and magnitude differences in monoamine-induced depression of DRPs and EFPs. Data points were obtained for each trial by averaging 5 stimulation episodes (1 minute per episode) and plotting the normalized peak amplitude. Monoamines were applied during the shaded periods. A. Time dependent depression of DRPs (blue) and EFPs (black) in an individual animal for 5HT, NA, and DA. B. Average data across animals (n = 4, 3, 4, respectively). * indicates $p<0.05$ when paired t-test was completed for each time point. No differences in time course were found for DA. Scale bars are 5 minutes in all panels.
doi:10.1371/journal.pone.0047213.g008

that alter the $GABA_A$ receptors involved in PAD generation [77,78]. Using this system, we characterized spinal visceral afferent stimulation-evoked ventral root responses (reflexes and subthreshold VRPs), synaptic transmission in the dorsal horn (EFPs), as well as PAD-mediated presynaptic inhibition (DRPs). To our knowledge, we also undertook the first studies on modulation of visceral afferent-evoked PAD by the monoamine transmitters 5HT, NA, and DA. Overall, we observed that all three monoamines acted to suppress visceral afferent-evoked responses while concomitantly increasing ventral root spiking and SPN excitability. 5HT, NA, and DA were also found to inhibit visceral afferent evoked synaptic transmission in the dorsal horn and PAD. In sum, 5HT, NA and DA had similar actions and modulated several spinal pathways to provide a global modulatory shift in the autonomic regulation of visceral afferent and sympathetic efferent function.

Triple labeling for CGRP, TH, and GFP in HB9-GFP transgenic mice indicated the presence of 3 distinct fiber populations that travel between the paravertebral sympathetic ganglia. $CGRP^+$ visceral afferents did not appear to synapse on TH^+ sympathetic postganglionic neurons, often avoiding postganglionic cell bodies entirely, unlike direct synapses reported between afferents and postganglionic neurons in pre-vertebral ganglia [79,80]. Consistent with the presence of $CGRP^+$ afferents, splanchnic nerve stimulation induced afferent volleys, DRPs, and VRPs (often with superimposed reflexes) in multiple spinal segments, supporting known projections of afferents originating in the greater splanchnic nerve [2], and demonstrating that splanchnic afferents act over their broad projection territory. The rostral and caudal extent of these actions remains to be characterized systematically in mouse, but in cat it is generally from T3-L1 dorsal roots [2]. Given the relative scarcity of visceral input to the spinal cord compared to their somatic counterparts, the extent of the visceral afferent-mediated responses is noteworthy.

Monoaminergic Modulation of Motor Output

The descending monoaminergic systems are known to strongly modulate somatic afferent and efferent activity (e.g. [22,24]) and their activity level varies with behavioral state [81,82]. However, few studies have looked at modulatory actions of these systems on visceral afferent dependent activity. In this study, all three monoamines tested potently depressed splanchnic-evoked excitatory actions on ventral root responses (VRP depression).

Whole-cell recordings assessed direct actions on SPNs. All monoamines preferentially facilitated SPN excitability. 5HT always depolarized SPNs and both 5HT and NA always increased SPN firing properties. Since NA and DA could also lead to membrane hyperpolarization and DA to reduced excitability in a minority of SPNs, it is clear that the monoamines can act bidirectionally. Differences in modulatory actions may be related to actions on differentiable subpopulations of SPNs including those previously differentiated by difference in cell membrane properties [54].

Observed monoamine modulatory actions compare favorably to previous studies in both rat and cat. 5HT induced membrane depolarizations in the neonatal rat *in vitro* [47,83,84] and observed excitability increases were previously seen with iontophoretically applied 5HT in SPN firing in cats [85]. The mixed membrane responses observed here with NA are also consistent with that reported in the neonatal rat and adult cat

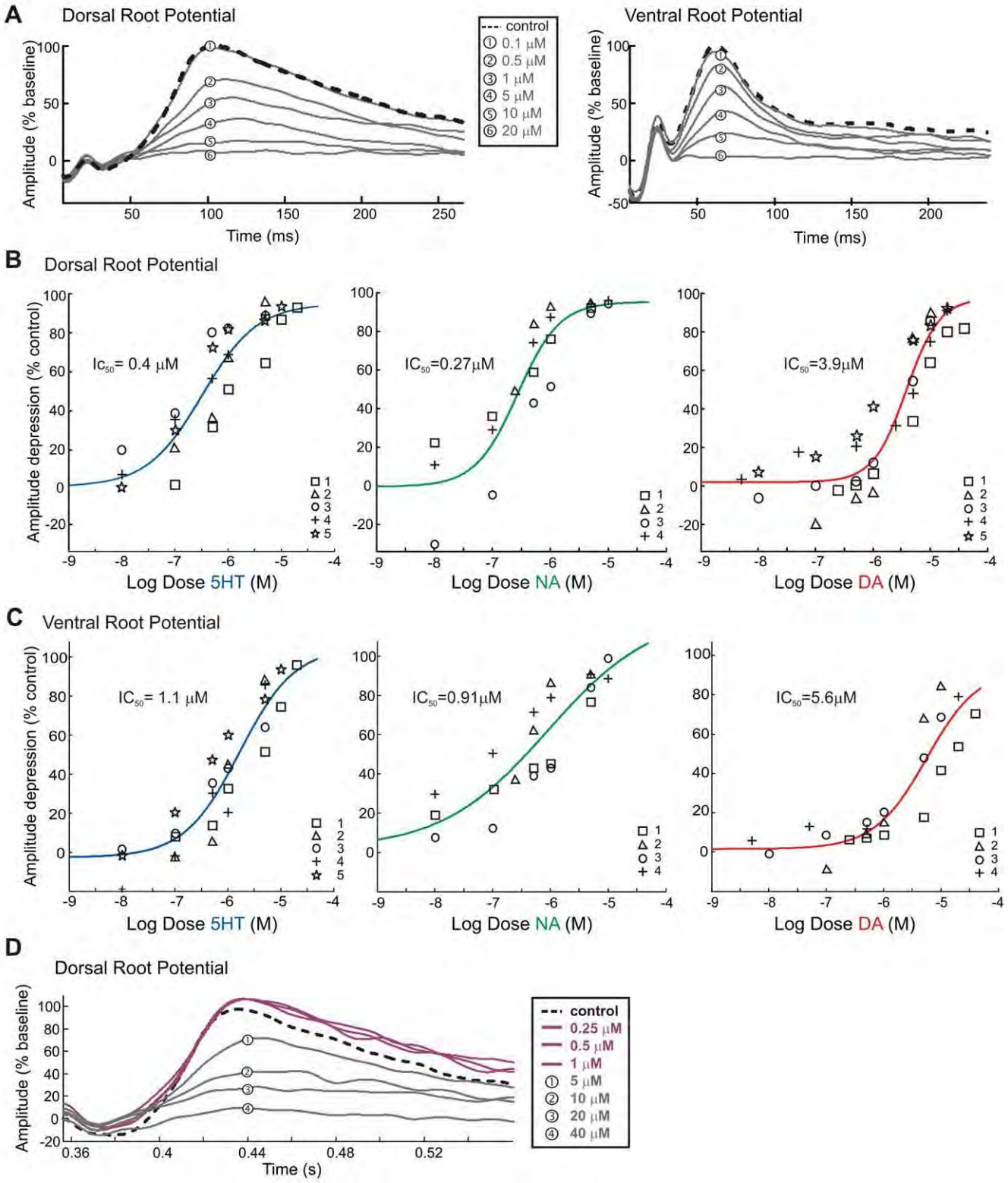

Figure 9. Dose-dependent actions on splanchnic evoked dorsal and ventral root potentials. A. Sample of dorsal root potentials (left) and ventral root potentials (right) evoked by splanchnic nerve stimulation. Each trace is the mean, normalized, and filtered trace of 5 sweeps for each dose increment, after 5 minutes of drug application. Control trace is dashed and other traces are number coded to corresponding dosage. B &C. Dose response curves for 5HT, NA, and DA, with each trial a distinct marker. Amplitude depression is shown as a % of control values for dorsal root (B) and ventral root (C) peak values. Line is a best fit dose-response equation to all data points, IC_{50} value is the dose at which the evoked response is half the control value. Note 10 fold increase in IC_{50} values between NA and DA for DRP depression. D. Sample dorsal root potentials for DA application. Control trace is dashed. Magenta traces denote low doses of DA which facilitated the DRP. Facilitation at low doses was seen in 3/5 trials. Numbers are coded to corresponding higher doses.

doi:10.1371/journal.pone.0047213.g009

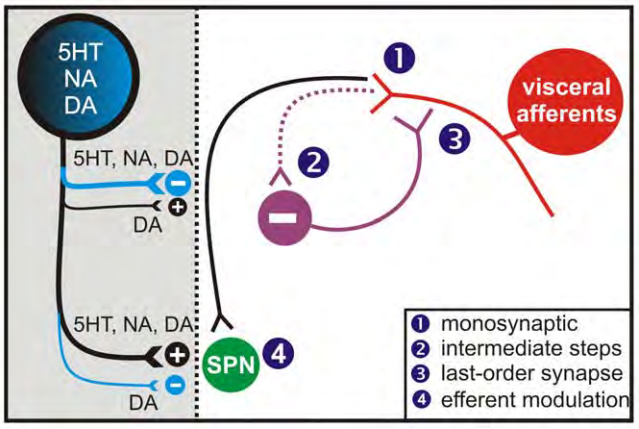

Figure 10. Potential sites of action of monoamines. 5-HT, NA and DA may exert actions on one or many of the following locations: 1) presynaptically directly inhibiting afferent transmission to the spinal cord, 2) inhibiting synaptic transmission to putative interneurons or altering their excitability so that fewer are recruited to produce PAD, or 3) inhibiting last order GABAergic transmission to the afferents producing PAD. 4) Monoamines also usually act to increase SPN excitability.
doi:10.1371/journal.pone.0047213.g010

[49,51,52,86]. Similarly, mixed DA responses on membrane potential were reported previously in the neonatal rat [48], while opposite actions on SPN firing have been reported in the adult rat [87] and cat [88].

Given the generally increased excitability of sympathetic efferents (SPNs) produced by the monoamines but decreased sensory-evoked efferent responses, the monoamines appear to modulate SPN activity away from sensory control, thereby shifting the influence of sympathetic function toward centrally driven events. As we also showed that this trend occurs in a dose-dependent manner, the strength of descending monoaminergic modulatory drives presumably shape the physiological level of afferent influence, as explored further below.

Dorsal Root Potentials and Primary Afferent Depolarization

Splanchnic and sympathetic chain stimulation produced a DRP, a measure of PAD, in dorsal roots of multiple thoracic spinal segments. The measured DRP duration was comparable to that reported previously after the stimulation of muscle and cutaneous afferents (e.g. [33,67,89]). These DRPs were also abolished by bicuculline as similarly observed in cutaneous and muscle afferent evoked DRPs, supporting PAD as mediated by last-order GABAergic interneurons ([32,33]; but see [33]).

The average latency to DRP onset of visceral-afferent evoked responses occurred much later than those reported in response to low threshold segmental afferent stimulation [68,78], here being greater than 30 ms after the first afferent volley was detected. Visceral afferent evoked DRPs have also been reported to occur much later than the shortest latency responses observed following cutaneous afferent stimulation [36]. As these DRPs also occurred ~20 ms after VRPs were recorded in our preparation, distinct afferent populations and/or distinct last-order interneuronal populations are implicated in their occurrence. Multi-segmental longer-latency DRPs have been observed previously with dorsal root stimulation [65], and it is conceivable that the long-latency visceral afferent-evoked DRPs seen presently converges onto a common set of interneurons. In contrast, both cutaneous and muscle afferent-evoked PAD are well known to utilize much shorter latency pathways [68,90]. Short-latency cutaneous and muscle afferent pathways may be required for greater temporal and spatial resolution as well as local negative feedback control mechanisms not as relevant to the control of visceral afferent signaling.

Visceral Afferent-evoked Field Potentials

EFPs were recorded to investigate the modulation of visceral afferent synaptic transmission in the spinal cord. Tracking experiments identified maximal responses in the deep dorsal horn, consistent with the location of spinal neurons activated by visceral afferents in the cat and rat [12,19] as well as anatomical labeling studies of visceral afferent projections in the spinal cord [10,15]. While the earliest measured EFP onset was 4.5 ms, consistent with monosynaptic transmission [91], latencies were highly variable, averaging 13 ms. Such longer latencies may reflect di- or tri-synaptic actions. Alternatively, as components of the afferent volley could spread over many milliseconds (e.g. Figure 7) longer-latency EFPs may instead arise monosynaptically from afferents with slower conduction velocities. Further studies that use approaches to identify monosynaptic actions are warranted [68]. Regardless, given that the observed monoaminergic depressant actions occurred uniformly on evoked EFPs regardless of latency, observed actions can be conservatively interpreted as at least partly reflecting modulation of afferent monosynaptic transmission onto first-order interneurons in the deep dorsal horn.

Modulation of Dorsal Root Potentials, Intraspinal Field Potentials and Dorsal Root Reflexes

The monoamines are known have differentiable depressant actions on somatic afferent interneuronal pathways [38,39], but the modulatory actions of 5HT, NA, and DA on spinal visceral afferent processing is not well known. The reduction in population excitatory postsynaptic potentials ($\downarrow$EFP) produced by the monoamines support a depression of visceral afferent input. This interpretation is consistent with previous work showing that the monoamines generally depress afferent-evoked monosynaptic transmission to individual neurons in the deep dorsal horn [37]. Depressed afferent transmission is consistent with the concomitantly observed reduction in reflex/VRP efferent responses.

Assuming observed EFPs reflect transmission at the first synapse in interneuronal pathways that generate the DRP (our measure of PAD), a reduction in the EFP would lead to a reduced DRP amplitude. This highlights the need for caution in interpreting reductions in the DRP as a reduction in presynaptic inhibition via depression of the interneuronal populations producing PAD. Here, the visceral-afferent evoked DRP was strongly depressed by the 5HT, NA, and DA, with IC_{50} values of 0.33, 0.27, and 3.9 μM, respectively. If the DRP reduction is an expression of PAD-evoked presynaptic inhibition, this effect suggests that descending monoaminergic systems strengthen visceral afferent evoked responses by reducing presynaptic inhibition. On the other hand, if the DRP reduction is due simply to reduced transmission in the stimulated afferents, then the conclusion is that descending monoamines serve to weaken afferent actions. In separate unpublished studies, evidence for depression of the DRP independent of afferent transmission was seen in response to muscle and cutaneous afferent stimulation [69,92].

In the present study, the observed EFP results clearly support monoamine depressant modulatory actions at incoming afferent synapses. Evidence of additional distinct depressant actions on downstream interneurons that lead to the production of PAD is supported by two observations (Figure 8). First, the EFP recovered

from depression after washout faster than did the DRP, implying the delayed DRP recovery was due to a temporally slower recovery in the PAD producing synapses. Second, at least for 5HT, the DRP was more strongly depressed than the EFP, suggesting additional modulatory actions on PAD producing synapses.

Overall then, it appears that the monoamines modify spinal processing of visceral afferent input in at least two ways: 1) decreasing visceral afferent transmission to the spinal cord ($\downarrow$ EFP) and 2) increasing repetitive synaptic actions by limiting PAD-mediated presynaptic inhibition ($\downarrow$ DRP). Differentiable sites of action with apparent opposite physiological consequence require more detailed studies to fully understand, but need not be dichotomous. For example, a reduction in primary afferent transmission ($\downarrow$ EFP) would reduce the influence of tonic low-frequency afferent activity on spinal circuits, while a reduced interneuronal activity-dependent presynaptic inhibition ($\downarrow$ DRP) would support a comparative facilitation of transmission during periods of higher frequency afferent activity.

Under control conditions evoked DRPs were usually of sufficient magnitude to recruit backward-propagating dorsal root reflexes. The monoamines 5HT, NA, and DA not only greatly depressed DRPs; they consequently also blocked the accompanying dorsal root reflexes. Dorsal root reflexes produce back-propagating spikes and can lead to peripherally-released neuromodulators (e.g. CGRP) and/or other signaling molecules that alter organ function and blood flow [93,94]. The monoamines may therefore also play a role in reducing peripheral sensitization via a depression of dorsal root reflexes. Further study is needed to assess this intriguing control of sensory actions at their peripheral endings by descending modulatory systems.

Putative Sites of Action

As there are many monoaminergic receptor subtypes present in spinal neurons and primary afferents (see [95] for review), the monoamines can affect neuronal function by activating metabotropic receptors (and ionotropic for $5HT_3$) that both modulate ion channels directly and/or modulate common signal transduction pathways (e.g. [96,97]). Observed similarities and differences in action between the monoamines at a given site could thus be based on the complement of receptors expressed. For example, $5HT_1$, $D_{2\text{-like}}$ and α_2 receptors are all G_i-coupled, and co-localization of these receptors at the same site may lead to comparable actions. Differing receptor expression patterns, actions on different signal transduction pathways, or dose-dependent differences in receptor affinity would be expected to lead to more complex actions. One such difference was observed with DA, where lower doses could facilitate the DRP while larger doses were depressant. Indeed, different DA receptors having different affinity has been shown in the pre-frontal cortex, where low doses of DA preferentially produce actions via $D_{1\text{-like}}$ receptors and higher doses of DA masked these effects by activation of $D_{2\text{-like}}$ receptors [98,99].

While a determination of receptor subtype identity and their specific sites of action is well beyond the scope of the present study, a schematic of these potential locations is conceptually instructive and shown in Figure 10. The site of modulation may therefore be: (1) presynaptically, by directly inhibiting afferent transmission to the spinal cord, (2) postsynaptically, inhibiting synaptic transmission or altering the excitability of interposed interneurons so that fewer are recruited to produce PAD, (3) inhibiting transmission of the last-order interneurons producing PAD, and/or (4) directly on SPNs to alter efferent excitability.

In summary, this work combined used of a novel *in vitro* spinal cord/sympathetic chain preparation with cellular studies of SPNs in a slice preparation to demonstrate that the monoamines all broadly act to facilitate sympathetic efferent activity while simultaneously suppressing visceral afferent evoked actions. These results lay the foundation for subsequent studies on central sites of action as well as studies on the behavioral relevance of such wide-ranging modulatory actions on the spinal autonomic nervous system.

Author Contributions

Conceived and designed the experiments: ALZ SH. Performed the experiments: ALZ MS SH. Analyzed the data: ALZ. Contributed reagents/materials/analysis tools: ALZ SH. Wrote the paper: ALZ SH.

References

1. Jänig W (1996) Neurobiology of visceral afferent neurons: neuroanatomy, functions, organ regulations and sensations. Biological Psychology 42: 29–51.
2. Bain WA, Irving JT, McSwiney BA (1935) The afferent fibres from the abdomen in the splanchnic nerves. The Journal of Physiology 84: 323–333.
3. Berthoud HR, Neuhuber WL (2000) Functional and chemical anatomy of the afferent vagal system. Autonomic Neuroscience 85: 1–17.
4. Cervero F (1985) Visceral Nociception: Peripheral and Central Aspects of Visceral Nociceptive Systems. Philos Trans R Soc Lond B Biol Sci 308: 325–337.
5. Vera PL, Nadelhaft I (2000) Anatomical evidence for two spinal 'afferent-interneuron-efferent' reflex pathways involved in micturition in the rat: a 'pelvic nerve' reflex pathway and a 'sacrolumbar intersegmental' reflex pathway. Brain Research 883: 107–118.
6. Cabot JB, Alessi V, Carroll J, Ligorio M (1994) Spinal cord lamina V and lamina VII interneuronal projections to sympathetic preganglionic neurons. The Journal of Comparative Neurology 347: 515–530.
7. Buéno L, Fioramonti J, Garcia-Villar R (2000) III. Visceral afferent pathways: a source of new therapeutic targets for abdominal pain. Am J Physiol Gastrointest Liver Physiol 278: G670–G676.
8. Ness TJ, Gebhart GF (1990) Visceral pain: a review of experimental studies. Pain 41: 167–234.
9. Danzebrink RM, Gebhart GF (1990) Antinociceptive effects of intrathecal adrenoceptor agonists in a rat model of visceral nociception. Journal of Pharmacology and Experimental Therapeutics 253: 698–705.
10. Neuhuber WL, Sandoz PA, Fryscak T (1986) The central projections of primary afferent neurons of greater splanchnic and intercostal nerves in the rat. Anatomy and Embryology 174: 123–144.
11. Kuo DC, Yang GCH, Yamasaki DS, Krauthamer GM (1982) A wide field electron microscopic analysis of the fiber constituents of the major splanchnic nerve in cat. The Journal of Comparative Neurology 210: 49–58.
12. Akeyson EW, Schramm LP (1994) Processing of splanchnic and somatic input in thoracic spinal cord of the rat. Am J Physiol Regul Integr Comp Physiol 266: R257–R267.
13. Cervero F, Connell LA, Lawson SN (1984) Somatic and visceral primary afferents in the lower thoracic dorsal root ganglia of the cat. The Journal of Comparative Neurology 228: 422–431.
14. Downman CBB, Evans MH (1957) The distribution of splanchnic afferents in the spinal cord of cat. The Journal of Physiology 137: 66–79.
15. Cervero F, Connell LA (1984) Distribution of somatic and visceral primary afferent fibres within the thoracic spinal cord of the cat. The Journal of Comparative Neurology 230: 88–98.
16. Sugiura Y, Terui N, Hosoya Y (1989) Difference in distribution of central terminals between visceral and somatic unmyelinated (C) primary afferent fibers. Journal of Neurophysiology 62: 834–840.
17. Sugiura Y, Terui N, Hosoya Y, Tonosaki Y, Nishiyama K, et al. (1993) Quantitative analysis of central terminal projections of visceral and somatic unmyelinated (C) primary afferent fibers in the guinea pig. The Journal of Comparative Neurology 332: 315–325.
18. Downman CB (1955) Skeletal muscle reflexes of splanchnic and intercostal nerve origin in acute spinal and decerebrate cats. Journal of Neurophysiology 18: 217–235.
19. Tattersall JE, Cervero F, Lumb BM (1986) Viscerosomatic neurons in the lower thoracic spinal cord of the cat: excitations and inhibitions evoked by splanchnic and somatic nerve volleys and by stimulation of brain stem nuclei. Journal of Neurophysiology 56: 1411–1423.

20. Albano JP, Garnier L (1983) Bulbo-spinal respiratory effects originating from the splanchnic afferents. Respiration Physiology 51: 229–239.
21. Franz D, Evans M, Perl E (1966) Characteristics of viscerosympathetic reflexes in the spinal cat. American Journal of Physiology – Legacy Content 211: 1292–1298.
22. Bell JA, Matsumiya T (1981) Inhibitory effects of dorsal horn and excitant effects of ventral horn intraspinal microinjections of norepinephrine and serotonin in the cat. Life Sciences 29: 1507–1514.
23. Madden CJ, Morrison SF (2008) Brown adipose tissue sympathetic nerve activity is potentiated by activation of 5-hydroxytryptamine (5-HT)1A/5-HT7 receptors in the rat spinal cord. Neuropharmacology 54: 487–496.
24. Madriaga MA, McPhee LC, Chersa T, Christie KJ, Whelan PJ (2004) Modulation of Locomotor Activity by Multiple 5-HT and Dopaminergic Receptor Subtypes in the Neonatal Mouse Spinal Cord. Journal of Neurophysiology 92: 1566–1576.
25. Pertovaara A (1993) Antinociception induced by alpha-2-adrenoceptor agonists, with special emphasis on medetomidine studies. Progress in Neurobiology 40: 691–709.
26. Schotland J, Shupliakov O, Wikstrom M, Brodin L, Srinivasan M, et al. (1995) Control of lamprey locomotor neurons by colocalized monoamine transmitters. Nature 374: 266–268.
27. Sillar KT, Reith CA, McDearmid JR (1998) Development and Aminergic Neuromodulation of a Spinal Locomotor Network Controlling Swimming in Xenopus Larvaea. Annals of the New York Academy of Sciences 860: 318–332.
28. Gordon IT, Whelan PJ (2006) Monoaminergic Control of Cauda-Equina-Evoked Locomotion in the Neonatal Mouse Spinal Cord. Journal of Neurophysiology 96: 3122–3129.
29. McPherson DR, Kemnitz CP (1994) Modulation of lamprey fictive swimming and motoneuron physiology by dopamine, and its immunocytochemical localization in the spinal cord. Neuroscience Letters 166: 23–26.
30. Danzebrink RM, Gebhart GF (1991) Evidence that spinal 5-HT1, 5-HT2 and 5-HT3 receptor subtypes modulate responses to noxious colorectal distension in the rat. Brain Research 538: 64–75.
31. Wu HC, Chiu CH, Tung KC, Chen GD, Peng HY, et al. (2010) Dopaminergic D2 receptors activate PKA to inhibit spinal pelvic-urethra reflex in rats. American Journal of Physiology - Renal Physiology 299: F681–F686.
32. Rudomin P, Schmidt RF (1999) Presynaptic inhibition in the vertebrate spinal cord revisited. Experimental Brain Research 129: 1–37.
33. Hochman S, Shreckengost J, Kimura H, Quevedo J (2010) Presynaptic inhibition of primary afferents by depolarization: observations supporting nontraditional mechanisms. Annals of the New York Academy of Sciences 1198: 140–152.
34. Khasabov SG, Lopez-Garcia JA, Asghar AUR, King AE (1999) Modulation of afferent-evoked neurotransmission by 5-HT3 receptors in young rat dorsal horn neurones in vitro: a putative mechanism of 5-HT3 induced anti-nociception. British Journal of Pharmacology 127: 843–852.
35. Bardoni R, Torsney C, Tong CK, Prandini M, MacDermott AB (2004) Presynaptic NMDA Receptors Modulate Glutamate Release from Primary Sensory Neurons in Rat Spinal Cord Dorsal Horn. The Journal of Neuroscience 24: 2774–2781.
36. Selzer M, Spencer WA (1969) Interactions between visceral and cutaneous afferents in the spinal cord: Reciprocal primary afferent fiber depolarization. Brain Research 14: 349–366.
37. Garraway SM, Hochman S (2001) Modulatory Actions of Serotonin, Norepinephrine, Dopamine, and Acetylcholine in Spinal Cord Deep Dorsal Horn Neurons. Journal of Neurophysiology 86: 2183–2194.
38. Jankowska E, Hammar I, Chojnicka B, Hedén CH (2000) Effects of monoamines on interneurons in four spinal reflex pathways from group I and/or group II muscle afferents. European Journal of Neuroscience 12: 701–714.
39. Bras H, Cavallari P, Jankowska E, McCrea D (1989) Comparison of effects of monoamines on transmission in spinal pathways from group I and II muscle afferents in the cat. Experimental Brain Research 76: 27–37.
40. Fleetwood-Walker SM, Mitchell R, Hope PJ, Molony V, Iggo A (1985) An [alpha]2 receptor mediates the selective inhibition by noradrenaline of nociceptive responses of identified dorsal horn neurones. Brain Research 334: 243–254.
41. Petras JM, Cummings JF (1972) Autonomic neurons in the spinal cord of the rhesus monkey: A correlation of the findings of cytoarchitectonics and sympathectomy with fiber degeneration following dorsal rhizotomy. The Journal of Comparative Neurology 146: 189–218.
42. Anderson CR, McLachlan EM, Srb-Christie O (1989) Distribution of sympathetic preganglionic neurons and monoaminergic nerve terminals in the spinal cord of the rat. The Journal of Comparative Neurology 283: 269–284.
43. Fleetwood-Walker SM, Coote JH (1981) Contribution of noradrenaline-, dopamine- and adrenaline-containing axons to the innervation of different regions of the spinal cord of the cat. Brain Research 206: 95–106.
44. Milner TA, Morrison SF, Abate C, Reis DJ (1988) Phenylethanolamine N-methyltransferase-containing terminals synapse directly on sympathetic preganglionic neurons in the rat. Brain Research 448: 205–222.
45. Björklund A, Skagerberg G (1979) Evidence for a major spinal cord projection from the diencephalic A11 dopamine cell group in the rat using transmitter-specific fluorescent retrograde tracing. Brain Research 177: 170–175.
46. Westlund KN, Bowker RM, Ziegler MG, Coulter JD (1983) Noradrenergic projections to the spinal cord of the rat. Brain Research 263: 15–31.
47. Lewis DI, Sermasi E, Coote JH (1993) Excitatory and indirect inhibitory actions of 5-hydroxytryptamine on sympathetic preganglionic neurones in the neonate rat spinal cord in vitro. Brain Research 610: 267–275.
48. Gladwell SJ, Coote JH (1999) Inhibitory and indirect excitatory effects of dopamine on sympathetic preganglionic neurones in the neonatal rat spinal cord in vitro. Brain Research 818: 397–407.
49. Yoshimura M, Polosa C, Nishi S (1987) Slow EPSP and the depolarizing action of noradrenaline on sympathetic preganglionic neurons. Brain Research 414: 138–142.
50. Pickering AE, Spanswick D, Logan SD (1994) 5-Hydoxytryptamine evokes depolarizations and membrane potential oscillations in rat sympathetic preganglionic neurones. The Journal of Physiology 480: 109–121.
51. Inokuchi H, Yoshimura M, Polosa C, Nishi S (1992) Adrenergic receptors (alpha 1 and alpha 2) modulate different potassium conductances in sympathetic preganglionic neurons. Can J Physiol Pharmacol 70: S92–97.
52. Yoshimura M, Polosa C, Nishi S (1987) Slow IPSP and the noradrenaline-induced inhibition of the cat sympathetic preganglionic neuron in vitro. Brain Research 419: 383–386.
53. Guyenet PG, Cabot JB (1981) Inhibition of sympathetic preganglionic neurons by catecholamines and clonidine: mediation by an alpha-adrenergic receptor. Journal of Neuroscience 1: 908–917.
54. Zimmerman AL, Hochman S (2010) Heterogeneity of membrane properties in sympathetic preganglionic neurons of neonatal mice: Evidence of four subpopulations in the intermediolateral nucleus. Journal of Neurophysiology 103: 490–498.
55. Sandkühler J, Chen JG, Cheng G, Randić M (1997) Low-frequency stimulation of afferent Aδ-fibers induces long-term depression at primary afferent synapses with substantia gelatinosa neurons in the rat. The Journal of Neuroscience 17: 6483–6491.
56. Chesnoy-Marchais D, Barthe J (1996) Voltage-dependent block of NMDA responses by 5-HT agonists in ventral spinal cord neurones. British Journal of Pharmacology 117.1 133–141.
57. Ammons WS, Blair RW, Foreman RD (1984) Greater splanchnic excitation of primate T1–T5 spinothalamic neurons. Journal of Neurophysiology 51: 592–603.
58. Molander C, Ygge J, Dalsgaard CJ (1987) Substance P-, somatostatin- and calcitonin gene-related peptide-like immunoreactivity and fluoride resistant acid phosphatase-activity in relation to retrogradely labeled cutaneous, muscular and visceral primary sensory neurons in the rat. Neuroscience Letters 74: 37–42.
59. Kashiba H, Senba E, Ueda Y, Tohyama M (1991) Cell size and cell type analysis of calcitonin gene-related peptide-containing cutaneous and splanchnic sensory neurons in the rat. Peptides 12: 101–106.
60. Jänig W (2006) The integrative action of the autonomic nervous system: neurobiology of homeostasis. New York: Cambridge University Press.
61. Wilson JM, Hartley R, Maxwell DJ, Todd AJ, Lieberam I, et al. (2005) Conditional Rhythmicity of Ventral Spinal Interneurons Defined by Expression of the Hb9 Homeodomain Protein. Journal of Neuroscience 25: 5710–5719.
62. Sharkey KA, Sobrino JA, Cervero F, Varro A, Dockray GJ (1989) Visceral and somatic afferent origin of calcitonin gene-related peptide immunoreactivity in the lower thoracic spinal cord of the rat. Neuroscience 32: 169–179.
63. Biscoe TJ, Nickels SM, Stirling CA (1982) Numbers and sizes of nerve fibres in mouse spinal roots. Experimental Physiology 67: 473–494.
64. Low PA, Dyck PJ (1977) Splanchnic preganglionic neurons in man: II. Morphometry of myelinated fibers of T7 ventral spinal root. Acta Neuropathologica 40: 219–225.
65. Lidierth M (2006) Local and diffuse mechanisms of primary afferent depolarization and presynaptic inhibition in the rat spinal cord. The Journal of Physiology 576: 309–327.
66. Jankowska E, Riddell JS (1995) Interneurones mediating presynaptic inhibition of group II muscle afferents in the cat spinal cord. The Journal of Physiology 483: 461–471.
67. Riddell JS, Jankowska E, Huber J (1995) Organization of neuronal systems mediating presynaptic inhibition of group II muscle afferents in the cat. The Journal of Physiology 483: 443–460.
68. Shreckengost J, Calvo J, Quevedo J, Hochman S (2010) Bicuculline-sensitive primary afferent depolarization remains after greatly restricting synaptic transmission in the mammalian spinal cord. The Journal of Neuroscience 30: 5283–5288.
69. Calvo JR, Hernandez-Rodriguez M, Hochman S, Quevedo JN (2006) Monoaminergic modulation of pathways mediating sensory-evoked pad in the hemisected spinal cord of the mouse Soc Neurosci Abstr Vol 32.
70. Takahashi T (1992) The minimal inhibitory synaptic currents evoked in neonatal rat motoneurones. The Journal of Physiology 450: 593–611.
71. Jonas P, Bischofberger J, Sandkuhler J (1998) Corelease of two fast neurotransmitters at a central synapse. Science 281: 419.
72. Lopez-Garcia JA, King AE (1996) Pre- and post-synaptic actions of 5-hydroxytryptamine in the rat lumbar dorsal horn in vitro: implications for somatosensory Transmission. European Journal of Neuroscience 8: 2188–2197.
73. Lew WY, Longhurst JC (1986) Substance P, 5-hydroxytryptamine, and bradykinin stimulate abdominal visceral afferents. Am J Physiol Regul Integr Comp Physiol 250: R465–R473.

74. Bahns E, Ernsberger U, Jänig W, Nelke A (1986) Functional characteristics of lumbar visceral afferent fibres from the urinary bladder and the urethra in the cat. Pflügers Arch 407: 510–518.
75. Angel MJ, Fyda D, McCrea DA, Shefchyk SJ (1994) Primary afferent depolarization of cat pudendal afferents during micturition and segmental afferent stimulation. The Journal of Physiology 479: 451–461.
76. Buss RR, Shefchyk SJ (1999) Excitability changes in sacral afferents innervating the urethra, perineum and hindlimb skin of the cat during micturition. The Journal of Physiology 514: 593–607.
77. Franks NP, Lieb WR (1994) Molecular and cellular mechanisms of general anaesthesia. Nature 367: 607–614.
78. Eccles JC, Schmidt R, Willis WD (1963) Pharmacological studies on presynaptic inhibition. The Journal of Physiology 168: 500–530.
79. King BF, Szurszewski JH (1989) Peripheral reflex pathways involving abdominal viscera: transmission of impulses through prevertebral ganglia. Am J Physiol Gastrointest Liver Physiol 256: G581–G588.
80. Quigg M, Elfvin LG, Aldskogius H (1990) Anterograde transsynaptic transport of WGA-HRP from spinal afferents to postganglionic sympathetic cells of the stellate ganglion of the guinea pig. Brain Research 518: 173–178.
81. Jacobs BL, Fornal CA (1993) 5-HT and motor control: a hypothesis. Trends in Neurosciences 16: 346–352.
82. Berridge CW, Waterhouse BD (2003) The locus coeruleus–noradrenergic system: modulation of behavioral state and state-dependent cognitive processes. Brain Research Reviews 42: 33–84.
83. Sah P, McLachlan EM (1995) Membrane properties and synaptic potentials in rat sympathetic preganglionic neurons studied in horizontal spinal cord slices in vitro. Journal of the Autonomic Nervous System 53: 1–15.
84. Ma RC, Dun NJ (1986) Excitation of lateral horn neurons of the neonatal rat spinal cord by 5-hydroxytryptamine. Developmental Brain Research 24: 89–98.
85. Gilbey MP, Stein RD (1991) Characteristics of sympathetic preganglionic neurones in the lumbar spinal cord of the cat. J Physiol 432: 427–443.
86. Miyazaki T, Coote JH, Dun NJ (1989) Excitatory and inhibitory effects of epinephrine on neonatal rat sympathetic preganglionic neurons in vitro. Brain Research 497: 108–116.
87. Lewis DI, Coote JH (1990) Excitation and inhibition of rat sympathetic preganglionic neurones by catecholamines. Brain Research 530: 229–234.
88. Coote JH, Macleod VH, Fleetwood-Walker S, Gilbey MP (1981) The response of individual sympathetic preganglionic neurones to microelectrophoretically applied endogenous monoamines. Brain Research 215: 135–145.
89. Eccles JC, Schmidt RF, Willis WD (1962) Presynaptic inhibition of the spinal monosynaptic reflex pathway. The Journal of Physiology 161: 282–297.
90. Bannatyne BA, Liu TT, Hammar I, Stecina K, Jankowska E, et al. (2009) Excitatory and inhibitory intermediate zone interneurons in pathways from feline group I and II afferents: differences in axonal projections and input. The Journal of Physiology 587: 379–399.
91. Takahashi T (1992) The minimal inhibitory synaptic currents evoked in neonatal rat motoneurones. Journal of Physiology 450: 593–611.
92. Calvo JR, Hochman S, Quevedo JN (2008) Modulation of sensory-evoked field potentials by monoamines in the hemisect spinal cord of the mouse. Soc Neurosci Abstr 34.
93. Holzer P (1998) Neurogenic vasodilatation and plasma leakage in the skin. General Pharmacology 30: 5–11.
94. Willis Jr WD (1999) Dorsal root potentials and dorsal root reflexes: a double-edged sword. Experimental Brain Research 124: 395–421.
95. Millan MJ (2002) Descending control of pain. Progress in Neurobiology 66: 355–474.
96. Eisenach JC, Zhang Y, Duflo F (2005) [alpha]2-adrenoceptors inhibit the intracellular Ca2+ response to electrical stimulation in normal and injured sensory neurons, with increased inhibition of calcitonin gene-related peptide expressing neurons after injury. Neuroscience 131: 189–197.
97. Formenti A, Martina M, Plebani A, Mancia M (1998) Multiple modulatory effects of dopamine on calcium channel kinetics in adult rat sensory neurons. The Journal of Physiology 509: 395–409.
98. Zheng P, Zhang XX, Bunney BS, Shi WX (1999) Opposite modulation of cortical N-methyl–aspartate receptor-mediated responses by low and high concentrations of dopamine. Neuroscience 91: 527–535.
99. Trantham-Davidson H, Neely LC, Lavin A, Seamans JK (2004) Mechanisms underlying differential D1 versus D2 dopamine receptor regulation of inhibition in prefrontal cortex. The Journal of Neuroscience 24: 10652–10659.

[Frontiers in Bioscience 17, 2158-2180, June 1, 2012]

Enabling techniques for *in vitro* studies on mammalian spinal locomotor mechanisms

Shawn Hochman[1,2], Elizabeth A. Gozal[1], Heather B. Hayes[3], JoAnna T. Anderson[2], Stephen P. DeWeerth[2], Young-Hui Chang[4]

[1]Department of Physiology, Emory University School of Medicine, Atlanta, Georgia, [2]Department of Biomedical Engineering, Georgia Institute of Technology and Emory University, Atlanta, Georgia, [3]Center for Rehabilitation Medicine, Emory University School of Medicine, Atlanta, Georgia, [4]School of Applied Physiology, Georgia Institute of Technology, Atlanta, Georgia

TABLE OF CONTENTS

1. ABSTRACT

The neonatal rodent spinal cord maintained *in vitro* is a powerful model system to understand the central properties of spinal circuits generating mammalian locomotion. We describe three enabling approaches that incorporate afferent input and attached hindlimbs. (i) Sacral dorsal column stimulation recruits and strengthens ongoing locomotor-like activity, and implementation of a closed positive-feedback paradigm is shown to support its stimulation as an untapped therapeutic site for locomotor modulation. (ii) The spinal cord hindlimbs-restrained preparation allows suction electrode electromyographic recordings from many muscles. Inducible complex motor patterns resemble natural locomotion, and insights into circuit organization are demonstrated during spontaneous motor burst 'deletions', or following sensory stimuli such as tail and paw pinch. (iii) The spinal cord hindlimbs-pendant preparation produces unrestrained hindlimb stepping. It incorporates mechanical limb perturbations, kinematic analyses, ground reaction force monitoring, and the use of treadmills to study spinal circuit operation with movement-related patterns of sensory feedback while providing for stable whole-cell recordings from spinal neurons. Such techniques promise to provide important additional insights into locomotor circuit organization.

2. INTRODUCTION

Locomotion is defined as the act of moving from one place to another, and sufficient complexity in neural circuit operations is needed to allow for the range of locomotor behaviors observed. Limbed vertebrates must coordinate limb and trunk musculature to achieve smooth movements that integrate with postural and cardiorespiratory activity. The circuitry required for generating mammalian (and lower vertebrate) locomotor activity resides in the spinal cord (1), and many reviews consider its organization (e.g. (2-9)). Locomotor central pattern generators (CPGs) consist of sets of interconnected neurons that can generate rhythmical output patterns in the absence of phasic input. A fundamental CPG output for limbed locomotion comprises a 'half-center' alternation between flexors and extensors in a single limb and left-right alternation in flexors and extensors between limbs. It is thought that the CPG may be composed of multiple units, such as series of unit burst oscillators which can be flexibly coupled to produce different behaviors (2, 10) or a multi-level hierarchical structure with one level responsible for setting the timing (rhythm generator) and the pattern (pattern generators) (6). Several schematics have been drawn to explain experimental findings (e.g. (2, 11-16) including recent computational models by Rybak, McCrea

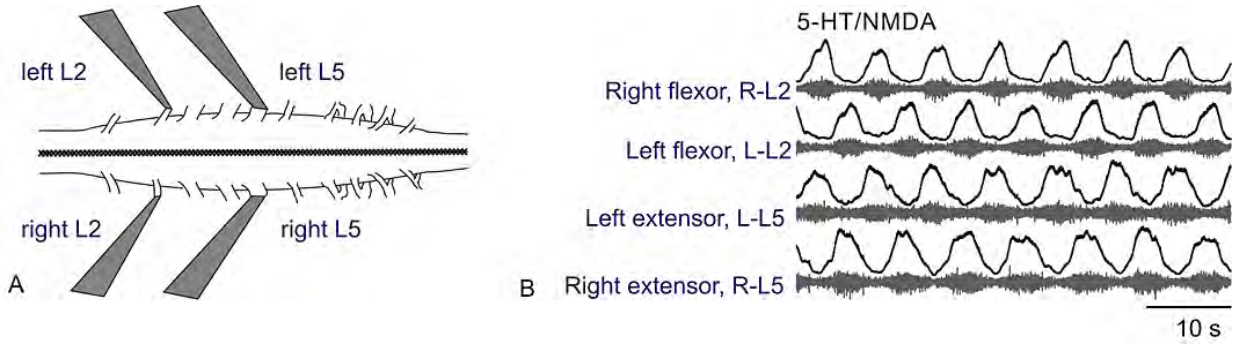

Figure 1. Experimental setup. (a) For *in vitro* studies on locomotor-like motor rhythms, suction electrodes are placed on lumbar L2 and L5 ventral roots bilaterally to monitor population motoneuron flexor and extensor activity. Drugs are applied to the bath. (b) Example of locomotor-like activity. Locomotor-like activity (LLA) is recruited with the addition of various neurochemicals with the combination of NMDA and 5-HT being the most common and illustrated here. Activity recorded from L2 ventral roots typically report flexor motoneuron activity while L5 ventral roots predominantly reflect extensor motoneuron activity. Rectified and low-pass filtered (top record) and raw records are displayed for each root recording.

and colleagues based on hypothesized half-center dynamics of a single cat hindlimb during locomotion (6, 17-19). Below, we explore the *in vitro* neonatal rodent (rat and mouse) spinal cord preparation as a model system to study properties of mammalian locomotion and the underlying circuitry. We provide a MATLAB-based code to analyze important measures of locomotor circuit operation. We then focus on experimental approaches that emphasize the contribution of sensory feedback and the importance of keeping hindlimbs attached.

2.1. The neonatal rodent spinal cord maintained *in vitro* for studies on locomotion

In mouse and rat, locomotor CPGs are present at birth and the spinal cord can be isolated from the brain and maintained *in vitro* (20). When activated by neurochemicals or electrical stimulation, the isolated spinal cord preparation produces a motor pattern consistent with locomotion that can be measured by using suction electrodes on ventral motor nerve roots or recordings from hindlimb muscles (21). While the full locomotor repertoire does not mature until a few weeks postnatal in rat (22), when the hindlimbs are left intact, the isolated spinal cord can produce limb kinematics and muscle activity patterns that are remarkably comparable to those seen in the adult (23-27). The greatest similarity to the adult requires specific afferent feedback, without which the pattern may more closely reflect a neonatal air-stepping pattern (23). One obvious difference between the adult and *in vitro* neonatal cord preparation, however, is in frequency, with those in the neonate being considerably slower than for adult locomotion *in vivo* (28).

Locomotion studies in the isolated *in vitro* spinal cord (taken at room temperature) afford distinct methodological advantages. Due to its small size, passive diffusion of oxygen in the CO2/bicarbonate buffered artificial cerebrospinal fluid (aCSF) maintains viability for many hours (21), though it is important to consider tissue depth-dependent gradients in pH, P02, and drug concentration (29-31). The extracellular medium can be controlled, and transport of drugs into the cord is not limited by the blood brain barrier, vastly expanding drug choice. The isolated cord also allows easy access for manipulation through global or restricted pharmacology, stimulation, and lesioning. Further, the surgery and electrode placement is relatively simple, and the absence of mechanical cardiorespiratory perturbations allows for stable whole-cell patch clamp recordings (16, 32). Defining the circuitry and function of CPGs in mammals has been greatly aided with the incorporation of complementary genetic approaches to this *in vitro* model. This includes expression-based neuron identification, conditional neuronal knockout/silencing of molecularly distinct cell populations, and optogenetics (3, 4, 7, 33-35).

While numerous bath-applied neuroactive substances can generate a patterned motor output consistent with locomotion, a combination of serotonin (5-HT) and N-methyl-D-aspartate (NMDA) is widely used to generate stable and long-lasting activity patterns consistent with a locomotor rhythm. The motor output recorded from lumbar L2 and L5/L6 ventral roots usually corresponds to activity in flexors and extensors, respectively, (36, 37) with left/right and ipsilateral alternation of bursts between these predominant flexor and extensor-reporting roots (Figure 1)(38, 39). When using the isolated spinal cord preparation the bursting pattern from ventral root neurograms is thought to provide a signature for activation of the locomotor circuitry and is commonly referred to as locomotor-like activity (LLA).

Normally, CPG circuit operation is initiated and controlled by activity in descending systems and/or primary sensory afferents. The intact *in vitro* brainstem-spinal cord preparation permits locomotor circuit activation via descending bulbospinal pathways (40-42). These pathways are clearly of great importance to understanding locomotor circuit operation. Recent *in vitro* studies have incorporated selective stimulation of descending pathways (33, 41), including activity-dependent imaging of recruited spinal neurons (43, 44) that promise to hasten our understanding of bulbospinal circuit function in locomotion.

Afferent activity-based recruitment of spinal locomotor circuits has also been demonstrated in the *in vitro* rodent spinal cord (35, 37, 45-52). However, activity-dependent afferent fatigue, difficulty in afferent fiber modality identification, and the lack of studies on movement-dependent sensory feedback on the operation of locomotor circuits make the study of afferents in the *in vitro* neonatal cord comparatively recalcitrant to detailed characterization (described further in Section 2 below).

Overall, while locomotor studies prior to weight-bearing may represent an inherent weakness of the neonatal *in vitro* model system for some studies (however, see (53)), the circuitry already expresses a mature motor pattern. This, in concert with discussed advantages, has catapulted the system into prominence in studies of mammalian locomotor circuits. Below we highlight enabling approaches and techniques that provide additional opportunities for experimentation in the *in vitro* model system.

2.2. Provision of a MATLAB-based code to analyze important measures of locomotion

To aid in quantifying and comparing rhythmic locomotor patterns, we developed a custom MATLAB® Graphical User Interface (GUI) called SpinalMOD (Spinal Motor Output Detector) for the analysis of LLA (Figure 2A & B). SpinalMOD determines the onset and offset of the bursts to calculate statistics on several variables including cycle period, frequency, burst duration, duty cycle, and phase (Figure 2C). SpinalMOD is a simple yet rather comprehensive single-screen GUI designed for ease of operation. SpinalMOD can open files collected with pCLAMP acquisition software, or files collected elsewhere and exported to appropriate Microsoft Excel formats. Four channels of data can be imported and compared at one time. Once opened, the raw data is rectified and processed through a low-pass filter. The burst threshold is calculated, and a series of IF-THEN logic statements are used for burst detection. This program is used for many of the subsequent analyses, and can be freely downloaded as-is from our website http://userwww.service.emory.edu/~shochm2/main_menu.html).

3. AFFERENT ACTIVITY-BASED RECRUITMENT, MODULATION AND FEEDBACK CONTROL OF LOCOMOTION

3.1. Introduction

Locomotor activity is regulated by ongoing afferent feedback recruited during the behavior (54). How afferent input can alter LLA in the *in vitro* neonatal cord preparation, and how afferent input properties differ from the adult remain an important but under-investigated area. Repetitive stimulation of afferents in sacral or lumbar dorsal roots, or the cauda equina is capable of recruiting LLA in the isolated spinal cord (27, 35, 37, 45-49, 51, 52). In comparison to neurochemical induction of LLA, which can be maintained for epochs of over an hour (55, 56), or to brainstem electrical stimulation-induced locomotion that can last for many minutes (40) afferent electrical stimulation-based recruitment of LLA is typically short-lived. Studies on sensory stimulation-based recruitment of LLA utilize trains of low frequency stimuli (generally less than 5 Hz) to generate an activity that builds up, stabilizes, and then fatigues within about one minute (35, 37, 49, 57, 58). LLA cannot be reinstated by stimulation of the same afferents for over a minute due to a required recovery from fatigue, presumably due to transmitter depletion in afferent terminals in the neonate (48, 59).

The dorsal column is a white matter tract predominantly composed of primary afferents carrying touch, vibration and proprioceptive information as well as information from visceral afferents (60, 61). It issues collaterals as it ascends to influence and possibly recruit, coordinate, and control locomotion. In the adult rat dorsal column, most axons are fast-conducting myelinated Aβ fibers; however, almost one-third of the axons appear to be unmyelinated primary afferents (62). While sacral caudal afferent stimulation is a useful strategy for electrically evoked control of motor circuitry, as a white matter tract, stimulation of the sDC may provide a unique therapeutic opportunity when incorporated into the use of conformable multi-electrode arrays for surface stimulation (63). In support of this proposition, previous studies involving epidural stimulation in humans, cats, and rats implanted wire electrodes on the dorsal surface to activate locomotion, and based on their positioning, these are likely also activating dorsal column pathways (64-67).

3.2. General methods

For the studies in this section, the spinal cords of postnatal day (P) 0-3 rats were isolated and maintained in a static solution of oxygenated aCSF with the dorsal aspect of the cord facing upward. Glass suction electrodes were applied to ventral lumbar roots (L2s and L5s) for recording. For stimulation, glass suction electrodes were applied to a sacral dorsal root, or to the dorsal surface midline region (with ~30 μm tip diameter) of the sacral dorsal column (sDC) between segments S2 and S4. Rhythmic activity was induced with trains of stimuli between 1 and 2 Hz.

3.3. Effects of sacral dorsal column stimulation on activated locomotor-like activity

Figure 3A&B show that electrical stimulation of the sDC recruits afferents that activate the locomotor CPG with properties comparable to that observed following stimulation of sacral dorsal roots (e.g. (37, 47)). Figure 3B and subsequent panels are shown following stimulus artifact removal (a feature provided in SpinalMOD). Note that recruitment of alternating L2 ventral root activity does not necessarily couple to comparable activity in L5 ventral roots and so may not always recruit a full locomotor pattern. The observed fatigue can be overcome by stimulating alternate afferent fiber populations using multiple stimulation sites, as shown previously with switching stimulation to contralateral dorsal roots (57). Examples of the effects of recruiting additional populations of afferents to reinstate a motor rhythm after activity-dependent fatigue, either in dorsal roots or dorsal column, are shown in Figure 3C&D, respectively. These results demonstrate the possibility of extending the duration of

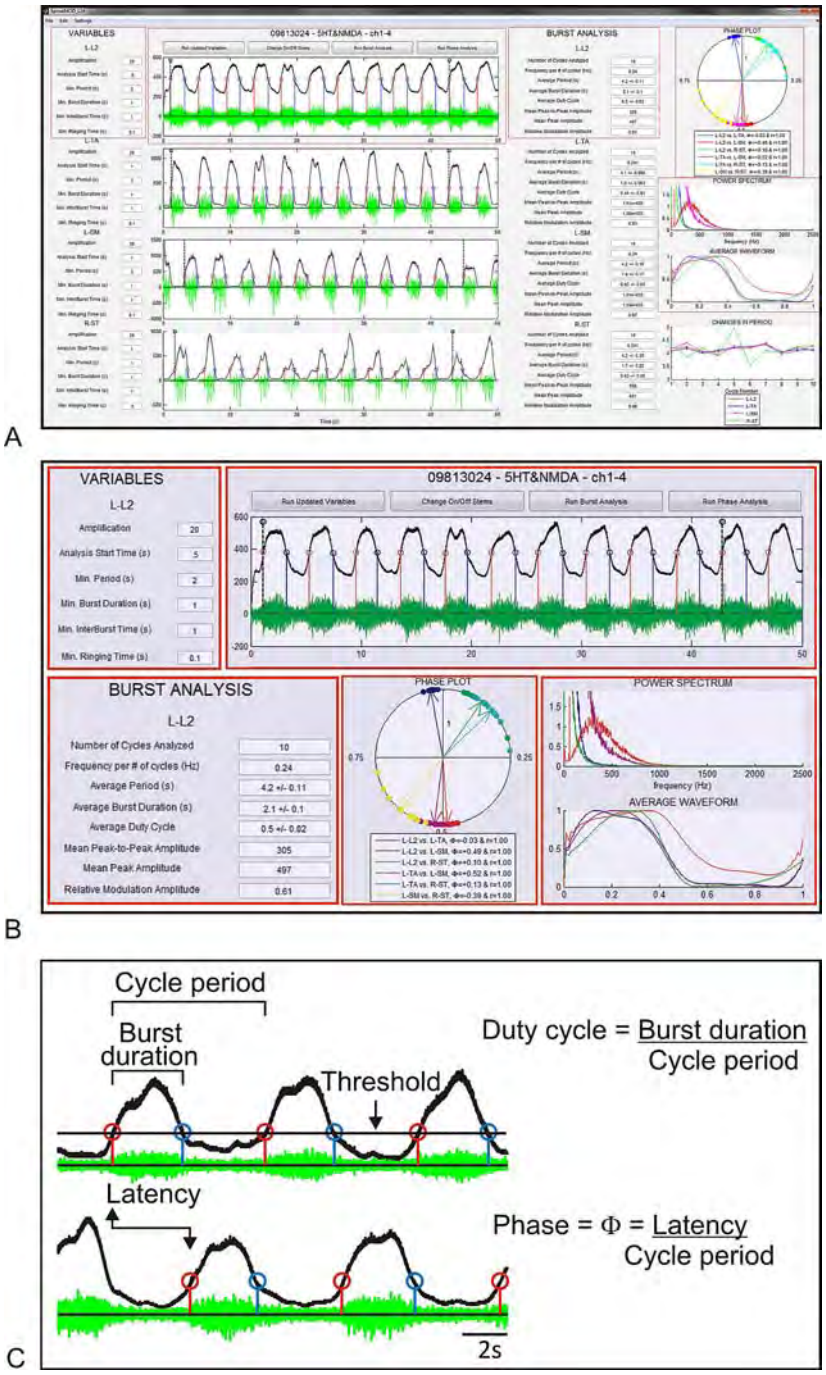

Figure 2. Commonly measured variables to describe locomotion analyzed with a custom Matlab-based GUI. SpinalMOD is designed to analyze ventral root, dorsal root, or muscle bursting for up to four channels. (a) Screenshot of the GUI with boxed regions enlarged in panel (b). Input variables are shown to the left and readily changed by the user by clicking in the box. The raw (green) and filtered (black) waveforms are graphed in the middle. Following burst detection, burst onset (red) and offset (blue) are denoted by vertical stems. "Run Updated Variables" allows the user to adjust the input variables and rerun the detection algorithm to correct misplaced burst markers. The stems can be also manually changed with "Change On/Off Stem Marks." Once burst detection is acceptable, burst analysis is run by selecting "Run Burst Analysis." The user then identifies the first burst to analyze and provides the number of bursts to be analyzed. Dashed black stems mark the beginning and end of the analyzed period. Once analyzed, the values calculated are shown in tabular and graphical form the Burst Analysis section to the right of the GUI. A phase plot figure as well as three of six other graphs, (average waveform, period, peak height, duty cycle, burst duration, and power spectrum), can be chosen for display. Finally, tabulated value and figures can be exported to Excel for subsequent use. (c). Blow-up of example raw and filtered waveform data shows commonly measured variables used to describe locomotion. For more information and to download SpinalMOD freely go to http://userwww.service.emory.edu/~shochm2/main_menu.html.

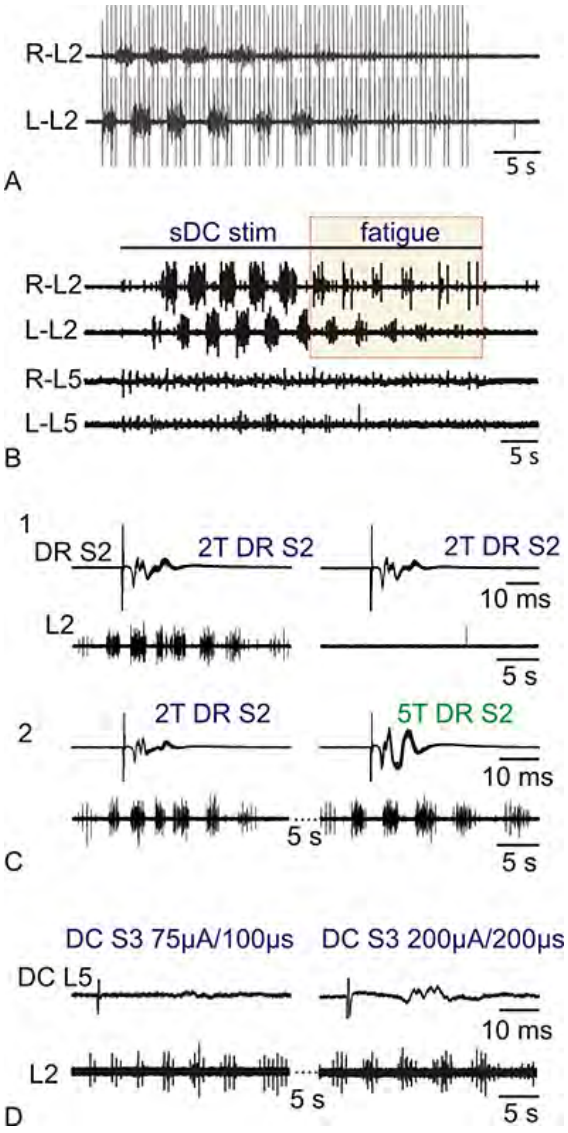

Figure 3. Afferent activity-dependent recruitment of rhythmic motor activity. (a) Sacral dorsal column (sDC) stimulation evoked rhythmic alternation in lumbar (L2) ventral roots shown in the presence of stimulation artifacts. Notice how the rhythm slowly fatigues even as stimuli are continually applied. (b) Continuous stimulation of the sDC recruits a rhythmic alternating pattern of motor activity with alternation between left and right L2 ventral roots. The recruited activity clearly beings to fatigue within 30s of its onset (2 Hz). Fatigability can last several minutes. (c and d) Stimulation intensity dependent recovery of fatigability in fiber pathways recruited in either sacral dorsal roots (sDR) or sDC. Top panels show fiber volleys recorded in the same dorsal root as stimulated (c) or in the same dorsal column tract as stimulated (d). Bottom rows show activity on a longer time scale in ventral roots. (c1) Stimuli were delivered to the sacral dorsal root (2 times threshold for afferent volley detection (2T) at 2 Hz) until motor activity fatigued. After a brief pause (less than five seconds), the stimulus train was repeated without recruitment of rhythmic L2 ventral root motor output. (c2) Fatigue of rhythmic activity at 2T can be quickly reinstated by recruiting a previously unstimulated fiber population at 5T to rescue the rhythm. (d) Similarly, when stimuli were delivered to the sacral dorsal column to fatigue the pattern (2 Hz) and subsequently delivered at higher intensity, rhythmic output was reinstated.

afferent stimulation-evoked LLA by interleaving stimulation at different sites.

In summary, primary afferent-evoked LLA fatigues quickly in the *in vitro* neonatal preparation. Strategies for interleaving recruitment of afferent fiber subpopulations or recruitment by natural afferent stimuli with more asynchronous recruitment may help considerably (23, 68). Further systematic exploration of these methods is needed especially as continuous afferent activation with epidural stimulation can recruit the hindlimb locomotor CPG after chronic spinal injury (66, 69-71).

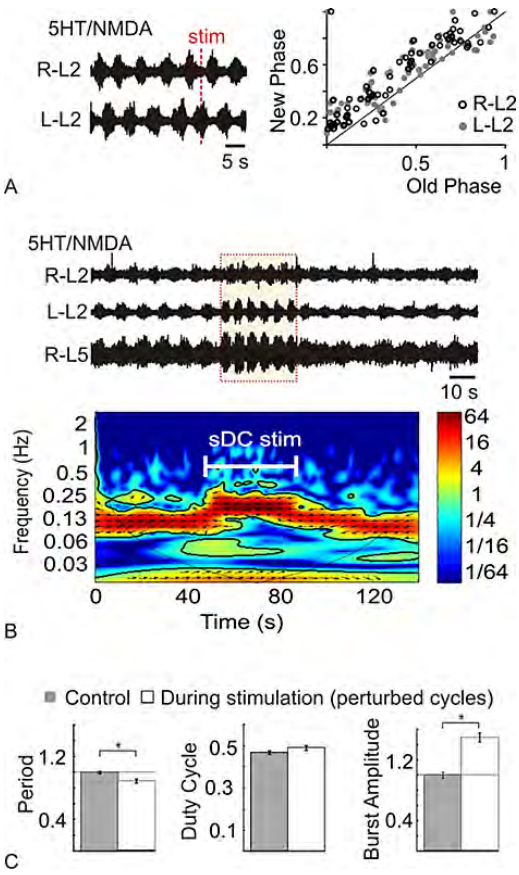

Figure 4. (a) Single pulses of sDC stimulation during 5HT/NMDA induced locomotor-like activity abruptly altered the bursting ventral root's activity. When analyzed for phase changes, these pulses result in shifts in the expected phase. These shifts are generally phase advances in both ventral roots regardless of the phase at which the stimuli occur as shown at right. To calculate the phase of the CPG, a "zero phase marker" (ZPM) was defined as the onset of bursting. At the time of stimulation, the "old phase", φ_{old}, was calculated as:

$$\varphi_{old} = \frac{t_{stim} - t_{ZPM}^{N}}{\bar{T}}$$

where t_{stim} is the time of stimulation, t_{ZPM}^{N} is the time of the most recent burst onset, and $\bar{T}$ is the mean cycle length measured during unperturbed bursting. After the stimulus occurs, the "new phase", φ_{new}, was calculated as:

$$\varphi_{new} = 1 - \frac{t_{ZPM}^{N+1} - t_{stim}}{\bar{T}}$$

where t_{ZPM}^{N+1} is the time of the next burst onset after the stimulation. Each stimulus pulse, therefore, generates a pair of "old" and "new" phases (φ_{old}, φ_{new}), which is plotted as a phase response curve. If the stimulus has no effect on the ongoing rhythm, then the old phase will equal the new phase. (b) Stimulus trains (2 Hz) significantly changed the cycle period and burst amplitude of the 5HT/NMDA locomotor-like activity. Wavelet analysis visualization of changes in frequency and phase over time for this data is provided below the raw data. Note that during stimulation there is a shift in the power of the low frequency component at locomotor frequency to a larger value that then returns to its original values after termination of stimulation. (c) Combined results from analysis of three experiments as in (b) are shown in (c). Data is displayed as mean ± S.E.M. Asterisks indicate significance with $p<0.05$.

3.4. Effects of sacral dorsal column stimulation during ongoing neurochemical locomotion

Previous studies have demonstrated that afferent activation can reset or entrain locomotor rhythms (39, 72-76). Resetting occurs when a stimulus alters the length of the ongoing flexor or extensor burst resulting in a phase delay or advancement of future bursts which occur at the same frequency as before (76). Entrainment occurs when the frequency of the CPG locomotion is altered by and follows the frequency of an external stimulus (15, 39, 75).

In comparison to in vivo studies predominantly undertaken in cat, where intensity of electrical stimuli correlates well with recruitment of afferent fiber modalities (e.g. (77, 78)), it

is much more difficult to target specific afferent fiber populations in the neonatal rodent using electrical stimulation (e.g. (79)) at least in part due to incomplete myelination (80). Nonetheless, activation of muscle afferents during 5-HT/NMDA-induced rhythms also produces resetting in the neonate (73, 81) and stimulation of lumbar dorsal roots may entrain locomotion (39). Last, locomotor frequency can be modulated by thermal stimuli applied selectively to the tail (82) or hindlimb (68) with frequency reversibly increasing and decreasing as a function of temperature deviations from physiological skin temperature (68).

Here we show that single pulse stimuli delivered to the sDC alter LLA, but do not cause phase resetting of the rhythmic pattern (Figure 4A). To analyze effects, changes in phase were calculated and displayed as a phase response curve (83) (see Figure 4 legend). In such plots, phase advances lie above the equality diagonal, and phase delays lie below. In three experiments, we found that the vast majority (87%) of stimulus pulses resulted in a phase advance in both right and left ventral roots (Figure 4A). This demonstrates that a single afferent stimulus acts on the rhythm generator to support a brief locomotor frequency increase. In comparison, short trains of pulses (500 µA/200 µs, 1-2 Hz) delivered to the sDC during ongoing 5-HT/NMDA LLA increased both burst amplitude and frequency (n=3/3; Figure 4B&C). The rhythm did not entrain to the stimulus frequency, and there was no change in duty cycle, suggesting the trains of stimuli provide additional excitatory drive to the neurochemically-activated locomotor CPG. Overall, these data demonstrate that sDC afferent stimuli facilitate locomotion. This is of potential importance to the development of future neuroprosthetic devices, such as spinal cord stimulators in closed-loop feedback strategies as considered below.

As shown in Figure 4B, the stimulation-induced increase in locomotor frequency coincides with a corresponding shift in predominant wavelet coherence. Wavelet spectral analysis is advantageous over traditional Fourier analyses for visualizing coherent frequency components and phase relationships for biological signals since many biological signals are nonstationary, and wavelet analysis methods do not assume stationarity. Moreover, its sensitivity facilitates detection and comparison of signals weakened by lesioning or pharmacological means (84, 85).

3.5. Afferent stimulation in closed-loop feedback strategies for locomotor control

The importance of afferent activity in the control of locomotor output is well established, and can be used to control locomotion after injury. For example, Edgerton and colleagues demonstrated that continuous epidural afferent stimulation recruits locomotor activity in the chronic spinal rat (66, 69-71). In cases of incomplete injury, a strategic output-based control of afferent stimulation may be preferred in order to augment but not overwhelm compromised locomotion. Below we discuss and explore close-loop feedback as a control strategy. Closed-loop feedback control strategies enable the system to autonomously operate and alter the inputs by comparing the output to a desired outcome. This methodology utilizes information regarding the input-output relationships of different system parameters to develop algorithms for feedback control. For example, in the cat, Mushahwar and colleagues used intraspinal microstimulation to show that basic proportional-derivative controllers mimic the phasic nature of neural signals and could produce locomotor stepping rhythms using a surprisingly small number of stimulating electrodes (86). Additionally, Vogelstein and colleagues developed a closed-loop control scheme to regulate directionality of simulated lamprey swimming using electrical stimulation of a spinal hemicord (87).

There are two basic forms of feedback control. Negative feedback works to maintain an equilibrium set point by altering the feedback to negate the error in the output. Positive feedback loops augment small perturbations to the system. If left unchecked, positive feedback systems are unstable, requiring an external variable or counter-signal to break the loop and limit the positive feedback. In the case of locomotion, the circuitry itself may intrinsically limit positive feedback controls due to neural fatigability, in their afferent inputs or in the CPG itself.

Using the isolated neonatal rat spinal cord preparation, we developed a simple positive feedback system based on detecting locomotor bursts in real-time. With sufficient levels of 5-HT/NMDA to induce a subthreshold erratic bursting pattern, a thresholding closed-loop simulation protocol was used to ascertain the impact of sDC stimulation on the ongoing locomotor pattern. The rectified, low-pass filtered signal from a single, flexor-related L2 ventral root was used. A burst was identified as beginning once the filtered trace rose above a specified threshold. At the onset of a detected burst, a stimulus pulse was delivered to the sDC. The stimuli served as positive reinforcement, presumably by providing additional excitatory input to the locomotor CPG. Prior to instituting the closed-loop feedback system, the phase relationships between the recorded ventral roots were irregular with a rather variable cycle period. After the closed-loop was initiated, cycle period variability was reduced to provide a more stable rhythm (n=3). An example of the effects of closed-loop stimulation is shown in Figure 5. While theoretically closed-loop positive feedback stimuli should become unstable, as demonstrated above, if afferent transmission fatigues or is limited by presynaptic inhibitory mechanisms, such mechanisms could limit the duration of productive afferent stimulation-induced actions. Because fatigue-based negative feedback may lessen with development, alternatively, a stopping external signal may be programmed into the closed-loop feedback to control for any tendency towards instability by inhibiting the rhythm or by simply ceasing the positive-feedback stimulation temporarily.

We conclude that afferent stimulation may be incorporated in closed-loop feedback strategies for locomotor control, and the *in vitro* model provides for a highly accessible high-throughput system to explore such strategies (63).

4. METHODOLOGIES TO STUDY CIRCUIT OPERATION WITH INTACT HINDLIMBS: THE *IN VITRO* SPINAL CORD HINDLIMBS-RESTRAINED PREPARATION

4.1. Introduction

While ventral root recordings offer a simple way to monitor spinal motor output, they do not identify nor report recruitment of individual muscles. Individual lumbar ventral roots contain axons projecting to flexors and extensors (88, 89), axial musculature (90), and sympathetic preganglionic neurons that exit from thoracic and upper lumbar segments (91). Thus, one cannot a priori assume that observed rhythmical activity in these roots reliably

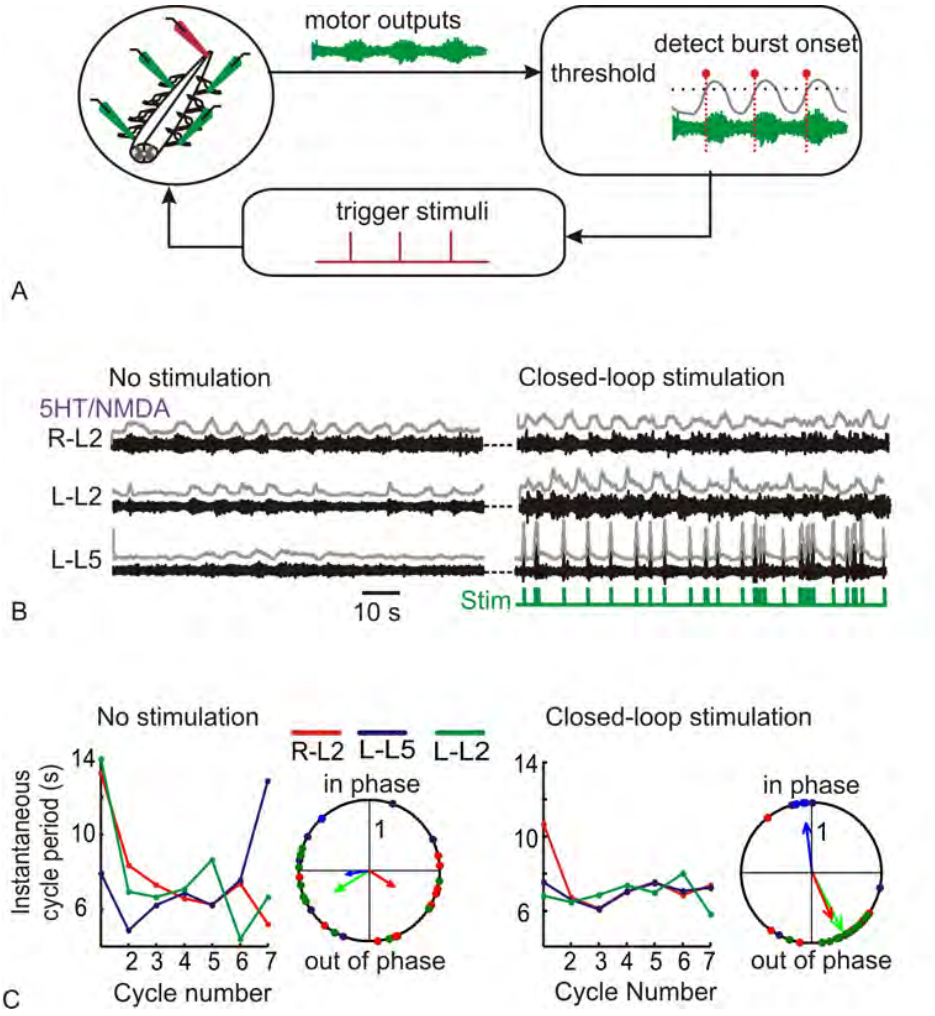

Figure 5. (a) Real-time burst detection feedback for triggering stimuli to alter ongoing 5HT/NMDA locomotion. (b) Irregular locomotor patterns with inconsistent instantaneous ventral root phase relationships. (c) Closed-loop stimulation reinforced the motor pattern, and phase relationships between roots were more consistent. Phase plots compare indicated root pairs.

represent the activity of individual flexors and extensors (92), particularly after experimental interventions that could alter actions on efferents not associated with hindlimb movement. For example, sympathetic preganglionic axons also exit the L2 ventral root, and may also express rhythmical patterns of activity (93, 94). An additional limitation of ventral root recordings is that important information on motor coordination is lost, including sequential activation of muscles, and distinctive patterns that reflect activation of different locomotor programs (e.g. swim vs. step) as can be observed with different bath-applied neuromodulators or following afferent electrical stimulation (25, 27). Finally, without the hindlimbs and their innervation intact, the influences of distinguishable sensory inputs on circuit function are limited. Demonstrated advantages of the SCH-R for studies on locomotion are shown below.

4.2. General methods

The *in vitro* spinal cord hindlimbs-restrained preparation (SCH-R) permits EMG recordings with suction electrodes attached to hindlimb muscles. In order to accomplish this, the spinal cord and attached hindlimbs are immobilized ventral side upward with insect pins affixed to Sylgard-lined chamber bottom (Dow Corning). Lower thoracic and the lumbar ventral roots innervating the hindlimbs remain intact, and the vertebral column surrounding the cervical and most of the thoracic spinal cord is removed to allow for sufficient cord superfusion. Thoracic and lumbar dorsal roots were cut in experiments on neurochemically-evoked locomotion, but remained intact for studies on afferent feedback. Independent micromanipulators with attached glass suction electrodes are used. We typically record from lumbar L2 ventral root en passant and 7 hindlimb muscles (Figure 6A) (see also (27)). Example recordings provided here were acquired from the following muscles: tibialis anterior (TA; ankle flexor), medial gastrocnemius (MG; ankle extensor), semitendinosus (St; knee flexor / hip extensor), semimembranosus (Sm; knee flexor / hip extensor), vastus medialis (VM; knee extensor), rectus femoris (RF; knee extensor / hip flexor), and adductor magnus (AM; hip

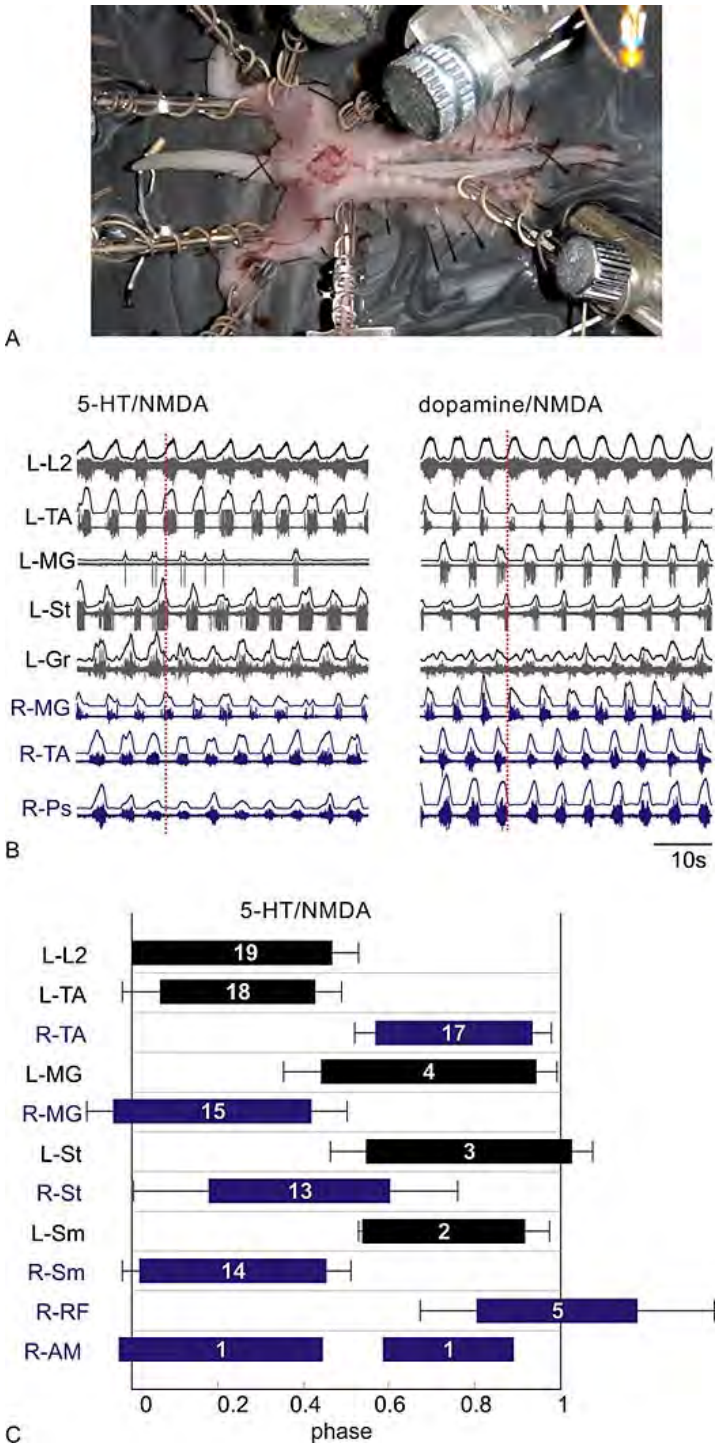

Figure 6. Multiple suction EMG electrode recordings in the *in vitro* neonatal rodent cord provide information regarding the locomotor pattern. (a) The isolated neonatal rat spinal cord with attached hindlimbs maintained *in vitro*. For studies on the output of muscle coordination, glass suction electrodes are placed on the left lumbar L2 ventral root and typically 7 muscles of the hindlimb. Drugs are applied to the bath. (b) EMG recording of LLA comparing motor patterns recruited in an animal in the presence of 5-HT and NMDA (left) or dopamine and NMDA (right). (c) Phase diagram summarizing activity periods observed during 5-HT/NMDA LLA. All phases are referenced to the onset of the L-L2 ventral root. Bars represent the average burst duration of muscles normalized to cycle duration. Burst onset is on the left and burst termination on the right. The number of rats used to obtain the diagrams is given in the middle. One difference observed from the earlier reports using 5-HT (Kiehn and Kjaerulff 1996) or 5-HT and NMDA (Klein *et al.* 2010) is that AM can also be observed during the flexor phase.

adductor), gracilis (Gr; hip flexor / hip adductor), iliopsoas (Ip; hip flexor), and paraspinal (Ps; movement of vertebrae). The left lumbar L2 ventral root (L-L2VR) was always recorded: (i) to enable comparison of the ventral root activity profile obtained in the isolated spinal cord preparation, and (ii) to provide a common reliable comparison between experiments where muscle EMG recruitment was variable (see also (27)).

4.3. Recording muscle EMG recruitment patterns during locomotion: complex phasing and expression of spontaneous burst deletions

Bath-applied 5-HT with NMDA produced EMG locomotor phase relations consistent with those seen previously for 5-HT by Kiehn and Kjaerulff, or 5-HT with NMDA by Tresch and colleagues (25, 27) (Figure 6B, left). While there was inter-animal variability in muscle recruitment, TA and MG were active during the flexor and extensor phases, respectively. The phase diagram in Figure 6C compares these phase relations and those of other recorded muscles in the sample population. Under these conditions Sm and St, both knee flexor and hip extensors, were usually both active during the extensor phase, while RF, a knee extensor and hip flexor was active during the flexor phase. Locomotor rhythms generated with bath-applied dopamine were previously reported to be slower, more variable, and require much higher doses than 5-HT (25). Interestingly, though flexor/extensor coordination patterns were preserved, they observed clear phase differences in recruitment patterns of bifunctional muscles, supporting a neuromodulator-dependent recruitment of different locomotor programs. Here, when applied with NMDA, 5-HT or dopamine generated locomotor rhythms that occurred at comparable frequencies and with muscle recruitment patterns (Figure 6B, right; n=4). Though preliminary, these findings highlight the contribution of co-applied NMDA to locomotor pattern expression.

Spontaneous absences of bursting in specific motor pools, often referred to as deletions, provide clues to the underlying modular organization of CPGs in vertebrate limb pattern generation. For mammalian hindlimb locomotion, McCrea and colleagues examined spontaneous burst deletions observed in motor pools from one hindlimb of the decerebrate cat during electrical stimulation of the mesencephalic locomotor region (MLR). These deletions are of two forms; non-resetting and resetting. Non-resetting deletions are identified when the reappearing activity emerges without phase shift in the locomotor cycle. In contrast, resetting deletions undergo a shift in the phase of the re-emerging rhythm relative to the rhythm that preceded it. The presence of resetting and non-resetting deletions provided strong evidence of a minimally two-layered CPG organization with rhythm-generating and subordinate pattern-generating circuits to control ipsilateral patterns of locomotor activity (6, 18, 19, 95). While compelling, these studies are nevertheless limited to the experimental model system utilized. Studies incorporating bilateral hindlimb and forelimb EMG or ENG recordings, will undoubtedly provide more complete insight into the organization of locomotor CPGs (24, 96). In comparison, Stein and colleagues undertook an analysis of deletions and the modular structure of the turtle rostral scratch CPG and observed an organization consistent with independent 'unit burst generators' as originally hypothesized by Grillner (2, 97).

Deletions are also observed during LLA in the isolated *in vitro* neonatal spinal cord of mouse (Ron Harris-Warrick, personal communication) and rat (below). Comparison of expressed deletions to the adult decerebrate cat may identify both conserved deletions and interesting differences in deletions during the uncoupling of modular elements of the activated locomotor circuit. Experimental approach, species, and developmental stage could all conceivably alter deletion expression patterns. To our knowledge locomotor studies examining spontaneous motor pool or muscle activity deletions in the *in vitro* hindlimbs-attached preparations have yet to be utilized. Here, with bilateral EMG recordings, many spontaneous deletions are observed during neurochemically-induced locomotion. For example, Figure 7A shows a non-resetting deletion in the left ankle flexor TA during the flexion phase and this occurs without obvious changes in activity in its strict antagonist MG, or in right flexor and extensors. These results are consistent with independent flexor and extensor pattern generators across a joint, an observation supporting Grillner's unit burst generator hypothesis (2). As loss of left TA activity is not associated with a loss in left L2 VR activity, rhythmic activity in ipsilateral flexors can be independently controlled. Figure 7B shows spontaneous coincident deletions of activity in left TA and right MG with corresponding complementary actions in the opposite limb: prolonged activity in right TA and left MG (shaded bars). Such deletions support the existence of a bilateral pattern generator that couples flexor activity in one limb with extensor activity in the opposite limb. This is consistent with a deletion in the population of descending contralateral interneurons identified by Butt and Kiehn (2003) that couple ipsilateral flexion with contralateral extension (98). Spontaneous resetting deletions are also seen in this preparation as shown in Figure 7C. Loss of the right TA corresponds with continued right extensor MG and Sm EMG activity with a subsequent maintained phase shift in timing. While the data presented here is preliminary, deletions during neurochemical locomotion were observed in most experiments, and the variations remain to be fully analyzed.

Overall, the much greater ease of interneuronal recordings, and flexibility for manipulation of motor output in the *in vitro* preparation, provides a high-yield platform to dissect the organization of locomotor pattern-generating circuits. When integrated with the guidance of genetic manipulations that now include optogenetics and high-throughput connectivity mapping (33, 99), a rather complete dissection of mammalian locomotor operation seems tantalizingly within reach. Yet, it is important to acknowledge evidence of at least two, and possibly three, distinct interneuronal circuits that generate locomotion in the phylogenetically older limbless vertebrates (100, 101). It is reasonable to assume these circuits are evolutionarily

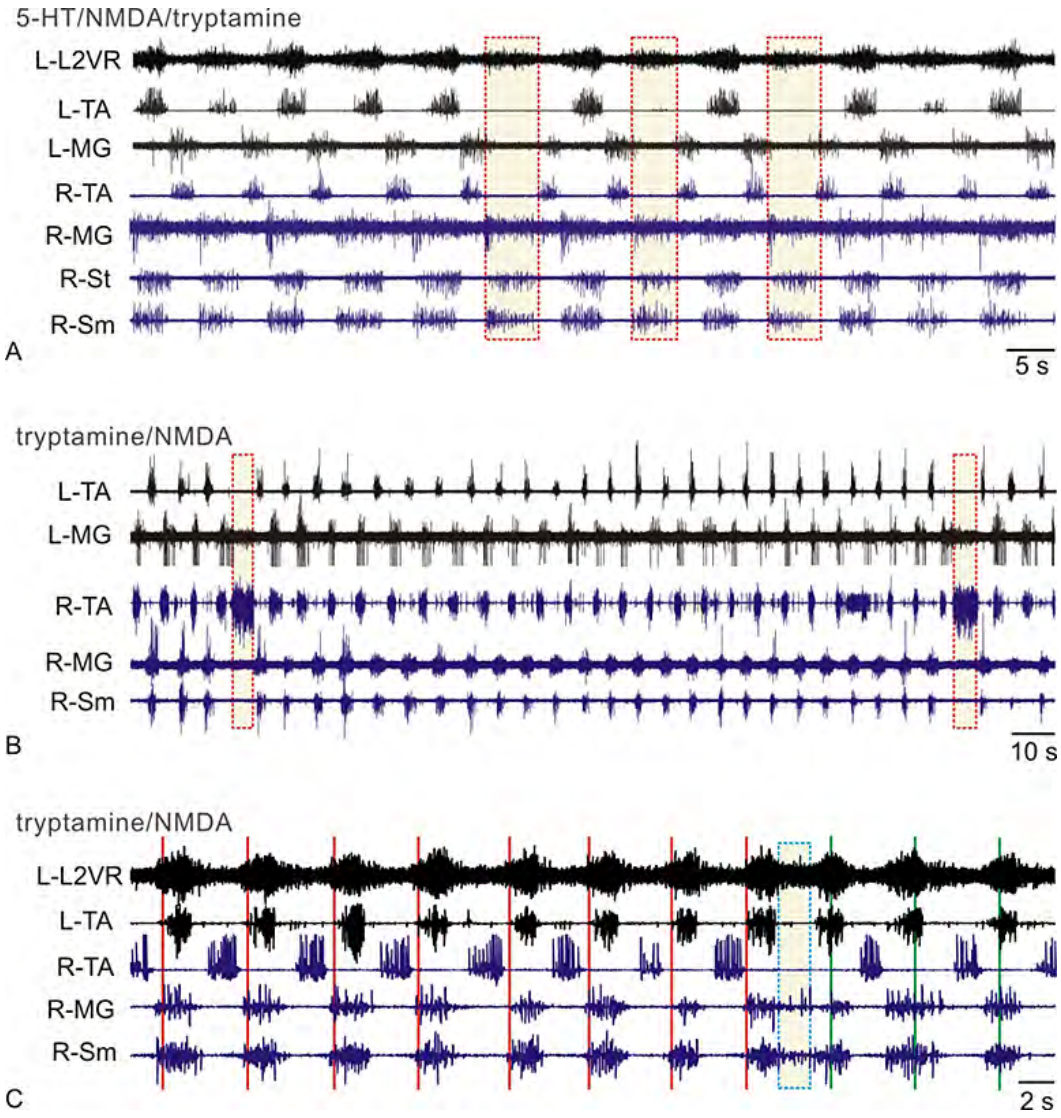

Figure 7. Multiple EMG recordings provide insight into the organization of central patterns generators based on spontaneous intermittent loss in muscle recruitment (deletions). (a) The left TA flexor phase burst is absent at expected time (shaded bars) but there is otherwise no obvious alteration in EMG activity in extensor phase or flexor phase activity in other channels recorded bilaterally. Note the loss of left TA activity is associated with only a reduction in left L2 ventral root amplitude. These results are consistent with several flexor modules, as well as an independence from extensor module. (b) Spontaneous coincident deletions of activity in left TA and right MG associate with corresponding complementary actions in opposite limb (prolonged activity in right TA and left MG (shaded bars). Such deletions support a bilateral pattern generator of mutual inhibitory interactions between flexors and extensors. (c) Evidence of a spontaneous resetting deletion. Red lines mark approximate same locomotor phase (onset of left TA activity), whose average duration is used to predict subsequent burst onsets (green lines). Note that after spontaneous deletion of the right TA and corresponding continued right extensor activity, subsequent locomotor activity has undergone a phase shift in timing consistent with a resetting of the locomotor rhythm.

conserved in limbed vertebrates including mammals. If true, studies undertaken during differing behavioral drives and/or afferent input patterns, particularly when combined with the silencing of distinct neuronal populations (3, 4) may uncover additional independent mammalian locomotor CPG circuitries, with differing modular organizational structures. The SCH-R and spinal cord hindlimbs-pendant preparation (SCH-P; see section 5 below) provide powerful model systems for such analyses.

4.4. Afferent activity can perturb ongoing locomotion: Activation of nociceptive flexion reflexes

Nociceptors and other higher-threshold afferents that converge onto interneuronal populations to produce ipsilateral flexion reflexes can be classified as flexor-reflex afferents (FRA) (72, 102-105). This includes the longer-latency FRA pathways unmasked by L-dopa in the spinal cat that generate spinal stepping (13, 106). Flexor reflex afferents can reset fictive locomotion to flexion in the cat

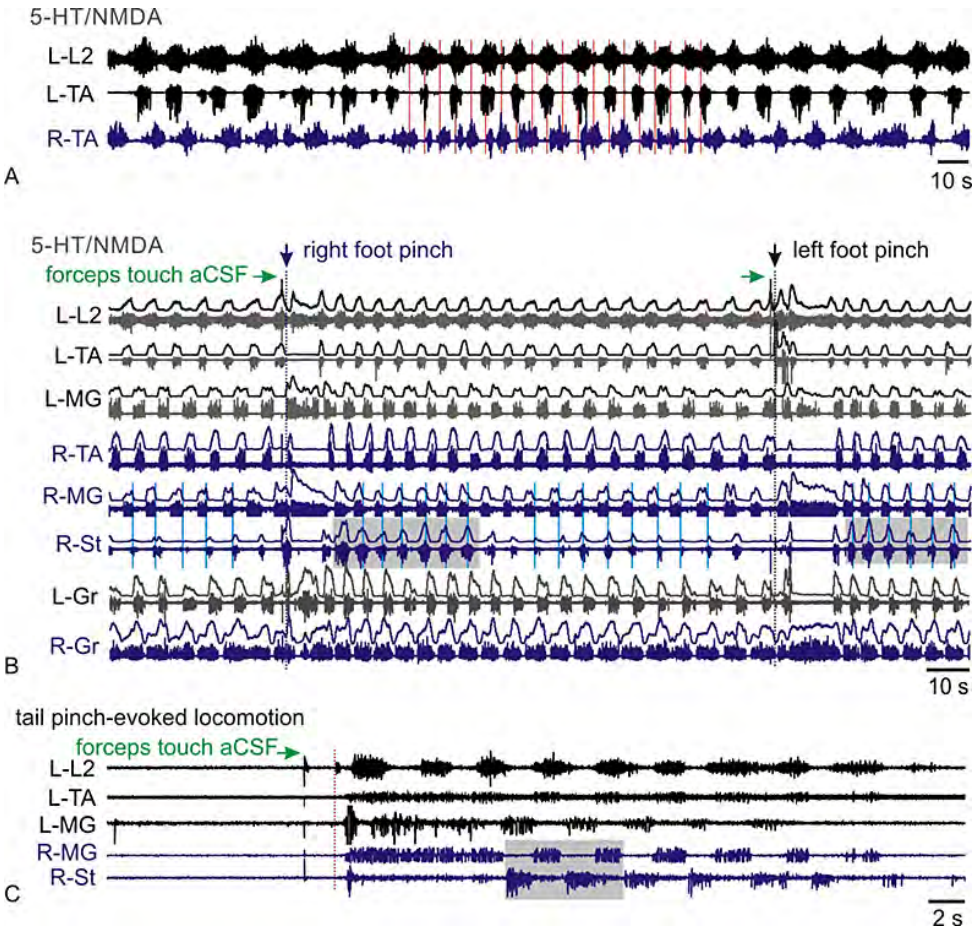

Figure 8. Sensory stimuli modify locomotor pattern expression. (a) High intensity lumbar dorsal root stimulation (1 mA, 1 ms) is able to increase and entrain frequency at half the simulation frequency (0.2 Hz at red bar) with signs of 1:1 entrainment at the end of the stimulus train. (b) Pinch evoked increase in locomotor frequency. Fast initial right pinch or left pinch-evoked ipsilateral right or left flexion reflexes, respectively, but this is difficult to discern on the slow time scale displayed. After initial response, both pinch events result in a suppression of ankle flexor muscle actions bilaterally with coincident bilateral strong recruitment of extensors. This event precedes a subsequent frequency increase that couples to greatly facilitated activity in the knee flexor, St, which now includes temporal overlap with ankle extensor activity (blue timing lines in gray shaded boxes). (c) Tail pinch-evoked action on locomotor circuits. Tail pinch (at red bar) initiates several cycles of LLA (top series) that is faster than neurochemically-evoked LLA (bottom series).

(107), and high threshold sensory stimuli in the neonate also reset to flexion (73). Studies in the *in vitro* neonatal spinal cord have demonstrated nociceptor activation of LLA (82) as well as facilitation of ongoing LLA as measured from ventral root recordings (68, 79). Ventral root recordings of LLA obviously limit interpretations of afferent-evoked alterations in LLA and motor coordination. In contrast, the response signature recorded from many muscles can provide a more complete assessment of afferent-evoked changes – from those that span multiple joints, that includes actions on bi-functional muscles, adductors and abductors, and even in the associated axial musculature (e.g. paraspinal muscle in Figure 6B).

We provide example actions of high threshold afferent electrical stimulation as well as mechanonociceptor pinch-evoked actions on EMG activity recorded bilaterally from several hindlimb muscles. High intensity lumbar dorsal root stimulation increased locomotor frequency and locomotion entrained to the stimulus frequency of 0.2 Hz (Figure 8A). Observations based on multiple EMG recordings identify recruitment patterns clearly more complex than observable from ventral roots. EMG recordings from many individual muscles during hindlimb pinch provided an interesting and complex sequence of motor coordination transitions, as shown in Figure 8B. Left or right hindlimb pinch produced an initial ipsilateral activation of flexors (flexion reflex) followed by a longer-lasting bilateral suppression of ankle flexors (TA) with concomitant strong recruitment of ankle extensors (MG). Note that the hip flexor/adductor Gr had more differentiated actions. Thereafter, a frequency increase emerged, lasting several cycles. This increase included a phase shift in patterning as St switched from flexor-related to extensor related activity, and with greatly facilitated motor recruitment. Figure 8C shows that tail pinch initiated

several bouts of locomotion in the absence of ongoing neurochemically-induced locomotion. This included several cycles of continuous bilateral tonic EMG activity. While the behavioral relevance of the aforementioned examples require additional study and interpretation, it is clear that hindlimb-attached preparations greatly extend the power of the *in vitro* studies of spinal locomotor circuits.

In summary, the SCH-R allows for easy placement of suction EMG electrodes that can be maneuvered for EMG recordings from multiple muscles bilaterally. Combined with the capacity for studying locomotor modifiability with various neurochemicals, both electrical and natural afferent stimulation, and expression of spontaneous deletions, it is clear that this approach will enable considerable further insight into locomotor mechanisms.

5. METHODOLOGIES TO STUDY CIRCUIT OPERATION WITH INTACT HINDLIMBS: UNRESTRAINED HINDLIMB LOCOMOTION

5.1. Introduction

While aspects of sensory feedback can be studied as described above, these studies cannot recreate the complex interactions between sensory modalities produced by natural limb movement, nor determine the behavioral impact of pharmacological, electrical, or mechanical manipulations on hindlimb kinematics. To overcome these limitations, we developed a novel *in vitro* spinal cord hindlimbs-pendant preparation (SCH-P) in the neonatal rat that combines the neural accessibility of the classic *in vitro* preparations with the natural patterns of sensory feedback and behavioral observability of more intact preparations (23). The SCH-P is composed of the nearly isolated, fully exposed neonatal rat spinal cord oriented dorsal-up and maintained in continuously oxygenated aCSF. The hindlimbs, as well as the corresponding dorsal and ventral lumbosacral roots, are left intact, with the limbs hanging pendant for stepping (Figure 9). Hindlimb stepping can then be activated by bath application of 5-HT or dopamine with or without NMDA. Sensory-modulated behavior can then be characterized using sagittal plane kinematics, EMG recordings of muscle activity, ventral and dorsal root recordings, and intracellular recordings. Thus, the SCH-P allows us to relate behavior to underlying neural substrates and to quantify the effect of pharmacological, electrical, or mechanical manipulations on neural function and behavior in ways not typically possible *in vitro*. Here we review the technologies developed for use with the SCH-P, demonstrate the use of the SCH-P to study sensory modulation and reinforcement of spinally-generated locomotion, and report the first intracellular recordings undertaken during unrestrained hindlimb locomotion.

5.2. General methods

Because dorsal-up hindlimb stepping had not been previously undertaken *in vitro*, several enabling technologies were needed to establish an environment amenable to hindlimb stepping and to enable extensive mechanical characterizations. First, we developed a custom perfusion chamber and treadmill system to facilitate stepping in the aqueous solution and at the slow speeds characteristics of *in vitro* preparations (23) (Figure 9A&B). The spinal cord was mounted dorsal-up on a Sylgard step with a small canal under the ventral surface to direct the incoming aCSF for sufficient ventral perfusion and drug diffusion. The treadmill belt was constructed from a 30mm wide by 130mm long polyurethane belt (McMaster-Carr) and mounted around two metal shafts with plastic rollers (Tamiya Inc). The shafts passed through holes in the perfusion chamber walls that were subsequently sealed with epoxy or petroleum jelly. The treadmill was front-driven by one of two radio-controlled car motors, a brushed DC motor (Tamiya Inc, GM7) or a brushless DC motor with electronic speed controller (Novak, Goat Brushless Crawler System). The back rollers were passively turned by friction with the belt. Treadmill speed could be adjusted between 2-12 mm/s to match the slow step frequency of *in vitro* stepping. Altering treadmill speed could also entrain SCH-P stepping frequency across a narrow range of speeds (23). The treadmill allowed us to monitor stepping more similar to that of the intact rat, rather than stepping without ground interaction or having to overcome high friction interactions with the perfusion chamber floor.

Ground reaction forces are commonly monitored in the intact animal to quantify the strength of limb-environment interactions and joint torques (e.g.(108-110)). Typical force platform systems are unsuitable for an aqueous environment and are insensitive to the small forces exerted by neonatal limbs *in vitro*. Thus, we developed miniaturized 2D force platforms specialized for the SCH-P and capable of measuring both vertical and fore-aft forces of each hindlimb (Figure 9C&D). The basics of design were similar to previous models (111), but specialized for the *in vitro* SCH-P using force plates composed of an acrylic-based photopolymer (Objet 3D printer) and highly sensitive strain gauges (Omega Engineering) to transduce the smaller forces. An example of the monitored forces is shown in Figure 9E. Measuring ground reaction forces allows us to relate muscle activity, ventral root activity, or single neuron activity to the forces exerted on the environment. We can also consider how neural activity and circuit function is modulated by the forces experienced by the limbs and their mechanical interactions. Finally, the force platforms can be readily repositioned to alter ground height, slope, or even temporarily eliminate ground interaction.

5.3. Studies on sensory modulation and reinforcement in the spinal cord-hindlimbs pendant preparation

Studies in the intact animal indicate that sensory cues related to limb posture and limb loading play significant roles in determining the spatiotemporal features of motor output (112, 113). Sensory feedback regulates both timing and amplitude of muscle activation, particularly the timing of flexor activation (114, 115) and the amplitude of extensor activation (116, 117). Initial studies in the SCH-P confirmed the importance of these sensory cues in establishing intact rat-like motor patterns *in vitro* (23). To understand the influence of limb posture and limb loading in the SCH-P, we compared joint kinematics and muscle activation patterns produced during unloaded

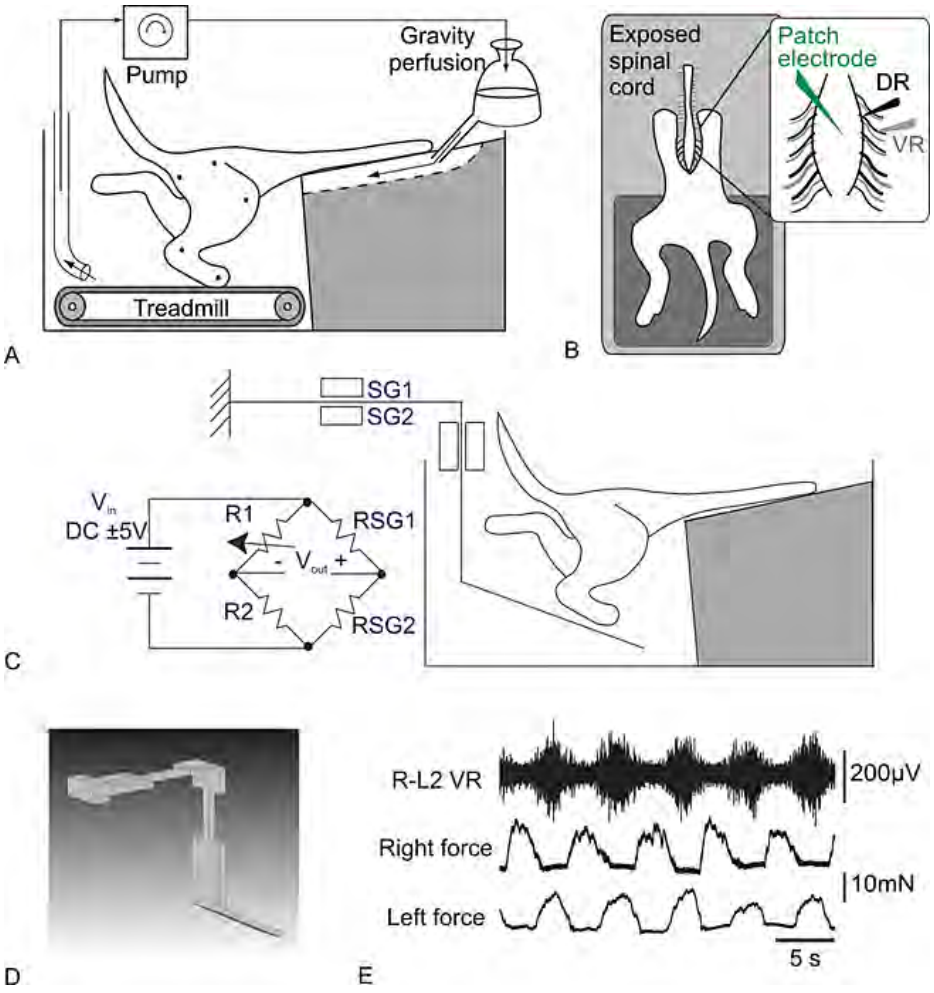

Figure 9. *In vitro* spinal cord-hindlimb preparation (SCH-P) experimental methods. (a) Sagittal view of the SCH-P oriented dorsal-up with hindlimbs hanging pendant to walk on a custom-built treadmill. The spinal cord and limbs are maintained in continuously oxygenated aCSF circulated by a peristaltic pump and gravity-fed perfusion system. aCSF was directed through a canal under the ventral surface to facilitate cord perfusion and drug diffusion to the ventral motor circuitry. The joint centers of the right hindlimb are marked for sagittal plane video collection and kinematic analyses. (b) Overhead view of the SCH-P. The inlay shows the setup for extracellular recordings at the ventral and dorsal roots (VR and DR) and intracellular patch clamp recordings in the exposed spinal cord. (c) 2D force platform to monitor forces exerted by a single hindlimb. Sagittal view of SCH-P-force platform interaction and accompanying Wheatstone bridge circuitry. Strain produced by strain gauges SG1 and SG2 of Sensor 1 and fed into the Wheatstone bridge circuit. Strain sensed by Sensor 2 is fed into a separate but identical Wheatstone bridge circuit. Output voltages are amplified by a DC amplifier and then converted to vertical and fore-aft forces offline. (d) Schematic2D force platform as shown in C with the SCH-P. The force platforms were calibrated by applying n known weights. The influence matrix (I) was then calculated according to: (V2xn) = (I2x2) · (L2xn) such that (I2x2) = (V2xn) · (L2xn)-1 where (V) is the voltage output in response to the known applied loads in μV, (L) is the known loads in mN, (I) is the influence matrix describing the relationship, and n is the number of known weights. After calibration, vertical and fore-aft forces could be computed from the recorded voltage responses according to: (F2xn) = (I2x2)-1 · (V2xn) where (I2x2)-1 = { (V2xn) · (F2xn)-1}-1 where (F) is the force matrix that includes both vertical and fore-aft forces computed from the conversion matrix (I)-1 . (e) Samples recordings of right and left hindlimb vertical ground reaction forces measured during locomotion and displayed relative to the right L2 ventral root activity (R-L2 VR).

ventral-up stepping to those produced during loaded dorsal-up treadmill stepping. Representative patterns are show in Figure 10. In the absence of ground contact, the hip, knee, and ankle joint trajectories were all in-phase, going through mass extension during stance and mass flexion during swing. In contrast, in the dorsal-up posture with ground contract, the knee trajectory was nearly reversed, such that the knee flexed during stance. The dorsal-up pattern much more closely resembled patterns typically observed in the intact rat (23, 118).

The muscle activation patterns also differed significantly between the ventral-up and dorsal-up conditions (23). For example, the phasing between flexors

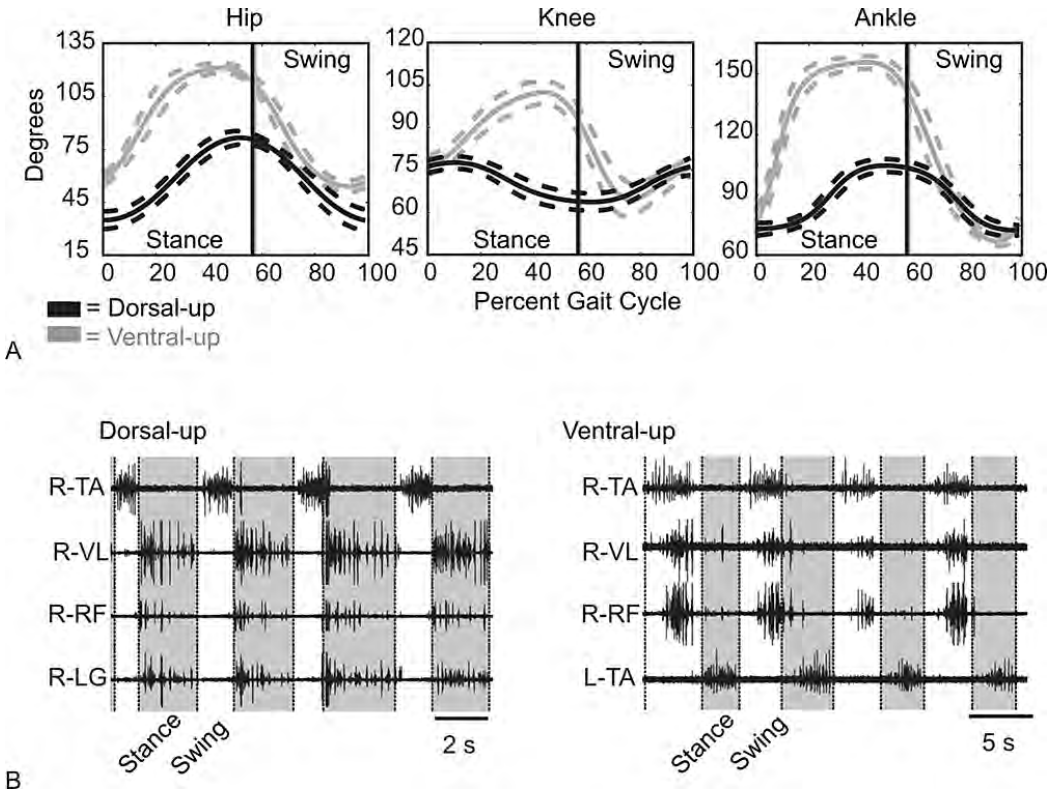

Figure 10. Kinematics and EMG activity during dorsal-up treadmill stepping and ventral-up stepping (adapted from Hayes *et al* 2009). (a) Kinematic joint angle trajectories from dorsal-up (black) and ventral-up (gray) stepping. Joint angle trajectories at the hip, knee, and ankle were time normalized and averaged across 17 cycles and plotted across the gait cycle. Average trajectories (17 cycles) are shown as mean (solid) plus or minus standard deviation (dashed). Increasing angles indicate joint extension and decreasing angles flexion. 0% gait cycle indicates stance onset (anterior extreme position). Vertical lines indicate swing onset (posterior extreme position). (b) Muscle activation patterns from four cycles of dorsal-up (left) and ventral-up (right) stepping are shown for the right tibialis anterior (R-TA), vastus lateralis (R-VL), rectus femoris (R-RF), lateral gastrocnemius (R-LG), and left tibialis anterior (L-TA). Gray shaded boxes represent stance phase.

and extensors differed significantly between the two conditions. In addition, extensors exhibited longer duty cycles than flexors during dorsal-up stepping, whereas flexor duty cycles tended to exceed extensor duty cycles during ventral-up stepping. The extensor-dominated patterns exhibited in the dorsal-up posture is characteristic of rat stepping, particularly at slower speeds like those seen *in vitro*, while flexor-dominated patterns are often seen during fictive locomotion in which muscle have been paralyzed and no sensory feedback is present.

Together these results suggest that ground contact and limb posture are important for establishing intact rat-like limb movements because they establish the appropriate sensory cues for locomotion, such as stretch and loading. Such cues have been previously shown to enhance extensor activation for body-weight support (116, 119). Loading and ground contact have also been shown to affect reflex patterns, joint kinematics, and muscle activation in humans (120, 121) Without these sensory cues, the isolated spinal circuitry functions without the vital influences of sensory feedback that is known to alter both its properties and final output, preventing us from studying this circuitry in a behaviorally-relevant context. By providing appropriate sensory cues, the SCH-P allows us to harness the many advantages of *in vitro* preparations, such as neural and pharmacological access, without reducing behavioral relevance.

Most importantly though, retaining sensory feedback from ongoing limb movement creates a more robust model for studying locomotion *in vitro* by reinforcing or even initiating spinally-generated locomotion. For example, cyclical sensory cues provided by applying repetitive swing assistance on the plantar surface of the hindlimb paw reinforced initially weak and irregular locomotion, resulting in a more regular frequency and reliable bursting in previously inactive muscles. This more robust pattern persisted after termination of the assistance (Figure 11A, (23)). Similarly, when drugs failed to initiate locomotion, alternating cyclical assistance on both limbs could actually initiate strong locomotion for the first time that persisted after bilateral assistance was terminated (Figure 11B). Thus, retaining the hindlimbs and sensory feedback can not only establish a behaviorally-relevant context, but can also be used to reinforce and

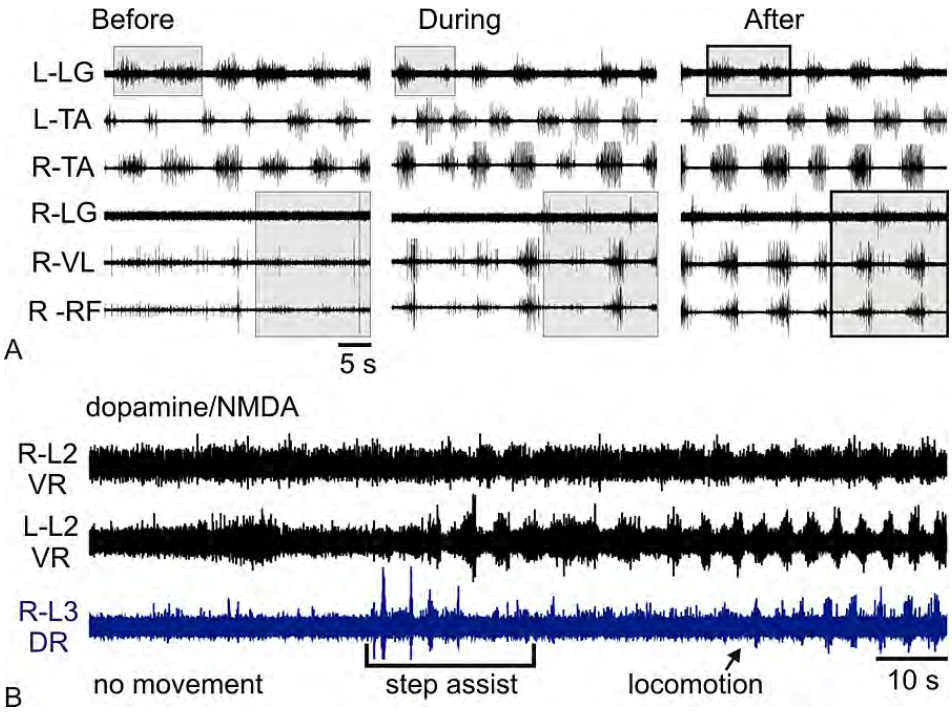

Figure 11. Unilateral swing assistance reinforced ongoing weak locomotion and bilateral stepping-like assistance initiated locomotion. (a) Application of swing assistance with a glass probe pushing on the right plantar paw surface reinforced otherwise weak locomotion (adapted from Hayes *et al* 2009). Forty seconds of muscle activation patterns from right (R-) or left (L-) lateral gastrocnemius (LG), tibialis anterior (TA), vastus lateralis (VL), and rectus femoris (RF) are shown before, during, and after application of swing assistance. Gray boxes emphasize changes in frequency and muscle bursting. (b) Bilateral cyclical stepping-like assistance initiated locomotion. Root activity from the right lumbar ventral root (R-L2 VR), left lumbar ventral root (L-L2 VR), and right lumbar dorsal root (R-L3 DR, blue) are shown before, during, and after assistive stepping-like movements. The bracket shows the period in which the limbs were cyclically moved through stepping-like patterns. Before entrainment, the sub-threshold concentration of neurochemicals failed to initiate rhythmic bursting in the ventral an dorsal roots. Stepping-like assistance initiated rhythmic locomotor bursting in all roots, which persisted after the assistance period.

facilitate CPG activation, making the SCH-P a powerful model for relating the spinal circuitry of locomotion to movement-related sensory feedback.

5.4. Intracellular recordings during unrestrained hindlimb stepping in the spinal cord-hindlimbs pendant preparation

One of the greatest advantages of the SCH-P is the potential for studying interneuronal activity and CPG function during natural, sensory-influenced behavior. Many have performed intracellular recordings in the isolated spinal cord without limbs attached or with neuromuscular blockage or deafferentation (e.g. (122, 123), for review see (124)). Although these studies provide insight into the neuronal contributions to rhythmogenesis, without movement-related sensory feedback, numerous inputs to these neurons are inactive. Because sensory inputs have profound effects on motor output, they undoubtedly influence the functioning of neurons including those comprising spinal locomotor circuitry.

Intracellular recordings performed during sensory-modulated, behaviorally-relevant locomotion provide additional insight into the functional synaptic and cellular properties of spinal interneuronal populations during locomotion. Wheatley and Stein made progress towards incorporating limb movement with intracellular recordings by developing the mudpuppy spinal cord-forelimb preparation (125), but no such model exists for mammals or for hindlimb locomotion. Further, impalement by the traditional sharp electrodes, as used in the mudpuppy, may induce current leaks that alter the passive membrane properties, while whole-cell patch recordings are thought to more accurately report these properties (126).

Using the dorsal-up SCH-P, we recently achieved whole-cell patch recordings from spinal interneurons during unrestrained locomotion. Stable recordings were easily achieved with adequate cord stabilization with insect pins. An example recording is shown in Figure 12. This T12 dorsal horn interneuron was recruited into spiking during locomotion and exhibited rhythmic spiking that increased with ipsilateral L3 dorsal root activity and reached maximum during ipsilateral flexion (Figure 12). Slightly hyperpolarizing the membrane with current injection revealed rhythmic depolarizing drive potentials (Figure 12B) similar to those previously observed in

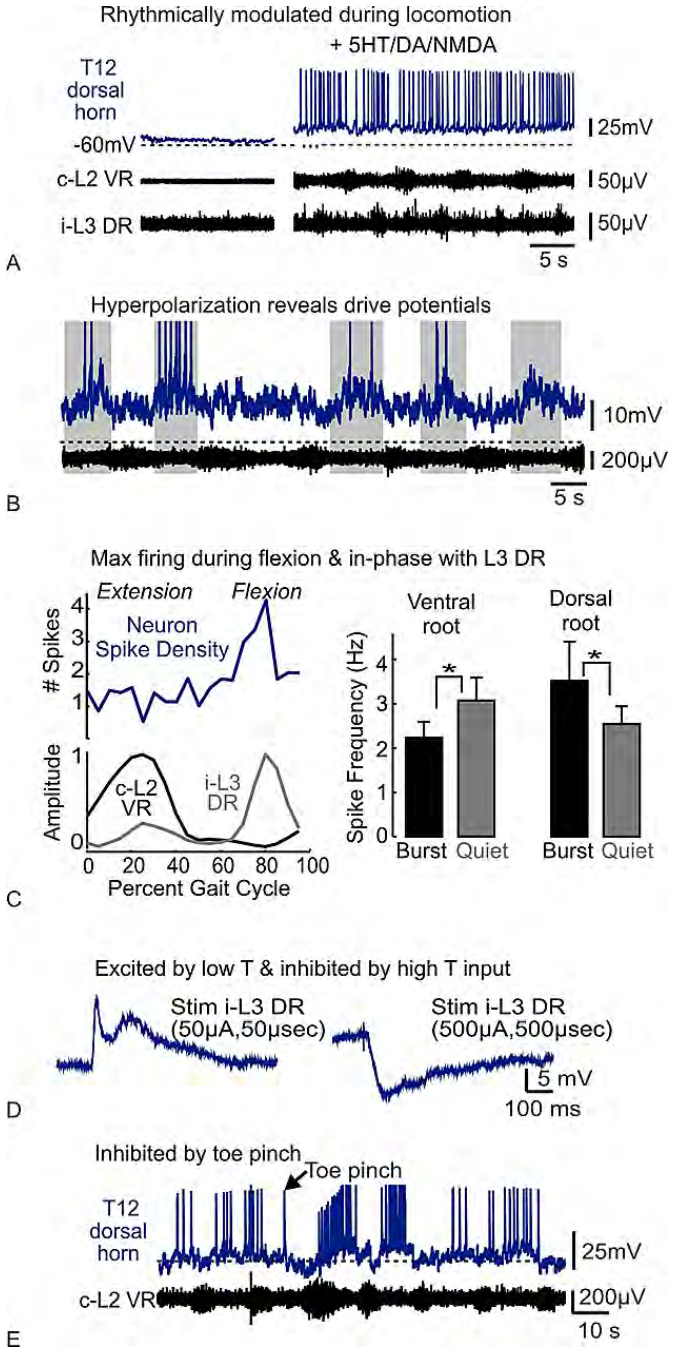

Figure 12. Intracellular patch clamp recordings during unrestrained hindlimb stepping. Activity from a T12 dorsal horn interneuron was recorded using whole cell patch clamp techniques. Interneuron activity (blue) is shown relative to ipsilateral (i-) and contralateral (c-) ventral root (VR) and dorsal root (DR) activity (black). As reported previously, the L2 VR activity corresponds to the flexion phase. (a) Resting membrane potential for this neuron was near -60mV. The neuron was quiescent at rest, but rhythmically spiked during neurochemically-induced locomotion. (b) Slightly hyperpolarizing the membrane potential revealed rhythmic drive potentials underlying the neuron's rhythmic spiking. (c) Left: Mean spike density (# spikes/bin) is shown relative to rectified integrated root activity were averaged across 47 cycles at 5% time bins. Spike density was maximum during the flexion phase, out-of-phase with c-L2 VR activity, and in-phase with i-L3 DR activity. Right: Mean spike frequency was significantly higher during cL2 VR quiescence and i-L3 DR bursting ($p < 0.05$). (d) Stimulation of the ipsilateral L3 dorsal root (i-L3 DR) showed that the neuron was excited by low-threshold stimulation (50µA, 50µsec), but inhibited by high-threshold stimulation (500µA, 500µsec). (e) Toe pinch showed that natural high-threshold noxious stimuli also inhibited the neuron's firing. Inhibition was followed by rebounding spiking.

motoneurons and interneurons (16, 32, 127). During locomotion, spike frequency for this interneuron was significantly higher during L3 dorsal root bursting and lower during contralateral L2 ventral root activity (i.e. out-of-phase with contralateral flexion, in-phase with ipsilateral flexion) (Figure 12C). In the dorsal horn, rhythmic drive potentials likely reflect afferent mediated synaptic actions from cyclic limb movements and may well contribute to locomotor drive potentials involved in the shaping of rhythmic motor output (122). This interneuron received strong, excitatory low-threshold afferent input, but was inhibited by high threshold inputs (Figure 12D). Toe pinch during locomotion evoked inhibition followed by rebound firing (Figure 12E), consistent with inhibition from high threshold stimulation.

Stable intracellular recordings and various imaging approaches (e.g. two–photon Ca2+ imaging) maintained through unrestrained hindlimb locomotion should further advance the understanding of spinal locomotor circuitry.

6. CONCLUSIONS

It has been known for over two decades that the isolated neonatal *in vitro* spinal cord offers distinct methodological advantages for the study of mammalian locomotor circuits. This includes easy access for pharmacology, stimulation, and lesioning, as well as stability for whole-cell patch clamp recordings. The more recent addition of complementary genetic approaches has provided for unprecedented identification and control of distinct neuronal populations implicated in locomotor rhythmogenesis. However, interpretations are limited when based solely on ventral root recordings that contain heterogeneity in motor and autonomic axons. Further integration of the *in vitro* model with afferent feedback and intact hindlimbs, particularly the SCH-P that can assess locomotor function with techniques previously restricted to *in vivo* studies, promise to provide important additional insights into locomotor circuit organization.

7. ACKNOWLEDGEMENTS

The authors are indebted to Dr. Patrick Whelan for providing helpful comments to improve the manuscript. The authors generously acknowledge the support of various funding agencies. S.H. - Christopher and Dana Reeve Foundation, Craig Neilsen Foundation, Paralyzed Veterans of America, National Science Foundation #0745164, NIH awards EB006179, NS 045248, NS40893, NS40440. E.G. - NIH NRSA. H.H. and J.A. - NSF IGERT DGE-0333411, and NSF GRFPs. S.D. – NIH EB006179. Y-H. C. - NIH AR054760.

8. REFERENCES

1. T G Brown: The intrinsic factors in the act of progression in the mammal. *Proceedings of the Royal Society of London*, 84, 308-319 (1911)

2. S Grillner: Control of locomotion in bipeds,tetrapods, and fish. In: *Handbook of Physiology-The Nervous System II*. (1981)

3. M. Goulding: Circuits controlling vertebrate locomotion: moving in a new direction. *Nature reviews. Neuroscience*, 10(7), 507-18 (2009)

4. O Kiehn: Locomotor circuits in the mammalian spinal cord. *Annu.Rev.Neurosci*, 29, 279-306 (2006)

5. PA Guertin: The mammalian central pattern generator for locomotion. *Brain research reviews*, 62(1), 45-56 (2009)

6. DA McCrea, IA Rybak: Organization of mammalian locomotor rhythm and pattern generation. *Brain research reviews*, 57(1), 134-46 (2008)

7. RM Brownstone, TV Bui: Spinal interneurons providing input to the final common path during locomotion. *Prog Brain Res*, 187, 81-95 (2010)

8. PJ Whelan: Shining light into the black box of spinal locomotor networks. *Philosophical transactions of the Royal Society of London. Series B, Biological sciences*, 365(1551), 2383-95 (2010)

9. RM Harris-Warrick: General principles of rhythmogenesis in central pattern generator networks. *Progress in brain research*, 187, 213-22 (2010)

10. PS Stein: Alternation of agonists and antagonists during turtle hindlimb motor rhythms. *Annals of the New York Academy of Sciences*, 1198, 105-18 (2010)

11. RM Brownstone, JM Wilson: Strategies for delineating spinal locomotor rhythm-generating networks and the possible role of Hb9 interneurones in rhythmogenesis. *Brain research reviews*, 57(1), 64-76 (2008)

12. T Endo, O Kiehn: Asymmetric operation of the locomotor central pattern generator in the neonatal mouse spinal cord. *Journal of neurophysiology*, 100(6), 3043-54 (2008)

13. A Lundberg: Half-centres revisited. In: *Regulatory Functions of the CNS. Motion and Organization Principles*. Ed P. M. edited by Szentagotheu J&a. H. J. Pergamon, Budapest, Hungary: (1981)

14. RE Burke: The central pattern generator for locomotion in mammals. *Advances in neurology*, 87, 11-24 (2001)

15. DJ Kriellaars, RM Brownstone, BR Noga, LM Jordan: Mechanical entrainment of fictive locomotion in the decerebrate cat. *J.Neurophysiol.*, 71, 2074-2086 (1994)

16. S Hochman, BJ Schmidt: Whole cell recordings of lumbar motoneurons during locomotor like activity in the

in vitro neonatal rat spinal cord. *Journal of Neurophysiology*, 79(2), 743-752 (1998)

17. DA McCrea, IA Rybak: Modeling the mammalian locomotor CPG: insights from mistakes and perturbations. *Progress in brain research*, 165, 235-53 (2007)

18. IA Rybak, K Stecina, NA Shevtsova, DA McCrea: Modelling spinal circuitry involved in locomotor pattern generation: insights from the effects of afferent stimulation. *The Journal of physiology*, 577(Pt 2), 641-58 (2006)

19. IA Rybak, NA Shevtsova, M Lafreniere-Roula, DA McCrea: Modelling spinal circuitry involved in locomotor pattern generation: insights from deletions during fictive locomotion. *The Journal of physiology*, 577(Pt 2), 617-39 (2006)

20. H Nishimaru, N Kudo: Formation of the central pattern generator for locomotion in the rat and mouse. *Brain research bulletin*, 53(5), 661-9 (2000)

21. JC Smith, JL Feldman, BJ Schmidt: Neural mechanisms generating locomotion studied in mammalian brain stem-spinal cord *in vitro*. *FASEB J.* 2(7):2283-8 (1988)

22. J Westerga, A Gramsbergen: The development of locomotion in the rat. *Developmental Brain Research*, 57, 163-174 (1990)

23. HB Hayes, YH Chang, S Hochman: An *in vitro* spinal cord-hindlimb preparation for studying behaviorally relevant rat locomotor function. *Journal of neurophysiology*, 101(2), 1114-22 (2009)

24. L Juvin, J Simmers, D Morin: Propriospinal circuitry underlying interlimb coordination in mammalian quadrupedal locomotion. *J.Neurosci*, 25(25), 6025-6035 (2005)

25. O Kiehn, O Kjaerulff: Spatiotemporal characteristics of 5-HT and dopamine-induced rhythmic hindlimb activity in the *in vitro* neonatal rat. *J.Neurophysiol.*, 75, 1472-1482 (1996)

26. DA Klein, MC Tresch: Specificity of intramuscular activation during rhythms produced by spinal patterning systems in the *in vitro* neonatal rat with hindlimb attached preparation. *Journal of neurophysiology*, 104(4), 2158-68 (2010)

27. DA Klein, A Patino, MC Tresch: Flexibility of motor pattern generation across stimulation conditions by the neonatal rat spinal cord. *Journal of neurophysiology*, 103(3), 1580-90 (2010)

28. T Akay, HJ Acharya, K Fouad, KG Pearson: Behavioral and electromyographic characterization of mice lacking EphA4 receptors. *Journal of neurophysiology*, 96(2), 642-51 (2006)

29. RJ Wilson, T Chersa, PJ Whelan: Tissue PO2 and the effects of hypoxia on the generation of locomotor-like activity in the *in vitro* spinal cord of the neonatal mouse. *Neuroscience*, 117(1), 183-196 (2003)

30. Y Okada, K Muckenhoff, G Holtermann, H Acker, P Scheid: Depth profiles of pH and PO2 in the isolated brain stem-spinal cord of the neonatal rat. *Respiration physiology*, 93(3), 315-26 (1993)

31. KC Murray, MJ Stephens, EW Ballou, CJ Heckman, DJ Bennett: Motoneuron excitability and muscle spasms are regulated by 5-HT2B and 5-HT2C receptor activity. *Journal of neurophysiology*, 105(2), 731-48 (2011)

32. O Kiehn, BR Johnson, M Raastad: Plateau properties in mammalian spinal interneurons during transmitter-induced locomotor activity. *Neuroscience*, 75(1), 263-273 (1996)

33. M Hagglund, L Borgius, KJ Dougherty, O Kiehn: Activation of groups of excitatory neurons in the mammalian spinal cord or hindbrain evokes locomotion. *Nature neuroscience*, 13(2), 246-52 (2010)

34. S Grillner, TM Jessell: Measured motion: searching for simplicity in spinal locomotor networks. *Current opinion in neurobiology*, 19(6), 572-86 (2009)

35. IT Gordon, PJ Whelan: Deciphering the organization and modulation of spinal locomotor central pattern generators. *The Journal of experimental biology*, 209(Pt 11), 2007-14 (2006)

36. O Kiehn, RM Harris-Warrick, LM Jordan, H Hultborn, N Kudo: Neuronal Mechanisms for Generating Locomotor Activity. The New York Academy of Sciences, New York (1998)

37. P Whelan, A Bonnot, MJ O'Donovan: Properties of rhythmic activity generated by the isolated spinal cord of the neonatal mouse. *Journal of neurophysiology*, 84(6), 2821-33 (2000)

38. O Kiehn, O Kjaerulff: Distribution of central pattern generators for rhythmic motor outputs in the spinal cord of limbed vertebrates. *Annals of the New York Academy of Sciences*, 860, 110-129 (1998)

39. Y Sqalli-Houssaini, JR Cazalets, F Clarac: Oscillatory properties of the central pattern generator for locomotion in neonatal rats. *J.Neurophysiol*., 70, 803-813 (1993)

40. E Zaporozhets, KC Cowley, BJ Schmidt: A reliable technique for the induction of locomotor-like activity in the in vitro neonatal rat spinal cord using brainstem electrical stimulation. *Journal of neuroscience methods*, 139(1), 33-41 (2004)

41. J Liu, LM Jordan: Stimulation of the parapyramidal region of the neonatal rat brain stem produces locomotor-like activity involving spinal 5-HT7 and 5-HT2A receptors. *J Neurophysiol*., 94(2), 1392-1404 (2005)

42. IT Gordon, PJ Whelan: Brainstem modulation of locomotion in the neonatal mouse spinal cord. *The Journal of physiology*, 586(10), 2487-97 (2008)

43. K Szokol, JC Glover, MC Perreault: Organization of Functional Synaptic Connections between Medullary Reticulospinal Neurons and Lumbar Descending Commissural Interneurons in the Neonatal Mouse. *The Journal of neuroscience*, 31(12), 4731-42 (2011)

44. N Kasumacic, JC Glover, MC Perreault: Segmental patterns of vestibular-mediated synaptic inputs to axial and limb motoneurons in the neonatal mouse assessed by optical recording. *The Journal of physiology*, 588(Pt 24), 4905-25 (2010)

45. A Bonnot, D Morin, D Viala: Organization of rhythmic motor patterns in the lumbosacral spinal cord of neonate mouse. *Annals of the New York Academy of Sciences*, 860, 432-435 (1998)

46. H Gabbay, I Delvolve, A Lev-Tov: Pattern generation in caudal-lumbar and sacrococcygeal segments of the neonatal rat spinal cord. *J Neurophysiol.*, 88(2), 732-739 (2002)

47. A Lev-Tov, I Delvolve, E Kremer: Sacrocaudal afferents induce rhythmic efferent bursting in isolated spinal cords of neonatal rats. *J Neurophysiol.*, 83(2), 888-894 (2000)

48. A Lev-Tov, M Pinco: *In vitro* studies of prolonged synaptic depression in the neonatal rat spinal cord. *Journal of Physiology*, 447, 149-169 (1992)

49. C Marchetti, M Beato, A Nistri: Alternating rhythmic activity induced by dorsal root stimulation in the neonatal rat spinal cord *in vitro*. *J Physiol*, 530(Pt 1), 105-112 (2001)

50. JL Todd, SP DeWeerth, S Hochman : Sacral spinal dorsal column stimulation activates locomotor-like activity via a cholinergic pathway in the neonatal rat spinal cord. *Soc. Neurosci. Abst*, 33 (2007)

51. GZ Mentis, FJ Alvarez, A Bonnot, DS Richards, D Gonzalez-Forero, R Zerda, MJ O'Donovan: Noncholinergic excitatory actions of motoneurons in the neonatal mammalian spinal cord. *Proc.Natl.Acad.Sci.U.S.A*, 102(20), 7344-7349 (2005)

52. A Bonnot, PJ Whelan, GZ Mentis, MJ O'Donovan: Locomotor-like activity generated by the neonatal mouse spinal cord. *Brain Res Brain Res Rev.*, 40(1-3), 141-151 (2002)

53. JC Norreel, JF Pflieger, E Pearlstein, J Simeoni-Alias, F Clarac, L Vinay: Reversible disorganization of the locomotor pattern after neonatal spinal cord transection in the rat. *The Journal of neuroscience:* 23(5), 1924-32 (2003)

54. S Rossignol, R Dubuc, JP Gossard: Dynamic sensorimotor interactions in locomotion. *Physiol Rev.*, 86(1), 89-154 (2006)

55. C Cina, S Hochman: Diffuse distribution of sulforhodamine-labeled neurons during serotonin-evoked locomotion in the neonatal rat thoracolumbar spinal cord. *J.Comp Neurol.*, 423(4), 590-602 (2000)

56. O Kjaerulff, I Barajon, O Kiehn: Sulphorhodamine-labelled cells in the neonatal rat spinal cord following chemically induced locomotor activity *in vitro Journal of Physiology*, 478, 265-273 (1994)

57. I Delvolve, H Gabbay, A Lev-Tov: The motor output and behavior produced by rhythmogenic sacrocaudal networks in spinal cords of neonatal rats. *J Neurophysiol.*, 85(5), 2100-2110 (2001)

58. I Strauss, A Lev-Tov: Neural pathways between sacrocaudal afferents and lumbar pattern generators in neonatal rats. *J Neurophysiol.*, 89(2), 773-784 (2003)

59. Y Li, RE Burke: Developmental changes in short-term synaptic depression in the neonatal mouse spinal cord. *J Neurophysiol.*, 88(6), 3218-3231 (2002)

60. WD Willis, RE Coggeshall: Sensory Mechanisms of the Spinal Cord. Plenum, New York (1991)

61. WD Willis, Jr., KN Westlund: The role of the dorsal column pathway in visceral nociception. *Current pain and headache reports*, 5(1), 20-6 (2001)

62. JT Patterson, PA Head, DL McNeill, K Chung, RE Coggeshall: Ascending unmyelinated primary afferent fibers in the dorsal funiculus. *Journal of Comparative Neurology*, 290, 384-390 (1989)

63. KW Meacham, L Guo, SP DeWeerth, S Hochman: Selective Stimulation of the Spinal Cord Surface Using a Conformable Microelectrode Array. *Frontiers in Neuroengineering*, Apr 21;4:5 (2011)

64. MR Dimitrijevic, Y Gerasimenko, MM Pinter: Evidence for a spinal central pattern generator in humans. *Annals of the New York Academy of Sciences*, 860, 360-376 (1998)

65. YP Gerasimenko, VD Avelev, OA Nikitin, IA Lavrov: Initiation of locomotor activity in spinal cats by epidural stimulation of the spinal cord. *Neurosci.Behav.Physiol*, 33(3), 247-254 (2003)

66. Y Gerasimenko, RR Roy, VR Edgerton: Epidural stimulation: comparison of the spinal circuits that generate and control locomotion in rats, cats and humans. *Experimental neurology*, 209(2), 417-25 (2008)

67. S Harkema, Y Gerasimenko, J Hodes, J Burdick, C Angeli, Y Chen, C Ferreira, A Willhite, E Rejc, RG Grossman, VR Edgerton: Effect of epidural stimulation of the lumbosacral spinal cord on voluntary movement, standing, and assisted stepping after motor complete paraplegia: a case study. *Lancet*, 377(9781), 1938-47 (2011)

68. S Mandadi, PJ Whelan: A new method to study sensory modulation of locomotor networks by activation of thermosensitive cutaneous afferents using a hindlimb attached spinal cord preparation. *Journal of neuroscience methods*, 182(2), 255-9 (2009)

69. RM Ichiyama, YP Gerasimenko, H Zhong, RR Roy and VR Edgerton: Hindlimb stepping movements in complete spinal rats induced by epidural spinal cord stimulation. *Neurosci.Lett.* (2005)

70. I Lavrov, G Courtine, CJ Dy, R van den Brand, AJ Fong, Y Gerasimenko, H Zhong, RR Roy, VR Edgerton: Facilitation of stepping with epidural stimulation in spinal rats: role of sensory input. *The Journal of neuroscience:* 28(31), 7774-80 (2008)

71. I Lavrov, CJ Dy, AJ Fong, Y Gerasimenko, G Courtine, H Zhong, RR Roy, VR Edgerton: Epidural stimulation induced modulation of spinal locomotor networks in adult spinal rats. *The Journal of neuroscience:* 28(23), 6022-9 (2008)

72. ED Schomburg, N Petersen, I Barajon, H Hultborn: Flexor reflex afferents reset the step cycle during fictive locomotion in the cat. *Experimental Brain Research*, 122(3), 339-350 (1998)

73. M Iizuka, O Kiehn, N Kudo: Development in neonatal rats of the sensory resetting of the locomotor rhythm induced by NMDA and 5-HT. *Experimental Brain Research*, 114(2), 193-204 (1997)

74. DA McCrea: Neuronal basis of afferent-evoked enhancement of locomotor activity. *Annals of the New York Academy of Sciences*, 860, 216-225 (1998)

75. BA Conway, H Hultborn, O Kiehn: Proprioceptive input resets central locomotor rhythm in the spinal cat. *Experimental Brain Research*, 68, 643-656 (1987)

76. H Hultborn, BA Conway, JP Gossard, R Brownstone, B Fedirchuk, ED Schomburg, M Enr¡quez-Denton, MC Perreault: How do we approach the locomotor network in the mammalian spinal cord? *Annals of the New York Academy of Sciences*, 860, 70-82 (1998)

77. DA McCrea: Spinal circuitry of sensorimotor control of locomotion. *J Physiol*, 533(Pt 1), 41-50 (2001)

78. K Bradley, JC Eccles: Analysis of the fast afferent impulses from thigh muscles. *J Physiol*, 122(3), 462-473 (1953)

79. S Mandadi, ST Nakanishi, Y Takashima, A Dhaka, A Patapoutian, DD McKemy, PJ Whelan: Locomotor networks are targets of modulation by sensory transient receptor potential vanilloid 1 and transient receptor potential melastatin 8 channels. *Neuroscience*, 162(4), 1377-97 (2009)

80. DR Foran, AC Peterson: Myelin acquisition in the central nervous system of the mouse revealed by an MBP-Lac Z transgene. *The Journal of neuroscience:* 12(12), 4890-7 (1992)

81. O Kiehn, M Iizuka, N Kudo: Resetting from low threshold afferents of N -methyl-D-aspartate- induced locomotor rhythm in the isolated spinal cord-hindlimb preparation from newborn rats. *Neurosci.Lett.*, 148, 43-46 (1992)

82. D Blivis, GZ Mentis, MJ O'Donovan, A Lev-Tov: Differential effects of opioids on sacrocaudal afferent pathways and central pattern generators in the neonatal rat spinal cord. *Journal of neurophysiology*, 97(4), 2875-86 (2007)

83. RJ Vogelstein, R Etienne-Cummings, NV Thakor, AH Cohen: Phase-dependent effects of spinal cord stimulation on locomotor activity. *IEEE transactions on neural systems and rehabilitation engineering*, 14(3), 257-65 (2006)

84. Y Mor, A Lev-Tov: Analysis of rhythmic patterns produced by spinal neural networks. *Journal of neurophysiology*, 98(5), 2807-17 (2007)

85. BW Gallarda, TO Sharpee, SL Pfaff, WA Alaynick: Defining rhythmic locomotor burst patterns using a continuous wavelet transform. *Annals of the New York Academy of Sciences*, 1198, 133-9 (2010)

86. VK Mushahwar, DM Gillard, MJ Gauthier, A Prochazka: Intraspinal micro stimulation generates locomotor-like and feedback-controlled movements. *IEEE Trans.Neural Syst.Rehabil.Eng*, 10(1), 68-81 (2002)

87. RJ Vogelstein, F Tenore, R Etienne-Cummings, MA Lewis and A. H. Cohen: Dynamic control of the central pattern generator for locomotion. *Biological cybernetics*, 95(6), 555-66 (2006)

88. S Nicolopoulos-Stournaras, JF Iles: Motor Neuron Columns in the Lumbar Spinal Cord of the Rat. *Journal of Comparative Neurology*, 217, 75-85 (1983)

89. S McHanwell, TJ Biscoe: The sizes of motoneurons supplying hindlimb muscles in the mouse. *Proc.R.Soc.Lond B Biol.Sci.*, 213(1191), 201-216 (1981)

90. VGJM Vanderhorst, G Holstege: Organization of lumbosacral motoneuronal cell groups innervating hindlimb, pelvic floor, and axial muscles in the cat. *Journal of Comparative Neurology*, 382(1), 46-76 (1997)

91. CR Anderson, JR Keast, EM McLachlan: Spinal autonomic preganglionic neurons: the visceral efferent system of the spinal cord. In: *The spinal cord*. Ed C. Waton, Paxinos, G., and Kayalioglu, G. Elsevier, Amsterdam (2009)

92. KC Cowley, BJ Schmidt: Some limitations of ventral root recordings for monitoring locomotion in the *in vitro* neonatal rat spinal cord preparation. *Neurosci.Lett.*, 171, 142-146 (1994)

93. ED Schomburg, H Steffens, K Dembowsky: Rhythmic phrenic, intercostal and sympathetic activity in relation to limb and trunk motor activity in spinal cats. *Neurosci.Res*, 46(2), 229-240 (2003)

94. AE Pickering, D Spanswick, SD Logan: 5-Hydoxytryptamine evokes depolarizations and membrane potential oscillations in rat sympathetic preganglionic neurones. *Journal of Physiology*, 480, 109-121 (1994)

95. M Lafreniere-Roula, DA McCrea: Deletions of rhythmic motoneuron activity during fictive locomotion and scratch provide clues to the organization of the mammalian central pattern generator. *J Neurophysiol.* (2005)

96. L Juvin, J Simmers, D Morin: Locomotor rhythmogenesis in the isolated rat spinal cord: a phase-coupled set of symmetrical flexion extension oscillators. *J.Physiol*, 583(Pt 1), 115-128 (2007)

97. PS Stein: Motor pattern deletions and modular organization of turtle spinal cord. *Brain research reviews*, 57(1), 118-24 (2008)

98. SJ Butt, O Kiehn: Functional identification of interneurons responsible for left-right coordination of hindlimbs in mammals. *Neuron*, 38(6), 953-963 (2003)

99. AE Stepien, M Tripodi, S Arber: Monosynaptic rabies virus reveals premotor network organization and synaptic specificity of cholinergic partition cells. *Neuron*, 68(3), 456-72 (2010)

100. DL McLean, J Fan, S Higashijima, ME Hale, JR Fetcho: A topographic map of recruitment in spinal cord. *Nature*, 446(7131), 71-75 (2007)

101. C Wyart, F Del Bene, E Warp, EK Scott, D Trauner, H Baier, EY Isacoff: Optogenetic dissection of a behavioural module in the vertebrate spinal cord. *Nature*, 461(7262), 407-410 (2009)

102. RM Eccles, A Lundberg: Synaptic actions in motoneurones by afferents which may evoke the flexion reflex. *Arch.Ital.Biol.*(97), 199-221 (1959)

103. NE Anden, MG Jukes, A Lundberg, L Vyklicky: A NEW SPINAL FLEXOR REFLEX. *Nature*, 202, 1344-1345 (1964)

104. E Jankowska, MGM Jukes, S Lund, A Lundberg: The effect of DOPA on the spinal cord. 6. Half-centre organization of interneurones transmitting effects from the flexor reflex afferents. *Acta Physiologica Scandinavica*, 68, 389-403 (1967)

105. H Steffens, ED Schomburg: Convergence in segmental reflex pathways from nociceptive and non-nociceptive afferents to à-motoneurones in the cat. *Journal of Physiology*, 466, 191-211 (1993)

106. ED Schomburg, H Steffens: Comparative analysis of L-DOPA actions on nociceptive and non-nociceptive spinal reflex pathways in the cat. *Neuroscience Research*, 31(4), 307-316 (1998)

107. ED Schomburg, N Petersen, I Barajon, H Hultborn: Flexor reflex afferents reset the step cycle during fictive locomotion in the cat. *Exp.Brain Res*, 122(3), 339-350 (1998)

108. PO Riley, G Paolini, U Della Croce, KW Paylo, DC Kerrigan: A kinematic and kinetic comparison of overground and treadmill walking in healthy subjects. *Gait & posture*, 26(1), 17-24 (2007)

109. JT Yen, AG Auyang, YH. Chang: Joint-level kinetic redundancy is exploited to control limb-level forces during human hopping. *Experimental brain research* 196(3), 439-51 (2009)

110. J Nilsson, A Thorstensson: Ground reaction forces at different speeds of human walking and running. *Acta physiologica Scandinavica*, 136(2), 217-27 (1989)

111. YH Chang, JE Bertram, A Ruina: A dynamic force and moment analysis system for brachiation. *The Journal of experimental biology*, 200(Pt 23), 3013-20 (1997)

112. S Rossignol: Plasticity of connections underlying locomotor recovery after central and/or peripheral lesions in the adult mammals. *Philos.Trans.R.Soc.Lond B Biol.Sci.*, 361(1473), 1647-1671 (2006)

113. KG Pearson, JE Misiaszek, K Fouad: Enhancement and resetting of locomotor activity by muscle afferents. *Annals of the New York Academy of Sciences*, 860, 203-215 (1998)

114. S Grillner, S Rossignol: On the initiation of the swing phase of locomotion in chronic spinal cats. *Brain research*, 146(2), 269-77 (1978)

115. GW Hiebert, PJ Whelan, A Prochazka, KG Pearson: Contribution of hind limb flexor muscle afferents to the timing of phase transitions in the cat step cycle. *Journal of neurophysiology*, 75(3), 1126-37 (1996)

116. JM Donelan, KG Pearson: Contribution of force feedback to ankle extensor activity in decerebrate walking cats. *Journal of neurophysiology*, 92(4), 2093-104 (2004)

117. GW Hiebert, KG Pearson: Contribution of sensory feedback to the generation of extensor activity during walking in the decerebrate cat. *Journal of Neurophysiology*, 81(2), 758-770 (1999)

118. AK Thota, SC Watson, E Knapp, B Thompson, R Jung: Neuromechanical control of locomotion in the rat. *Journal of neurotrauma*, 22(4), 442-65 (2005)

119. V Dietz, J Duysens: Significance of load receptor input during locomotion: a review. *Gait & posture*, 11(2), 102-10 (2000)
120. M Faist, C Hoefer, M Hodapp, V Dietz, W Berger, J Duysens: In humans Ib facilitation depends on locomotion while suppression of Ib inhibition requires loading. *Brain research*, 1076(1), 87-92 (2006)

121. DP Ferris, P Aagaard, EB Simonsen, CT Farley, P Dyhre-Poulsen: Soleus H-reflex gain in humans walking and running under simulated reduced gravity. *The Journal of physiology*, 530(Pt 1), 167-80 (2001)
122. O Kiehn, O Kjaerulff, MC Tresch, RM Harris-Warrick: Contributions of intrinsic motor neuron properties to the production of rhythmic motor output in the mammalian spinal cord. *Brain Research Bulletin*, 53(5), 649-659 (2000)

123. MC Tresch, O. Kiehn: Coding of locomotor phase in populations of neurons in rostral and caudal segments of the neonatal rat lumbar spinal cord. *J.Neurophysiol.*, 82(6), 3563-3574 (1999)

124. O Kiehn, SJ Butt: Physiological, anatomical and genetic identification of CPG neurons in the developing mammalian spinal cord. *Progress in Neurobiology*, 70(4), 347-361 (2003)

125. M Wheatley, M Edamura, RB Stein: A comparison of intact and in-vitro locomotion in an adult amphibian. *Experimental Brain Research*, 88, 609-614 (1992)

126. KJ Staley, TS Otis, I Mody: Membrane properties of dentate gyrus granule cells: Comparison of sharp microelectrode and whole-cell recordings. *J.Neurophysiol.*, 67, 1346-1358 (1992)

127. LM Jordan: Factors determining motoneuron rhythmicity during fictive locomotion. *Soc.Exp.Biol.Symp.*, 37, 423-444 (1983)

Key Words: Spinal cord, Locomotion, *In vitro*, Dorsal column, EMG, Central pattern generator, CPG, Rhythmic, Review, Afferent, Sensory, Review

Send correspondence to: Shawn Hochman**,** Department of Physiology, Emory University School of Medicine, Atlanta, Georgia, Tel: 404-712-3131, Fax: 404-727-2648, E-mail: shawn.hochman@emory.edu

J Neurophysiol 106: 2794–2795, 2011.
First published September 28, 2011; doi:10.1152/jn.00873.2011.

Long-term patch recordings from adult spinal neurons herald new era of opportunity

Shawn Hochman
Department of Physiology, Emory University School of Medicine, Atlanta, Georgia

Submitted 26 September 2011; accepted in final form 26 September 2011

Hochman S. Long-term patch recordings from adult spinal neurons herald new era of opportunity. *J Neurophysiol* 106: 2794–2795, 2011. First published September 28, 2011; doi:10.1152/jn.00873.2011.— Recently, Andreas Husch, Nathan Cramer, and Ronald M. Harris-Warrick achieved a remarkable breakthrough in patch-clamp recordings of ventral horn neurons in the adult spinal cord slice preparation. This landmark study that breaks the "age barrier" is titled "Long-duration perforated patch recordings from spinal interneurons of adult mice" (Husch et al., in press). In it, the authors demonstrate the unprecedented ability to undertake day-long (up to 12 h), and utterly stable perforated patch recordings. A description of the methodology is detailed in their paper. Here, I give a brief overview before providing context to this extraordinary achievement.

spinal cord; perforated patch; interneuron

HUSCH ET AL. (IN PRESS) DESCRIBE THE INCORPORATION of two technical strategies that combine to enable stable and very long-duration recordings. The first technique emphasizes the surgical approach and preparation of spinal cord slices, and the second technique is on the use of the perforated patch approach with amphotericin B. Overall, while the method has notable challenges, when implemented successfully, it will undoubtedly open a tantalizingly broad window for experimentation, on neural function, neurological dysfunction, and aging in the adult spinal cord.

Isolating the spinal cord. The authors first limit hypoxia by optimizing removal of the spinal cord by a method similar to that undertaken by Bennett's group in rat (Li et al. 2004). This is accomplished by cord exposure via laminectomy with subsequent local surface application of an ice-cold modified artificial cerebrospinal fluid solution to reduce metabolism. Further enhancing oxygenation by providing 100% O_2 for the mice to breathe was not included in this approach [cf. (Li et al. 2004), but may be needed to afford greater protection from hypoxia if motoneurons are targeted]. Carp and colleagues (2008) successfully recorded with sharp electrodes from adult rat motoneurons in spinal slice by a comparable method, but like their predecessors (Aghajanian and Rasmussen 1989; Hori et al. 2001), they also included transcardial perfusion of ice-cold modified artificial cerebrospinal fluid. Again, this added layer of neuroprotection may afford greater survival of motoneurons from hypoxia, but was clearly not necessary for the interneurons targeted in the Husch et al. study (in press).

Perforated patch-clamp recordings. Successful implementation of the perforated patch technique plainly requires meticulous attention to detail (Rae et al. 1991). Pore-forming molecules like amphotericin B prevent the formation of gigaohm seals, so the electrode tip must be filled in solution without it. As recordings in slices are typically below the surface, positive pressure is required to clear debris, so cell targeting and subsequent membrane suction must occur before pore-forming molecules reach the electrode tip. However, if they are too far from the tip, pore formation would be too slow and incomplete to obtain the desired low series resistance. So, the right electrode tapers, the right amount amphotericin-free solution at the tip, and the right amount of positive pressure undertaken for the right amount of time all must be tightly calibrated to bring this approach to fruition. While not explored, the possibility of utilizing this technique in "blind" targeting approaches from thicker slices (Blanton et al. 1989) is also feasible within the same time constraints (Hall et al. 1999).

Time is a treasure. When it comes to cellular physiology, there are few luxuries greater than time and recording stability. With these luxuries come reproducible application of agonists and antagonists, time to study long-term changes, and dose/physiological-response relations can be undertaken without the worry of cell dialysis-induced time-dependent changes in function. A systematic pharmacological dissection of the prospective role of many metabotropic and ionotropic receptors within an individual neuron also becomes feasible. Moreover, due to the remarkable recording stability, as stated by Husch et al. (in press), "it is possible to discern even subtle effects of neuromodulators on the intrinsic properties of neurons, which were previously difficult to measure due to the rundown of various intrinsic currents in whole cell recordings."

A window into disease, injury, and aging. Most central nervous system (CNS) disorders present in adulthood, and many include alterations in spinal circuit function. This includes neurodegenerative disorders (e.g., amyotrophic lateral sclerosis), epilepsies (e.g., spinal myoclonus), and injury-induced disorders (e.g., spinal cord injury). For instance, spinal cord injury imposes alterations in sensory, motor, and autonomic circuits with clear interneuronal involvement. How interneuronal properties are altered has not been examined in vitro in adult interneurons, and so has remained the territory of in vivo approaches with inherent limitations in neuron identity, recording stability, and drug access. The same limitations could be said for studies of other disorders with spinal cord involvement. Moreover, how aging-induced alterations in motor coordination reflect alterations in spinal interneuronal function could now be explored using this recording approach.

How generalizable are these findings, and what is the secret for long-duration recordings? In this study, the oldest animals were 3 mo old, but there is no reason to believe that older animals will restrict success. However, nothing is said about whether ensheathing perineuronal nets (PNNs), a likely physical barrier to membrane access, were encountered while using this method. Not all neurons are encapsulated in PNNs, and the genetically identified V2A interneuron population was selectively targeted. The spinal cord ventral horn has the greatest percentage of neurons enshrouded in PNNs (~60%) than any

Address for reprint requests and other correspondence: S. Hochman, Dept. of Physiology, Emory Univ. School of Medicine, 615 Michael St., Atlanta, GA 30322 (e-mail: shawn.hochman@emory.edu).

other CNS region (Bertolotto et al. 1996). In dorsal horn, less than 15% of neuron cell bodies are draped in PNNs. An intriguing possibility is that the patch electrode was able to locally breach an ensheathing PNN, but its continued presence (perhaps dependent on lack of cell dialysis) helped maintain structural integrity to greatly enhance recording duration and stability. If a relationship between PNNs and recording stability exists, this method would not be uniformly applicable to all spinal neurons and may differ after procedures that alter neuronal ensheathment [e.g., chondroitinase treatment-induced plasticity after spinal cord injury (e.g., Alilain et al. 2011)]. More generally, why consistently long-duration recordings have not been highlighted in other CNS regions, and whether this relates to an absence of PNNs (Bertolotto et al. 1996) and/or lack of use of amphotericin B (Kawamura and Wahler 1994) remains to be determined.

In summary, the Husch et al. (in press) paper will undoubtedly inspire a new era of experimentation. While neither the approach to spinal cord isolation nor the use of perforated patch recordings is technically novel, the combination leads to a landmark and absolutely transformative advance in the study of adult spinal cord interneurons implicated in motor control. It is no exaggeration to say that the present study breaks a critical barrier in electrophysiological studies on spinal neuronal function, providing for the first time a gateway into age-appropriate studies on spinal disease mechanisms. Moreover, the approach should generalize to many other spinal neurons. Last, the capacity for very long-term stable recordings moves characterization of a wide range of physiological properties in individual neurons from fantasy to reality.

GRANTS

The author is indebted to the following funding agencies: Christopher and Dana Reeve Foundation, Craig Neilsen Foundation, Paralyzed Veterans of America, National Science Foundation #0745164, National Institutes of Health awards EB-006179, NS-045248, NS-40893, and NS-40440.

DISCLOSURES

No conflicts of interest, financial or otherwise, are declared by the author(s).

AUTHOR CONTRIBUTIONS

Author contributions: S. H. drafted manuscript; S. H. edited and revised manuscript; S. H. approved final version of manuscript.

REFERENCES

Aghajanian GK, Rasmussen K. Intracellular studies in the facial nucleus illustrating a simple new method for obtaining viable motoneurons in adult rat brain slices. *Synapse* 3: 331–338, 1989.

Alilain WJ, Horn KP, Hu H, Dick TE, Silver J. Functional regeneration of respiratory pathways after spinal cord injury. *Nature* 475: 196–200, 2011.

Bertolotto A, Manzardo E, Guglielmone R. Immunohistochemical mapping of perineuronal nets containing chondroitin unsulfated proteoglycan in the rat central nervous system. *Cell Tissue Res* 283: 283–295, 1996.

Blanton MG, Lo Torco JJ, Kriegstein AR. Whole cell recording from neurons in slices of reptilian and mammalian cerebral cortex. *J Neurosci Methods* 30: 203–210, 1989.

Carp JS, Tennissen AM, Mongeluzi DL, Dudek CJ, Chen XY, Wolpaw JR. An in vitro protocol for recording from spinal motoneurons of adult rats. *J Neurophysiol* 100: 474–481, 2008.

Hall AC, Earle-Cruikshanks G, Harrington ME. Role of membrane conductances and protein synthesis in subjective day phase advances of the hamster circadian clock by neuropeptide Y. *Eur J Neurosci* 11: 3424–3432, 1999.

Hori N, Tan Y, Strominger NL, Carpenter DO. Intracellular activity of rat spinal cord motoneurons in slices. *J Neurosci Methods* 112: 185–191, 2001.

Husch A, Cramer N, Harris-Warrick RM. Long-duration perforated patch recordings from spinal interneurons of adult mice. *J Neurophysiol*; published ahead of print September 7, 2011, doi:10.1152/jn.00673.2011.

Kawamura A, Wahler GM. Perforated-patch recording does not enhance effect of 3-isobutyl-1-methylxanthine on cardiac calcium current. *Am J Physiol Cell Physiol* 266: C1619–C1627, 1994.

Li Y, Harvey PJ, Li X, Bennett DJ. Spastic long-lasting reflexes of the chronic spinal rat studied in vitro. *J Neurophysiol* 91: 2236–2246, 2004.

Rae J, Cooper K, Gates P, Watsky M. Low access resistance perforated patch recordings using amphotericin B. *J Neurosci Methods* 37: 15–26, 1991.

Selective optogenetic activation of ChAT-Cre/channelrhodopsin-expressing primary afferents.

Somatosensory inflow to the central nervous system is complexly regulated at the primary afferent synaptic relay to the spinal cord dorsal horn. Presynaptic nicotinic acetylcholine receptors (n**AChRs**) modulate synaptic transmission and are abundantly distributed on primary afferent terminals. Possible sources for cholinergic modulation of these nAChRs include dorsal horn islet-like interneurons, rostral ventrolateral medulla, and primary afferent fibers expressing a choline acetyltransferase (ChAT) splice-form specific to peripheral neurons (peripheral or **pChAT**). GM24-Gsat/ChAT-Cre mice (GENSAT) express Cre recombinase from the initiation site of the first coding exon shared by both ChAT/pChAT. We previously demonstrated reporter-based expression in known spinal cholinergic neurons as well as in a subpopulation of primary afferents that span the rostrocaudal neuraxis and includes cutaneous mechanoreceptors (Speigel et al. Society for Neuroscience 2013).

Here, ChAT-Cre mice were crossed with the channel channelrhodopsin (ChR2) expressing Ai32D Cre-dependent line to examine the spinal actions of selectively recruited ChAT expressing primary afferents. We first show ChR2 trafficked to dorsal root ganglia (DRG), dorsal root axons, spinal projections and peripheral nerve fibers, enabling further studies on possible optical excitability. We then used the isolated hemicord to assess optical excitability in juvenileChAT::ChR2 mice. In P7-10 preparations with attached hindlimbs, blue laser-diode light delivered through optical fibers positioned onto peripheral nerves evoked compound action potentials in recordings from sciatic nerve or lumbar dorsal roots. When recording from the thoracic or lumbar dorsal root entry zone of juvenile ChAT::ChR2 isolated hemicords, optical activation of afferents in DRG or dorsal roots elicited dorsal root potentials consistent with primary afferent depolarization, a form of presynaptic inhibition. We conclude that ChAT expressing primary afferents modulate spinal somatosensory transmission, and ongoing studies will determine whether evoked responses include activation of nAChRs.

Support NS-065949 and NS086370-01A1

Sympathetic preganglionic and afferent stimulation-evoked responses in paravertebral thoracic chain ganglia

Mallika Halder, Mike Sawchuk, Shawn Hochman

Paravertebral sympathetic postganglionic neurons (SPNs) located in thoracic chain sympathetic ganglia represent the predominant sympathetic control of vascular function in the upper and middle extremities. These ganglia are practically inaccessible for *in vivo* studies, and consequently have barely been directly studied (Blackman and Purves J Pysiol 1969; Lichtman et al J Physiol 1980). We developed an *in vitro* adult mouse model to examine evoked population responses following stimulation of segmental sympathetic preganglionic and primary afferents axons. The approach retains the adult mouse thoracic sympathetic chain ganglia *in situ* with connections to dorsal root ganglia, dorsal roots and ventral roots. Dorsal roots were stimulated to examine primary afferent evoked responses, and ventral root stimulation was used to recruit axons of sympathetic preganglionic neurons. Responses in individual ganglia were recorded with suction electrodes attached to cut inter-ganglia nerve bundles. We first characterized the multisegmental axonal composition in individual chain ganglia. When recording from T12 ganglia, we observed orthodromic responses following stimulation of T7-T12 ventral roots and antidromic responses from T4-T12 dorsal roots. In addition to recordings of compound action potentials, dorsal and ventral root stimulation evoked synaptically-mediated spiking responses were seen and subsequently blocked in a high Mg2+/low Ca2+ solution or in the presence of ionotropic receptor antagonists. Both dorsal and ventral root stimulation evoked responses showed sensitivity to ionotropic glutamatergic and cholinergic receptor antagonists while ventral root-evoked synaptic actions were also facilitated in the presence of the nitric oxide donor DEANO. The observation of considerable synaptic actions arising from visceral afferents was unexpected. To further support this observation, we undertook post-experiment immunolabeling within the chain and found CGRP+ puncta in a position to interact synaptically with SPNs. Overall, we conclude that most thoracic ganglia receive widely divergent input from multiple spinal segments. Moreover, the visceral afferents within chain ganglia can project many spinal segments prior to entry into the spinal cord and also appear to issue collaterals within the ganglia and have synaptic actions on SPNs.

Ruby Lam

Abstract: Final

Limited incidence of tyrosine hydroxylase-expressing C-fiber low-threshold mechanoreceptors in the first two weeks of postnatal development of mouse

Gentle mechanical stimuli that correlate with the highest pleasantness ratings activate C tactile (CT) afferents in humans (Olausson et al, Nature 5, 2002). The corresponding fibers in mice are C-fiber low-threshold mechanoreceptors (C-LTMRs). One population of C-LTMRs can be identified by selective expression of tyrosine hydroxylase (TH), and these C-LTMRs have the highest incidence of expression in thoracic and sacral spinal dorsal root ganglia (DRG) (Li et al Cell 147, 2011). These afferents are likely recruited during licking, and since maternal licking is important in the development of prosocial behavior, we sought to determine incidence of expression of C-LTMRs in DRGs during development.

C-LTMRs were identified by crossing TH-Cre with Cre-dependent tdTomato reporter mice (TH::tdTomato). Mice were perfused at predetermined critical time points during early postnatal development (P7, P10, P14 and P21) and as adults (P33). In the adult, we observed that the incidence and rostrocaudal pattern of tdTomato expression was somewhat lower but comparable to that reported previously with TH immunofluorescence (Li et al 2011). In contrast, there was a much lower incidence of expression in DRGs from mice at postnatal days P21 and earlier. This suggests that C-LTMRs express a mature phenotype rather late in development. Understanding the developmental plasticity of C-LTMRs and the behavioral events associated with their activation should further our understanding of their role in affiliative behaviors.

Light Touch: Optogenetic Activation of Tyrosine Hydroxylase-expressing C-fiber Mechanoreceptors

Watkins, K., Sawchuk, M., and Hochman, S. (2014) Soc. Neurosci. Abst. 40.

Affiliative, pleasurable touch imparts numerous benefits for socioemotional and physical health, including modulation of stress reactivity, anxiety, blood pressure, and pain. A functionally distinct population of cutaneous sensory fibers, the C-tactile (CT) afferents, is purportedly involved in sensing and coding these pleasurable tactile stimuli in humans. Progress in characterizing the neural pathway to the brain has been severely hindered, however, by the inability to selectively activate this population of sensory afferents in a model organism. This barrier restricts investigation into the neural circuitry, behavioral effects, and clinical use of the affective tactile system. We used an optogenetic approach in transgenic mice to selectively activate a population of tyrosine hydroxylase-expressing C-fiber low-threshold mechanoreceptors (TH^+ C-LTMRs), a distinct group of afferents likely corresponding to human CT afferents (Li et al. Cell 147, 2011). We crossed TH-Cre and Cre-dependent channelrhodopsin (CHR2)-YFP mice. Using an *ex-vivo* isolated skin and dorsal cutaneous nerve preparation, we observed that the units recruited through optogenetic stimulation have similar physiological characteristics as C-LTMRs responding to brush strokes. Furthermore, analysis of the tissue revealed ChR2-YFP expressing neurons innervating nearly all hair follicles, consistent with results previously reported for TH^+ C-LTMRs (Li et al. Cell 147, 2011). Studies are underway to further characterize TH^+ C-LTMR response properties and assess the effects of their activation on behavior.

Neuroscience 2013

Control/Tracking Number: 2013-S-16261-SfN
Activity: Scientific Abstract
Current Date/Time: 5/13/2013 10:25:26 AM

Do sympathetic preganglionic neurons modulate locomotion by intraspinal activity-dependent release of nitric oxide?

AUTHOR BLOCK: *P. LOSEY, S. HOCHMAN;
Physiol., Emory Univ. Sch. of Med., Atlanta, GA

Abstract:
Though known to receive common input from several descending pathways involved in behavioral drives, intraspinal interactions between activity in sympathetic preganglionic neurons (SPNs) and motor neurons are not thought to occur. Interestingly, only SPNs express nitric oxide synthase (e.g. Dun et al 1992), and intraspinal nitric oxide (NO) complexly modulates vertebrate motor output including locomotor activity (e.g. Kyriakatos et al 2009). Here we sought to determine whether SPN neuronal activity derived NO can contribute to the modulation of locomotor like activity (LLA) in the isolated mammalian spinal cord.
We undertook studies in the isolated neonatal rat spinal cord, some with intact sympathetic chain to independently record SPN activity. We stimulated caudal lumbar or sacral dorsal roots to evoke LLA recorded predominantly in L1 and L2 ventral roots (VRs) known to also contain SPN efferent axons. We observed that during afferent stimulation-induced LLA, SPNs are also recruited to spike. When sympathetic bursting activity continued after stimulation epochs, these bursts were synchronous with those seen in VRs bilaterally. This indicates that some of the rhythmic activity observed in L1-2 VRs reflects firing in SPNs.
We wondered whether spiking activity in SPNs could modulate ongoing LLA via a nitrergic mechanism since Wu and Dun (1995) showed that high frequency activity in SPNs was sufficient to induce facilitation of excitatory transmission via Ca2+ dependent release of NO. Repetitive trains of stimuli were delivered to VRs at intervening periods between bouts of stimulation evoked LLA (3x10 epochs at 50 Hz) or concomitant with DR stimulation induced LLA (4x5 pulses at 30-50 Hz; n=4). In all cases the amplitude of motor output was facilitated on the contralateral side while ipsilateral motor activity was depressed. Both facilitatory and depressant actions appeared long-lasting (> 1 hour). To associate these actions with NO we tested the effects of the NO donor DEANO (50 ε M) on LLA. In the presence of DEANO, motor burst amplitude changes were complex and included amplitude increases and decreases with amplitude increases more consistently observed following washout across all VRs (n=4). These preliminary results suggest spiking activity in SPNs may utilize intraspinal nitrergic volume transmission to directly modulate motor function.
:

Presentation Preference (Complete): Poster Only

Linking Group (Complete): None selected
Nanosymposium Information (Complete):
Theme and Topic (Complete): D.11.c. Neuromodulation
Keyword (Complete): SPINAL CORD ; LOCOMOTOR ACTIVITY ; SYMPATHETIC
Support (Complete):
Support: Yes
Grant/Other Support: : Craig Neilsen Foundation

Special Requests (Complete):
Would you be interested in being considered for a dynamic poster?: No, I am not interested in presenting a Dynamic Poster

Is the first (presenting) author of this abstract a high school or undergraduate student?: None

Religious Conflict?: No Religious Conflict
Additional Conflict?: No

Status: Finalized

OASIS Helpdesk

Leave OASIS Feedback

Neuroscience 2013

Print this Page for Your Records Close Window

Control/Tracking Number: 2013-S-12891-SfN
Activity: Scientific Abstract
Current Date/Time: 7/29/2013 1:40:38 PM

Visualization of putative peripheral ChAT-expressing primary afferent cell bodies and spinal projections using ChAT-cre/Gsat transgenic mice

AUTHOR BLOCK: *I. A. SPEIGEL[1], M. SAWCHUK[1], F. J. ALVAREZ[1], H. KIMURA[2], S. HOCHMAN[1];
[1]Emory Univ., Atlanta, GA; [2]Mol. Neurosci. Res. Ctr., Shiga Univ. of Med. Sci., Otsu, Japan

Abstract:
Cholinergic neurons are distinguishable by expression of the acetylcholine (ACh) synthesis enzyme choline acetyltransferase (ChAT). A recently identified ChAT splice variant is expressed only in neurons of the peripheral nervous system (peripheral or pChAT). In the dorsal root ganglia, pChAT immunostaining is observed in a considerable number of small and medium size diameter neurons (Hanada et al, Cell Tissue Res, 2012). While we have reported on their intraspinal projections in preliminary fashion in rat (Hochman et al., NYAS 2010), details on protein co-expression patterns, central projections, and biological significance remain largely uncharacterized.
The two goals of this study were to genetically label pChAT expressing primary afferents in mice and compare their anatomical properties to those of pChAT immunolabeled primary afferents. pChAT intraspinal staining was observed throughout the rostrocaudal cord neuraxis and comparable in rat and mouse. Thus, mouse studies should integrate with previous work in rat. To introduce genetic targeting methods, we used a Cre/Lox recombination strategy to express the tdTomato fluorescent reporter protein in cells wherein the ChAT promoter is transcriptionally active, targeting both central and peripheral cholinergic structures. Specifically, we used a GENSAT derived ChAT-cre transgenic mouse line with a previously uncharacterized spinal expression pattern.
In the resulting ChAT::tdTomato transgenic mouse, we observed the expected genetic labeling of known intrinsic spinal cord cholinergic neuronal populations. Additionally a large number of primary afferent cell bodies were genetically labeled in dorsal root ganglia, consistent with reported pChAT immunolabeling of a mixed population of small and medium diameter neurons (Bellier at al, J Neurochem 2007; Hanada et al 2012). Afferent intraspinal projection patterns also appeared to mirror pChAT immunolabeling (Hochman et al 2010) with similar spinal axonal projections in dorsal column and dorsal horn. Studies are underway to ascertain the correspondence between pChAT immunoreactivity and the afferents targeted in these ChAT-Cre mice, including in relation to chemical neuroanatomy and sensory phenotype.
Support: NIH NS45248.
:

Presentation Preference (Complete): Poster Only
Linking Group (Complete): None selected

Nanosymposium Information (Complete):
Mapped Theme : Senses & Perception

Theme and Topic (Complete): D.09.d. Functional organization
Keyword (Complete): DORSAL ROOT GANGLION ; DORSAL HORN ; ACETYLCHOLINE
Support (Complete):
Support: Yes
Grant/Other Support: : NIH NS45248.

Special Requests (Complete):
Would you be interested in being considered for a dynamic poster?: No, I am not interested in presenting a Dynamic Poster

Is the first (presenting) author of this abstract a high school or undergraduate student?: None

Religious Conflict?: No Religious Conflict
Additional Conflict?: No
Mapped Theme One : Senses & Perception

Status: Finalized

O'NEILL, E.O., ZIMMERMAN,A., SAWCHUK, M., & HOCHMAN, S.,. Changes in mouse serotonin and dopamine receptor labeling in the intermediolateral nucleus after spinal cord injury. EB (2012).

Autonomic dysreflexia (AD), a neurological condition associated with spinal cord injury (SCI), is a hypertensive crisis initiated following activation of peripheral pain fibers. As descending monoaminergic neuromodulatory transmitter systems project densely to thoracic spinal cord sympathetic preganglionic regions, lost connections after SCI may contribute to altered autonomic function. Using immunohistochemistry (IHC), this study examined the distributions of three receptors; serotonergic 5HT2A, and dopaminergic D2 and D3 in the intermediolateral nucleus (IML), the location of sympathetic preganglionic neurons (SPNs) in a mouse model of AD. Labeling was explored in control cords at ~P70, and in littermates 3 weeks following spinalization at high thoracic levels (T1/T2). Analysis focused on SPNs in the IML, efferent neurons that are presumably responsible for blood pressure increases.

In controls, IHC showed labeling of processes adjacent to the IML for 5HT2A receptors and somatic/perisomatic labeling of SPNs for D2 and D3 receptors. In injured mice, D2 and D3 receptor expression significantly decreased below the injury, both close to the injury site (thoracic levels T2-T7) as well as caudally distant from the injury site (thoracic level T9-T12) ($p<0.01$). Though 5HT2A receptor expression was also decreased at more rostral thoracic regions ($p<0.01$), expression increased in a rostrocaudal gradient, with expression levels in the lower thoracic cord comparable to controls ($p=.081$). 5HT2A receptors can be constitutively active and facilitate sympathetic motor output. We hypothesize that their constitutive activity, unrestrained by descending inhibitory influences that include actions on D2 and D3 receptors, help support a substrate for afferent-induced over-activation of SPNs in AD. This work is funded by the Department of Defense, SC090469.

SALK Motor Control Meeting 2010

MONOAMINERGIC RECEPTORS ASSOCIATED WITH AUTONOMIC AND SOMATIC MOTONEURONS: IMMUNOCYTOCHEMICAL COMPARISON AND OBSERVED MODULATORY ACTIVITIES.

Brannan O'Neill[1], Amanda Zimmerman[2], Mike Sawchuk[2], Kelly Lohr[2] & Shawn Hochman[1].

[1]*Department of Physiology, Emory University*

[2]*Department of Biomedical Engineering, Emory University/Georgia Institute of Technology*

There is a known correlated recruitment of sympathetic and motor activity during locomotion. Monoaminergic descending pathways have been implicated in the recruitment of both systems, and noradrenergic, serotonergic, and dopaminergic fibers densely innervate the intermediolateral column (IML) and lamina IX, where sympathetic preganglionic neurons (SPNs) and motoneurons (MNs) reside, respectively.

The present study sought to compare the monoamine receptor subtypes found in the IML and associated with motoneurons in the lamina IX of the adult caudal thoracic and rostral lumbar spinal cord obtained from HB9-GFP labeled transgenic mice. Immunohistochemistry was used to assess the presence and distribution of monoamine receptor subtypes in both neuronal populations.

We investigated the presence of $5HT_{1A}$, $5HT_{1D}$, $5HT_{1F}$, $5HT_{2A}$, and $5HT_7$ serotonergic receptors, D_1, D_2, D_3, and D_5 dopaminergic receptors, and α_{1A}, $\alpha_{2A,}$ β_1, and β_3 adrenoceptors. We saw widespread $5HT_{2a}$ somatic and process labeling in both SPNs and MNs, including strong labeling in GFP+ processes in the lateral funiculus associated with the IML and in the ventral root exit zone. $5HT_{1d}$ and $5HT_7$ labeling was also seen. Adrenergic receptors α_{1A} and α_{2A} strongly and selectively labeled both populations of MNs, suggesting a profound modulatory role of descending adrenergic systems as these two receptors act on different 2^{nd} messenger systems. Similary, both D_2 and D_3 (Gi-coupled) and D_5 (Gs-coupled) receptors intensely labeled both populations perisomatically and on processes. This wide variety of receptor subtypes suggests complex neuromodulation, dependent on the concentration of ligands and receptor affinity.

Lastly, we characterized the effects of monoamines on locomotor and sympathetic rhythmicity using an *in vitro* spinal cord-sympathetic chain preparation. While lumbar ventral roots (responsible for locomotor output) had no inherent rhythmicity in this preparation, intrinsic rhythmic patterns could be distinguished in the sympathetic output recorded from the sympathetic chain and white rami. Exogenously applied noradrenaline, dopamine, and serotonin led to changes in the overall activity level, periodicity, and rhythmic coupling between sympathetic and locomotor outputs. Future studies investigate concentration and agonist dependence of monoamine-induced responses.

Supported by DoD.

Print this Page

Presentation Abstract

Program#/Poster#:	585.9/YY3
Title:	Somatotopic relationships between motor and autonomic physiology and afferent axonal anatomy in a multi-segmental spinal pain reflex
Location:	Halls B-H
Presentation Time:	Tuesday, Nov 16, 2010, 8:00 AM - 9:00 AM
Authors:	***K. E. TANSEY**[1], M. SAWCHUK[2], S. HOCHMAN[2], B. R. BOTTERMAN[3]; [1]SCI Research/Neurology & Physiology/SCI Clin., Shepherd Center/Emory University/Atlanta VA, ATLANTA, GA; [2]Physiol., Emory Univ. Sch. of Med., Atlanta, GA; [3]Cell Biol., Univ. of Texas Southwestern Med. Ctr., Dallas, TX
Abstract:	We have been studying a multi-segmental spinal pain reflex following spinal cord injury (SCI) and have found that activation of the afferents in this reflex can generate both altered motor and autonomic physiology. This observation led us to investigate the relationship between the somatotopic organization of 1) the reflex motor response, 2) the autonomic effect of reflex afferent activation and 3) the axonal populations making up these afferents in normal animals. The cutaneus trunci muscle (CTM) reflex produces a skin “shrug” in response to pinch on a rat's back and is mediated by a three neuron circuit: 1) A-δ and C fiber afferents in segmental dorsal cutaneous nerves (DCNs) from lumbar to thoracic levels, 2) ascending propriospinal interneurons, and 3) the CTM motoneuron pool located at the cervical-thoracic junction. The reflex can be quantified by recording the neurogram from a CTM muscle nerve branch in response to electrical stimulation of the DCNs and blood pressure effects of activating this reflex can be measured via carotid artery cannulation. For this study, we are also investigating the ultrastructural characteristics of the axonal populations in segmental DCNs from L1 to T6. The motor response to DCN activation consists of A-δ and C fiber specific components. The A-δ component is different in response to different level DCN activation with the largest responses coming from T11 and T12. The C-fiber response is largest when evoked from the most caudal DCNs (T12 to L1) and is

rather small when evoked from the most rostral DCNs (T6 and T7). The blood pressure changes to DCN activation in normal animals under pentobarbital anesthesia are actually depressor in nature and they also depend on the DCN being stimulated. While this response shows greater variability animal to animal, its average profile across the DCNs matches closely the profile of the A-δ component of the motor response.
Preliminary anatomical analysis shows that the diameter of the DCNs seems to vary in parallel to the motor and autonomic effects with the lower thoracic DCNs being the largest. The DCNs clearly contain large numbers of C-fibers, fewer A-δ fibers but even some A-β and A-α fibers (which do not contribute to the CTM reflex in normals). We are currently quantifying the total axon counts of the different axon populations across the DCNs from L1 to T6 to determine how well different axonal populations correlate with the somatotopically distributed motor and autonomic physiology. This will provide valuable information for future studies investigating pain afferent plasticity after SCI and its relationship to the development of pathological pain and autonomic dysfunction.

Disclosures: **K.E. Tansey**, None; **M. Sawchuk**, None; **S. Hochman**, None; **B.R. Botterman**, None.

Keyword(s): intersegmental reflex

cutaneus trunci muscle

dorsal cutaneous nerve

Support: Mobility Foundation Center

[Authors]. [Abstract Title]. Program No. XXX.XX. 2010 Neuroscience Meeting Planner. San Diego, CA: Society for Neuroscience, 2010. Online.

Control/Tracking Number: 2011-S-10392-SfN
Activity: Scientific Abstract
Current Date/Time: 5/12/2011 2:39:23 PM

Temporal dynamics of motor and autonomic physiology in a multi-segmental spinal cutaneous pain reflex

AUTHOR BLOCK: *J. M. WHITE[1,4], J. S. TIDWELL[2,3,6], H. J. LEE[2,3], S. P. DEWEERTH[4,5,7], K. E. TANSEY[2,3,6,8]; [1]Biomed. Engin., [2]Neurol., [3]Physiol., Emory Univ., Atlanta, GA; [4]Biomed. Engin., [5]Electrical Engin., Georgia Tech., Atlanta, GA; [6]Spinal Cord Injury Res. Program, Shepherd Ctr., Atlanta, GA; [7]Biomed. Engin., Khalifa Univ., Abu Dhabi, United Arab Emirates; [8]Spinal Cord Injury Clin., Atlanta Veterans Admin. Med. Ctr., Atlanta, GA

Abstract:
The cutaneus trunci muscle (CTM) reflex produces a skin “shrug” in response to pinch on a rat's back, and is mediated by a three neuron circuit: 1) A-delta and C fiber afferents in segmental dorsal cutaneous nerves (DCNs) from lumbar to thoracic levels, 2) ascending propriospinal interneurons, and 3) the CTM motoneuron pool located at the cervicothoracic junction. We quantified the reflex by recording the neurogram from a CTM nerve branch in response to electrical stimulation of individual DCNs (T6-L1) with 3-5 mA at 1, 2, 5, or 10 Hz for 20 seconds. Responses were divided into an early (A-delta mediated) and a late (C fiber mediated) response, which are temporally non-overlapping. The effects of nociceptive stimulation on the autonomic system were assessed by cannulating the carotid artery to measure blood pressure.
Our data shows that the size of both the early (A-delta) and late (C) motor responses varied depending on the DCN stimulation frequency used and the timing of the specific stimulus in the train (1st, 2nd, 5th ...). The greatest A-delta responses tended to occur at 1 Hz, and generally, the first stimulus in the train produced the largest A-delta response at all stimulation frequencies. The C responses consistently increased over the course of the stimulus train, reaching their peak around the 5th stimulus at 1 Hz and around the 80th stimulus at 10 Hz. Of all the stimulation frequencies, 5 Hz consistently produced the largest individual C fiber responses. Additionally, the blood pressure showed a depressor response to the noxious input that followed the size and timing of the C response at all frequencies tested.
We found segmental differences in the responses as well. The largest (A-delta) response was consistently from T9-T11. Additionally, in these initial experiments, there was evidence that the segments from T7-T11 showed a reduced drop off in size of the A-delta responses over time at 10 Hz. Our early data also showed the facilitation in the C responses at higher stimulation frequencies (5 and 10 Hz) was noticeably less apparent in the most caudal segments (T13-L1).
These results demonstrate that the CTM reflex response has many of the temporal dynamics seen in pain systems. First, the C fiber response facilitation is consistent with the “wind up” phenomenon observed in other pain reflexes. Second, the early (A-delta) response depresses quickly, similar to the sharp “first pain”, which reduces significantly with continued stimulation.
Lastly, blood pressure appears to follow the C fiber motor response more closely at all tested frequencies, which provides evidence C fibers modulate the autonomic system.
:

Presentation Preference (Complete): Poster Only
Linking Group (Complete): None selected
Nanosymposium Information (Complete):
Theme and Topic (Complete): D.08.f. Spinal cord processing: Anatomy and physiology ; D.08.p. Pain models: Physiology
Keyword (Complete): Cutaneus Trunci Muscle ; SENSORIMOTOR ; Spinal Cord Processing
Support (Complete):
Support: Yes
Grant/Other Support: : DoD Grant SC090469
Grant/Other Support: : Kustar Predoctoral Fellowship

Special Requests (Complete):
Is the first (presenting) author of this abstract a high school or undergraduate student?: None

Religious Conflict?: No Religious Conflict
Additional Conflict?: No

Status: Finalized

OASIS Helpdesk

Leave OASIS Feedback

NEUROSCIENCE 2012

Print this Page for Your Records Close Window

Control/Tracking Number: 2012-S-6177-SfN
Activity: Scientific Abstract
Current Date/Time: 5/10/2012 4:07:39 PM

Central projection patterns of segmental cutaneous pain afferents in the rat spinal cord

AUTHOR BLOCK: *H. LEE[1,2], J. S. TIDWELL[1,2,5], J. M. WHITE[3,6], P. S. MALONE[4], K. E. TANSEY[1,2,5,7];
[1]Dept. of Neurol., [2]Dept. of Physiol., [3]Dept. of Biomed. Engin., [4]Neurosci. and Behavioral Biol., Emory Univ., Atlanta, GA; [5]Spinal Cord Injury Res., Shepherd Ctr., Atlanta, GA; [6]Dept. of Biomed. Engin., Georgia Inst. of Technol., Atlanta, GA; [7]Spinal Cord Injury Clin., Atlanta VA Med. Ctr., Atlanta, GA

Abstract:
The cutaneus trunci muscle (CTM) reflex produces a “skin shrug” in response to pinch on a rat’s back, and is mediated by a three neuron circuit: 1) A-delta and C fiber afferents in segmental dorsal cutaneous nerves (DCNs), 2) ascending propriospinal interneurons, and 3) the CTM motoneuron pool. The evoked CTM neurogram consists of an early (A-delta) and a late (C fiber) response and depends on which DCN is stimulated. We found little difference in the number of axons of different types across peripheral DCNs so we are now looking at their central projection patterns. We have shown physiological plasticity in this reflex after spinal cord injury (SCI), including nociceptive hypereflexia and dysautonomia, and we wonder if there is related cutaneous afferent anatomical plasticity. To evaluate any changes in the central projection patterns of these afferents after SCI, we first need to characterize them in normal rats.
In this study we injected axonal tracers, either cholera toxin subunit B (CTB) for myelinated A fibers or isolectin B4 (IB4) for unmyelinated C fibers, into the T7 and T13 DCNs to develop an anatomical profile of pain afferent central projections. Both IB4 labeled C fibers and CTB labeled A fibers were mainly found in the ipsilateral dorsal horn. C fibers were concentrated in laminae I-II whereas A fibers were distributed widely in laminae III-V.
Immunohistochemistry of calcitonin gene related peptide (CGRP), expressed in peptidergic C fibers, was detected in laminae I and co-localized with a few IB4 positive C fibers but not with CTB positive A fibers. Immunohistochemistry of synaptophysin, a synaptic vesicle marker, showed synaptic termination of A and C fibers in approximately 30% of both IB4 and CTB labeled axons in 20 µm thick transverse spinal cord sections at T7 and T13. Quantitative estimation of central projection density and rostral-caudal distribution of DCN afferents was performed. The density of IB4 labeled C fibers was apparently greater in T13 compared to T7 while A fibers appeared similarly at both levels. The rostral-caudal extent of CTB labeled A fibers, and to a lesser extent IB4 labeled C fibers, however, was apparently greater in T7 compared to T13.
These data demonstrate that the central projection patterns of A and C fibers vary between T7 and T13 DCNs suggesting that segmental differences in afferent anatomy may contribute to the different physiological responses seen across this multi-segmental pain reflex. To investigate the relationship between anatomical and physiological changes after SCI, we are evaluating the central projections of A and C fibers from DCNs above and below a mid thoracic spinal cord hemisection injury.
:

Presentation Preference (Complete): Poster Only
Linking Group (Complete): OliveOrchid
Nanosymposium Information (Complete):
Theme and Topic (Complete): D.10.d. Plasticity: Neurophysiology ; D.08.f. Spinal cord processing: Anatomy and physiology
Keyword (Complete): cutaneus trunci muscle ; PLASTICITY ; NEUROPATHIC PAIN
Support (Complete):
Support: Yes
Grant/Other Support: : DoD SC090469
Grant/Other Support: : NIH EB006179

Special Requests (Complete):
Is the first (presenting) author of this abstract a high school or undergraduate student?: None

Religious Conflict?: No Religious Conflict
Additional Conflict?: No

Status: Finalized

OASIS Helpdesk

Leave OASIS Feedback

Print this Page

NEUROSCIENCE 2012

Presentation Abstract

Program#/Poster#: 378.17/TT13

Presentation Title: Complex neural plasticity in an intersegmental cutaneous pain reflex after spinal cord injury

Location: Hall F-J

Presentation time: Monday, Oct 15, 2012, 8:00 AM - 9:00 AM

Authors: ***P. S. MALONE**[1,2], J. S. TIDWELL[3,4,6], J. M. WHITE[5,7], H. LEE[3,4], K. E. TANSEY[3,4,6,8]; [1]Akron, OH; [2]Neurosci. and Behavioral Biol., [3]Dept. of Neurol., [4]Dept. of Physiol., [5]Dept. of Biomed. Engin., Emory Univ., Atlanta, GA; [6]Spinal Cord Injury Res., Shepherd Ctr., Atlanta, GA; [7]Dept. of Biomed. Engin., Georgia Inst. of Technol., Atlanta, GA; [8]Spinal Cord Injury Clin., Atlanta VA Med. Ctr., Atlanta, GA

Abstract: The cutaneus trunci muscle (CTM) reflex produces a “skin shrug” in response to pinch on a rat’s back, and is mediated by a three neuron circuit: 1) A-delta and C fiber afferents in segmental dorsal cutaneous nerves (DCNs) from lumbar to thoracic levels, 2) ascending propiospinal interneurons, and 3) the CTM motoneuron pool located at the cervico-thoracic junction. The reflex is bilateral but asymmetric such that a larger reflex response in the CTM is seen with cutaneous stimulation of the ipsilateral side. We have previously shown that the CTM response has many of the temporal dynamics seen in pain systems, such as C fiber evoked response facilitation consistent with a “wind up” phenomenon.

Female Long Evans rats were divided into 4 groups (n=8) for electrophysiological recording: uninjured controls and animals 1, 3, and 6 weeks after T10 hemisection contralateral to the side where CTM neurograms were to be recorded. The reflex neurogram was recorded from a CTM nerve branch in response to electrical stimulation of individual DCNs (L01, T12, T08, and T06) ipsilateral to the recording site (contralateral to the hemisection) and contralateral to recording site (ipsilateral to the hemisection) with 5 mA at 1 Hz for 20 seconds and 5 Hz for 10 seconds. Responses were divided into two temporally non-overlapping phases: an early (A-delta mediated) and a late (C fiber mediated) response. Injured animals were then perfused and their spinal cords were harvested to assess the extent of hemisection.

The analysis of CTM neurograms revealed several differences between uninjured and injured animals. Changes in reflexes evoked from DCN stimulation on both the side of hemisection and on the uninjured side as well as from both above and below the level of injury were seen. Following injury, there was an increased C fiber evoked response from all DCNs, an increase in response size with ipsilateral (uninjured side) stimulation and the appearance of a C fiber evoked response with contralateral (injured side) stimulation. There was also an increase in the size of the A-delta evoked response from the contralateral (injured) side. Some greater background activity in the CTM neurogram was observed after spinal cord injury. Preliminary anatomical evaluation revealed no clear relationship between the extent of hemisection and the reflex changes.

A complex increased stimulus response after spinal cord injury could be characterized in this neural circuit as “nociceptive hypereflexia.” This raises the possibility that the CTM reflex

could serve as an animal model for some aspects of neuropathic pain after spinal cord injury.

Disclosures: **P.S. Malone:** None. **J.S. Tidwell:** None. **J.M. White:** None. **H. Lee:** None. **K.E. Tansey:** None.

Keyword(s): ELECTROPHYSIOLOGY

NEUROPATHIC PAIN

CUTANEUS TRUNCI MUSCLE

Support: DoD SC090469

NIH EB006179

[Authors]. [Abstract Title]. Program No. XXX.XX. 2012 Neuroscience Meeting Planner. New Orleans, LA: Society for Neuroscience, 2012. Online.

4th International Congress on Neuropathic Pain, 2013, Toronto, Canada.

COMPLEX NOCICEPTIVE HYPEREFLEXIA IN A RAT INTERSEGMENTAL CUTANEOUS REFLEX AFTER SPINAL CORD INJURY

Malone PS, Tidwell JS, White JM, Lee HJ, Tansey KE.

Background:
The cutaneus trunci muscle (CTM) reflex produces a “skin shrug” in response to pinch on a rat’s back, and is mediated by a three neuron circuit: 1) A-delta and C fiber afferents in segmental dorsal cutaneous nerves (DCNs), 2) ascending propiospinal interneurons, and 3) the CTM motoneuron pool. The reflex is bilateral but asymmetric with a larger reflex response with ipsilateral stimulation.
Methods:
Electrophysiological recordings were made in 4 groups (n=8) of female Long Evans rats: uninjured controls and animals 1, 3, and 6 weeks after T10 spinal cord hemisection contralateral to the CTM neurogram recording site. The reflex was recorded from a CTM nerve branch in response to electrical stimulation of individual DCNs (L01, T12, T08, and T06) ipsilateral and contralateral to the recording site (contralateral and ipsilateral to the hemisection) with 5mA at 1Hz for 20s and 5Hz for 10s. Both early (A-delta) and late (C fiber) responses were analyzed.
Results:
Changes, most often increases, in DCN stimulation evoked CTM reflexes were observed on both the side of the hemisection and on the uninjured side as well as from both above and below the level of injury. This was true for both A-delta and C fiber evoked responses.
Conclusions:
Complex nociceptive hypereflexia can be demonstrated in this intersegmental cutaneous reflex after spinal cord injury, raising the possibility that it could serve as an animal model for aspects of human neuropathic pain after SCI, at least the altered processing of noxious stimuli by the injured spinal cord.

Introduction
TBI is the leading cause of death in children and young adults. Furthermore many patients were left with substantial cognitive impairment, motor dysfunction and epilepsy. There is no effective treatment for these disorders. The discovery of neural stem cells in adult brain raises a potential strategy for repairing CNS injury.

Methods
We used immunostaining or retrovirus to visualize the new generated neurons after TBI in hippocampus to assess their migration.

Results
Our previous study showed that TBI promotes NSC proliferation in an attempt to initial an innate repair and/or plasticity mechanisms. When we tracked the migration of newly generated neurons in the adult hippocampus after TBI, we found that a large percentage of immature neurons migrate pass their normal stopping site at the inner granular cell layer, and misplace in the outer granular cell layer of the hippocampal dentate gyrus. The aberrant migration of adult-born neurons in the hippocampus occurs 3 days after TBI, and lasts for 7 weeks, resulting in a great number of newly generated neurons misplaced in the outer granular layer in the hippocampus.

Conclusions
The newborn neurons at the displaced position will not be able to make correct connections with their appropriate targets, and may even make wrong connections with inappropriate nearby targets in the pre-existing neural network. Abnormal migration has been shown to cause several diseases including dyslexia, schizophrenia, and epilepsy. These results suggest that stimulation of endogenous adult neural stem cells following TBI might offer new avenues for cell-based therapy, but additional intervention is required to further enhance successful neurogenesis for repairing the damaged brain.

Acknowledgments
This work was supported by funding from the Life and Health Science Initiative (LSHI) of Indiana University School of medicine, Ralph W. and Grace M. Showalter Research Award, Indiana University Biological Research Grant, NIH grants RR025761, and 1R21NS072631-01A to J Chen.

Key words
migration, neurogenesis, TBI

A149

ASSESSMENT OF NGR1 FUNCTION *IN VIVO* AFTER SPINAL CORD INJURY

Jason H. Huang, Jing Tong, Ming Liang
University of Rochester

Introduction
Neuronal Nogo-66 receptor 1 (NgR1) has been the focus of intense investigation as a converging point for mediating the effects of myelin-associate inhibitory ligands in the central nervous system. However, the importance of NgR1 has been undermined by several studies that have shown the lack of substantial axon regeneration following spinal cord injury in NgR1 knockout or knockdown animal models.

Methods
To investigate the factors that may be contributing to the discrepancy in these findings, we used mice carrying either a homozygous or heterozygous null mutation in the NgR1 gene and subjected them to either a moderate or severe spinal cord injury.

Results
Locomotor function assessments revealed that the level of functional recovery is affected by the degree of injury suffered. Tract tracing of the corticospinal (CST) tract fibers revealed that, while none or few of the severed axons regenerated past the injury site to caudal spinal cord, NgR1 ablation enhanced local collateral sprouting to the contralateral spinal cord in the mutant mice. Reactive astrocytes and chondroitin sulfate proteoglycans (CSPGs), which are known to inhibit neurite outgrowth, are upregulated surrounding the injury site. MMP-9, which has been shown to degrade CSPGs, was significantly upregulated in the homozygous mutant mice compared to the heterozygous or wild-type mice. However, CSPG levels remained higher in the homozygous compared to the heterozygous mice, suggesting that the CSPG-degrading activity of MMP-9 may require the presence of NgR1.

Conclusions
Together, these results suggest that NgR1 has important physiological functions, which may have been masked by redundant pathways or confounding factors in previous studies. Therapeutic strategies based on NgR1 antagonism, in combination with other treatment approaches, can have functionally important outcomes for patients suffering from spinal cord injury.

Acknowledgments
The authors would like to thank Dr. Roman J. Giger for providing NgR1 KO mice. This work was supported, in part, by a University of Rochester SPAC grant (JHH), and by NIH-R01-NS-067435 (JHH).

Key words
chondroitin sulfate proteoglycans, glial scar, matrix metalloproteinases, NgR1, spinal cord injury

A150

CENTRAL PLASTICITY OF SEGMENTAL CUTANEOUS NOCICEPTIVE PRIMARY AFFERENTS AFTER SPINAL CORD HEMISECTION INJURY IN RATS

Hyun Joon Lee, Natalee K. Wilson, Jumi Chung, Patrick S. Malone, Jason S. Tidwell, Keith Tansey
Emory University

Introduction
The cutaneus trunci muscle (CTM) nociceptive intersegmental spinal reflex results from stimulation of segmental dorsal cutaneous nerves (DCNs) and demonstrates complex neurophysiological plasticity after spinal cord hemisection injury (SCI). The central projection patterns of Aδ and C fibers in DCNs after SCI were compared to normal animals.

Methods
Female Long Evans rats (n = 8) were subjected to a T10 spinal cord hemisection on one side of the animal. After 6 weeks, retrograde axonal tracers, cholera toxin subunit B (CTB) for myelinated A fibers or isolectin B4 (IB4) for non-peptidergic, unmyelinated C fibers, were injected into bilateral T7 and T13 DCNs, one tracer on one side and the other on the other side. Animals were transcardially perfused with 4% PFA 3 days after injection and the spinal cords were harvested. Immunohistochemistry was performed on serial transverse sections of the spinal cord at T7 and T13. The projection fields of labeled A and C fibers were measured quantitatively as immunoreactive areas in the T7 and T13 dorsal horns. Their projection patterns were analyzed in terms of laminar, medial/lateral, dorsal/ventral, and rostral/caudal distribution. Synaptophysin, a synaptic vesicle protein, is being used to identify the synaptic terminations of the A and C fibers.

Results
Neurophysiological changes of both Aδ and C fiber evoked reflex responses have been shown after spinal cord hemisection injury, both above and below the level of injury and on the side of hemisection and on the uninjured side. In this study we developed central projection profiles of bilateral A and C fibers of T7 and T13 DCNs 6 weeks after a unilateral T10 hemisection injury and in uninjured animals. Both A and C fiber projection areas increased overall in T7 and T13 after injury compared to normals. However, the greatest mean increase was seen in C fibers at T7 whereas increases of A fibers were the next greatest at T13. Only C fibers at T7 showed a significant difference between the injured and uninjured sides, with injury side being greater. The rostro-caudal distributions of both A and C fiber projections expanded in both rostral and caudal directions after injury. Not only was there greater area of labeled A and C fiber neurites, they covered a greater territory of the dorsal horn after injury.

Conclusions
After hemisection SCI, the altered projection patterns of DCN A and C fibers in the dorsal horn demonstrate central plasticity of the nociceptive inputs of the CTM reflex. These changes are consistent with the neurophysiological plasticity seen in this reflex after injury. Ongoing work with synaptophysin will help to determine whether these afferent projection area changes also represent synaptogenesis following injury.
These data demonstrate that anatomical changes of sensory fibers in the CTM pain reflex probably contribute to the ''nociceptive hyperreflexia'' observed neurophysiologically after hemisection injury. This supports the idea that the CTM reflex could be a good animal model in which to study the neuroplasticity associated with neuropathic pain after SCI that can be quantitatively analyzed, at least for the altered spinal processing of nociceptive signals.

Acknowledgments
This work has been supported by U.S. Department of Defense Grant, DoD SC090469 and by the Emory University's Integrated Cellular Imaging Microscopy Core in the Department of Physiology.

Key words
myelinated A fiber, pain, retrograde tracers, sprouting, unmyelinated C fiber

A151

A MINIMAL INFORMATION STANDARD FOR SPINAL CORD INJURY EXPERIMENTS

Vance P. Lemmon[1], Adam R. Ferguson[2], Phillip G. Popovich[3], Diane M. Snow[4], Carol A. Mason[5], Michihiro Igarashi[6], Xiao-Ming Xu[7], Christine Beattie[3], John L. Bixby[8]
[1]*University of Miami Miller School of Medicine,* [2]*University of California San Francisco,* [3]*The Ohio State University,* [4]*University of Kentucky,* [5]*Columbia University,* [6]*Niigata University, Japan,* [7]*Indiana University School of Medicine,* [8]*University of Miami Miller School of Medicine*

Introduction
It is well documented across many areas of biological science that reproducibility of experiments among labs is challenging (Prinz, Schlange et al. 2011, Begley and Ellis 2012). A number of factors contribute to this problem; chief among them is the relatively poor documentation of experimental methods in many papers.

Methods
Recent failures to replicate significant findings in the spinal cord injury field demonstrate a need for improved documentation of experimental metadata (Landis, Amara et al. 2012, Steward, Popovich et al. 2012). In collaboration with a group of 35 U.S. and Japanese scientists, we have developed a draft standard for Minimal Information About a Spinal Cord Injury experiment (MIASCI). Guidelines developed by the Minimum Information for Biological and Biomedical Investigations (MIBBI) project (Taylor, Field et al. 2008) were used to develop the MIASCI. After the MIASCI was assembled, surveys were done to rank the importance of items in the MIASCI, as judged by domain experts.

Results
The MIASCI covers a wide range of topics such as animal housing, surgery conditions, treatments (drugs, RNAi, cell transplants, etc), histology, imaging, and behavioral testing. At present the MIASCI has approximately 350 items in the checklist. We will present the preliminary results summarizing the polling data and rank-ordering of the draft MIASCI items. Further refinement will need additional input from the SCI community.

Conclusions
The long-term goal is to produce a standard that is both comprehensive and concise so that authors, editors and reviewers can easily comply with the recommendations. The MIASCI will also greatly facilitate future data mining and knowledge discovery in the SCI domain.

Acknowledgments
The efforts of the participants in the RegenBase meeting in Oct. 2012 are greatly appreciated. Supported by NIH NS080145, NS067092 and HD057632.

Key words
minimal information standard, spinal cord injury

A152

NEUOPROTECTIVE EFFECT OF FINGOLIMOD FOLLOWING TRAUMATIC BRAIN INJURY

Dong Sun, Andrew Rolfe, Dong Chen, Nitai Hait, Sarah Spiegel
Virginia Commonweath University

Introduction
Fingolimod is a recently FDA approved drug as an immune modulator for treating Multiple Sclerosis. Fingolimod exerts immunomodulatory actions by affecting lymphocyte trafficking through Sphingosine 1-phosphate receptors. In this study, we aimed at exploring the therapeutic effects of Fingolimod following TBI and its molecular mechanisms of neuroprotective action.

Methods
In this study, three months old male Sprague-Dawley rats were used. Animals were subjected to a moderate cortical impact injury. At thirty minutes following injury, Fingolimod was administrated orally at the dose of 1mg/kg. Thereafter, six more daily single doses were given. Motor functions were tested at 1, 3, 7 and 14 days post-injury using beam walking, rotarod and neurological scoring methods. Cognitive functions were tested using Fear Conditioning tests at 8–10 days post-injury and Morris Water Maze tests 11–15 days post-injury. Animals were sacrificed at 15 days post-injury. Brain tissues were processed for histological examination for lesion volume, neuronal cell survival and inflammatory cell reactions.

Results
We have found that following a moderate cortical impact injury, 7-day post-TBI oral delivery of Fingolimod can ameliorate both motor and cognitive functions in the injured animals. Further studies examining Fingolimod treatment on lesion volume, neuronal cell survival and inflammatory cell reactions are ongoing.

Abstract for ASNR 2013

Central plasticity of segmental cutaneous nociceptive primary afferents is associated with evoked nociceptive hypereflexia after hemisection spinal cord injury in rats

Patrick S. Malone[1,2], Natalee K. Wilson[1,2], Jumi Chung[1,2], Jason S. Tidwell[1,2,4], Jason M. White[3,4], Hyun Joon Lee[1,2], Keith E. Tansey[1,2,4,5]

[1]Neurology, [2]Physiology, Emory University, Atlanta, GA [3]Biomedical Engineering, Emory University/Georgia Institute of Technology, Atlanta, GA; [4]Spinal Cord Injury Research Program, Shepherd Center, Atlanta, GA; [5]Spinal Cord Injury Clinic, Atlanta Veterans Administration Medical Center, Atlanta, GA

441 / 450 words

The cutaneus trunci muscle (CTM) nociceptive intersegmental spinal reflex results from stimulation of segmental dorsal cutaneous nerves (DCNs) and demonstrates complex neurophysiological plasticity after hemisection spinal cord injury (SCI). The central projection patterns of A and C fibers in DCNs were analyzed 6 weeks after a unilateral T10 spinal cord hemisection. Retrograde axonal tracers, cholera toxin subunit B (CTB) for myelinated A fibers or isolectin B4 (IB4) for non-peptidergic, unmyelinated C fibers, were injected into bilateral T7 and T13 DCNs, one tracer on one side and the other on the other side. Immunohistochemistry was performed on serial transverse sections of the spinal cord at T7 and T13 to measure the projection fields of labeled A and C fibers quantitatively as immunoreactive areas. Synaptophysin, a synaptic vesicle protein, is being used to identify the synaptic terminations of the A and C fibers.

Neurophysiological changes of both Aδ and C fiber evoked reflex responses have been shown after spinal cord hemisection injury, both above and below the level of injury and on the side of hemisection and on the uninjured side. In this study we investigated the central projection profiles of bilateral A and C fibers of T7 and T13 DCNs 6 weeks after a unilateral T10 hemisection injury and in uninjured animals. Both A and C fiber projection areas increased overall in T7 and T13 after injury compared to normals. However, the greatest mean increase was seen in C fibers at T7 whereas increases of A fibers were the next greatest at T13. Only C fibers at T7 showed a significant difference between the injured and uninjured sides, with injury side being greater. The rostro-caudal distributions of both A and C fiber projections expanded in both rostral and caudal directions after injury. Not only was there greater area of labeled A and C fiber neurites, they covered a greater territory of the dorsal horn after injury.

After hemisection SCI, the altered projection patterns of DCN A and C fibers in the dorsal horn demonstrate central plasticity of the nociceptive inputs of the CTM reflex. These changes are

consistent with the neurophysiological plasticity seen in this reflex after injury. Preliminary work with synaptophysin has shown that these afferent projection area changes also represent overall synaptogenesis following injury. These data demonstrate that anatomical changes of sensory fibers in the CTM pain reflex probably contribute to the “nociceptive hyperreflexia” observed neurophysiologically after hemisection injury. This supports the idea that the CTM reflex could be a good animal model in which to study the neuroplasticity associated with neuropathic pain after SCI that can be quantitatively analyzed, at least for the altered spinal processing of nociceptive signals.

Abstract for ASNR 2013

Central plasticity of segmental cutaneous nociceptive primary afferents is associated with evoked dysautonomia after cervical spinal cord injury in rats

Hyun Joon Lee[1,2], Jason S. Tidwell[1,2,4], Jumi Chung[1,2], Natalee K. Wilson[1,2], Jason M. White[3,4], Keith E. Tansey[1,2,4,5]

[1]Neurology, [2]Physiology, Emory University, Atlanta, GA [3]Biomedical Engineering, Emory University/Georgia Institute of Technology, Atlanta, GA; [4]Spinal Cord Injury Research Program, Shepherd Center, Atlanta, GA; [5]Spinal Cord Injury Clinic, Atlanta Veterans Administration Medical Center, Atlanta, GA

381 / 450 words

The cutaneus trunci muscle (CTM) nociceptive intersegmental spinal reflex results from stimulation of segmental dorsal cutaneous nerves (DCNs). DCN stimulation also generates a depressor blood pressure response via the autonomic nervous system in normal animals but can generate a pressor response after severe cervical spinal cord crush injury (SCI). The central projection patterns of A and C fibers in DCNs were analyzed 2 and 4 weeks after a C7 bilateral crush SCI. Retrograde axonal tracers, cholera toxin subunit B (CTB) for myelinated A fibers or isolectin B4 (IB4) for non-peptidergic, unmyelinated C fibers, were injected into bilateral T7 and T13 DCNs, one tracer on one side and the other on the other side. Immunohistochemistry was performed on serial transverse sections of the spinal cord at T7 and T13 to measure the projection fields of labeled A and C fibers quantitatively as immunoreactive areas. Synaptophysin, a synaptic vesicle protein, is being used to identify the synaptic terminations of the A and C fibers. Responses of the autonomic system to electrical DCN stimulations were assessed by cannulation of the carotid artery to measure blood pressure.

Blood pressure changes to DCN stimulation in cervical injured rats range from mild dysautonomia to frank autonomic dysreflexia and were usually more pathological with rostral DCN stimulation relative to caudal DCN stimulation. In this study we investigated the central projection profiles of bilateral A and C fibers of T7 and T13 DCNs 2 and 4 weeks after injury and in uninjured animals. C fiber projection areas, more so than A fiber projection areas, increased in T7 and T13 after C7 bilateral crush injury compared to normals. The rostro-caudal distributions of both A and C fiber projections expanded in both rostral and caudal directions after injury. Not only was there greater area of labeled A and C fiber neurites, they covered a greater territory of the dorsal horn after injury.

Current measurements are underway to compare the extent of afferent sprouting at T7 vs T13 to see if the rostral/caudal physiological observations are paralleled by anatomical changes.

We are also measuring the extent to which afferent sprouting is associated with synaptogenesis after cervical SCI. Nevertheless, it seems clear that anatomical changes, especially in C fiber central projection patterns are associated with the physiological changes of dysautonomia following cervical SCI.

PLASTICITY IN CENTRAL PROJECTIONS OF CUTANEOUS NOCICEPTIVE AFFERENTS MATCHES THE NOCICEPTIVE HYPEREFLEXIA AND DYSAUTONOMIA SEEN AFTER SPINAL CORD INJURY IN RATS

K. E. Tansey[1,2,4,5], P. S. Malone[1,2], J. S. Tidwell[1,2,4], J. Chung[1,2], N. K. Wilson[1,2], J. M. White[3,4], H. J. Lee[1,2]

[1]Neurology, [2]Physiology, Emory University, Atlanta, GA [3]Biomedical Engineering, Emory University/Georgia Institute of Technology, Atlanta, GA; [4]Spinal Cord Injury Research Program, Shepherd Center, Atlanta, GA; [5]Spinal Cord Injury Clinic, Atlanta Veterans Administration Medical Center, Atlanta, GA

The cutaneus trunci muscle (CTM) spinal reflex results from stimulation of segmental dorsal cutaneous nerves (DCNs) and demonstrates neurophysiological plasticity after unilateral T10 hemisection spinal cord injury (SCI). DCN stimulation also generates a depressor blood pressure response in normal animals but can generate dysautonomia after severe bilateral C7 crush SCI.

The central projection patterns of A and C fibers in DCNs were analyzed after thoracic hemisection injury or cervical crush injury. Retrograde axonal tracers, cholera toxin subunit B (CTB) for myelinated A fibers or isolectin B4 (IB4) for non-peptidergic, unmyelinated C fibers, were injected into bilateral T7 and T13 DCNs, one tracer on one side and one on the other. Immunohistochemistry was performed on serial sections of the spinal cord at T7 and T13 to measure the projection fields of labeled A and C fibers.

Following cervical crush injury, a spectrum of blood pressure responses are seen, ranging from mild dysautonomia to the frank pressor response of autonomic dysreflexia, with rostral DCN stimulation generating greater pathology than caudal DCN stimulation. In these animals, there is sprouting of the central projections of C fibers at both T7 and T13 much more so than A fibers. Following unilateral thoracic hemisection injury, we record predominantly nociceptive hypereflexia to DCN stimulation both at A delta strength stimulation as well as to combined A delta and C fiber strength stimulation, both above and below the hemisection, and both on the injured and uninjured sides of the spinal cord. In these animals, there is sprouting of the central projections of both A and C fibers at both T7 and T13 with some A fibers now invading C fiber territory in lamina II.

It seems plasticity in central projections of cutaneous nociceptive afferents matches the nociceptive hypereflexia and dysautonomia seen after spinal cord injury.

Control/Tracking Number: 2014-S-5564-SfN
Activity: Scientific Abstract
Current Date/Time: 5/6/2014 12:41:21 PM

Cardiovascular responses to cutaneous nociceptive input after cervical spinal cord injury: role of pain afferent types and their plasticity

AUTHOR BLOCK: *H. LEE[1,2], J. CHUNG[1,2], K. E. TANSEY[1,2,3];
[1]Dept. of Neurol., [2]Dept. of Physiol., Emory Univ., Atlanta, GA; [3]Spinal Cord Injury Clin., VAMC, Atlanta, GA

Abstract:
In normal, anesthetized rats, stimulation of segmental (T6 - L1) dorsal cutaneous nerves (DCNs) generates different cardiovascular responses depending on which pain afferent types are activated. Stimulation of A delta fibers alone (0.5 mA) generates increases in heart rate (HR) but relatively limited decreases in blood pressure (BP), with this effect on BP being greater at higher stimulation frequencies (10 Hz vs 1, 2 or 5 Hz). Stimulation of both A delta and C fibers together (5 mA) generates the same increase in HR but now a greater drop in BP, especially at higher stimulation frequencies (2, 5, & 10 Hz). The temporal relationships between BP and HR changes show an initial drop in BP followed by an increase in HR followed by a recovery in BP and then a recovery in HR.
Following C7 crush spinal cord injury (SCI), we have found three cardiovascular responses based on BP, a depressor (normal) response where DCN stimulation at A delta and C fiber strength (5 mA) almost always generates a drop in BP, a pressor (autonomic dysreflexia) response where DCN stimulation almost always generates an increase in BP, and a dysautonomia response where there are mixed depressor and pressor responses to DCN stimulation at different spinal levels. We have now investigated the BP vs. HR relationships within these groups and found that the depressor response after injury is different than the normal response in that the final recovery of increased HR is delayed. This finding is also true in the dysautonomia response. In the pressor response, there are simultaneous increases in both BP and HR and both BP and HR are delayed in their return to baseline. In this last group, the effect is much greater in response to rostral DCN stimulation than to caudal DCN stimulation.
To relate these cardiovascular responses to pain afferent anatomical plasticity in the spinal cord dorsal horn, we transganglionically labeled A and C fibers with CTB and IB4 respectively in the T7 and T13 DCNs. In all injury cardiovascular responses, we found increased A fiber sprouting from both DCNs relative to uninjured animals. C fibers were fewer than, or the same as, in uninjured animals in both the depressor and dysautonomia response groups but

showed sprouting in the pressor response group, significantly more so at T7 than at T13. Taken together, the normal animal data and the spectrum of cardiovascular responses and anatomical plasticity after cervical SCI, it would seem that A delta afferent input and plasticity preferentially affect HR responses and C fiber input and plasticity preferentially affect BP responses. This may mean that A delta effects could be predominantly cardiac while C fiber effects could be predominantly on vascular tone.
:

Presentation Preference (Complete): Poster Only
Linking Group (Complete): None selected
Nanosymposium Information (Complete):
Theme and Topic (Complete): D.10.d. Plasticity: Neurophysiology ; E.04.a. Cardiovascular regulation
Keyword (Complete): AUTONOMIC ; HEART RATE, BLOOD PRESSURE ; SPROUTING
Support (Complete):
Support: Yes
Grant/Other Support: : DoD SC090469
Grant/Other Support: : Craig H. Neilsen 284874

Special Requests (Complete):
Would you be interested in being considered for a dynamic poster?: No, I am not interested in presenting a Dynamic Poster

Is the first (presenting) author of this abstract a high school or undergraduate student?: None

Religious Conflict?: No Religious Conflict
Additional Conflict?: No

Status: Finalized